Quantum Vacuum Nonlinearities in Strong Electromagnetic Fields

Habilitationsschrift
vorgelegt am 26.06.2023
der Physikalisch-Astronomischen Fakultät
der Friedrich-Schiller-Universität Jena
von
Felix Karbstein
aus Sonthofen

Gutachter

1. Prof. Dr. Holger Gies
2. Prof. Dr. Gerald V. Dunne
3. Prof. Dr. Thomas Heinzl

Erteilung der Lehrbefähigung am 07.02.2024

Abstract

The physical vacuum of a relativistic quantum field theory amounts to a non-trivial quantum state. It encodes information about the full particle content of the underlying microscopic theory in the form of virtual processes, also referred to as vacuum fluctuations. If the theory features charged particles, fluctuations of the latter give rise to nonlinear effective couplings between electromagnetic fields that vanish in the formal limit of $\hbar \to 0$, but persist for a nonzero physical value of Planck's constant $\hbar$. In turn, they inherently modify Maxwell's linear theory of classical electrodynamics. However, for the field strengths reached by macroscopic electromagnetic fields currently available in the laboratory the quantum vacuum nonlinearities induced by Standard Model particles are parametrically suppressed relatively to the linear contribution by inverse powers of the electron mass and thus very small. As a consequence, this fundamental tenet has remained experimentally challenging and is yet to be tested in the laboratory. The present work is devoted to the study of quantum vacuum nonlinearities in strong electromagnetic fields arising from quantum electrodynamics. It provides a detailed account of the state of the art of analytical theory. On the one hand, it focuses on fundamental theoretical aspects concerning the structure and behavior of the Heisenberg-Euler effective action, which supersedes the classical Maxwell action in governing the physics of strong macroscopic electromagnetic fields in the quantum vacuum. On the other hand, it is concerned with questions of direct phenomenological relevance like the systematic study of photonic quantum vacuum signals accessible with state-of-the-art laser technology.

Contents

Chapter 1

Introduction

In contrast to the classical notion of the vacuum, describing the absence of anything, the physical quantum vacuum amounts to a highly non-trivial state. It is characterized by the omnipresence of quantum fluctuations of all dynamical degrees of freedom of the underlying microscopic quantum field theory (QFT). These fluctuations effectively endow the quantum vacuum with medium-like properties which can be probed, e.g., by imposing physical boundary conditions [1], or with macroscopic electromagnetic fields [2].

In the first example the experimental signature is the Casimir effect, which reveals fluctuation-induced matter-matter interactions. These manifest themselves in forces between macroscopic objects which could already be successfully measured in experiment. In the second example the fluctuation-induced effective self-interactions of the electromagnetic fields result in a nonlinear response to the applied macroscopic field. So far, this response has never been observed in experiment. It is in particular triggered by fluctuations of charged particles which couple directly to electromagnetic fields, but – at least in principle – depends on the charges and masses of all existing particles. Correspondingly, the vacuum associated with the world we live in even constitutes a portal to new physics beyond the Standard Model (SM) of particle physics. Within the SM the leading effective interactions between electromagnetic fields are governed by quantum electrodynamics (QED), which describes the interaction of electrons and positrons of mass m and charge $\mp e$ – the lightest free charged SM particles – with photons. The contributions of other particle sectors of the SM are parametrically suppressed with powers of $(m/M)^2 \ll 1$ because their effective masses M fulfill $M \gg m$ while their charges are of the same order as e. *

The present work is devoted to the theoretical study of the quantum vacuum subjected to a non-quantized macroscopic electromagnetic field $\bar{F}^{\mu\nu} = \partial^\mu \bar{A}^\nu - \partial^\nu \bar{A}^\mu$ which is typically expressed in terms of a gauge field $\bar{A}^\mu$. Macroscopic fields approximately preserve their characteristic properties, such as frequency and associated cycle-averaged energy density, on scales much larger than the inherent ref-

*This statement does not seem to hold for the lightest quarks. However, these couple directly to gluons and their physics is governed by quantum chromodynamics (QCD). Central properties of QCD are color confinement and infrared slavery, which implies strong coupling at low energies. Hence, it is to be expected that upon integrating out the gluons, the spectrum of QCD at low energies is characterized by colourless composite states made up of quarks and gluons. Their lightest representatives are the pions fulfilling $M \gg m$.

erence scale of the considered microscopic theory. To be specific, this work focuses on two rather different directions: first, the foundations of the effective field theory framework facilitating the solid theoretical study of quantum vacuum phenomena in prescribed external electromagnetic fields as well as fundamental aspects of the theory. And second, on strategies allowing to provide quantitatively accurate phenomenological predictions for quantum vacuum signals accessible in discovery experiments based on state-of-the-art laser technology while retaining analytical control. Throughout this work we focus exclusively on the vacuum of QED in $d = 3 + 1$ space-time dimensions: we are absolutely convinced that a thorough understanding of quantum vacuum processes in external fields within the SM is required prior to extending the considerations to the widely unconstrained physics beyond the SM. On the other hand, precise SM predictions usually allow for improved constraints on beyond SM contributions. In the realm of QED, a macroscopic field $\bar{F}^{\mu\nu}$ exhibits no significant changes in its cycle-averaged energy density (which is proportional to the square of the field amplitude) and oscillation frequency on distances $\lambda \gg \lambda\!\!\!^{-}_{\mathrm{C}}$ and durations $\tau \gg \tau_{\mathrm{C}}$, with Compton wavelength $\lambda\!\!\!^{-}_{\mathrm{C}} = \hbar/mc \simeq 3.8 \times 10^{-13}$ m and time $\tau_{\mathrm{C}} = \lambda\!\!\!^{-}_{\mathrm{C}}/c \simeq 1.3 \times 10^{-21}$ s set by the electron mass. The latter constitutes the only dimensionful scale of the QED vacuum at zero field. This in particular implies that static electromagnetic fields and coherent light fields generated by lasers amount to macroscopic fields.

A central quantity in the theoretical study of the QED vacuum in the presence of an external electromagnetic field $\bar{A}^{\mu}$ is the Heisenberg-Euler effective action $\Gamma_{\mathrm{HE}}[\bar{A}]$ [2–4]. It arises from the microscopic theory of QED by introducing an appropriately chosen source for the photon field and integrating out the dynamical degrees of freedom, namely the quantized spinor fields describing electrons and positrons, and the quantum photon field. In this way, quantum vacuum fluctuations are encoded in effective nonlinear couplings of the electromagnetic field $\bar{F}^{\mu\nu}$; gauge invariance of QED ensures that there is no explicit dependence on $\bar{A}^{\mu}$. This theory can be considered as the true theory of external electromagnetic fields in the QED vacuum superseding Maxwell's classical theory of electrodynamics. As opposed to the latter, it is no longer linear in the field on the level of the equations of motion which immediately implies light-by-light scattering phenomena and violations of the celebrated superposition principle of electromagnetic fields [5–10], which is a cornerstone of Maxwell's theory. In terms of Feynman diagrams $\Gamma_{\mathrm{HE}}[\bar{A}]$ can be represented as an infinite set of vacuum diagrams, with the charged particle lines dressed to all orders in the external field and its derivatives. Vacuum diagrams are Feynman diagrams without external lines representing incoming and outgoing quantum fields, respectively. The simplest quantum corrections arise from a one-loop diagram. As in QED at zero field, diagrams featuring more loops are parametrically suppressed with powers of the fine structure constant, which in the low-energy limit, i.e., at the energy scale of the electron mass m, is given by $\alpha = e^2/(4\pi\epsilon_0\hbar c) \simeq 1/137 \ll 1$.

Apart from the applied electromagnetic field $\bar{F}^{\mu\nu}$ and potentially derivatives thereof, at zero temperature and vanishing chemical potential the only physical parameters available for parameterizing fluctuation-induced corrections to the classical Maxwell action are the electron mass m and the elementary charge e mediating the coupling between charges and electromagnetic fields. As the quantum fields only appear as virtual states, their momenta are integrated over and hence not determined, eliminating the possibility of any explicit reference to them. Upon combination with the speed of light c and the Planck constant $\hbar$ the inverse of the electron mass can be converted into length and time scales.

As noted above, these are $\lambda\!\!\!^{-}_{\mathrm{C}}$ and τ_{C}. Analogously, the ratio of m^2 and e can be converted into electric $E_{\mathrm{cr}} = m^2c^3/(e\hbar) \simeq 1.3\times10^{18}\,\mathrm{V/m}$ and magnetic $B_{\mathrm{cr}} = E_{\mathrm{cr}}/c \simeq 4\times10^{9}\,\mathrm{T}$ field strengths. These quantities constitute the QED inherent reference scales the applied electric and magnetic fields and their scales of variation are compared to. Because all macroscopic electric $\vec{E}$ and magnetic $\vec{B}$ fields currently available in the laboratory fulfill $|\vec{E}|/E_{\mathrm{cr}} \ll 1$ and $|\vec{B}|/B_{\mathrm{cr}} \ll 1$, quantum vacuum nonlinearities are generically very small and suppressed relative to the Maxwell term. For fields varying on typical spatial and temporal scales much larger than $\lambda\!\!\!^{-}_{\mathrm{C}}$ and τ_{C} in addition also derivative contributions are negligible.

In fact, precisely this is the reason for the great success of Maxwell electrodynamics in the very accurate description of essentially all measurable classical optics phenomena. At the same time, it explains why quantum vacuum nonlinearities have not yet been observed in experiments with macroscopic electromagnetic fields. However, recent technological advances resulting in the availability of high-intensity lasers of the petawatt class in numerous laboratories worldwide in conjunction with high-definition detection schemes allowing to measure signals on the single photon level should provide a golden opportunity to measure nonlinear quantum vacuum signals in the near future for the first time. Seizing this opportunity in experiment requires a profound understanding of the underlying physics with regard to both genuine theoretical (e.g., identifying the contributions to be accounted for in the relevant parameter regime and putting forward strategies to determine the signal) and more phenomenological (e.g., modeling the experimentally realistic field configurations driving the signal consistently and finding ways to enhance it) aspects. Here we exclusively focus on an accurate analytical modeling of quantum vacuum signals. While accurate analytical approximations accounting for central parameter dependences of the induced quantum vacuum signals are especially important to assist the planning of such discovery experiments, an unambiguous discovery will eventually require quantitative numerical first-principle results evaluated in the specific field configurations used in experiment. We emphasize that this does not require any new conceptual insights and thus can be considered as a straightforward extension of the formalism presented here. For other recent advances in QED with intense background fields see the topical review [11] and references therein.

As noted already above, the present work is concerned with the full range of topics: it in particular (i) tackles fundamental research questions at the foundations of external-field QED, such as the emergence of $\Gamma_{\mathrm{HE}}[\bar{A}]$, its relation to the microscopic theory of QED and its diagrammatic structure, (ii) reviews and complements explicit analytical results for $\Gamma_{\mathrm{HE}}[\bar{A}]$ in different parameter regimes, (iii) highlights the role of one-particle reducible contributions to $\Gamma_{\mathrm{HE}}[\bar{A}]$ and provides analytical insights into the manifestly nonperturbative strong field limit of the theory receiving contributions from all loop orders, (iv) introduces and advocates the vacuum emission picture as a convenient approach allowing for the quantitatively reliable determination of photonic quantum vacuum signals in manifestly inhomogeneous electromagnetic fields, (v) emphasizes the importance of accounting for the details of the driving field configurations in assessing the discernibility of quantum vacuum signals, and finally (vi) focuses on phenomenological applications relevant for experiment, such as new strategies allowing to enhance the signal-to-background separation in laser pulse collisions. We present this rich material in two main chapters, each of which consists of several subsections. While Chapter 2 focuses on fundamental theory and is centered on the topics (i) to (iii), Chapter 3 is devoted to more phenomenological aspects and elaborates on topics (iv) to

(vi). Finally, we end with conclusions and an outlook in Chapter 4.

Throughout this work, we use the Heaviside-Lorentz System with $c = \hbar = \epsilon_0 = 1$; our metric convention is $g^{\mu\nu} = \mathrm{diag}(-1, +1, +1, +1)$.

Chapter 2

The quantum vacuum in an external electromagnetic field

This chapter outlines the theoretical framework used to study quantum vacuum phenomena in external electromagnetic fields. It is centered on the Heisenberg-Euler effective action $\Gamma_{\rm HE}[\bar{A}]$ which governs the physics of external electromagnetic fields $\bar{A}^\mu$ beyond the classical Maxwell action by accounting for the quantum vacuum fluctuations of quantum electrodynamics. The definition and general structure of $\Gamma_{\rm HE}[\bar{A}]$ is elucidated, and important results obtained in the last century following the original works of Heisenberg and Euler [2], and Weisskopf [2] are reviewed and revisited. A central focus is on the role of one-particle reducible contributions to $\Gamma_{\rm HE}[\bar{A}]$ which were until recently and erroneously completely discarded in the low-frequency limit [12]. The latter in particular have a profound impact on the strong field limit of the theory.

2.1 From microscopic to strong-field QED

The microscopic theory of QED is defined by the Lagrangian

$$\mathcal{L}_{\rm QED} = -\frac{1}{4}F_{\mu\nu}F^{\mu\nu} + \bar{\psi}(\mathrm{i}\not{D}[A] - m)\psi\,, \tag{2.1}$$

with $\bar{\psi} = \psi^\dagger\gamma^0$ and $\not{D} = \gamma^\mu D_\mu$, which governs the dynamics and interactions of the gauge field A^μ and a four-component massive Dirac spinor field ψ describing charged spin-1/2 fermions. Both fields are quantized: the field A^μ in terms of photons, and the matter field ψ in terms of both electrons and positrons. Equation (2.1) is invariant under U(1) gauge transformations; $D_\mu[A] = \partial_\mu - \mathrm{i}eA_\mu$ is the gauge covariant derivative, and $F^{\mu\nu} = \frac{\mathrm{i}}{e}[D^\mu, D^\nu] = \partial^\mu A^\nu - \partial^\nu A^\mu$ is the field strength tensor. The defining property of the Dirac gamma matrices γ^μ is $\{\gamma^\mu, \gamma^\nu\} = -2g^{\mu\nu}\mathbb{1}$. The associated action is $S_{\rm QED}[A, \bar{\psi}, \psi] = \int \mathcal{L}_{\rm QED}$.* A

*Throughout this work we use the shorthand forms $\int_x \equiv \int \mathrm{d}^4x$ and $\int_p \equiv \int \frac{\mathrm{d}^4p}{(2\pi)^4}$ for integrations over position and momentum space. Moreover, we use $\int$ if the integration can be performed in position or momentum space.

slightly different representation of Eq. (2.1) is

$$\mathcal{L}_{\mathrm{QED}} = -\frac{1}{4}F_{\mu\nu}F^{\mu\nu} + \bar{\psi}(\mathrm{i}\partial\!\!\!/ - m)\psi + eA^{\mu}\bar{\psi}\gamma_{\mu}\psi\,, \tag{2.2}$$

where we split $\mathcal{L}_{\mathrm{QED}}$ into three terms: The first one is the Maxwell Lagrangian, describing the dynamics of free electromagnetic fields. The second one is the Dirac Lagrangian governing the dynamics of free spin-$1/2$ charges. Finally, the third one accounts for the interaction of electromagnetic and matter fields mediated by the elementary charge.

In the absence of sources directly supplying the considered system with real charges, the associated partition function is a functional of the current J^{μ} sourcing the field A^{μ} and reads

$$\begin{aligned} Z[J] &= \int \mathcal{D}A \int \mathcal{D}\bar{\psi} \int \mathcal{D}\psi \, \mathrm{e}^{\mathrm{i}S_{\mathrm{QED}}[A,\bar{\psi},\psi]+\mathrm{i}\int J_{\mu}A^{\mu}} \\ &= \int \mathcal{D}A \, \mathrm{e}^{\mathrm{i}\int(-\frac{1}{4}F_{\mu\nu}F^{\mu\nu}+J_{\mu}A^{\mu})} \, \mathrm{e}^{\mathrm{i}S_{\psi}[A]}\,. \end{aligned} \tag{2.3}$$

Here and throughout this work, the integration over the gauge field A^{μ} is implicitly understood to be only over gauge-inequivalent configurations and to preserve both the Lorentz and the gauge symmetry. This can be explicitly ensured via the Faddeev-Popov procedure [13]. Moreover, we introduced the shorthand notation

$$\mathrm{e}^{\mathrm{i}S_{\psi}[A]} = \int \mathcal{D}\bar{\psi} \int \mathcal{D}\psi \, \mathrm{e}^{\mathrm{i}\int \bar{\psi}(\mathrm{i}\partial\!\!\!/[A]-m)\psi}\,. \tag{2.4}$$

The generalization of Eq. (2.3) to explicitly account for sources for the fermions is straightforward. It is immediately clear that upon performing the integration over the fermion fields ψ and $\bar{\psi}$ Eq. (2.4) generates effective nonlinear self-couplings of the photon field A^{μ} of arbitrary order; cf. also the detailed discussion of this point in Sec. 2.2 below.

In a next step we aim at constructing the consistent effective field theory of QED in the presence of a prescribed non-quantized *external* electromagnetic field which is considered to be given from the outside. Our main focus is on the effective theory of external electromagnetic fields in the QED vacuum, i.e., the state where the quantum fields of the microscopic theory occur solely as virtual particles – or equivalently – have been integrated out. We note that from a fundamental viewpoint, the concept of a non-quantized external field seems somewhat redundant because the world ultimately is fully quantum. Besides, a separation into internal and external fields may look purely academic. On the other hand, this concept nicely aligns with our perception of a real experiment using classically controlled sources and detectors and thus is very useful in practice.

To this end, we formally decompose the gauge field as $A^{\mu} \to \bar{A}^{\mu} + A^{\mu}$ into two components, where $\bar{A}^{\mu}$ is eventually to be identified with the external field. With this decomposition, Eq. (2.3) can be rewritten identically as

$$Z[J] = \mathrm{e}^{\mathrm{i}\int(-\frac{1}{4}\bar{F}_{\mu\nu}\bar{F}^{\mu\nu}+J_{\mu}\bar{A}^{\mu})} \int \mathcal{D}A \, \mathrm{e}^{\mathrm{i}\int[-\frac{1}{4}F_{\mu\nu}F^{\mu\nu}+(\partial_{\mu}\bar{F}^{\mu\nu}+J^{\nu})A_{\nu}]} \, \mathrm{e}^{\mathrm{i}S_{\psi}[\bar{A}+A]}\,, \tag{2.5}$$

where we employed a partial integration and appropriate boundary conditions which eliminate surface

contributions. This can for instance be ensured by assuming $\bar{F}^{\mu\nu} = \partial^\mu \bar{A}^\nu - \partial^\nu \bar{A}^\mu$ and $F^{\mu\nu}$ to vanish at the boundary of the considered space-time region. Throughout this work we assume such surface terms to be rendered irrelevant by appropriately chosen boundary conditions. We emphasize that despite the explicit appearance of $\bar{A}^\mu$ on its right-hand side, the partition function (2.5), of course, still does not depend on $\bar{A}^\mu$ and remains a functional of the source J^μ only. In addition, we highlight that in contrast to the standard QFT treatment where J^μ often plays the role of an auxiliary variable, in the present context it is needed to sustain the external field.

At the same time, Eq. (2.5) implies that only a particular choice of J^μ is consistent with the concept of $\bar{A}^\mu$ being an external field, namely the one ensuring that

$$\int_x (\partial_\mu \bar{F}^{\mu\nu} + J^\nu) = 0 \quad \leftrightarrow \quad J^\nu = -\partial_\mu \bar{F}^{\mu\nu} =: -(\partial \bar{F})^\nu \,. \tag{2.6}$$

With this identification the fluctuation field A^μ only couples to the electron-positron field, while any direct coupling to $\bar{A}^\mu$ is inhibited. For any violation of Eq. (2.6), i.e., $\partial_\mu \bar{F}^{\mu\nu} + J^\nu = \mathcal{J}^\nu \neq 0$, the remnant source $\mathcal{J}^\nu$ may induce a nonvanishing expectation value of the quantum field $\langle A^\mu \rangle = -\mathrm{i}\, \delta/\delta \mathcal{J}_\mu \ln Z[\mathcal{J}] - \langle \bar{A}^\mu \rangle \neq 0$, which could mix with $\bar{A}^\mu = \langle \bar{A}^\mu \rangle$ and thereby lead to inconsistencies with the external field concept. Moreover, by adopting the choice in Eq. (2.6) the current J^ν is conserved by definition because $\partial_\nu J^\nu = -\partial_\mu \partial_\nu \bar{F}^{\mu\nu} = 0$.

Hence, upon implementing the constraint (2.6) in Eq. (2.5) the partition function acquires an explicit dependence on $\bar{A}^\mu$ and the latter is promoted to a physical external field. Indeed, for sources fulfilling Eq. (2.6), we can write

$$\mathrm{e}^{\mathrm{i}\Gamma_{\mathrm{HE}}[\bar{A}]} := \mathrm{e}^{\mathrm{i}\int(-J_\mu \bar{A}^\mu)} Z[J]\Big|_{J=-(\partial \bar{F})} = \mathrm{e}^{\mathrm{i}\int(-\frac{1}{4}\bar{F}_{\mu\nu}\bar{F}^{\mu\nu})} \int \mathcal{D}A\, \mathrm{e}^{\mathrm{i}\int(-\frac{1}{4}F_{\mu\nu}F^{\mu\nu})}\, \mathrm{e}^{\mathrm{i}S_\psi[\bar{A}+A]} \,, \tag{2.7}$$

which is a functional of $\bar{A}^\mu$ and, as a direct consequence of the Ward identity [14], invariant under its U(1) gauge transformations; cf. also Eq. (2.77) below. Here, we normalized the resulting expression by multiplying with an overall phase term such that in the absence of the quantum fields ψ, $\bar{\psi}$ and A^μ the exponential on the right-hand side reduces to $\exp\{\mathrm{i}(\Gamma_{\mathrm{MW}}[\bar{A}] + C)\}$, where $\Gamma_{\mathrm{MW}}[\bar{A}] = -\frac{1}{4}\int \bar{F}_{\mu\nu}\bar{F}^{\mu\nu}$ is the classical Maxwell action for the external field $\bar{A}^\mu$ and C denotes a constant (independent of $\bar{A}^\mu$). Correspondingly, in Eq. (2.7) all quantum vacuum fluctuation induced modifications of the latter are encoded in the expression under the functional integral over A^μ. As detailed in Sec. 2.2 below, this gives rise to nonlinear and nonlocal self-interactions of $\bar{A}^\mu$. The effective action

$$\Gamma_{\mathrm{HE}}[\bar{A}] = \Big(-\int J_\mu \bar{A}^\mu - \mathrm{i} \ln Z[J]\Big)\Big|_{J=-(\partial \bar{F})} \tag{2.8}$$

is commonly known as the Heisenberg-Euler [2] effective action, and the associated Lagrangian $\mathcal{L}_{\mathrm{HE}}$ fulfilling $\Gamma_{\mathrm{HE}} = \int \mathcal{L}_{\mathrm{HE}}$ as the Heisenberg-Euler effective Lagrangian. However, we remark that in the literature this term is sometimes used exclusively for the effective action in a constant electromagnetic field, or even just the one-loop constant-field result (2.61). Because $-\mathrm{i} \ln Z[J] =: W[J]$ is the Schwinger functional which generates all connected correlation functions Eq. (2.8) comprises only connected con-

tributions.

We note that Eq. (2.8) closely resembles the form of a standard one-particle irreducible (1PI) effective action defined via a Legendre transform of the partition function as

$$\Gamma_{\rm 1PI}[\mathcal{A}] = \sup_J \left(-\int J_\mu \mathcal{A}^\mu - \mathrm{i} \ln Z[J] \right) \tag{2.9}$$

in terms of the *classical* gauge field $\mathcal{A}^\mu$. The supremum prescription in Eq. (2.9) identifies $\mathcal{A}^\mu$ with the expectation value of the fluctuating quantum field,

$$\mathcal{A}^\mu = -\mathrm{i} \frac{\delta}{\delta J_\mu} \ln Z[J] = \langle A^\mu \rangle \,, \tag{2.10}$$

which thus emerges as the result of a quantum averaging process. Equation (2.9) governs the physics of classical electromagnetic fields in the quantum vacuum in the absence of real quantum particles as well as classical charges; by the introduction of fermionic sources it can be readily generalized to also account for the presence of classical charged particle fields. However, apart from structural resemblances between Eqs. (2.8) and (2.9) there are also important differences. Equation (2.8), wherein the source is subject to the constraint (2.6), clearly does not constitute a Legendre transform. As a consequence, it comprises both 1PI and one-particle reducible (1PR) contributions; see Sec. 2.2 below. Moreover, it contains no information about the dynamics that creates $\bar{A}^\mu$ in the first place. This has to be provided by a separate theory for the external field.

In the absence of quantum fluctuations, a consistent external field would obey an action principle with action $\Gamma_{\rm MW}[\bar{A}]$ and correspondingly solve the associated equations of motion,

$$\frac{\delta \Gamma_{\rm MW}[\bar{A}]}{\delta \bar{A}_\mu} = -\bar{J}^\mu \quad \leftrightarrow \quad \partial_\mu \bar{F}^{\mu\nu} = -\bar{J}^\nu \,, \tag{2.11}$$

where the classical source $\bar{J}^\mu = \bar{J}^\mu_{\rm in} + \bar{J}^\mu_{\rm out}$ governs the creation "in" as well as the detection and absorption "out" of the external electromagnetic field, i.e., strictly speaking, accounts for both sources and sinks of this field. These two components of the source typically exhibit a causal ordering in time. Equation (2.11) amounts to the classical inhomogeneous Maxwell equations.

Subsequently, we generalize Eq. (2.11) to the presence of quantum vacuum fluctuations while keeping the assumption that the external field is controlled by $\bar{J}^\mu$. In this context, we further clarify and elaborate on different aspects of the external field concept. To this end, it is convenient to decompose the external field as $\bar{A}^\mu = \bar{A}^\mu_{\rm in} + \bar{A}^\mu_{\rm signal}$ into an initially applied component generated by $\bar{J}^\mu_{\rm in}$ and a signal field, which encodes the quantum vacuum fluctuation mediated nonlinear response to $\bar{A}^\mu_{\rm in}$. For definiteness, we envisage a situation where the different constituents to $\bar{J}^\mu$ (lasers, magnets, detectors, etc.) are macroscopically separated from an *interaction region* $V_{\rm I}$, which is the space-time region wherein the effective self-interactions of the external field $\bar{A}^\mu$ mediated by quantum vacuum fluctuations may become sizable (focal volume, overlap region of various driving fields, etc.). Outside $V_{\rm I}$ such quantum vacuum nonlinearities by definition play no role: they are dramatically suppressed and essentially vanish due to the fact that here the external field is much weaker than the Schwinger field in combination with the locality

of QED. This establishes a formal partitioning of the system into an internal interaction and an external Maxwellian region, and thus allows for an operational definition of $\bar{A}^\mu$ in the outside region, where it is related to to the source $\bar{J}^\mu$ governing both the creation of $\bar{A}^\mu_{\rm in}$ and the detection of $\bar{A}^\mu_{\rm signal}$. It should be noted that, from a conceptual point of view, the specifics of the choice of $V_{\rm I}$ do not matter. At the same time, the considered scenario closely matches the typical physical setting of experiments aiming at the verification of strong-field QED effects. For completeness, we also note that especially for field strengths well below the Schwinger field, resulting only in very small effective nonlinear couplings between electromagnetic fields, the signal $\bar{A}^\mu_{\rm signal}$ may often be on the single photon level, i.e., of *quantum nature*. However, as it is ultimately assumed to be detected as an asymptotic state far outside $V_{\rm I}$ it is still useful and natural to attribute this signal to the external field.

This discussion implies that in the presence of quantum fluctuations the equations of motion to be fulfilled by a consistent external field $\bar{A}^\mu$ can be cast in the following form,

$$\partial_\mu \bar{F}^{\mu\nu} + C^\nu[\bar{A}] = -\bar{J}^\nu \,, \tag{2.12}$$

where $C^\nu[\bar{A}]$ parameterizes quantum corrections which become negligible outside $V_{\rm I}$. Correspondingly, in the outside region we have $C^\nu[\bar{A}] \to 0$ and Eq. (2.11) is recovered. By contrast, $C^\nu[\bar{A}]$ can become relevant inside $V_{\rm I}$, where however $\bar{J}^\nu = 0$. In QED, $C^\nu[\bar{A}]$ is perturbatively of $O(\alpha)$ and nonlinear and nonlocal in the field, with the nonlinearities and nonlocalities typically controlled by the Compton scale; cf. Sec. 2.3 below. To be precise, we emphasize that the above reasoning is only true for external fields fulfilling

$$\left| \bar{F}_{\mu\nu}(x)\, \partial^2 \bar{F}^{\mu\nu}(x) \right| \ll m^2 \left| \bar{F}_{\mu\nu}(x) \bar{F}^{\mu\nu}(x) \right| , \tag{2.13}$$

i.e., fields varying on typical spatio-temporal scales much larger than the Compton wavelength $\lambda\!\!\!^{-}_{\rm C} = 1/m$ of the electron, or fields being sufficiently light-like such that $\partial^2 \bar{F}^{\mu\nu} \approx 0$ [15]. Equation (2.13) is a direct consequence of the structure of the vacuum polarization tensor (2.83) mediating between two gauge fields which, in turn, is dictated by the gauge symmetry; see also Sec. 2.3.3 below. For generic high-frequency fields refinements are needed: in this case the higher-derivative terms linear in $\bar{F}^{\mu\nu}$ encoded in $C^\nu[\bar{A}]$ can become sizable also outside V_I, resulting in deviations from Eq. (2.11) also there and thus inhibiting the definition of an external Maxwellian region. We remark that adapting the discussion to arbitrarily strongly varying external fields is not a problem per se, but just requires a slightly different partitioning of the effective action into contributions quadratic and nonlinear in $\bar{F}^{\mu\nu}$. However, particularly as the physically relevant classical electromagnetic fields of high frequency, e.g., ultra-energetic gamma beams, are light fields fulfilling Eq. (2.13), throughout this work we consider only external fields meeting the criterion (2.13). This is also in accordance with the original work of Heisenberg and Euler focusing on the low-energy effective theory of external electromagnetic fields in the quantum vacuum.

Accounting for the fact that, as we have established above, the vacuum fluctuation induced effective couplings of $\bar{A}^\mu$ are governed by

$$\tilde{\Gamma}_{\rm HE}[\bar{A}] := \Gamma_{\rm HE}[\bar{A}] - \Gamma_{\rm MW}[\bar{A}] = W[J]|_{J=-(\partial\bar{F})} \,, \tag{2.14}$$

it is straightforward to infer that $C^\nu[\bar{A}] = \delta\tilde{\Gamma}_{\rm HE}[\bar{A}]/\delta\bar{A}_\nu$; Eq. (2.14) immediately implies that $\tilde{\Gamma}^{\ell\text{-loop}}_{\rm HE} = \Gamma^{\ell\text{-loop}}_{\rm HE}$ for $\ell \geq 1$. In turn, in the presence of quantum fluctuations Eq. (2.11) is superseded by

$$\frac{\delta\Gamma_{\rm HE}[\bar{A}]}{\delta\bar{A}_\mu} = -\bar{J}^\mu \quad \leftrightarrow \quad \partial_\mu \bar{F}^{\mu\nu} = -\bar{J}^\nu - \frac{\delta\tilde{\Gamma}_{\rm HE}[\bar{A}]}{\delta\bar{A}_\nu}\,, \tag{2.15}$$

a solution of which constitutes a consistent external field in Eq. (2.8). Thus, once $\Gamma_{\rm HE}[\bar{A}]$ is obtained, it can be used for determining $\bar{A}^\mu$ via Eq. (2.15) either by purely classical means or using a Fock space representation in a quantum optical setting. Both treatments are useful and legitimate. In particular, it is natural to adopt a mixed representation which treats the applied field $\bar{A}^\mu_{\rm in}$ classically and the induced weak signal fields $\bar{A}^\mu_{\rm signal}$ in terms of Fock space states, as has been put forward in the vacuum emission picture [16]. We remark that in practice an explicit evaluation of Eq. (2.8) for arbitrary field profiles is clearly impossible, such that approximate solution strategies of Eq. (2.15) are needed; see the discussion in the context of Eq. (2.24) below for further details. Moreover, a comparison of Eqs. (2.15) and (2.6) allows us to infer that the particular choice of the current J^μ which inhibits that $\bar{A}^\mu$ as well as $\bar{J}^\mu$ provide a source for the fluctuation field A^μ can alternatively be represented as

$$J^\nu = \bar{J}^\nu + \frac{\delta\tilde{\Gamma}_{\rm HE}[\bar{A}]}{\delta\bar{A}_\nu}\,. \tag{2.16}$$

Hence, a shift of the source term as $\bar{J}^\mu \to J^\mu$ generalizes the equations of motions for the external field in the absence of quantum vacuum fluctuations (2.11) to their presence and ensures that the external quantities $\bar{A}^\mu$ and $\bar{J}^\mu$ do not couple directly to A^μ.

It should also be noted that the argument of the exponential on the right-hand side of Eq. (2.7) can be interpreted as the microscopic action of *external-* or *strong-field* QED (sfQED) defined in terms of the quantum fields ψ, $\bar{\psi}$, A^μ and the external field $\bar{A}^\mu$, such that

$$\mathrm{e}^{\mathrm{i}\Gamma_{\rm HE}[\bar{A}]} = \int \mathcal{D}A \int \mathcal{D}\bar{\psi} \int \mathcal{D}\psi\, \mathrm{e}^{\mathrm{i}S_{\rm sfQED}[\psi,\bar{\psi},A|\bar{A}]}\,. \tag{2.17}$$

This action is given by $S_{\rm sfQED}[\psi,\bar{\psi},A|\bar{A}] = \int \mathcal{L}_{\rm sfQED}$ with Lagrangian (cf., e.g., Ref. [11])

$$\mathcal{L}_{\rm sfQED} = -\frac{1}{4}\bar{F}_{\mu\nu}\bar{F}^{\mu\nu} - \frac{1}{4}F_{\mu\nu}F^{\mu\nu} + \bar{\psi}(\mathrm{i}\not{D}[A+\bar{A}] - m)\psi\,. \tag{2.18}$$

Here, the attribute microscopic refers to its explicit dependence on the quantum fields. Equation (2.18) is very similar to Eq. (2.1), but features two different gauge fields $\bar{A}^\mu$ and A^μ representing external and internal electromagnetic fields, respectively. As detailed above, by construction these different types of fields do not exhibit a direct (tree-level) coupling. In the calculation of physical amplitudes within this theory the quantum field A^μ is typically integrated over and thus can be associated with internal lines in Feynman diagrams. Conversely, external fields only appear as external lines and represent asymptotic in- and outgoing fields.

We highlight that Eqs. (2.7), (2.8) and (2.17) fix $\Gamma_{\rm HE}[\bar{A}]$ up to a constant which can be associated with

the (missing) normalization of the partition function. It is convenient to choose this constant such that $\Gamma_{\rm HE}[\bar{A}]$ vanishes identically for $\bar{A}^\mu = 0$; this amounts to normalizing the partition function by $Z[J=0]$, i.e., replacing $Z[J] \to Z[J]/Z[0]$ in the above expressions.

For the following discussion, we recall that in QFT n-point correlation functions of quantum fields $\phi(x)$ are defined as $\langle\phi(x_1)\dots\phi(x_n)\rangle := \langle 0|T\{\hat{\phi}(x_1)\dots\hat{\phi}(x_n)\}|0\rangle$, where $\hat{\phi}(x)$ denotes the field operator associated with the field $\phi(x)$ in the Heisenberg picture, $T\{\cdots\}$ is the time-ordering operator and $|0\rangle$ is a vacuum state at every point in spacetime. In the path integral formulation of QFT, we have $\langle\phi(x_1)\dots\phi(x_n)\rangle = \int\mathcal{D}\phi\,\phi(x_1)\dots\phi(x_n)\,\mathrm{e}^{\mathrm{i}S[\phi]}/\int\mathcal{D}\phi\,\mathrm{e}^{\mathrm{i}S[\phi]}$, where $S[\phi]$ is the microscopic action of the considered quantum theory. The propagators of the fields are encoded in two-point correlators.

Hence, by identifying $S[\phi] \to S_{\rm sfQED}[\psi,\bar{\psi},A|\bar{A}]$, starting from Eq. (2.18) one can then, for instance, determine the full photon propagator in the presence of the external field in position space as $(\mathcal{D}[\bar{A}])^{\mu\nu}(x,y) = \mathrm{i}\langle A^\mu(x)A^\nu(y)\rangle_{\rm sfQED}$. To indicate over which microscopic action the averaging is performed we have introduced a label here for clarity. This propagator can conveniently be extracted by momentarily introducing an auxiliary current sourcing the field A^μ for parameter differentiation which is set to zero afterwards. By comparison, one can then easily show that the result of this calculation can be expressed as

$$(\mathcal{D}[\bar{A}])^{\mu\nu} = D^{\mu\nu} - D^{\mu\alpha}\Big(\frac{\delta^2\tilde{\Gamma}_{\rm HE}[\bar{A}]}{\delta\bar{A}^\alpha\delta\bar{A}^\beta} + \mathrm{i}\frac{\delta\tilde{\Gamma}_{\rm HE}[\bar{A}]}{\delta\bar{A}^\alpha}\frac{\delta\tilde{\Gamma}_{\rm HE}[\bar{A}]}{\delta\bar{A}^\beta}\Big)D^{\beta\nu} \tag{2.19}$$

in terms of functional derivatives of $\tilde{\Gamma}_{\rm HE}[\bar{A}]$ as defined in Eq. (2.14) and the bare photon propagator $D^{\mu\nu}$. The inverse of the latter appears in the Maxwell term $\frac{1}{4}F_{\mu\nu}F^{\mu\nu} = \frac{1}{2}A_\mu(D^{-1})^{\mu\nu}A_\nu$ + total derivative. In momentum space and accounting for a gauge fixing term (generalized Lorenz gauge) we have

$$D^{\mu\nu}(p,p') = (2\pi)^4\delta(p+p')\,\frac{1}{p^2-\mathrm{i}0^+}\Big(g^{\mu\nu} - (1-\xi)\frac{p^\mu p^\nu}{p^2-\mathrm{i}0^+}\Big), \tag{2.20}$$

with $\xi = 1$ in Feynman gauge; we use all-incoming conventions, which implies that all external momenta in a given Feynman diagram are formally considered as incoming and thus come with the same sign. Due to translational invariance in the field-free vacuum the free photon propagator only depends on the momentum transfer p^μ. We emphasize that this is in general no longer the case in inhomogeneous external fields that can transfer momentum to the photon line via the coupling to charged particle fluctuations. This effect is encoded in the second term in Eq. (2.19) which accounts for all possible modifications of photon propagation due to quantum fluctuations of virtual electrons, positrons and photons in the external field. Because external fields can source photons, Eq. (2.19) comprises both connected and disconnected contributions [12]. To understand and illustrate this, we recall that the exact Lagrangian describing photon propagation in the quantum vacuum subjected to $\bar{A}^\mu$ can be parameterized as

$$\mathcal{L} = -\frac{1}{2}A_\mu(D^{-1} + \Pi[\bar{A}])^{\mu\nu}A_\nu + j_\mu A^\mu \tag{2.21}$$

in terms of the photon polarization tensor $(\Pi[\bar{A}])^{\mu\nu}$ and an induced photon current $(j[\bar{A}])^\mu$. By definition, on the level of the Lagrangian propagation effects are encoded in contributions up to quadratic order in the considered field. A comparison of the photon propagator arising from Eq. (2.21) with Eq. (2.19)

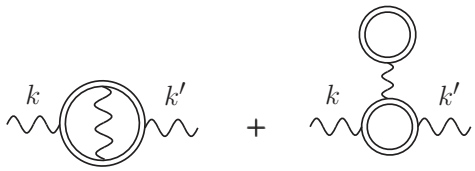

Figure 2.1: Representative Feynman diagrams that constitute $(\Pi[\bar{A}])^{\mu\nu}$ at two loops. There are both 1PI (left) and 1PR (right) contributions [12]. The double line denotes the Dirac propagator dressed to all orders in the external field $\bar{A}^\mu$ and the wiggly line represents a photon propagator; cf. also Fig. 2.2 below.

allows to establish the following relations,

$$\text{(i):}\ \frac{\delta^2\tilde{\Gamma}_{\text{HE}}[\bar{A}]}{\delta\bar{A}^\alpha\delta\bar{A}^\beta} = -\Big[\Pi[\bar{A}](1+D\Pi[\bar{A}])^{-1}\Big]_{\alpha\beta} \quad \text{and} \quad \text{(ii):}\ \frac{\delta\tilde{\Gamma}_{\text{HE}}[\bar{A}]}{\delta\bar{A}^\alpha} = \Big[j[\bar{A}](1+D\Pi[\bar{A}])^{-1}\Big]_{\alpha}\,. \tag{2.22}$$

These expressions reflect the fact that beyond one loop the functional derivatives of $\Gamma_{\text{HE}}[\bar{A}]$ for $\bar{A}^\mu$ account for both 1PI and 1PR structures that (i) mediate the interaction between the two open indices, and (ii) connect the current $(j[\bar{A}])^\mu$ with the open index. Conversely, $(\Pi[\bar{A}])^{\mu\nu}$ and $(j[\bar{A}])^\mu$ are manifestly 1PI with regard to the diagrammatic structure (i) mediating between the two indices, and (ii) ending at the open index. This means that, as opposed to the former quantities, it is impossible to truncate any of the diagrams constituting the latter ones by cutting a single photon line and subsequently moving an open index further inside. At the same time this provides us with a prescription allowing to extract the latter from the former on a diagrammatic level: draw all diagrams constituting the former and eliminate all those which can be further amputated with regard to the open indices by cutting a single photon line. Note that this nevertheless does not render $(\Pi[\bar{A}])^{\mu\nu}$ completely one-particle irreducible because in external fields it can still contain 1PR tadpole structures [12, 17]. See Fig. 2.1 for an example.

Moreover, we explicitly highlight that the above definition of exact correlation functions in the presence of an external field, such as Eq. (2.19), based on the microscopic action of strong-field QED involves a normalization by the partition function of this theory. The latter actually describes the vacuum in the presence of the external field. Alternatively one may rather want to capture all effects beyond the vacuum of QED at zero field by correlation functions like the photon propagator. This can be easily implemented by multiplication of the quoted result with a factor of $\int\mathcal{D}\phi\,\mathrm{e}^{\mathrm{i}S_{\text{sfQED}}[\phi|\bar{A}]}/\int\mathcal{D}\phi\,\mathrm{e}^{\mathrm{i}S_{\text{QED}}[\phi]} = \mathrm{e}^{\mathrm{i}\Gamma_{\text{HE}}[\bar{A}]}$, which immediately ensures the desired normalization on the QED vacuum at zero field. Note, however, that this transformation to another physical vacuum generically gives rise to (additional) disconnected contributions to correlation functions that have to be consistently accounted for.

Finally, we provide yet another representation of $\Gamma_{\text{HE}}[\bar{A}]$. Using the definitions just introduced, it is obvious that the appropriately normalized variant of Eq. (2.17) can be compactly represented as

$$\mathrm{e}^{\mathrm{i}\Gamma_{\text{HE}}[\bar{A}]} = \Big\langle \mathrm{e}^{\mathrm{i}\int(-\frac{1}{4}\bar{F}_{\mu\nu}\bar{F}^{\mu\nu}+\bar{j}_\mu\bar{A}^\mu)}\Big\rangle_{\text{QED}}\,, \tag{2.23}$$

with tree-level quantum current $\bar{j}_\mu = e\bar{\psi}\gamma_\mu\psi$. The integrand in the exponential on the right-hand side of Eq. (2.23) clearly resembles the Lagrangian of classical electrodynamics characterized by a gauge potential $\bar{A}^\mu$ coupled to a charged-particle current $\bar{j}_\mu$. In the absence of the latter, the free Maxwell

theory is recovered. From the representation (2.23) it is also evident that $\exp\{\mathrm{i}\Gamma_{\mathrm{HE}}[\bar{A}]\}$ amounts to the vacuum persistence amplitude parameterizing the probability amplitude for the initial vacuum state to persist in the presence of the external field $\bar{A}^\mu$ [4].

We emphasize that gauge and Lorentz invariance severely constrain the structure of $\mathcal{L}_{\mathrm{HE}}$: the entire dependence on the external field $\bar{A}^\mu$ is to be encoded in the field strength tensor $\bar{F}^{\mu\nu}$ and its dual ${}^\star\bar{F}_{\mu\nu} = \frac{1}{2}\epsilon_{\mu\nu\rho\sigma}\bar{F}^{\rho\sigma}$, which in turn is fully determined by $\bar{F}^{\mu\nu}$. Recall that the explicit occurrence of the gauge field in the QED Lagrangian (2.1) is a direct consequence of the gauge transformation of the Dirac field which has been integrated out in the derivation of $\mathcal{L}_{\mathrm{HE}}$. In position space, the only viable additional building block is the derivative operator ∂^μ. As $\mathcal{L}_{\mathrm{HE}}$ is a Lorentz scalar all Minkowski indices have to be contracted, which directly implies evenness in ∂^μ. Correspondingly, $\mathcal{L}_{\mathrm{HE}}$ can be organized in terms of a derivative expansion, where the $2n$th-order contribution contains $2n$ powers of the derivative operator and $n \in \mathbb{N}_0$. In turn, the Heisenberg-Euler effective action can be schematically expressed as

$$\Gamma_{\mathrm{HE}}[\bar{A}] = \int \mathrm{d}^4x\, \mathcal{L}_{\mathrm{HE}}(\bar{F}, \partial\bar{F}, \partial^2\bar{F}, \ldots)\,, \tag{2.24}$$

where the Lagrangian $\mathcal{L}_{\mathrm{HE}}$ is a function of $\bar{F}^{\mu\nu}$ and arbitrary powers of derivatives thereof. This derivative expansion constitutes a very important approach: at least in principle, it allows to ensure the above requirement on $\bar{A}^\mu$ to be a solution of Eq. (2.15) at each order of the expansion without needing to evaluate Eq. (2.8) for generic space-time dependent $\bar{A}^\mu$ from the outset. Note, however, that higher-derivative theories often come with inherent conceptual limitations on the parameter regime which can be reliably studied on their basis [18] and ultimately resummations will be necessary.

Also note that $\bar{F}^{0i} = E_i$ and $\bar{F}^{ij} = \epsilon_{ijk}B_k$. In fact, all Lorentz-contracted monomials of the field strength tensor and its dual are reducible to the gauge-invariant Lorentz scalars

$$\mathcal{F} = \frac{1}{4}\bar{F}_{\mu\nu}\bar{F}^{\mu\nu} = \frac{1}{2}(\vec{B}^2 - \vec{E}^2) \quad \text{and} \quad \mathcal{G} = \frac{1}{4}\bar{F}_{\mu\nu}{}^\star\bar{F}^{\mu\nu} = -\vec{B}\cdot\vec{E} \tag{2.25}$$

by the identities [19]

$$\begin{aligned} \bar{F}^{\mu\alpha}\bar{F}^{\nu}{}_{\alpha} - {}^\star\bar{F}^{\mu\alpha}{}^\star\bar{F}^{\nu}{}_{\alpha} &= 2\mathcal{F}g^{\mu\nu}\,, \\ \bar{F}^{\mu\alpha}{}^\star\bar{F}^{\nu}{}_{\alpha} = {}^\star\bar{F}^{\mu\alpha}\bar{F}^{\nu}{}_{\alpha} &= \mathcal{G}g^{\mu\nu}\,, \end{aligned} \tag{2.26}$$

such that the external field dependence of the contribution involving no derivatives acing on $\bar{F}^{\mu\nu}$ can be expressed in terms of $\mathcal{F}$ and $\mathcal{G}$ only. As a consequence of the fact that QED is CP invariant, i.e., respects a charge conjugation parity symmetry, and because of *Furry's theorem* [20] (charge conjugation invariance of the QED vacuum) $\Gamma_{\mathrm{HE}}[\bar{A}]$ in fact is even in the elementary charge e as well as both $\bar{F}^{\mu\nu}$ and ${}^\star\bar{F}^{\mu\nu}$. This directly implies evenness of the zero-derivative contribution to $\mathcal{L}_{\mathrm{HE}}$ in the *pseudoscalar* $\mathcal{G}$. Instead of $\mathcal{F}$ and $\mathcal{G}^2$ often also the so-called *secular* invariants

$$c_\pm = (\sqrt{\mathcal{F}^2 + \mathcal{G}^2} \pm \mathcal{F})^{1/2} \tag{2.27}$$

are used. Note that also $\mathcal{G}^2$ can be expressed in terms of the field strength tensor alone; cf. Eq. (A.1).

2.2 Heisenberg-Euler effective action

As detailed above, an explicit determination of $\Gamma_{\rm HE}[\bar{A}]$ requires evaluating the functional integrals over the fluctuation fields ψ, $\bar{\psi}$ and A^μ. Performing the integrations over the fermion fields ψ and $\bar{\psi}$ in Eq. (2.4) in the form as it enters Eq. (2.7) with the help of the identity $\int \mathcal{D}\bar{\psi} \int \mathcal{D}\psi \exp\{-\mathrm{i} \int \bar{\psi} M \psi\} = \det M$ yields

$$S_\psi[\bar{A}+A] = -\mathrm{i} \ln\det(G^{-1}[\bar{A}+A])\,, \tag{2.28}$$

where $G^{-1}[\bar{A}+A] = -\mathrm{i}\not{D}[\bar{A}+A]+m$ is the inverse Dirac propagator *dressed* to all orders in the combined field $\bar{A}^\mu + A^\mu$ and the functional determinant is over both spinor indices and coordinate space. In result, only the integration over A^μ in Eq. (2.7) remains to be carried out. Adopting this order of integration, the latter cannot be performed in closed form. It can however be tackled perturbatively by expanding Eq. (2.28) in powers of A^μ. The relevant all-order Taylor expansion of $S_\psi[\bar{A}+A]$ can be formally cast into the form

$$S_\psi[\bar{A}+A] = S_\psi[\bar{A}] + \sum_{n=1}^{\infty} \frac{1}{n!} \int \ldots \int (S_\psi^{(n)}[\bar{A}])^{\sigma_1\ldots\sigma_n} A_{\sigma_1} \ldots A_{\sigma_n}\,, \tag{2.29}$$

where we used the shorthand notation

$$(S_\psi^{(n)}[\bar{A}])^{\sigma_1\ldots\sigma_n} := \left.\frac{\delta^n S_\psi[A]}{\delta A_{\sigma_1}\ldots\delta A_{\sigma_n}}\right|_{A=\bar{A}} \tag{2.30}$$

for the effective vertices coupling n quantum fields. The nth contribution to Eq. (2.29) involves n integrals: each contraction of a pair of Minkowski indices comes with an integration over the associated common variable. Note that effective couplings of generic order $n \in \mathbb{N}$ are generated.

On the other hand, with the identity $\ln\det M = \mathrm{Tr}\ln M$ Eq. (2.28) can be represented as

$$S_\psi[\bar{A}+A] = S_\psi[\bar{A}] + \mathrm{i}\sum_{n=1}^{\infty} \frac{1}{n} \mathrm{Tr}\{(e\not{A} G[\bar{A}])^n\}\,. \tag{2.31}$$

Here, the trace $\mathrm{Tr}\{\cdot\} = \mathrm{tr}_\gamma \mathrm{tr}\{\cdot\}$ is over both spinor indices and coordinate space; we denote the Dirac trace over spinor indices by tr_γ and the trace over either position or momentum space by $\mathrm{tr}\{\cdot\} \equiv \int_x \langle x|\cdot|x\rangle = \int_p \langle p|\cdot|p\rangle$. A comparison of Eqs. (2.29) and (2.31) allows us to infer the following identity,

$$(S_\psi^{(n)}[\bar{A}])^{\sigma_1\ldots\sigma_n} = (n-1)!\,\mathrm{i}e^n\,\mathrm{Tr}\{\gamma^{\sigma_1} G[\bar{A}] \ldots \gamma^{\sigma_n} G[\bar{A}]\} \tag{2.32}$$

for $n \in \mathbb{N}$. Particularly from Eq. (2.32) it is obvious that the effective couplings $S_\psi^{(n)}[\bar{A}]$, and thus also $S_\psi[\bar{A}+A]$, are one-loop quantities arising from a single fermion loop. While accounting for the coupling to the external field $\bar{A}^\mu$ to all orders in the combined parameter $e\bar{A}^\mu$, the effective vertices exhibit an overall scaling $S_\psi^{(n)}[\bar{A}] \sim e^n$. This immediately implies that each joining of vertices by a photon line (both of two indices of the same vertex and of distinct vertices) comes with a factor of $e^2 \sim \alpha$. The functional integration over the dynamical photon field A^μ generically implements such contractions. In turn, upon plugging the expansion (2.29) into Eq. (2.7) the sum generates contributions to $\Gamma_{\rm HE}[\bar{A}]$ from

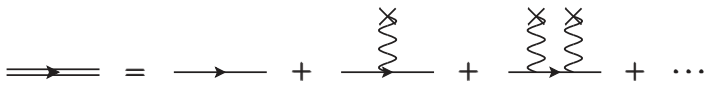

Figure 2.2: The double (single) straight line denotes the dressed (free) Dirac propagator accounting for arbitrarily many couplings to the external field $\bar{A}^\mu$ represented by wiggly lines ending at crosses.

order α onwards.

Thus in effect the perturbative expansion of Eq. (2.28) in the fluctuation field A^μ implies a perturbative expansion of $\Gamma_{\rm HE}[\bar{A}]$ in powers of α. Accounting for the fact that $S_\psi^{(n)}[\bar{A}]$ are one-loop quantities it is then straightforward to see that an ℓ-loop contribution to the Heisenberg-Euler effectively scales as $\Gamma_{\rm HE}^{\ell\text{-loop}}[\bar{A}] \sim \alpha^{\ell-1}$ for $\ell \in \mathbb{N}$. This in particular implies that $S_\psi[\bar{A}]$ constitutes the full one-loop correction to classical Maxwell theory, i.e., $\Gamma_{\rm HE}^{\text{1-loop}}[\bar{A}] = S_\psi[\bar{A}]$. As a direct consequence, $S_\psi^{(1)}[\bar{A}] = j^{\text{1-loop}}[\bar{A}]$ amounts to the one-loop photon current induced by $\bar{A}^\mu$, and $S_\psi^{(2)}[\bar{A}] = -\Pi^{\text{1-loop}}[\bar{A}]$ to the one-loop photon polarization tensor evaluated in the presence of $\bar{A}^\mu$ in line with Eq. (2.22).

On the other hand, it should also be noted that the occurrence of the disconnected contribution in Eq. (2.19) invalidates the equivalence between counting numbers of loops and powers of α for the full photon propagator in an external field. This is already obvious from the leading quantum correction, as clearly $(\Pi^{\text{1-loop}}[\bar{A}]) \sim (j^{\text{1-loop}}[\bar{A}])^2 \sim \alpha$ even though the current-current contribution comprises two loops.

Also note that upon adopting Eq. (2.31) with $\bar{A} \to 0$ and $A \to \bar{A}$ to expand $S_\psi[\bar{A}]$ in powers of $\bar{A}^\mu$ we obtain

$$S_\psi[\bar{A}] - S_\psi[0] = \mathrm{i}\sum_{n=1}^{\infty}\frac{1}{n}\mathrm{Tr}\{(e\bar{\not{A}}G[0])^n\} = \mathrm{i}\sum_{n=2}^{\infty}\frac{1}{2n}\mathrm{Tr}\{(e\bar{\not{A}}G[0])^{2n}\}\,, \tag{2.33}$$

with free inverse Dirac propagator $G^{-1}[0] = -\mathrm{i}\not{\partial} + m$. Here, we made use of the fact that effective couplings of an odd number of gauge fields vanish identically because of *Furry's theorem* [20] in the second step.[†] This implies that the one-loop result $S_\psi[\bar{A}]$ accounts for the effective coupling of arbitrary even powers of the combination $e\bar{A}^\mu$. Using a perturbative expansion of the Dirac propagator dressed in the external field (cf. Fig. 2.2),

$$G[\bar{A}] = G[0]\sum_{n=0}^{\infty}(e\bar{\not{A}}G[0])^n\,, \tag{2.34}$$

it can be readily shown that for the same reason $S_\psi^{(n)}[\bar{A}]$ with n odd (even) receives non-vanishing contributions only from terms odd (even) in $e\bar{A}^\mu$. This explains why the effective coupling of an odd number of A^μ mediated by a single fermion loop becomes possible in the presence of an external field as opposed to QED at zero field: in the constituting diagrams the odd coupling to A^μ is compensated by an odd coupling to $\bar{A}^\mu$ resulting in an overall even coupling to the gauge field compatible with Furry's theorem. As Eq. (2.28) is a priori defined up to an arbitrary additive constant, it is customary to define $S_\psi[\bar{A}]$ relative to the (divergent) vacuum contribution $S_\psi[0]$, which is to be subtracted; cf. Eq. (2.33). We will

[†]This can be easily shown by inserting the identity $C^{-1}C = \mathbb{1}$ with charge conjugation operator matrix C between each factor in Eq. (2.32) specialized to $\bar{A}^\mu = 0$ and using $C\gamma^\mu C^{-1} = -(\gamma^\mu)^T$; note that $CG(p)C^{-1} = G^T(-p)$ for the free Dirac propagator $G = G[0]$ in momentum space.

subsequently adopt this choice and set $S_\psi[\bar{A}] - S_\psi[0] \to S_\psi[\bar{A}]$.

In a next step, we aim at establishing the explicit form of higher order contributions to $\Gamma_{\mathrm{HE}}[\bar{A}]$ from Eq. (2.7). Upon insertion of Eq. (2.29) and employing the series representation of the exponential function, we obtain

$$\mathrm{e}^{\mathrm{i}\Gamma_{\mathrm{HE}}[\bar{A}]} = \mathrm{e}^{\mathrm{i}\int(-\frac{1}{4}\bar{F}_{\mu\nu}\bar{F}^{\mu\nu})}\,\mathrm{e}^{\mathrm{i}S_\psi[\bar{A}]}\int\mathcal{D}A\,\mathrm{e}^{\mathrm{i}S_{<3}[\bar{A},A]}\sum_{l=0}^{\infty}\frac{1}{l!}(\mathrm{i}S_{\geq 3}[\bar{A},A])^l\,, \tag{2.35}$$

where we split the terms in the exponential depending on the dynamical photon field in two contributions coupling less than three and three or more A^μ fields, respectively. To keep notations compact, we introduced the shorthand notations

$$\begin{aligned} S_{<3}[\bar{A},A] &:= \int (S_\psi^{(1)}[\bar{A}])^\mu A_\mu - \frac{1}{2}\iint A_\mu (D^{-1} - S_\psi^{(2)}[\bar{A}])^{\mu\nu} A_\nu\,, \\ S_{\geq 3}[\bar{A},A] &:= \sum_{n=3}^{\infty}\frac{1}{n!}\int\ldots\int (S_\psi^{(n)}[\bar{A}])^{\sigma_1\ldots\sigma_n} A_{\sigma_1}\ldots A_{\sigma_n}\,, \end{aligned} \tag{2.36}$$

where we rewrote the Maxwell term for the A^μ field in terms of the inverse bare photon propagator $(D^{-1})^{\mu\nu}$. The decomposition in Eq. (2.35) is motivated by the fact that Gaussian functional integrals can be performed explicitly. In the present case, this yields

$$\int\mathcal{D}A\,\mathrm{e}^{\mathrm{i}S_{<3}[\bar{A},A]} = \mathrm{e}^{\frac{\mathrm{i}}{2}\iint (S_\psi^{(1)}[\bar{A}])_\mu [(D^{-1}-S_\psi^{(2)}[\bar{A}])^{-1}]^{\mu\nu}(S_\psi^{(1)}[\bar{A}])_\nu}\,\det{}^{-1/2}(D^{-1} - S_\psi^{(2)}[\bar{A}])\,. \tag{2.37}$$

Taking the logarithm on both sides of Eq. (2.35) we arrive at the following representation of the effective action

$$\begin{aligned} \Gamma_{\mathrm{HE}}[\bar{A}] = -\frac{1}{4}\int \bar{F}_{\mu\nu}\bar{F}^{\mu\nu} + S_\psi[\bar{A}] - \mathrm{i}\ln\int\mathcal{D}A\,\mathrm{e}^{\mathrm{i}S_{<3}[\bar{A},A]} \\ - \mathrm{i}\ln\left(1 + \sum_{l=1}^{\infty}\frac{1}{l!}\int\mathcal{D}A\,\mathrm{e}^{\mathrm{i}S_{<3}[\bar{A},A]}(\mathrm{i}S_{\geq 3}[\bar{A},A])^l\Big/\int\mathcal{D}A\,\mathrm{e}^{\mathrm{i}S_{<3}[\bar{A},A]}\right), \end{aligned} \tag{2.38}$$

which can now be evaluated at any desired accuracy in a perturbative loop expansion using the series expansion of $\ln(1+\chi)$ about $\chi = 0$, yielding $\ln(1+\chi) = -\sum_{n=1}^{\infty}(-\chi)^n/n$. To this end it is particularly useful to shift $(S_\psi^{(1)})^\mu$ in Eq. (2.37) by a source term J^μ, allowing to generate powers of A^μ in the integrand in the second line of Eq. (2.38) by performing functional derivatives for this source term and setting $J^\mu = 0$ at the very end of the calculation. Therewith we can write

$$\begin{aligned} \Gamma_{\mathrm{HE}}[\bar{A}] = -\frac{1}{4}\int \bar{F}_{\mu\nu}\bar{F}^{\mu\nu} + S_\psi[\bar{A}] + \frac{\mathrm{i}}{2}\ln\det(D^{-1} - S_\psi^{(2)}[\bar{A}]) \\ + \frac{1}{2}\iint (S_\psi^{(1)}[\bar{A}])_\mu [(D^{-1} - S_\psi^{(2)}[\bar{A}])^{-1}]^{\mu\nu}(S_\psi^{(1)}[\bar{A}])_\nu \\ - \mathrm{i}\ln\left(1 + \sum_{l=1}^{\infty}\frac{1}{l!}\big(\mathrm{i}S_{\geq 3}[\bar{A},-\mathrm{i}\tfrac{\delta}{\delta J}]\big)^l\,\mathrm{e}^{\frac{\mathrm{i}}{2}\iint J_\mu[(D^{-1}-S_\psi^{(2)}[\bar{A}])^{-1}]^{\mu\nu}(J+2S_\psi^{(1)}[\bar{A}])_\nu}\right)\Bigg|_{J=0}. \end{aligned} \tag{2.39}$$

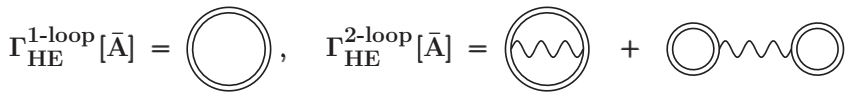

Figure 2.3: Diagrammatic representation of the Heisenberg-Euler effective action up to two loops. For the definition of the double line see Fig. 2.2.

Apart from the free Maxwell action and the one-loop effective action $S_\psi[\bar{A}]$, the first two lines of Eq. (2.39) account for scalar combinations involving generic powers of $S_\psi^{(1)}[\bar{A}]$ and $S_\psi^{(2)}[\bar{A}]$ contracted by photon propagators. This results in contributions of arbitrary order in α. Particularly the expression in the second line describes the effective interaction of two currents via the photon propagator dressed to all orders by the one-loop polarization tensor, i.e., comprises reducible one-loop bubble chains of arbitrarily order. On the other hand, the third line encompasses all contributions involving effective vertices $S_\psi^{(n)}[\bar{A}]$ with $n \geq 3$. Equation (2.39) in particular allows to read off the explicit expression for $\Gamma_{\text{HE}}^{2\text{-loop}}[\bar{A}]$. The latter can be represented as

$$\Gamma_{\text{HE}}^{2\text{-loop}}[\bar{A}] = -\frac{\mathrm{i}}{2}\mathrm{Tr}(DS_\psi^{(2)}[\bar{A}]) + \frac{1}{2}\iint (S_\psi^{(1)}[\bar{A}])_\mu D^{\mu\nu}(S_\psi^{(1)}[\bar{A}])_\nu\,, \tag{2.40}$$

where the trace $\mathrm{Tr}\{\cdot\}$ is now over both Minkowski indices and coordinate space. Equation (2.40) clearly decomposes into a 1PI (the first term) and a 1PR (the second term) contribution. See Fig. 2.3 for an illustration depicting the two-loop contributions in the same order as in Eq. (2.40).

The explicit determination of higher-loop contributions $\Gamma_{\text{HE}}^{\ell\text{-loop}}[\bar{A}]$ with $\ell \geq 3$ along these lines in addition requires parameter differentiations for J^μ and an expansion of the logarithm in the last line of Eq. (2.39).

For the sake of completeness, we note that alternatively one may, of course, perform the functional integration over A^μ prior to that over the charged particle field. Adopting this order of integrations, the functional integration over A^μ in Eq. (2.17) is of Gaussian type and can be carried out explicitly. Up to an overall field-independent normalization factor which can be dropped, this yields

$$\mathrm{e}^{\mathrm{i}\Gamma_{\text{HE}}[\bar{A}]} = \mathrm{e}^{\mathrm{i}\int(-\frac{1}{4}\bar{F}_{\mu\nu}\bar{F}^{\mu\nu})} \int \mathcal{D}\bar{\psi} \int \mathcal{D}\psi\; \mathrm{e}^{\mathrm{i}\int \bar{\psi}(\mathrm{i}\not{D}[\bar{A}]-m)\psi + \mathrm{i}\frac{1}{2}\iint e^2(\bar{\psi}\gamma^\mu\psi)D_{\mu\nu}(\bar{\psi}\gamma^\nu\psi)}\,. \tag{2.41}$$

Correspondingly, the resulting action in the exponential on the right-hand side of Eq. (2.41) features an effective, nonlocal four-fermion interaction. Aiming at the extraction of higher loop contribution from this expression, one can make use of a perturbative expansion in powers of the four-fermion interaction term, while at the same time accounting for the full dressing of the charged-particle propagator by the external field to all orders. The result for $\Gamma_{\text{HE}}^{\ell\text{-loop}}[\bar{A}]$ is then encoded in the contribution containing $\ell - 1$ powers of this interaction term. We point out that upon re-expressing the factor of e^2 governing the strength of the four-fermion interaction in terms of the fine structure constant, from Eq. (2.41) the distinct nature of the parameters e (parameterizing the coupling to the external field via $e\bar{A}^\mu$) and α (governing the loop expansion) becomes particularly transparent. Moreover, in this context we emphasize once again that, as opposed to QED at zero field, in the presence of an external field the vacuum expectation value of

$\langle\bar{\psi}\gamma^\mu\psi\rangle(x)$ is generically non-zero because it is effectively sourced by $\bar{A}^\mu$. This suggests that Eq. (2.41) defines a non-trivial mean field theory already in the Hartree approximation [21]. We note that to this end it is especially convenient to shift the fluctuation field in Eq. (2.17) as $A_\nu \to A_\nu + e\int\bar{\psi}\gamma^\mu\psi D_{\mu\nu} := \mathcal{J}_\nu$, which allows to rewrite it identically as

$$\mathrm{e}^{\mathrm{i}\Gamma_{\mathrm{HE}}[\bar{A}]} = \mathrm{e}^{\mathrm{i}\int(-\frac{1}{4}\bar{F}_{\mu\nu}\bar{F}^{\mu\nu})}\int\mathcal{D}\bar{\psi}\int\mathcal{D}\psi\int\mathcal{D}A\;\mathrm{e}^{\mathrm{i}\int\bar{\psi}(\mathrm{i}\not{D}[\bar{A}+\mathcal{J}]-m)\psi-\mathrm{i}\frac{1}{2}\iint\mathcal{J}_\mu(D^{-1})^{\mu\nu}\mathcal{J}_\nu}\,. \tag{2.42}$$

The Hartree approximation then amounts to simply identifying $\mathcal{J}_\nu$ with its expectation value $\bar{\mathcal{J}}_\nu := \langle\bar{\mathcal{J}}_\nu\rangle = e\int\langle\bar{\psi}\gamma^\mu\psi\rangle D_{\mu\nu}$; cf., e.g., Ref. [22]. For standard QED at zero field we clearly have $\bar{\mathcal{J}}^\mu = 0$ and the trivial theory of massive free fermions is recovered. We also remark that Eq. (2.42) can alternatively be understood as a Hubbard-Stratonovich transformation [23, 24] of the non-local four-fermion theory on the right-hand side of Eq. (2.41).

In a next step, we aim at providing an alternative representation of the one-loop effective action $S_\psi[\bar{A}]$. Therefore, we first note that with the help of Eq. (2.28) we can write

$$S_\psi[\bar{A}] = \quad - \quad = -\mathrm{i}\ln\det(-\mathrm{i}\not{D}[\bar{A}]+m) + \mathrm{i}\ln\det(-\mathrm{i}\not{\partial}+m)\,. \tag{2.43}$$

In even space-time dimensions we can define a matrix γ_5 (in four dimensions: $\gamma_5 = \mathrm{i}\gamma^0\gamma^1\gamma^2\gamma^3$) which anticommutes with the Dirac matrices γ^μ, i.e., fulfills $\{\gamma^\mu,\gamma_5\} = 0$ and $(\gamma_5)^2 = \mathbb{1}$. Upon insertion of this identity into the determinant it is easy to show that $\det(-\mathrm{i}\not{D}+m) = \det(\mathrm{i}\not{D}+m)$, such that

$$S_\psi[\bar{A}] = -\frac{\mathrm{i}}{2}\ln\det(\not{D}^2[\bar{A}]+m^2) + \frac{\mathrm{i}}{2}\ln\det(\not{\partial}^2+m^2)\,. \tag{2.44}$$

Using the defining property for the gamma matrices $\{\gamma^\mu,\gamma^\nu\} = -2g^{\mu\nu}\mathbb{1}$ and the definition $\sigma^{\mu\nu} := \frac{\mathrm{i}}{2}[\gamma^\mu,\gamma^\nu]$ one can straightforwardly show that $\not{D}^2[\bar{A}] = -D^2[\bar{A}] - \frac{e}{2}\sigma^{\mu\nu}\bar{F}_{\mu\nu}$.[‡] Therewith, we obtain

$$S_\psi[\bar{A}] = -\frac{\mathrm{i}}{2}\mathrm{Tr}\ln(-D^2[\bar{A}]+m^2-\tfrac{e}{2}\sigma^{\mu\nu}\bar{F}_{\mu\nu}) + \frac{\mathrm{i}}{2}\mathrm{Tr}\ln(-\partial^2+m^2)\,. \tag{2.45}$$

For completeness, we note that Eq. (2.45) closely resembles the analogous result for scalar electrodynamics[§]: the latter is recovered by multiplication with an overall minus sign, omitting the term $\sim\sigma^{\mu\nu}\bar{F}_{\mu\nu}$ and skipping the Dirac trace; cf. also the Appendix A.2. In addition using the parameter integral representation of the logarithm,

$$-\ln M + \ln M_0 = \int_0^\infty\frac{\mathrm{d}T}{T}(\mathrm{e}^{-\mathrm{i}MT}-\mathrm{e}^{-\mathrm{i}M_0T}) \quad\text{for}\quad \mathrm{Im}\{M,M_0\} < 0\,, \tag{2.46}$$

and taking into account the implicit prescription $m^2 \to m^2-\mathrm{i}0^+$, which can be traced back to the *Feynman prescription* in the propagator and is implied throughout this work, we arrive at the following integral

[‡]Subsequently we suppress the explicit notation of $\mathbb{1}$ whenever clear from the context.

[§]Scalar QED is the analogue of standard (or spinor) QED with the spinor field describing spin-1/2 fermions replaced by a spinless complex scalar field minimally coupling to the gauge potential.

representation of Eq. (2.43)

$$S_\psi[\bar{A}] = \frac{\mathrm{i}}{2}\int_0^\infty \frac{\mathrm{d}T}{T}\,\mathrm{e}^{-\mathrm{i}m^2T}\Big(\mathrm{Tr}\,\mathrm{e}^{\mathrm{i}(D^2[\bar{A}]+\frac{e}{2}\sigma^{\mu\nu}\bar{F}_{\mu\nu})T} - \mathrm{Tr}\,\mathrm{e}^{\mathrm{i}\partial^2 T}\Big). \tag{2.47}$$

An explicit evaluation of the traces for a given gauge field $\bar{A}^\mu$ in general requires the determination of the eigenvalues of the differential operators $D^2[\bar{A}] + \frac{e}{2}\sigma^{\mu\nu}\bar{F}_{\mu\nu}$ and ∂^2.

The exponential functions in Eq. (2.47) have the form of time evolution operators $\hat{U}(T) = \exp\{-\mathrm{i}\hat{H}T\}$ in quantum mechanics with time-independent Hamilton operator $\hat{H}$. In fact, the variable T can be identified with proper time [25] and a parameter integral representation like Eq. (2.47) is therefore often referred to as proper time representation [4]. Making use of the fact that the time evolution kernel $\langle x'|\hat{U}(T)|x\rangle$ can be expressed as a quantum mechanical path integral, we arrive at the *worldline* path integral representation of the one-loop effective action [26]. Of course, the worldline representation of the fermion propagator dressed in the external field can be constructed along the same lines.

Explicit analytical results for Eq. (2.47) accounting for all orders in the coupling to $e\bar{A}^\mu$ are only available for several special cases, namely constant electromagnetic fields, $\bar{F}^{\mu\nu} = \text{const.} \leftrightarrow \partial_\alpha \bar{F}^{\mu\nu} = 0$ [2–4], and specific one-dimensional field inhomogeneities [27–32]. However, we emphasize that in general the determination of higher-loop contributions to $\Gamma_{\mathrm{HE}}[\bar{A}]$ via Eq. (2.29) using functional derivatives (2.30) of course requires results for $S_\psi[\bar{A}]$ in arbitrary fields $\bar{A}^\mu$. A notable exception is the one-loop photon current $S_\psi^{(1)}[\bar{A}]$ in a constant field which can be obtained directly via functional differentiation from the constant-field one-loop effective action [12]. The reason for this is that constant fields cannot transfer momentum to a virtual charged particle loop; cf. Eq. (2.75) below.

On the other hand, making use of the fact that the dressed Dirac propagator $G[\bar{A}]$ is known explicitly in constant fields [4], though technical challenging, at least in principle Eq. (2.32) allows to work out all the relevant building blocks to determine a generic ℓ-loop contribution to $\Gamma_{\mathrm{HE}}[\bar{A}]$ in constant fields. The same is true for all inhomogeneous fields $\bar{A}^\mu$ for which the associated dressed Dirac propagator is available. Ritus [33] used this approach to provide an explicit expression for the 1PI contribution to $\Gamma_{\mathrm{HE}}^{\text{2-loop}}[\bar{A}]$ in a constant field. Along the same lines Batalin and Shabad [34] worked out the explicit result for the one-loop photon polarization tensor $S_\psi^{(2)}[\bar{A}]$ in a constant field; see also Sec. 2.3.2 below.

Finally, in this context we also note that $\Gamma_{\mathrm{HE}}[\bar{A}]$ vanishes identically in transverse null fields $\bar{F}^{\mu\nu} = \bar{F}^{\mu\nu}(\kappa\cdot x)$ that are characterized by $\kappa^2 = 0$ and $\kappa_\mu \bar{F}^{\mu\nu} = 0$ as well as $\mathcal{F} = \mathcal{G} = 0$. Prominent examples are either a single plane wave or a constant-crossed field [4]. This is a direct consequence of the fact that $\mathcal{L}_{\mathrm{HE}}$ depends on the external field only via monomials of $\bar{F}^{\mu\nu}$, ${}^\star\bar{F}^{\mu\nu}$ and derivatives ∂^μ thereof with all Minkowski indices contracted; cf. the paragraph below Eq. (2.23). In particular, recall that the zero-derivative contribution can be expressed exclusively in terms of the Lorentz scalar invariants $\mathcal{F}$ and $\mathcal{G}$.

2.3 Explicit analytical insights at one loop

2.3.1 Heisenberg-Euler effective Lagrangian

In a next step we explicitly work out the result for $\Gamma_{\text{HE}}^{\text{1-loop}}[\bar{A}] = S_\psi[\bar{A}]$ at zeroth order in a derivative expansion with respect to the strength $\bar{F}^{\mu\nu}$ of the external field. Because to this order the scalar invariants to be formed by contractions of $\bar{F}^{\mu\nu}$ and ${}^\star\bar{F}^{\mu\nu}$ are exactly the same as those for $\bar{F}^{\mu\nu} = \text{const.}$ we can without loss of generality formally perform the calculation for strictly constant fields. The corresponding expression has first been derived already in the mid-1930s by Heisenberg, Euler [2] and Weisskopf [3] for both spinor and scalar QED. Subsequently adopting the substitution $\bar{F}^{\mu\nu} \to \bar{F}^{\mu\nu}(x)$ in the result of the constant-field calculation we finally arrive at the expression which holds for fields of arbitrary space-time dependence. As long as the considered external fields vary so slowly that all higher-order derivative terms can be safely neglected this result even constitutes an excellent approximation to the full result for $\Gamma_{\text{HE}}[\bar{A}]$ at one loop.

For $\bar{F}^{\mu\nu} = \text{const.}$ we of course have $[D^2[\bar{A}], \bar{F}_{\mu\nu}] = 0$, such that $\exp\{\mathrm{i}(D^2[\bar{A}] + \frac{e}{2}\sigma^{\mu\nu}\bar{F}_{\mu\nu})T\} = \exp\{\mathrm{i}D^2[\bar{A}]T\}\exp\{\mathrm{i}\frac{e}{2}\sigma^{\mu\nu}\bar{F}_{\mu\nu}T\}$, where only the second factor has a nontrivial Dirac matrix structure. Aiming at performing the Dirac trace we first note that $(\frac{1}{2}\sigma^{\mu\nu}\bar{F}_{\mu\nu})^2 = \frac{1}{8}\{\sigma^{\mu\nu}, \sigma^{\alpha\beta}\}\bar{F}_{\mu\nu}\bar{F}_{\alpha\beta} = 2(\mathcal{F} + \mathrm{i}\gamma_5\mathcal{G})$, where we employed the identity $\frac{1}{2}\{\sigma^{\mu\nu}, \sigma^{\alpha\beta}\} = g^{\mu\alpha}g^{\nu\beta} - g^{\mu\beta}g^{\nu\alpha} + \mathrm{i}\gamma_5\epsilon^{\mu\nu\alpha\beta}$ [4]; the latter follows from the anticommutation relations of the Dirac matrices, $\mathrm{tr}_\gamma\gamma_5 = 0$ and $\mathrm{tr}_\gamma(\gamma_5\gamma^\mu\gamma^\nu\gamma^\alpha\gamma^\beta) = -4\mathrm{i}\epsilon^{\mu\nu\alpha\beta}$. Second, we note that because of $(\gamma_5)^2 = \mathbb{1}$ and $\mathrm{tr}_\gamma\gamma_5 = 0$ the eigenvalues of γ_5 in $3+1$ space-time dimensions are doubly degenerate and given by ± 1 [4]. This immediately implies that the eigenvalues of $(\frac{1}{2}\sigma^{\mu\nu}\bar{F}_{\mu\nu})^2$ are also doubly degenerate and read $2(\mathcal{F} \pm \mathrm{i}\mathcal{G})$ or equivalently $(c_+ \pm \mathrm{i}c_-)^2$; cf. Eq. (2.27). Taking into account that $\sigma^{\mu\nu}$ is traceless, it is then obvious that the four eigenvalues of $\frac{1}{2}\sigma^{\mu\nu}\bar{F}_{\mu\nu}$ are given by $\pm(c_+ \pm \mathrm{i}c_-)$, which implies

$$\mathrm{tr}_\gamma\, \mathrm{e}^{\mathrm{i}\frac{e}{2}\sigma^{\mu\nu}\bar{F}_{\mu\nu}T} = 4\cos(ec_+T)\cosh(ec_-T)\,. \tag{2.48}$$

Hence, in constant fields Eq. (2.47) can be expressed as

$$S_\psi[\bar{A}] = 2\mathrm{i}\int_0^\infty \frac{\mathrm{d}T}{T}\,\mathrm{e}^{-\mathrm{i}m^2T}\Big(\cos(ec_+T)\cosh(ec_-T)\,\mathrm{tr}\,\mathrm{e}^{\mathrm{i}D^2[\bar{A}]T} - \mathrm{tr}\,\mathrm{e}^{\mathrm{i}\partial^2T}\Big)\,, \tag{2.49}$$

where only the trace over coordinate space remains to be performed. The explicit evaluation of this trace can be significantly simplified by recalling that for constant fields $S_\psi[\bar{A}]$ depends on the external field only in terms of the two independent gauge-invariant Lorentz scalars $\mathcal{F}$ and $\mathcal{G}^2$, or $c_\pm$, respectively; see the corresponding discussion in the context of Eq. (2.26). In particular for the special case of $\vec{E} \parallel \vec{B}$ there is a one-to-one correspondence between the two sets of independent variables $B = |\vec{B}|$, $E = |\vec{E}|$ and c_+, c_-, namely $B \leftrightarrow c_+$ and $E \leftrightarrow c_-$. This implies that the result in arbitrary constant fields can be determined by actually performing a calculation for this special case only. Correspondingly, without loss of generality we choose the gauge potential $\bar{A}^\mu(x) = (0, 0, c_+\mathrm{x}, -c_-t)$ which ensures the electromagnetic fields to be given by $\vec{B} = c_+\vec{e}_\mathrm{z}$ and $\vec{E} = c_-\vec{e}_\mathrm{z}$. In turn, we have $D^2[\bar{A}] = \partial_\mathrm{x}^2 + (\partial_\mathrm{y} - \mathrm{i}ec_+\mathrm{x})^2 + (\partial_\mathrm{z} + \mathrm{i}ec_-t)^2 - \partial_t^2$.

The second trace in Eq. (2.49) can be evaluated straightforwardly in momentum space as $\partial_\mu = \mathrm{i}\hat{p}_\mu$, with momentum operator $\hat{p}_\mu$ fulfilling $\hat{p}_\mu|p_\mu\rangle = p_\mu|p_\mu\rangle$. Also note that $\langle p'_\mu|p_\mu\rangle = 2\pi\,\delta(p'_\mu - p_\mu)$ and

$\langle x'_\mu | x_\mu \rangle = \delta(x'_\mu - x_\mu)$, such that $\langle p_\mu | p_\mu \rangle = \int \mathrm{d}x_\mu$. Therewith we obtain

$$\mathrm{tr}\, \mathrm{e}^{\mathrm{i}\partial^2 T} = \int_p \langle p | \mathrm{e}^{\mathrm{i}\partial^2 T} | p \rangle = V^{(4)} \int_p \mathrm{e}^{-\mathrm{i}p^2 T} = -\mathrm{i} V^{(4)} \frac{1}{16\pi^2} \frac{1}{T^2}\,, \tag{2.50}$$

with space-time volume $V^{(4)}$. Similarly, the argument of the first trace in Eq. (2.49) depends on the y and z components only via ∂_y and ∂_z. On the other hand, it exhibits an explicit dependence on both ∂_x, ∂_t and x, t. We perform the trace over its y and z components in momentum space and that over its t and x components in position space. After shifting $t \to t - \frac{p_\mathrm{z}}{ec_-}$ and $\mathrm{x} \to \mathrm{x} + \frac{p_\mathrm{y}}{ec_+}$, this results in

$$\begin{aligned} \mathrm{tr}\, \mathrm{e}^{\mathrm{i}D^2[\bar{A}]T} = &\int \mathrm{d}\mathrm{y} \int \frac{\mathrm{d}p_\mathrm{y}}{2\pi} \int \mathrm{d}\mathrm{x}\, \langle \mathrm{x} |\, \mathrm{e}^{-\mathrm{i}2[\frac{1}{2}(-\mathrm{i}\partial_\mathrm{x})^2 + \frac{1}{2}(ec_+)^2 \mathrm{x}^2]T} | \mathrm{x} \rangle \\ &\times \int \mathrm{d}\mathrm{z} \int \frac{\mathrm{d}p_\mathrm{z}}{2\pi} \int \mathrm{d}t\, \langle t | \mathrm{e}^{\mathrm{i}2[\frac{1}{2}(-\mathrm{i}\partial_t)^2 + \frac{1}{2}(\mathrm{i}ec_-)^2 t^2]T} | t \rangle\,. \end{aligned} \tag{2.51}$$

It is now helpful to note that the expressions in the squared brackets in Eq. (2.51) can be interpreted as Hamilton operators of a quantum harmonic oscillator in one dimensions, $\hat{H} = \frac{1}{2m}\hat{p}_\mathrm{x}^2 + \frac{1}{2}m\omega^2 \hat{\mathrm{x}}^2$, whose eigenvalues are given by $E_n = \omega(n + \frac{1}{2})$, with $n \in \mathbb{N}_0$. For the expression in the upper line of Eq. (2.51) we have $\omega = ec_+$. The expression in the lower line is to be understood as harmonic oscillator with analytically continued frequency $\omega = \mathrm{i}ec_-$. This reflects the fact that as a direct consequence of $S_\psi[\bar{A}] = S_\psi(\mathcal{F}, \mathcal{G}^2)$ in a constant field and because of $\mathcal{F} = (c_+^2 - c_-^2)/2$ and $\mathcal{G}^2 = (c_+ c_-)^2$ there should exist a mapping $c_+^2 \leftrightarrow -c_-^2$ which leaves $S_\psi[\bar{A}]$ at zeroth order in a derivative expansion invariant. The seemingly equally justified identification $\omega = -\mathrm{i}ec_-$ would yield a divergent result, which would also be incompatible with the limit of $c_- \to 0$ considered in the second line of Eq. (2.53) below. Hence, we have

$$\begin{aligned} \mathrm{tr}\, \mathrm{e}^{\mathrm{i}D^2[\bar{A}]T} = &\sum_{n=0}^{\infty} \int \mathrm{d}\mathrm{y} \int \frac{\mathrm{d}p_\mathrm{y}}{2\pi} \int \mathrm{d}\mathrm{x}\, |\langle \mathrm{x} | n \rangle|^2\, \mathrm{e}^{-\mathrm{i}ec_+(2n+1)T} \\ &\times \sum_{n'=0}^{\infty} \int \mathrm{d}\mathrm{z} \int \frac{\mathrm{d}p_\mathrm{z}}{2\pi} \int \mathrm{d}t\, |\langle t | n' \rangle|^2\, \mathrm{e}^{-ec_-(2n'+1)T} \\ = &V^{(4)} \sum_{n=0}^{\infty} \rho(n)\, \mathrm{e}^{-\mathrm{i}ec_+(2n+1)T} \sum_{n'=0}^{\infty} \rho'(n')\, \mathrm{e}^{-ec_-(2n'+1)T}\,. \end{aligned} \tag{2.52}$$

where we introduced dimensionless densities of states $\rho(n)$ and $\rho'(n')$ associated with the discrete eigenvalues in the last step. These can be readily determined by accounting for the fact that the difference of Eqs. (2.52) and (2.50) have to vanish for $\{c_+, c_-\} \to 0$, which implies

$$\begin{aligned} \lim_{c_+ \to 0} \sum_{n=0}^{\infty} \rho(n)\, \mathrm{e}^{-\mathrm{i}ec_+(2n+1)T} &= \int \frac{\mathrm{d}p_\mathrm{x}}{2\pi} \int \frac{\mathrm{d}p_\mathrm{y}}{2\pi}\, \mathrm{e}^{-\mathrm{i}(p_\mathrm{x}^2 + p_\mathrm{y}^2)T}\,, \\ \lim_{c_- \to 0} \sum_{n'=0}^{\infty} \rho'(n')\, \mathrm{e}^{-ec_-(2n'+1)T} &= \int \frac{\mathrm{d}p_\mathrm{z}}{2\pi} \int \frac{\mathrm{d}p_t}{2\pi}\, \mathrm{e}^{-\mathrm{i}(p_\mathrm{z}^2 - p_t^2)T} = \int \frac{\mathrm{d}p_\mathrm{z}}{2\pi} \int \frac{\mathrm{d}p_t}{2\pi}\, \mathrm{e}^{-(p_\mathrm{z}^2 + p_t^2)T}\,. \end{aligned} \tag{2.53}$$

Defining $p_\perp^2 \equiv p_x^2 + p_y^2$ and $\Delta p_\perp^2 = 2ec_+$, the first line of Eq. (2.53) can be expressed as

$$\lim_{c_+\to 0} \sum_{n=0}^{\infty} \Delta p_\perp^2 \frac{\rho(n)}{2ec_+} \mathrm{e}^{-\mathrm{i}n\Delta p_\perp^2 T} = \frac{1}{4\pi} \int_0^\infty \mathrm{d}p_\perp^2 \, \mathrm{e}^{-\mathrm{i}p_\perp^2 T} \,, \tag{2.54}$$

allowing us to infer $\rho(n) = ec_+/(2\pi)$. Analogously, the second line yields $\rho'(n') = ec_-/(2\pi)$. In turn, Eq. (2.52) can be expressed in the compact form

$$\mathrm{tr}\, \mathrm{e}^{\mathrm{i}D^2[\bar{A}]T} = -\mathrm{i}V^{(4)} \frac{1}{16\pi^2} \frac{1}{T^2} \frac{(ec_+T)(ec_-T)}{\sin(ec_+T)\sinh(ec_-T)} \,. \tag{2.55}$$

Upon plugging Eqs. (2.50) and (2.55) into Eq. (2.49), we arrive at the compact expression

$$S_\psi[\bar{A}] = V^{(4)} \frac{1}{8\pi^2} \int_0^\infty \frac{\mathrm{d}T}{T^3} \mathrm{e}^{-\mathrm{i}m^2 T} \left(\frac{(ec_+T)(ec_-T)}{\tan(ec_+T)\tanh(ec_-T)} - 1 \right). \tag{2.56}$$

The integrand in Eq. (2.56) is clearly invariant under the mapping $c_+ \leftrightarrow -\mathrm{i}c_-$ compatible with Eq. (2.52). However, only if the integration contour of the proper time integration is assumed to lie slightly below the positive real T axis, no poles in the complex T plane are crossed when continuously deforming $c_+ \leftrightarrow -\mathrm{i}c_-$. This fixes the proper time integration contour in Eq. (2.56) to lie slightly below the positive real T axis [33, 35]. Also note that only a contour fulfilling $\mathrm{Im}\{T\} \leq 0$ is fully consistent with the Feynman prescription $m^2 \to m^2 - \mathrm{i}0^+$; otherwise ambiguities concerning the decay of the overall exponential factor $\mathrm{e}^{-\mathrm{i}m^2T}$ would arise for finite values of m and T. Employing the change of variable $T \to -\mathrm{i}T$ and a rotation of the integration contour in the complex plane which leaves the integral invariant, Eq. (2.56) can be alternatively represented as

$$S_\psi[\bar{A}] = -V^{(4)} \frac{1}{8\pi^2} \int_0^\infty \frac{\mathrm{d}T}{T^3} \mathrm{e}^{-m^2 T} \left(\frac{(ec_+T)(ec_-T)}{\tanh(ec_+T)\tan(ec_-T)} - 1 \right), \tag{2.57}$$

where the integration contour is now implicitly assumed to lie slightly above the positive real T axis. In the present context, this implies the following rule: for proper time representations featuring an overall factor of $\mathrm{e}^{-\mathrm{i}m^2T}$ (e^{-m^2T}) integrated along the positive real T axis, the integration contour is implicitly assumed to lie slightly below (above) the real axis.

The associated Lagrangian follows as $\mathcal{L}_{\mathrm{HE}}^{\text{1-loop}} = S_\psi[\bar{A}]/V^{(4)}$. Note however that this result is divergent and requires renormalization. The divergence arises from the small T behavior of the integrand in Eq. (2.57), namely the contribution $\sim T^2$ in the following expansion,

$$\frac{(ec_+T)(ec_-T)}{\tanh(ec_+T)\tan(ec_-T)} - 1 = \frac{2}{3}\mathcal{F}(eT)^2 + O(T^4) \,. \tag{2.58}$$

Isolating this UV divergent (recall that T has inverse mass dimension, i.e., small T correspond to large energies) contribution $\sim \mathcal{F}$ in Eq. (2.57) and introducing a regulator Λ of dimension mass, we obtain

$$\mathcal{L}_{\mathrm{HE}}^{\text{1-loop}} = -\mathcal{F}\frac{\alpha}{3\pi} \int_{1/\Lambda^2}^\infty \frac{\mathrm{d}T}{T} \mathrm{e}^{-m^2T} - \frac{1}{8\pi^2} \int_0^\infty \frac{\mathrm{d}T}{T^3} \mathrm{e}^{-m^2T} \left(\frac{(ec_+T)(ec_-T)}{\tanh(ec_+T)\tan(ec_-T)} - 1 - \frac{2}{3}(eT)^2\mathcal{F} \right), \tag{2.59}$$

where the limit of $\Lambda \to \infty$ is implicitly understood. Clearly, the second integral in Eq. (2.59) scales at least quartic in the external field $e\bar{F}^{\mu\nu}$. The first integral can be explicitly carried out, such that the divergent contribution becomes

$$\mathcal{L}_{\text{HE}}^{\text{1-loop}}\big|_{\sim\mathcal{F}} = -\mathcal{F}\frac{\alpha}{3\pi}\Big[\ln\Big(\frac{\Lambda^2}{m^2}\Big) - \gamma\Big] =: -\mathcal{F}(Z^{-1}(m^2) - 1)\,, \tag{2.60}$$

where γ denotes the Euler-Mascheroni constant and we neglected terms which vanish for $\Lambda \to \infty$.

Because of its linear scaling with $\mathcal{F}$, the divergent contribution (2.60) can be absorbed in the Maxwell term $\mathcal{L}_{\text{MW}} = -\mathcal{F}$. The form of the original Maxwell term is then recovered by rescaling the field strength as $\bar{F}^{\mu\nu} \to Z^{1/2}(m^2)\,\bar{F}^{\mu\nu}$, or equivalently the gauge field as $\bar{A}^{\mu\nu} \to Z^{1/2}(m^2)\,\bar{A}^{\mu\nu}$. For the interaction vertex of the external field $\bar{A}^{\mu}$ with the fermion fields in the Lagrangian (2.18) this rescaling implies $e\bar{A}^{\mu}\bar{\psi}\gamma_{\mu}\psi \to Z^{1/2}(m^2)\,e\bar{A}^{\mu}\bar{\psi}\gamma_{\mu}\psi$. The factor of $Z^{1/2}(m^2)$ in the last expression can be eliminated and the original interaction vertex restored by rescaling in addition $e \to Z^{-1/2}(m^2)\,e$. We emphasize that these rescalings effectively implement a transition to *renormalized quantities*, which depend on the renormalization scale μ. Here, we have clearly employed $\mu = m$, which is conventionally referred to as "on-shell" renormalization; note that $e^2(m^2)/(4\pi) = \alpha(m^2) \simeq 1/137$. The generalization to other renormalization scales is straightforward. The above considerations in particular imply that the combination $e\bar{F}^{\mu\nu}$ which remains invariant under these rescalings does not depend on the renormalization scale and thus forms a renormalization group (RG) invariant.

In turn, the (on-shell) renormalized one-loop Heisenberg Euler effective Lagrangian [2, 4] reads

$$\mathcal{L}_{\text{HE}}^{\text{1-loop}} = -\frac{1}{8\pi^2}\int_0^\infty \frac{\mathrm{d}T}{T^3}\,\mathrm{e}^{-m^2T}\Big(\frac{(ec_+T)(ec_-T)}{\tanh(ec_+T)\tan(ec_-T)} - 1 - \frac{(ec_+T)^2 - (ec_-T)^2}{3}\Big). \tag{2.61}$$

We emphasize that Eq. (2.61) accounts for all orders in $\mathcal{F}$ and $\mathcal{G}^2$, and (presuming the validity of a perturbative loop expansion) can be employed for the study of arbitrarily strong electromagnetic fields. It in particular provides access to phenomena which are nonperturbative in $e\bar{F}^{\mu\nu}$, most prominently vacuum decay via the Schwinger effect encoded in the imaginary part of the effective action. The latter can obviously be expressed as

$$\text{Im}\{\mathcal{L}_{\text{HE}}\} = \frac{1}{2\mathrm{i}}[\mathcal{L}_{\text{HE}} - (\mathcal{L}_{\text{HE}})^*]\,. \tag{2.62}$$

As the integrand in Eq. (2.61) is purely real-valued and the imaginary part stems only from the integration contour, which for the given representation lies slightly above the positive real T axis, the expression for $(\mathcal{L}_{\text{HE}}^{\text{1-loop}})^*$ looks identical to the one given for $\mathcal{L}_{\text{HE}}^{\text{1-loop}}$ in Eq. (2.61). However, now the integration contour is understood to lie slightly below the positive real T axis. By Cauchy's integral theorem, the difference in the square brackets on right side of Eq. (2.62) then corresponds to $-2\pi\mathrm{i}$ times the sum of the residues of the poles of the integrand lying on the positive real T axis. These are the poles of the inverse tangent located at $ec_-T = n\pi$ with $n \in \mathbb{N}$. Taking into account that in the vicinity of the pole located at $ec_-T = n\pi$ we have $1/\tan(ec_-T) = \frac{1}{ec_-}\frac{1}{T-\frac{n\pi}{ec_-}} + \mathcal{O}(T - \frac{n\pi}{ec_-})$, it is straightforwardly to infer that

$$\text{Res}\Big\{\frac{ec_-T}{\tan(ec_-T)}g(T)\Big\}\Big|_{ec_-T=n\pi} = \frac{n\pi}{ec_-}g(\tfrac{n\pi}{ec_-})\,, \tag{2.63}$$

where $g(T)$ is a function regular at $ec_-T = n\pi$. In turn, the imaginary part of $\mathcal{L}_{\text{HE}}^{\text{1-loop}}$ is given by [36],

$$\text{Im}\{\mathcal{L}_{\text{HE}}^{\text{1-loop}}\} \simeq \frac{(ec_-)^2}{8\pi^2}\frac{c_+}{c_-}\sum_{n=1}^{\infty}\frac{1}{n}\,\mathrm{e}^{-\frac{m^2}{ec_-}n\pi}\,\coth\!\left(\tfrac{c_+ n\pi}{c_-}\right), \tag{2.64}$$

and vanishes for $c_- = 0$. The characteristic feature of Eq. (2.64) is the manifestly nonperturbative dependence on ec_- in the exponential.

On the other hand, resorting to the identity $z/\tan z = \sum_{n=0}^{\infty}(-1)^n\mathcal{B}_{2n}/(2n)!\,(2z)^{2n}$ for $|z| < \pi$ with Bernoulli numbers $\mathcal{B}_{2n}$ ([37]: 1.411.7), noting that $z/\tanh z = \mathrm{i}z/\tan(\mathrm{i}z)$, and making use of the Cauchy product, Eq. (2.61) can be expanded as

$$\begin{aligned}
\mathcal{L}_{\text{HE}}^{\text{1-loop}} &\sim -\frac{1}{8\pi^2}\int_0^\infty\frac{\mathrm{d}T}{T^3}\,\mathrm{e}^{-m^2T}\left(\sum_{n=2}^{\infty}\sum_{k=0}^{n}(-1)^k\frac{\mathcal{B}_{2k}}{(2k)!}\frac{\mathcal{B}_{2n-2k}}{(2n-2k)!}(2ec_+T)^{2(n-k)}(2ec_-T)^{2k}\right)\\
&= -\frac{m^4}{8\pi^2}\sum_{n=2}^{\infty}\sum_{k=0}^{n}(-1)^k(2n-3)!\frac{\mathcal{B}_{2k}}{(2k)!}\frac{\mathcal{B}_{2n-2k}}{(2n-2k)!}\left(\frac{2ec_+}{m^2}\right)^{2(n-k)}\left(\frac{2ec_-}{m^2}\right)^{2k}\\
&= \frac{m^4}{360\pi^2}\left[\left(\frac{e}{m^2}\right)^4(4\mathcal{F}^2+7\mathcal{G}^2) - \frac{4}{7}\left(\frac{e}{m^2}\right)^6\mathcal{F}(8\mathcal{F}^2+13\mathcal{G}^2) + O\Big(\big(\tfrac{e\bar{F}}{m^2}\big)^8\Big)\right],
\end{aligned} \tag{2.65}$$

where the integration over T could be performed trivially as $\int_0^\infty \mathrm{d}T\,\mathrm{e}^{-m^2T}T^{2n-3} = (2n-3)!\,m^{4(1-n)}$. With the identity $\mathcal{B}_{2n} = (-1)^{n+1}2(2n)!\,\zeta(2n)/(2\pi)^{2n}$ ([38]: 5.152 and 5.157) the Bernoulli numbers can be expressed in terms of the Riemann zeta function, $\zeta(n) = \sum_{k=1}^{\infty}k^{-n}$ for $n \in \mathbb{N}$ and $\zeta(0) = -1/2$; clearly $\lim_{n\to\infty}\zeta(n) = 1$. Equation (2.65) constitutes an all-order perturbative weak field expansion, which should allow for reliable insights into the parameter regime where $c_\pm \ll m^2/e \;\leftrightarrow\; |\bar{F}^{\mu\nu}| \ll m^2/e$ [¶] or equivalently $\{|\mathcal{F}|, |\mathcal{G}|\} \ll (m^2/e)^2$. Note, however, that it amounts to a divergent asymptotic series because the expansion coefficients grow factorially fast with n.

Specifically also the regime of generic $\mathcal{F}$ but small $|\mathcal{G}| \ll (m^2/e)^2$, which covers the special cases of purely magnetic or electric fields, is of particular interest. To this end, we perform a perturbative weak field expansion in $\mathcal{G}$ and consider [39]

$$\mathcal{L}_{\text{HE}}^{\text{1-loop}} = \mathcal{L}_{\text{HE}}^{\text{1-loop}}\big|_{\mathcal{G}=0} + \frac{1}{2}\frac{\partial^2\mathcal{L}_{\text{HE}}^{\text{1-loop}}}{\partial\mathcal{G}^2}\bigg|_{\mathcal{G}=0}\mathcal{G}^2 + O(\mathcal{G}^4). \tag{2.66}$$

We explicitly account for terms up to $O(\mathcal{G}^2)$ in Eq. (2.66) because these are relevant for the study of probe photon propagation phenomena like vacuum birefringence in such field configurations and cannot be extracted from the contribution at $O(\mathcal{G}^0)$ alone [40].

In case of $\mathcal{G} = 0$ only one of the secular invariants (2.27) is nonvanishing: for $\mathcal{F} > 0$ we have $c_+ = \sqrt{2\mathcal{F}}$, while for $\mathcal{F} < 0$ we have $c_- = \sqrt{-2\mathcal{F}}$. Accounting for the invariance of the proper time representation of $\mathcal{L}_{\text{HE}}^{\text{1-loop}}$ under the mapping $c_+ \leftrightarrow -\mathrm{i}c_-$, without loss of generality both cases are accessible by a single calculation for $c_+ = \sqrt{2\mathcal{F}}$, $c_- = 0$, with the square root to be interpreted as

[¶] The notation $|\bar{F}^{\mu\nu}| \ll m^2/e$ is understood to imply that the modulus of each component of $\bar{F}^{\mu\nu}$ is much smaller than m^2/e.

$\sqrt{\mathcal{F}} = \sqrt{|\mathcal{F}|}[\Theta(\mathcal{F}) - \mathrm{i}\Theta(-\mathcal{F})]$. Also note that for $|\mathcal{F}| \gg |\mathcal{G}|$, we have

$$c_+ = \sqrt{2\mathcal{F}}\Big[1 + O\Big((\tfrac{\mathcal{G}}{\mathcal{F}})^2\Big)\Big] \quad \text{and} \quad c_- = \frac{|\mathcal{G}|}{\sqrt{2\mathcal{F}}}\Big[1 + O\Big((\tfrac{\mathcal{G}}{\mathcal{F}})^2\Big)\Big]. \tag{2.67}$$

Remarkably, the integrations over proper time T in Eq. (2.66) can even be carried out explicitly and expressed in terms of the Hurwitz zeta function $\zeta(s,\chi)$ and its derivative by resorting to the following two identities ([37]: 3.381.4 and 3.551.3),

$$\int_0^\infty \mathrm{d}T\,(aT)^{n-1+\epsilon}\,\mathrm{e}^{-m^2T} = \frac{1}{a}\Gamma(n+\epsilon)\Big(\frac{a}{m^2}\Big)^{n+\epsilon}, \tag{2.68}$$

$$\int_0^\infty \mathrm{d}T\,(aT)^{n+\epsilon}\,\mathrm{e}^{-m^2T}\coth(aT) = \frac{1}{a}\frac{\Gamma(n+1+\epsilon)}{2^{n+1+\epsilon}}\Big[2\zeta(n+1+\epsilon,\tfrac{m^2}{2a}) - \Big(\frac{2a}{m^2}\Big)^{n+1+\epsilon}\Big], \tag{2.69}$$

which hold for $n+\epsilon > 0$ and $a = |a|\,\mathrm{e}^{\mathrm{i}\delta}$ with $0 \leq \delta < \frac{\pi}{2}$, and derivatives thereof. The conditions on $n+\epsilon$ are rendered irrelevant upon combination of these integrals in the evaluation of manifestly finite contributions to $\mathcal{L}_{\mathrm{HE}}$. Equations (2.68) and (2.69) allow to derive closed-form expressions for $(\partial/\partial\mathcal{G})^n\mathcal{L}_{\mathrm{HE}}^{\text{1-loop}}\big|_{\mathcal{G}=0}$ with $n \in \mathbb{N}_0$ [41]. For the expressions written explicitly in Eq. (2.66) we obtain [39,40,42],

$$\mathcal{L}_{\mathrm{HE}}^{\text{1-loop}}\big|_{\mathcal{G}=0} = \frac{1}{\pi^2}e^2\mathcal{F}\Big\{\zeta'(-1,\chi) + \frac{\chi}{2}\Big[(1-\chi)\ln\chi + \frac{\chi}{2}\Big] - \frac{1}{12}(\ln\chi + 1)\Big\}, \tag{2.70}$$

$$\frac{\partial^2\mathcal{L}_{\mathrm{HE}}^{\text{1-loop}}}{\partial\mathcal{G}^2}\bigg|_{\mathcal{G}=0} = \frac{1}{8\pi^2}\frac{e^2}{\mathcal{F}}\Big\{4\zeta'(-1,\chi) - \chi[2\zeta'(0,\chi) - \ln\chi + \chi] - \frac{1}{6}\Big[2\psi(\chi) + \frac{1}{\chi} + 1\Big]\Big\}, \tag{2.71}$$

where we used the shorthand notation $\chi = m^2/(2e\sqrt{2\mathcal{F}})$ and $\psi(\chi) = \frac{\mathrm{d}}{\mathrm{d}\chi}\ln\Gamma(\chi)$ is the Digamma function. The strong field expansions of Eqs. (2.70) and (2.71) follow from the series representations of the first derivative of the Hurwitz zeta function as well as the Digamma function for small arguments [43,44] and read

$$\begin{aligned}\mathcal{L}_{\mathrm{HE}}^{\text{1-loop}}\big|_{\mathcal{G}=0} = \frac{1}{\pi^2}e^2\mathcal{F}\Big\{&-\frac{1}{12}\ln\chi + \zeta'(-1) - \frac{1}{12} - \frac{1}{2}\Big[\ln\chi + \ln(2\pi) - 1\Big]\chi \\ &- \frac{1}{2}\Big[\ln\chi - \frac{3}{2} + \gamma\Big]\chi^2 + \sum_{j=0}^{\infty}\frac{(-1)^j\zeta(j+2)}{(j+2)(j+3)}\chi^{j+3}\Big\},\end{aligned} \tag{2.72}$$

$$\begin{aligned}\frac{\partial^2\mathcal{L}_{\mathrm{HE}}^{\text{1-loop}}}{\partial\mathcal{G}^2}\bigg|_{\mathcal{G}=0} = \frac{1}{8\pi^2}\frac{e^2}{\mathcal{F}}\Big\{&\frac{1}{6}\chi^{-1} + \frac{\gamma}{3} + 4\zeta'(-1) - \frac{1}{6} - \Big[\ln\chi + \ln(2\pi) - 2 + \frac{\pi^2}{18}\Big]\chi \\ &+ \Big[1 + \frac{1}{3}\zeta(3)\Big]\chi^2 - \sum_{j=0}^{\infty}(-1)^j\Big[\frac{2(j+1)}{(j+2)(j+3)}\zeta(j+2) + \frac{1}{3}\zeta(j+4)\Big]\chi^{j+3}\Big\},\end{aligned} \tag{2.73}$$

where γ is the Euler-Mascheroni constant, $\zeta(\cdot)$ is the Riemann zeta function and $\zeta'(\cdot)$ is its derivative. As to be expected, in the limit of $\chi \ll 1$ the physical quantity setting the overall scale is the strong field $\mathcal{F}$; Eq. (2.72) has mass dimension 4 and scales linearly with $\mathcal{F}$, conversely Eq. (2.73) has mass dimension -4 and scales inversely with $\mathcal{F}$. Equations (2.66), (2.72) and (2.73) imply that the dominant

contributions to $\mathcal{L}_{\text{HE}}^{\text{1-loop}}$ in the limit of $|\mathcal{F}| \gg (m^2/e)^2$ while $|\mathcal{G}| \ll (m^2/e)^2$ are given by

$$\mathcal{L}_{\text{HE}}^{\text{1-loop}} = \frac{1}{12\pi^2}\left\{e^2\mathcal{F}\left[\ln\chi^{-1} + O(\chi^0)\right] + \frac{1}{8}\frac{e^2\mathcal{G}^2}{\mathcal{F}}\left[\chi^{-1} + O(\chi^0)\right]\right\} + O(\mathcal{G}^4)\,. \tag{2.74}$$

For completeness, we note that though this expression seems to suggest that the restriction on $\mathcal{G}$ can be relaxed to just $|\mathcal{G}| \ll |\mathcal{F}|$, this is generally not the case; cf also the discussion below Eq. (2.141). Particularly in the case of $\mathcal{F} > 0$ the perturbative weak field expansion in $\mathcal{G}$ employed in Eqs. (2.66) and (2.74) will of course be completely insensitive to the manifestly non-perturbative imaginary part of $\mathcal{L}_{\text{HE}}$ which may arise for finite values of $\mathcal{G}$. Equation (2.64) implies that the latter can be safely neglected as long as $m^2/(ec_-) \gg 1$. For $|\mathcal{F}| \gg |\mathcal{G}|$ this results in the condition $\mathcal{F}/|\mathcal{G}| \gg (e/m^2)^2|\mathcal{G}|$, which can be straightforwardly inferred with the help of Eq. (2.67). This criterion is perfectly fulfilled in the limit of $\mathcal{F} \gg (m^2/e)^2$ and $|\mathcal{G}| \ll (m^2/e)^2$.

Finally, we recall once again that though Eq. (2.61) was derived for constant fields, after substituting $\bar{F}^{\mu\nu} \to \bar{F}^{\mu\nu}(x)$ it accounts for all local effective interactions of the electromagnetic field $\bar{F}^{\mu\nu}(x)$ at one loop. As discussed in the context of Eq. (2.26), the leading derivative correction to this result scales as $\sim \partial^2$. In turn, Eq. (2.61) also allows determining the exact expressions for the effective one-loop couplings $S_\psi^{(n)}[\bar{A}]$ in Eq. (2.30) at order ∂^n‖; because the dependence on the gauge potential is encoded in $\bar{F}^{\mu\nu}$ a functional derivative for $\bar{A}^\mu$ generically results in a term scaling linearly with ∂^μ. The corrections which are inaccessible from the zeroth-order derivative expansion result for the effective Lagrangian (2.61) scale as ∂^{n+2}. Their explicit determination requires the evaluation of higher-order contributions in the derivative expansion of $\mathcal{L}_{\text{HE}}$. Particularly for the one-loop photon current sourced by the external field $S_\psi^{(1)}[\bar{A}]$ in position space we infer

$$\begin{aligned}(S_\psi^{(1)}[\bar{A}])_\sigma(x) &= \frac{\delta}{\delta\bar{A}^\sigma(x)}\int \mathrm{d}^4x'\, \mathcal{L}_{\text{HE}}^{\text{1-loop}}(\bar{F}(x')) + O(\partial^3)\\ &= 2\partial^\nu \frac{\partial\mathcal{L}_{\text{HE}}^{\text{1-loop}}(\bar{F})}{\partial\bar{F}^{\sigma\nu}}\bigg|_{\bar{F}=\bar{F}(x)} + O(\partial^3)\,,\end{aligned} \tag{2.75}$$

where we assumed that boundary terms vanish. Considered as an individual object the current (2.75) obviously vanishes in constant fields, reflecting the fact that a constant field cannot source on-shell photons. Conversely, if considered as a building block in a larger Feynman diagram to which it is sewed by a photon propagator, Eq. (2.75) may give rise to a finite contribution even in constant fields [12]. Here, the IR singularity of the photon propagator (2.20) in position space $\sim 1/\partial^2$ can compensate a contribution which scales quadratic with ∂. This becomes most evident in momentum space. Using the Fourier representation of the gauge field, $\bar{A}^\mu(x) = \int_k \mathrm{e}^{\mathrm{i}kx}\bar{A}^\mu(k)$, the effective couplings (2.30) in momentum space

‖Throughout this work we use the shorthand notation $O(\partial^n)$ with $n \in \mathbb{N}_0$ for contributions scaling as $\partial^{\sigma_1}\ldots\partial^{\sigma_n}$ and higher orders in the derivative operator as well as for four-vectors in general. Analogously we use $O(\bar{F}^n)$ for contributions scaling as $\bar{F}^{\sigma_1\rho_1}\ldots\bar{F}^{\sigma_n\rho_n}$ and higher orders in $\bar{F}^{\mu\nu}$ for (rank 2) tensors.

can be expressed as**

$$(S_\psi^{(n)}[\bar{A}])_{\sigma_1\ldots\sigma_n}(k_1,\ldots,k_n) = \mathrm{i}^n\int_x \mathrm{e}^{\mathrm{i}x(\sum_{j=1}^n k_j)}\left\{\prod_{j=1}^n k_j^{\mu_j}\left(\frac{\partial}{\partial\bar{F}^{\mu_j\sigma_j}}-\frac{\partial}{\partial\bar{F}^{\sigma_j\mu_j}}\right)\mathcal{L}_{\mathrm{HE}}^{\text{1-loop}}(\bar{F})+O(k^{n+2})\right\}\Big|_{\bar{F}=\bar{F}(x)}, \quad (2.76)$$

reflecting the fact that the derivative expansion amounts to a low-energy expansion; here we count $O(k) = O(k_i)$ for $i \in \{1,\ldots,n\}$. In accordance with the Ward identity [14] we have

$$k_i^{\sigma_i}(S_\psi^{(n)}[\bar{A}])_{\sigma_1\ldots\sigma_i\ldots\sigma_n}(k_1,\ldots,k_i,\ldots,k_n) = 0 \quad \text{for} \quad 0 \le i \le n. \quad (2.77)$$

For $\bar{F}^{\mu\nu} = \text{const.}$ the external field cannot transfer momentum to vacuum fluctuations, and the x integration in Eq. (2.76) can be performed right away, resulting in an overall delta function, $\int_x \mathrm{e}^{\mathrm{i}x(\sum_{j=1}^n k_j)} = (2\pi)^4\,\delta(\sum_{j=1}^n k_j)$, ensuring four-momentum conservation in the effective coupling of n photons. Correspondingly, the momentum-space version of Eq. (2.75) in a constant field reads

$$(S_\psi^{(1)}[\bar{A}])_\sigma(k) = 2\mathrm{i}(2\pi)^4\delta(k)\left(k^\nu\frac{\partial\mathcal{L}_{\mathrm{HE}}^{\text{1-loop}}(\bar{F})}{\partial\bar{F}^{\nu\sigma}} + O(k^3)\right), \quad (2.78)$$

while the photon propagator (2.20) scales as $\sim 1/k^2$. The linear dependence of this expression on k^ν is a direct consequence of the Ward identity (2.77). Sewing the current (2.78) to a contribution exhibiting an overall linear scaling $\sim k^\alpha$ with a photon propagator and integrating over the transferred momentum one effectively needs to evaluate the momentum integral

$$\int_k \frac{k^\nu k^\alpha}{k^2}(2\pi)^d\delta(k) = \int_k \frac{g^{\nu\alpha}}{d}(2\pi)^d\delta(k) = \frac{g^{\nu\alpha}}{d} \quad (2.79)$$

in $d = 4$ space-time dimensions. This integral obviously does not vanish; symmetry allows one to replace $k^\nu k^\alpha \to k^2 g^{\nu\alpha}/4$ in the integrand. Note that the delta function manifestly ensures the momenta contributing to this integral to stem from the regime $k^\mu \to 0$ compatible with the leading order derivative expansion invoked in the derivation of the current (2.75). At the same time, it is easy to see that in this limit higher-order contributions to the current which scale as $O(k^3)$ never result in finite corrections and thus can be neglected from the outset. Therefore, in the particular case of the photon current sourced by a constant electromagnetic field the zeroth-order derivative expansion for the effective action even allows to obtain an expression accounting for all the physically relevant contributions, i.e., the full result. In fact, this effectively implies that any 1PR tadpole part of a larger Feynman diagram in a constant external field can be dealt with exactly within a leading order derivative expansion for the 1PI sector of $\mathcal{L}_{\mathrm{HE}}$ [17]; see in particular also Sec. 2.4.3 below for the details. A contribution of this type arises, e.g., when sewing together two currents (2.75) with a photon propagator like in the second term of Eq. (2.40), which constitutes the 1PR contribution to $\mathcal{L}_{\mathrm{HE}}$ in a constant field at two loops discussed in Sec. 2.4.1. In this context, it is worthwhile to emphasize that until very recently [12] such terms were completely missed. They were erroneously believed to vanish identically because the current (2.78) is zero when

** In general, we use p^μ for loop momenta to be integrated over from the outset and k^μ for momenta which appear as external ones at a certain point of the discussion.

considered as an isolated object [33, 45–47].

2.3.2 Photon polarization tensor in an external field

On the other hand, the explicit expression for the one-loop photon polarization tensor $\Pi^{\text{1-loop}}[\bar{A}] = -S^{(2)}_{\psi}[\bar{A}]$ in momentum space extracted from Eq. (2.76) is

$$(\Pi^{\text{1-loop}}[\bar{A}])^{\mu\nu}(k,k') = \int_x e^{\mathrm{i}(k+k')x} \left\{ p_T^{\mu\nu}(k,k') \frac{\partial \mathcal{L}^{\text{1-loop}}_{\text{HE}}}{\partial \mathcal{F}} + p_\epsilon^{\mu\nu}(k,k') \frac{\partial \mathcal{L}^{\text{1-loop}}_{\text{HE}}}{\partial \mathcal{G}} + p_{\bar{F}\bar{F}}^{\mu\nu}(k,k') \frac{\partial^2 \mathcal{L}^{\text{1-loop}}_{\text{HE}}}{\partial \mathcal{F}^2} \right.$$
$$\left. + p_{\star\bar{F}\star\bar{F}}^{\mu\nu}(k,k') \frac{\partial^2 \mathcal{L}^{\text{1-loop}}_{\text{HE}}}{\partial \mathcal{G}^2} + p_{\star\bar{F}\bar{F}}^{\mu\nu}(k,k') \frac{\partial^2 \mathcal{L}^{\text{1-loop}}_{\text{HE}}}{\partial \mathcal{F}\partial \mathcal{G}} + O(k^4) \right\} \Bigg|_{\bar{F}=\bar{F}(x)}, \quad (2.80)$$

with tensor structures

$$\begin{aligned}
p_T^{\mu\nu}(k,k') &= (kk')g^{\mu\nu} - k'^\mu k^\nu\,,\\
p_\epsilon^{\mu\nu}(k,k') &= k'_\alpha k_\beta\, \epsilon^{\mu\nu\alpha\beta}\,,\\
p_{\bar{F}\bar{F}}^{\mu\nu}(k,k') &= (k\bar{F})^\mu (k'\bar{F})^\nu\,,\\
p_{\star\bar{F}\star\bar{F}}^{\mu\nu}(k,k') &= (k^\star\bar{F})^\mu (k'^\star\bar{F})^\nu\,,\\
p_{\star\bar{F}\bar{F}}^{\mu\nu}(k,k') &= (k^\star\bar{F})^\mu (k'\bar{F})^\nu + (k\bar{F})^\mu (k'^\star\bar{F})^\nu\,.
\end{aligned} \quad (2.81)$$

Here, we count $O(k) = O(k')$. To arrive at this result we made use of the fact that the zeroth order derivative expansion result for $\mathcal{L}^{\text{1-loop}}_{\text{HE}}$ depends on the external field only via $\mathcal{F}$ and $\mathcal{G}^2$; cf. Eq. (A.8) in the Appendix A.3. In the constant field limit all the expressions in the curly brackets are independent of x^μ and the integration over position space results in an overall delta function which ensures $k'^\mu = -k^\mu$. Specifically for this case we introduce the shorthand notation $p_i^{\mu\nu} := p_i^{\mu\nu}(k,k)$ with $i \in \{T, \epsilon, \bar{F}\bar{F}, {}^\star\bar{F}\star\bar{F}, {}^\star\bar{F}\bar{F}\}$, where we suppress the dependence on the single momentum k^μ; note that due to symmetry $p_\epsilon^{\mu\nu} = 0$.

In constant [19, 34, 48–52] and plane-wave backgrounds [53–55] also explicit results for the one-loop photon polarization tensor accounting for arbitrarily large momentum transfers are available. These results can, e.g., be worked out by evaluating the corresponding Feynman diagram with the charged-particle propagator $G[\bar{A}]$ dressed to all orders in the given external field $\bar{A}^\mu$; cf. Refs. [4] and [56] for this propagator in a constant and in a plane-wave field, respectively. Gauge invariance ensures the polarization tensor to depend on the external field $\bar{A}^\mu$ only via the field strength tensor $\bar{F}^{\mu\nu}$. In particular in a constant field and d space-time dimensions, this yields

$\Pi^{\mu\nu}(k,k'|\bar{F}) =$  $= (2\pi)^4 \delta(k+k')\, \mathrm{i}(\mathrm{i}e)^2\, \mathrm{tr}_\gamma \left\{ \int \frac{\mathrm{d}^d p}{(2\pi)^d}\, \gamma^\mu G[\bar{A}](p)\, \gamma^\nu G[\bar{A}](p+k) \right\}$, (2.82)

where the overall momentum conserving delta function reflects the fact that because of translational invariance in constant fields, implying $\Pi^{\mu\nu}(x,x'|\bar{F}) = \Pi^{\mu\nu}(x-x'|\bar{F})$ in position space, the photon four-momentum is conserved. In the absence of the external field, $\bar{A}^\mu = 0$, the momentum transfer k^μ through the loop constitutes the only four-vector available. Correspondingly, in this case the polarization tensor

at arbitrary loop order has the simple structure

$$\Pi^{\mu\nu}(k,k'|0) = (2\pi)^4\delta(k+k')\,p_T^{\mu\nu}\,\pi(k^2)\,. \tag{2.83}$$

The tensor structure in Eq. (2.83) is completely determined by the Ward identity (2.77) for $n = 2$, which requires $k_\mu\Pi^{\mu\nu}(k,k') = \Pi^{\mu\nu}(k,k')k'_\nu = 0$ to hold. Note that $p_T^{\mu\nu} = k^2 P_T^{\mu\nu}$, with transverse projector $P_T^{\mu\nu}$; the longitudinal projector is $P_L^{\mu\nu} = g^{\mu\nu} - P_T^{\mu\nu}$. This is the only non-vanishing tensor structure in Eq. (2.81) that does not depend on the external field.

At one-loop order, the scalar function encoding the non-trivial momentum dependence in Eq. (2.83) can be obtained by evaluating Eq. (2.82) for $\bar{A}^\mu = 0$. However, it diverges in $d = 4$ dimensions and thus requires regularization. Here, we use dimensional regularization to evaluate it. Performing the momentum integral in d generic space-time dimensions, we obtain

$$\pi^{\text{1-loop}}(k^2) = 2\alpha\,\frac{\Gamma\left(\frac{4-d}{2}\right)}{(4\pi)^{\frac{d-2}{2}}}\int_0^1 \mathrm{d}v\,(1-v^2)\left(\frac{1}{m^2+\frac{1-v^2}{4}k^2}\right)^{\frac{4-d}{2}}, \tag{2.84}$$

with gamma function $\Gamma(\cdot)$. Specializing Eq. (2.84) to $d = 4-\eta$ dimensions with $\eta \to 0^+$ and imposing the renormalization condition $\Pi(k^2 = 0) = 0$, which ensures that the Maxwell term in Eq. (2.21) remains unmodified, yields the renormalized one-loop photon polarization tensor at zero field in $d = 4$ dimensions. The corresponding scalar function reads

$$\pi^{\text{1-loop}}(k^2) = \frac{\alpha}{4\pi}\int_0^1 \mathrm{d}v\,v^2\left(\frac{v^2}{3}-1\right)\frac{k^2}{m^2+\frac{1-v^2}{4}k^2}\,, \tag{2.85}$$

For later reference, we also note that Eq. (2.85) has a convergent series representation for $\frac{k^2}{4m^2} < 1$, which reads

$$\pi^{\text{1-loop}}(k^2) = \frac{\alpha}{\pi}\sum_{n=0}^{\infty}\left(-\frac{k^2}{4m^2}\right)^{n+1}\frac{\sqrt{\pi}\,(2+n)\,\Gamma(1+n)}{4\,\Gamma(7/2+n)}\,. \tag{2.86}$$

In an external field the situation is more complicated as the field strength tensor $\bar{F}^{\mu\nu} \neq 0$ constitutes an additional building block to span the tensor structure of the polarization tensor (2.82) compatible with the Ward identity (2.77). More specifically, in the notations of [19], the photon polarization tensor in a constant field for which $\mathcal{G} \geq 0$ can be expressed as

$$\Pi^{\mu\nu}(k,k'|\bar{F}) = (2\pi)^4\delta(k+k')\left(\Pi_0 P_0^{\mu\nu} + \Pi_\perp P_\perp^{\mu\nu} + \Pi_\parallel P_\parallel^{\mu\nu} + \pi_Q Q^{\mu\nu}\right), \tag{2.87}$$

with scalar functions $\Pi_{0,\parallel,\perp}$ and π_Q which depend on both k^μ and $\bar{F}^{\mu\nu}$. Its tensor structure is spanned by

$$P_0^{\mu\nu} = P_T^{\mu\nu} - P_\perp^{\mu\nu} - P_\parallel^{\mu\nu}\,, \quad P_\perp^{\mu\nu} = \frac{v_\perp^\mu v_\perp^\nu}{v_\perp^2}\,, \quad P_\parallel^{\mu\nu} = \frac{v_\parallel^\mu v_\parallel^\nu}{v_\parallel^2}\,, \quad \text{and} \quad Q^{\mu\nu} = v_\parallel^\mu v_\perp^\nu + v_\perp^\mu v_\parallel^\nu\,, \tag{2.88}$$

with four-vectors

$$v^\mu_{\parallel/\perp} = \frac{c_\pm (k^\star \bar{F})^\mu \mp c_\mp (k\bar{F})^\mu}{c_+^2 + c_-^2}\,, \quad \text{fulfilling} \quad v^2_{\parallel/\perp} = \frac{(k\bar{F})^2 \mp k^2 c_\pm^2}{c_+^2 + c_-^2} \quad \text{and} \quad v_\perp^2 - v_\parallel^2 = k^2\,. \tag{2.89}$$

Here, we use the shorthand notation $(k\bar{F})^\mu = k_\nu \bar{F}^{\nu\mu}$, etc. The definitions in Eq. (2.88) are such that $P^{\mu\nu}_{0,\parallel,\perp}$ are projectors and fulfill the usual projector identities. The fourth tensor $Q^{\mu\nu}$ is only orthogonal to $P_0^{\mu\nu}$ and not a projector. Equation (2.87) can alternatively be represented as

$$\Pi^{\mu\nu}(k,k'|\bar{F}) = (2\pi)^4 \delta(k+k') \left(p_T^{\mu\nu}\, \pi_T + p^{\mu\nu}_{\bar{F}\bar{F}}\, \pi_{\bar{F}\bar{F}} + p^{\mu\nu}_{\star\bar{F}\star\bar{F}}\, \pi_{\star\bar{F}\star\bar{F}} + p^{\mu\nu}_{\star\bar{F}\bar{F}}\, \pi_{\star\bar{F}\bar{F}} \right), \tag{2.90}$$

in terms of the tensor structures defined in the context of Eq. (2.81). Here, we introduced the notations $\pi_T = \Pi_0/k^2$, $\pi_{\parallel/\perp} = (\Pi_{\parallel/\perp} - \Pi_0)/v^2_{\parallel/\perp}$ and

$$\begin{aligned}
\pi_{\bar{F}\bar{F}} &= \frac{1}{(c_+^2 + c_-^2)^2} \left[c_+^2 \pi_\perp + c_-^2 \pi_\parallel - 2 c_+ c_- \pi_Q \right], \\
\pi_{\star\bar{F}\star\bar{F}} &= \frac{1}{(c_+^2 + c_-^2)^2} \left[c_-^2 \pi_\perp + c_+^2 \pi_\parallel + 2 c_+ c_- \pi_Q \right], \\
\pi_{\star\bar{F}\bar{F}} &= \frac{1}{(c_+^2 + c_-^2)^2} \left[c_+ c_- (\pi_\perp - \pi_\parallel) + (c_+^2 - c_-^2) \pi_Q \right].
\end{aligned} \tag{2.91}$$

This is the representation that will be used in our explicit calculations below. We emphasize that the structure of Eqs. (2.87) and (2.90) is generic for constant external fields. Using the shorthand notations $z = e c_+ T$ and $z' = e c_- T$, at one loop order the explicit expressions for the scalar functions encoding the nontrivial dependences on $\bar{F}^{\mu\nu}$ and k^μ can be cast in the form

$$\begin{Bmatrix} \pi_T \\ \pi_\parallel \\ \pi_\perp \\ \pi_Q \end{Bmatrix} = \frac{\alpha}{2\pi} \int_0^\infty \frac{\mathrm{d}T}{T} \mathrm{e}^{-\mathrm{i}m^2 T} \left[\int_0^1 \mathrm{d}\nu\, \mathrm{e}^{\mathrm{i}(v_\parallel^2 n_1 - v_\perp^2 n_2)T} \frac{z z'}{\sin z \sinh z'} \begin{Bmatrix} N_0 \\ N_0 - N_1 \\ N_2 - N_0 \\ -N_3 \end{Bmatrix} - \begin{Bmatrix} \frac{2}{3} \\ 0 \\ 0 \\ 0 \end{Bmatrix} \right], \tag{2.92}$$

with

$$\begin{aligned}
N_0 &= \cos(\nu z) \cosh(\nu z') - \cot z \sin(\nu z) \coth z' \sinh(\nu z')\,, \\
N_1 &= 2 \cos z\, \frac{\cosh z' - \cosh(\nu z')}{\sinh^2 z'}\,, \quad N_2 = N_1|_{z \leftrightarrow -\mathrm{i}z'}\,, \\
N_3 &= \frac{1 - \cos z \cos(\nu z)}{\sin z} \frac{1 - \cosh z' \cosh(\nu z')}{\sinh z'} + \sin(\nu z) \sinh(\nu z')\,, \\
n_1 &= \frac{\cosh z' - \cosh(\nu z')}{2 z' \sinh z'}\,, \quad n_2 = n_1|_{z \leftrightarrow -\mathrm{i}z'}\,.
\end{aligned} \tag{2.93}$$

The contour of the proper time integration in Eq. (2.92) is implicitly assumed to lie slightly below the positive real T axis [57]; cf. also the paragraph below Eq. (2.57). A comparison of Eq. (2.90) with Eq. (2.80) unveils that the analogous result for $\mathcal{G} < 0$ follows by simultaneously replacing $c_+ c_- \to -c_+ c_-$

and $\pi_Q \to -\pi_Q$ in Eq. (2.91) as only $\pi_{\star\bar{F}\bar{F}}$ should be odd in $\mathcal{G}$. Moreover, we emphasize that the entire momentum dependence of Eq. (2.92) is encoded in the phase of the proper time integral over T via $v_\parallel^2$ and $v_\perp^2$. This implies that all the scalar functions $\pi_p = \pi_p(k|\bar{F})$ introduced above can be formally expanded as $\pi_p = \sum_{n=0}^{\infty} \pi_p^{(2n)}$ with $\pi_p^{(2n)} = k_{\sigma_1} \dots k_{\sigma_{2n}} (h_p^{(2n)})^{\sigma_1 \dots \sigma_{2n}}$. The tensors $h_p^{(2n)} = h_p^{(2n)}(\bar{F})$ account for generic couplings to the external field $\bar{F}^{\mu\nu}$. Because the tensor structures in Eq. (2.90) scale quadratically with k^μ, the scalar functions $\pi_p^{(2n)}$ with n fixed constitute the full result for $\Pi^{\mu\nu}(k, k'|\bar{F})$ at order k^{2n+2}. For completeness, we note that the photon polarization tensor in Eqs. (2.87) and (2.90) remains invariant under the mapping $c_+ \leftrightarrow -\mathrm{i}c_-$ while keeping the vectors $(k\bar{F})^\mu$, $(k^\star\bar{F})^\mu$ and their contractions unchanged. Finally, we remark that the explicit expression for the 1PR contribution to the constant-field photon polarization tensor at two loops depicted in Fig 2.1 (right) is also available [17]. It can be expressed in a form analogous to Eqs. (2.87) and (2.92).

2.3.3 Derivative corrections to the effective Lagrangian

In a next step, we use these results for the one-loop photon polarization tensor detailed in Sec. 2.3.2 to explicitly determine derivative corrections to $\mathcal{L}_{\mathrm{HE}}$. First, we turn to the vacuum polarization tensor at $\bar{A}^\mu = 0$. Upon omission of the irrelevant field-independent vacuum contribution $S_\psi[0]$, Eqs. (2.32) and (2.33) allow to infer that

$$\Gamma_{\mathrm{HE}}^{\text{1-loop}}[\bar{A}] = -\frac{1}{2} \iint \bar{A}_\mu (\Pi^{\text{1-loop}}[0])^{\mu\nu} \bar{A}_\nu + O(\bar{A}^4) \,. \tag{2.94}$$

Equation (2.94) clearly implies that the one-loop vacuum polarization tensor mediates the full effective interaction at quadratic order in the external field $\bar{A}^\mu$ of $\Gamma_{\mathrm{HE}}[\bar{A}]$ at one loop. Inserting Eq. (2.83) into Eq. (2.94), we obtain

$$\Gamma_{\mathrm{HE}}^{\text{1-loop}}[\bar{A}]\big|_{\sim \bar{A}^2} = -\frac{1}{2} \int_k \bar{A}_\mu(-k)(k^2 g^{\mu\nu} - k^\mu k^\nu)\, \pi^{\text{1-loop}}(k^2)\, \bar{A}_\nu(k) = \int_x \mathcal{L}_{\mathrm{HE}}^{\text{1-loop}}\big|_{\sim \bar{A}^2} \,, \tag{2.95}$$

with

$$\mathcal{L}_{\mathrm{HE}}^{\text{1-loop}}\big|_{\sim \bar{A}^2} = -\frac{1}{4} \bar{F}_{\mu\nu}(x)\, \pi^{\text{1-loop}}(-\partial^2)\, \bar{F}^{\mu\nu}(x) \,, \tag{2.96}$$

where in the second step we transformed from momentum to position space using the Fourier representation of the gauge field $\bar{A}^\mu(x) = \int_k \mathrm{e}^{\mathrm{i}kx} \bar{A}^\mu(k)$ introduced in the context of Eq. (2.76) above. The latter definition implies that $\bar{F}^{\mu\nu}(x) = \int_k \mathrm{e}^{\mathrm{i}kx} \bar{F}^{\mu\nu}(k)$ with $\bar{F}^{\mu\nu}(k) = \mathrm{i}(k^\mu \bar{A}^\nu(k) - k^\nu \bar{A}^\mu(k))$. Especially upon insertion of Eq. (2.86) into Eq. (2.96), which yields

$$\mathcal{L}_{\mathrm{HE}}^{\text{1-loop}}\big|_{\sim \bar{A}^2} = -\frac{1}{4} \frac{\alpha}{\pi} \sum_{n=0}^{\infty} \frac{\sqrt{\pi}\,(2+n)\,\Gamma(1+n)}{4\,\Gamma(7/2+n)} \bar{F}_{\mu\nu}(x) \left(\frac{\partial^2}{4m^2}\right)^{n+1} \bar{F}^{\mu\nu}(x) \,, \tag{2.97}$$

it is obvious that this result accounts for derivative corrections of arbitrary order. Moreover, in this particular case, we have now confirmed by an explicit calculation that the derivative operator is indeed rendered dimensionless by the electron/position mass. For completeness, also recall that with the renormalization condition invoked in the context of Eq. (2.84) we explicitly ensured the zeroth order derivative

contribution, which would have modified the classical Maxwell term, to vanish identically. One can easily convince oneself that the leading derivative correction $\sim \partial^2$ in Eq. (2.97) matches the corresponding results of Refs. [28, 58]. The apparent discrepancy between their expressions and our result is straightforwardly resolved by noting the identity $2\partial_\mu \bar{F}^{\mu\nu}\partial^\rho \bar{F}_{\rho\nu} = -\bar{F}_{\mu\nu}\partial^2 \bar{F}^{\mu\nu}$ + total derivative, which can be easily verified by insertion of $\bar{F}^{\mu\nu} = \partial^\mu \bar{A}^\nu - \partial^\nu \bar{A}^\mu$.

On the other hand, the result for the photon polarization tensor in a generic constant electromagnetic field (2.90) can be used to determine the contribution to $\Gamma_{\text{HE}}[\bar{A}]$ at quadratic order in a derivative expansion which accounts for arbitrarily high couplings to the external field [59]. For alternative approaches to determine this derivative correction, see Refs. [58, 60, 61]. Here, we explicitly determine this derivative correction at one-loop order. However, we emphasize that our approach is not limited to one loop, but could be adopted to arbitrary loop orders. The results for the photon polarization tensor evaluated in a homogeneous constant background field up to ℓ loops would allow for the determination of these quadratic derivative corrections to $\Gamma_{\text{HE}}[\bar{A}]$ up to ℓ loops. It should be noted that practically this would require considerable efforts because currently no explicit results for the polarization tensor at arbitrary momentum transfers are available in constant fields beyond one loop. To be precise, we recall that beyond one loop the relevant quantity to be determined for the extraction of the derivative correction is not $(\Pi^{\ell\text{-loop}}[\bar{A}])^{\mu\nu}$ but rather $\delta^2\Gamma^{\ell\text{-loop}}_{\text{HE}}[\bar{A}]/\delta\bar{A}^\mu\delta\bar{A}^\nu$; cf. also Eq. (2.22) above and Eq. (2.144) below.

To this end, we consider for a moment the one-loop effective action in the external field $\bar{A}^\mu + \bar{a}^\mu$, with the associated field strength tensors given by $\bar{F}^{\mu\nu} = \text{const.}$ and $\bar{f}^{\mu\nu}(x)$, respectively. In analogy to Eq. (2.94), this effective action can be expanded as

$$\Gamma^{\text{1-loop}}_{\text{HE}}[\bar{A}+\bar{a}] = -\frac{1}{2}\int_k\int_{k'} \bar{a}^\mu(k)\,\Pi^{\text{1-loop}}_{\mu\nu}(k,k'|\bar{F})\,\bar{a}^\nu(k') + O(\bar{a}^3)\,. \tag{2.98}$$

Recall, however, that in the presence of the field $\bar{A}^\mu$ also odd contributions in $\bar{a}^\mu$ are generated. The contribution linear in $\bar{a}^\mu$ vanishes in constant fields; cf. Eq. (2.75) and the corresponding discussion. With the above definitions it is easy to show that $(k\bar{F})^\nu \bar{a}_\nu(k) = -\mathrm{i}\bar{F}^{\rho\nu}\bar{f}_{\rho\nu}(k)/2$ and analogously $(k{}^\star\bar{F})^\nu \bar{a}_\nu(k) = -\mathrm{i}\,{}^\star\bar{F}^{\rho\nu}\bar{f}_{\rho\nu}(k)/2$. Using these identities, upon insertion of Eq. (2.90) the term written explicitly in Eq. (2.98) can be expressed in a manifestly gauge-invariant form as

$$\begin{aligned}\Gamma^{\text{1-loop}}_{\text{HE}}[\bar{A}+\bar{a}] = -\frac{1}{4}\int_k \Big\{ &\bar{f}_{\mu\nu}(-k)\bar{f}^{\mu\nu}(k)\,\pi_T \\ &+ \frac{1}{2}\bar{f}_{\sigma\mu}(-k)\bar{f}_{\rho\nu}(k)\big[\bar{F}^{\sigma\mu}\bar{F}^{\rho\nu}\pi_{\bar{F}\bar{F}} + {}^\star\bar{F}^{\sigma\mu}\,{}^\star\bar{F}^{\rho\nu}\pi_{\star\bar{F}\star\bar{F}} + 2{}^\star\bar{F}^{\sigma\mu}\bar{F}^{\rho\nu}\pi_{\star\bar{F}\bar{F}}\big]\Big\}\,,\end{aligned} \tag{2.99}$$

with $\pi_p = \pi_p(k|\bar{F})$. Upon limitation to the contribution scaling quadratic with k^μ in the integrand of Eq. (2.99), we obtain

$$\begin{aligned}\Gamma^{\text{1-loop}}_{\text{HE}}[\bar{A}+\bar{a}]\big|_{\sim\partial^2} &= \frac{1}{4}\int_k \Big\{(-k_\alpha)\bar{f}_{\mu\nu}(-k)\,k_\beta\bar{f}^{\mu\nu}(k)\,(h_T^{(2)})^{\alpha\beta} + \frac{1}{2}(-k_\alpha)\bar{f}_{\sigma\mu}(-k)\,k_\beta\bar{f}_{\rho\nu}(k) \\ &\qquad\times\Big[\bar{F}^{\sigma\mu}\bar{F}^{\rho\nu}(h^{(2)}_{\bar{F}\bar{F}})^{\alpha\beta} + {}^\star\bar{F}^{\sigma\mu}\,{}^\star\bar{F}^{\rho\nu}(h^{(2)}_{\star\bar{F}\star\bar{F}})^{\alpha\beta} + 2{}^\star\bar{F}^{\sigma\mu}\bar{F}^{\rho\nu}(h_{\star\bar{F}\bar{F}})^{\alpha\beta}\Big]\Big\} \qquad (2.100)\\ &= -\frac{1}{4}\int_x \Big\{\partial_\alpha\bar{f}_{\mu\nu}(x)\,\partial_\beta\bar{f}^{\mu\nu}(x)\,(h_T^{(2)})^{\alpha\beta} + \frac{1}{2}\partial_\alpha\bar{f}_{\sigma\mu}(x)\,\partial_\beta\bar{f}_{\rho\nu}(x)\end{aligned}$$

$$\times \Big[\bar{F}^{\sigma\mu}\bar{F}^{\rho\nu}(h^{(2)}_{\bar{F}\bar{F}})^{\alpha\beta} + {}^\star\bar{F}^{\sigma\mu}{}^\star\bar{F}^{\rho\nu}(h^{(2)}_{{}^\star\bar{F}{}^\star\bar{F}})^{\alpha\beta} + 2{}^\star\bar{F}^{\sigma\mu}\bar{F}^{\rho\nu}(h^{(2)}_{{}^\star\bar{F}\bar{F}})^{\alpha\beta} \Big] \Big\} . \tag{2.101}$$

The position space result (2.101) follows by using $\int_k \mathrm{e}^{\mathrm{i}kx}[k_\beta f_{\rho\nu}(k)] = -\mathrm{i}\partial_\beta f_{\rho\nu}(x)$ and $\int_k u(-k)v(k) = \int_x u(x)v(x)$. Identifying $\bar{F}^{\mu\nu} := \bar{F}^{\mu\nu}(x_0)$, which clearly fulfills $\partial^\rho \bar{F}^{\mu\nu}(x_0) = 0$, and $\partial_\beta \bar{f}_{\rho\nu}(x) := \partial_\beta \bar{F}_{\rho\nu}(x)|_{x=x_0}$, we arrive at the following effective Lagrangian,

$$\begin{aligned}
\mathcal{L}^{\text{1-loop}}_{\text{HE}}\big|_{\sim\partial^2} &= -\frac{1}{4}\partial_\alpha \bar{F}_{\mu\nu}\,\partial_\beta \bar{F}^{\mu\nu}\,(h^{(2)}_T)^{\alpha\beta} \\
&\quad - \frac{1}{8}\partial_\alpha \bar{F}_{\sigma\mu}\,\partial_\beta \bar{F}_{\rho\nu}\Big[\bar{F}^{\sigma\mu}\bar{F}^{\rho\nu}(h^{(2)}_{\bar{F}\bar{F}})^{\alpha\beta} + {}^\star\bar{F}^{\sigma\mu}{}^\star\bar{F}^{\rho\nu}(h^{(2)}_{{}^\star\bar{F}{}^\star\bar{F}})^{\alpha\beta} + 2{}^\star\bar{F}^{\sigma\mu}\bar{F}^{\rho\nu}(h^{(2)}_{{}^\star\bar{F}\bar{F}})^{\alpha\beta}\Big], \\
&= -\frac{1}{4}\partial_\alpha \bar{F}_{\mu\nu}\,\partial_\beta \bar{F}^{\mu\nu}\,(h^{(2)}_T)^{\alpha\beta} \\
&\quad - \frac{1}{2}\Big[\partial_\alpha\mathcal{F}\partial_\beta\mathcal{F}(h^{(2)}_{\bar{F}\bar{F}})^{\alpha\beta} + \partial_\alpha\mathcal{G}\partial_\beta\mathcal{G}(h^{(2)}_{{}^\star\bar{F}{}^\star\bar{F}})^{\alpha\beta} + 2\partial_\alpha\mathcal{G}\partial_\beta\mathcal{F}(h^{(2)}_{{}^\star\bar{F}\bar{F}})^{\alpha\beta}\Big],
\end{aligned} \tag{2.102}$$

which constitutes the desired leading derivative correction to $\mathcal{L}^{\text{1-loop}}_{\text{HE}}$ in the external field $\bar{F}^{\mu\nu} = \bar{F}^{\mu\nu}(x)$. In the second step in Eq. (2.102) we made use of $\partial_\alpha \bar{F}_{\sigma\mu}\bar{F}^{\sigma\mu} = 2\partial_\alpha\mathcal{F}$ and $\partial_\alpha \bar{F}_{\sigma\mu}{}^\star\bar{F}^{\sigma\mu} = 2\partial_\alpha\mathcal{G}$. As the derivation of $\Pi^{\mu\nu}(k,k'|\bar{F})$ explicitly accounts for all possible variants of coupling the fields $\bar{a}^\mu(k)$ and $\bar{a}^\nu(k')$ to the dressed charged particle loop, the procedure outlined above automatically ensures the same to be true for the derivatives of the field strength tensor in Eq. (2.102). We emphasize that for the consistent transition from Eq. (2.101) to Eq. (2.102) the regrouping of the terms such that each power of the field $\bar{f}^{\mu\nu}(x)$ comes with a single derivative acting on it is absolutely essential. In this context, we also note that, though the contribution to Eq. (2.99) with $\pi_p \to \pi^{(0)}_p = \mathcal{O}(k^0)$ yields an expression that contains no derivatives, is quadratic in $\bar{f}^{\mu\nu}$ and accounts for generic couplings to $\bar{F}^{\mu\nu}$, it does not reproduce the zero-derivative result for $\Gamma_{\text{HE}}[\bar{A}]$ in the limit of $\bar{f}^{\mu\nu} \to \bar{F}^{\mu\nu}$. The reason for this is the fact that in the derivation of the photon polarization tensor and Eq. (2.98) the fields $\bar{F}^{\mu\nu}$ and $\bar{f}^{\mu\nu}$ are assumed to be manifestly different. Inconsistencies arise as soon as (at least) one of the couplings to the field $\bar{f}^{\mu\nu}$ is identified with a coupling to the background field $\bar{F}^{\mu\nu}$. Note, that Eq. (2.102) simplifies significantly for fields fulfilling either $c_+ = 0$ or $c_- = 0$, which implies $\mathcal{G} = 0$ and thus

$$\mathcal{L}^{\text{1-loop}}_{\text{HE}}\big|_{\sim\partial^2} = -\frac{1}{4}\partial_\alpha \bar{F}_{\mu\nu}\partial_\beta \bar{F}^{\mu\nu}\,(h^{(2)}_T)^{\alpha\beta} - \frac{1}{2}\partial_\alpha\mathcal{F}\partial_\beta\mathcal{F}(h^{(2)}_{\bar{F}\bar{F}})^{\alpha\beta} . \tag{2.103}$$

The explicit determination of Eqs. (2.102) and (2.103) boils down to the evaluation of the scalar functions $\pi^{(2)}_p = k_\alpha k_\beta (h^{(2)}_p)^{\alpha\beta}$, or more precisely, the tensors $h^{(2)}_p$. As the quadratic term in k^μ arises from the contribution scaling linear with $(v^2_\parallel n_1 - v^2_\perp n_2)$ in Eq. (2.92), central building blocks to $h^{(2)}_p$ are clearly

$$\mathcal{N}_{1i} = \int_0^1 \mathrm{d}\nu\, n_1 N_i \quad \text{and} \quad \mathcal{N}_{2i} = \int_0^1 \mathrm{d}\nu\, n_2 N_i\,, \quad \text{with} \quad i \in \{0,1,2,3\}\,. \tag{2.104}$$

The integrals over ν in Eq. (2.104) can be performed analytically, yielding

$$\mathcal{N}_{10} = \frac{1}{z^2+4z'^2}\frac{z'}{z}\Big[\frac{3}{2}\frac{z^2}{z^2+z'^2}\coth z'\Big(\frac{\cosh z'}{\sin z} - \frac{z'}{z}\frac{\cos z}{\sinh z'}\Big) - \frac{\sin z}{\sinh z'}\Big]\text{‘},$$

$$
\begin{aligned}
\mathcal{N}_{11} &= \frac{1}{z'}\frac{\cos z}{\sinh z'}\Big[1+\frac{3}{2}\frac{1}{\sinh z'}\Big(\frac{1}{\sinh z'}-\frac{\cosh z'}{z'}\Big)\Big],\\
\mathcal{N}_{12} &= \frac{\cosh z'}{\sin z}\Big[\frac{1}{z^2+z'^2}\Big(\frac{z'}{z}\coth z'+\frac{z^2}{z'^2}\cot z\Big)-\frac{\cot z\coth z'}{z'}\Big],\\
\mathcal{N}_{13} &= \frac{3}{4}\frac{\coth z'}{\sin z}\frac{1}{z'}\Big(\frac{1}{\sinh z'}-\frac{\cosh z'}{z'}\Big)+\frac{1}{2}\frac{1}{z^2+z'^2}\frac{z^2}{z'^2}\frac{\sinh z'}{\sin z}\\
&\quad+\frac{3}{2}\frac{1}{z^2+4z'^2}\frac{z'^2}{z^2+z'^2}\Big[2\coth z'\Big(\frac{\cosh z'}{\sin z}-\frac{z'}{z}\frac{\cos z}{\sinh z'}\Big)-\frac{\sin z}{\sinh z'}\Big],
\end{aligned}
\tag{2.105}
$$

as well as $\mathcal{N}_{20}=\mathcal{N}_{10}|_{z\leftrightarrow -\mathrm{i}z'}$, $\mathcal{N}_{21}=\mathcal{N}_{12}|_{z\leftrightarrow -\mathrm{i}z'}$, $\mathcal{N}_{22}=\mathcal{N}_{11}|_{z\leftrightarrow -\mathrm{i}z'}$ and $\mathcal{N}_{23}=\mathcal{N}_{13}|_{z\leftrightarrow -\mathrm{i}z'}$. The leading contributions to the quantities (2.105) in a weak-field expansion are

$$
\begin{aligned}
\mathcal{N}_{10} &= \frac{2}{15}-\frac{e^2}{315}(c_+^2+2c_-^2)T^2+O(\bar{F}^4),\\
\mathcal{N}_{11} &= \frac{2}{15}-\frac{e^2}{315}(21c_+^2+13c_-^2)T^2+O(\bar{F}^4),\\
\mathcal{N}_{12} &= \frac{2}{15}+\frac{e^2}{315}(10c_+^2+18c_-^2)T^2+O(\bar{F}^4),\\
\mathcal{N}_{13} &= -\frac{e^2}{35}c_+c_-T^2+O(\bar{F}^4).
\end{aligned}
\tag{2.106}
$$

Also note that

$$
\frac{zz'}{\sin z\sinh z'}=1+\frac{e^2}{6}(c_+^2-c_-^2)T^2+O(\bar{F}^4). \tag{2.107}
$$

Using the shorthand notations

$$
\mathcal{N}_i^-=\mathcal{N}_{1i}-\mathcal{N}_{2i}\quad\text{and}\quad \mathcal{N}_i^+=\frac{c_+^2}{c_+^2+c_-^2}\mathcal{N}_{1i}+\frac{c_-^2}{c_+^2+c_-^2}\mathcal{N}_{2i}, \tag{2.108}
$$

the tensors $h_p^{(2)}$ can be compactly expressed as

$$
(h_p^{(2)})^{\alpha\beta}=\frac{\bar{F}^\alpha{}_\tau\bar{F}^{\beta\tau}}{c_+^2+c_-^2}h_p^{(2)-}-g^{\alpha\beta}h_p^{(2)+}, \tag{2.109}
$$

with scalar functions

$$
\begin{Bmatrix} h_T^{(2)\pm}\\ h_\parallel^{(2)\pm}\\ h_\perp^{(2)\pm}\\ h_Q^{(2)\pm}\end{Bmatrix}=\mathrm{i}\frac{\alpha}{2\pi}\int_0^\infty \mathrm{d}T\,\mathrm{e}^{-\mathrm{i}m^2T}\,\frac{zz'}{\sin z\sinh z'}\begin{Bmatrix}\mathcal{N}_0^\pm\\ \mathcal{N}_0^\pm-\mathcal{N}_1^\pm\\ \mathcal{N}_2^\pm-\mathcal{N}_0^\pm\\ -\mathcal{N}_3^\pm\end{Bmatrix}. \tag{2.110}
$$

Hence, similarly to Eq. (2.61) also the quadratic derivative correction to the Heisenberg-Euler Lagrangian at one loop (2.102) can be represented in terms of a single parameter integral. On the other hand, the expression for the latter is much more complicated. It is easy to show that the quantities defined in Eq. (2.110) fulfill $h_p^{(2)\pm}\big|_{c_+\leftrightarrow -\mathrm{i}c_-}=\pm h_p^{(2)\pm}$ for $p\in\{T,Q\}$, while $h_\parallel^{(2)\pm}\big|_{c_+\leftrightarrow -\mathrm{i}c_-}=\mp h_\perp^{(2)\pm}$. We note that Eqs. (2.91) and (2.109) imply that $(h_{\bar{F}\bar{F}}^{(2n)})^{\alpha\beta}$ relates to $(h_\perp^{(2n)})^{\alpha\beta}$, $(h_\parallel^{(2n)})^{\alpha\beta}$ and $(h_Q^{(2n)})^{\alpha\beta}$ – and likewise $h_{\bar{F}\bar{F}}^{(2\pm}$

to $h_\perp^{(2)\pm}$, $h_\parallel^{(2)\pm}$ and $h_Q^{(2)\pm}$ – in exactly the same way as $\pi_{\bar F\bar F}$ relates to $\pi_\perp$, $\pi_\parallel$ and π_Q, etc. This allows us to show that $h_p^{(2)\pm}\big|_{c_+\leftrightarrow -\mathrm{i}c_-} = \pm h_p^{(2)\pm}$ also for $p \in \{\bar F\bar F, {}^\star\bar F{}^\star\bar F, {}^\star\bar F\bar F\}$. In fact, the factor of $1/(c_+^2 + c_-^2)$ multiplying $h_p^{(2)-}$ in Eq. (2.109) flips sign under $c_+ \leftrightarrow -\mathrm{i}c_-$ and thus ensures that Eq. (2.102) remains invariant under the mapping $c_+ \leftrightarrow -\mathrm{i}c_-$ while keeping the explicit occurrences of the field strength tensor and its dual unchanged. This property is inherited from the polarization tensor; see Sec. 2.3.2. Also note that the structure of Eq. (2.102) with tensor structures (2.109) is generic and holds to all loop orders.

The fact that the functions $h_p^{(2)-}/(c_+^2 + c_-^2)$ and $h_p^{(2)+}$ in Eq. (2.109) are regular at $c_+ = c_- = 0$ and feature asymptotic expansions in terms of powers of combinations of c_+ and c_- is not at all obvious from the above results for generic fields. However, at least at low orders one can easily convince oneself that this is indeed the case by performing explicit expansions. In the special cases where only one of the two invariants $c_\pm$ does not vanish, and thus $\mathcal{G} = 0$, the situation is more transparent and the only quantities to be determined are the tensors $h_T^{(2)}$ and $h_{FF}^{(2)}$; cf. Eq. (2.103). Here, the all-order weak-field expansion can be readily worked out in closed form and reads [59]

$$
\begin{aligned}
h_T^{(2)+}\big|_{\mathcal{G}=0} &= -\frac{\alpha}{\pi}\frac{1}{m^2}\sum_{n=0}^{\infty}\frac{12\mathcal{B}_{2(n+2)}}{(2n+1)(2n+2)(2n+3)}\chi^{-2n},\\
h_T^{(2)-}\big|_{\mathcal{G}=0} &= \frac{\alpha}{\pi}\frac{1}{m^2}\sum_{n=1}^{\infty}\frac{1}{4}\frac{1}{n+1}\Big[\frac{3(2n-5)\mathcal{B}_{2(n+2)}}{(2n+1)(2n+3)} - \mathcal{B}_{2(n+1)}\Big]\chi^{-2n},\\
h_{\bar F\bar F}^{(2)+}\big|_{\mathcal{G}=0} &= -\frac{\alpha}{\pi}\frac{1}{m^2}\Big(\frac{e}{m^2}\Big)^2\sum_{n=0}^{\infty}4\,\frac{n+1}{n+2}\Big[\frac{4\mathcal{B}_{2(n+3)}}{(2n+3)(2n+5)} - \frac{\mathcal{B}_{2(n+2)}}{3}\Big]\chi^{-2n},\\
h_{\bar F\bar F}^{(2)-}\big|_{\mathcal{G}=0} &= \frac{\alpha}{\pi}\frac{1}{m^2}\Big(\frac{e}{m^2}\Big)^2\sum_{n=1}^{\infty}\frac{1}{n+2}\Big[\frac{16n^2+50n+49}{(2n+3)(2n+5)}\mathcal{B}_{2(n+3)} + \frac{4n+7}{3}\mathcal{B}_{2(n+2)}\Big]\chi^{-2n}.
\end{aligned}
\tag{2.111}
$$

The quantities in Eq. (2.111) labeled by + (−) start contributing with c_+^0 (c_+^2), which implies regularity of $h_p^{(2)-}/c_+^2\big|_{c_-=0}$ and $h_p^{(2)+}\big|_{c_-=0}$ for $c_+ \to 0$ as expected.

Given that either c_+ or c_- vanishes even the proper time integral in Eq. (2.110) can be performed explicitly and be expressed in terms of the Hurwitz zeta function and its derivatives. This results in expressions analogous to the zeroth-order derivative expansion results in Eqs. (2.70) and (2.71), namely

$$
\begin{aligned}
h_T^{(2)+}\big|_{\mathcal{G}=0} &= \frac{\alpha}{\pi}\frac{1}{m^2}\chi\Big\{-18\zeta'(-2,\chi) + 12\chi\,\zeta'(-1,\chi) + \frac{1}{2}(1+2\chi^2)\chi - \Big(3\chi-2\Big)\chi\ln\chi\Big\},\\
h_T^{(2)-}\big|_{\mathcal{G}=0} &= \frac{\alpha}{\pi}\frac{1}{m^2}\chi\Big\{-\frac{27}{2}\zeta'(-2,\chi) + 6\chi\,\zeta'(-1,\chi) + \frac{3}{2}\chi^2\zeta'(0,\chi)\\
&\qquad + \frac{1}{2}(1+3\chi^2)\chi - \Big(3\chi-\frac{5}{4}\Big)\chi\ln\chi + \frac{1}{2}\chi\,\psi(\chi) + \frac{1}{4}\Big\},\\
h_{\bar F\bar F}^{(2)+}\big|_{\mathcal{G}=0} &= \frac{1}{\mathcal{F}}\frac{\alpha}{\pi}\frac{1}{m^2}\chi\Big\{3\zeta'(-2,\chi) + 2\chi\,\zeta'(-1,\chi) - 2\chi^2\,\zeta'(0,\chi) - \frac{1}{12}(5+14\chi^2)\chi\\
&\qquad + \Big(\frac{3}{2}\chi-1\Big)\chi\ln\chi + \frac{1}{3}\chi\,\psi(\chi) + \frac{1}{6}\chi^2\,\zeta(2,\chi) + \frac{1}{12}\Big\},\\
h_{\bar F\bar F}^{(2)-}\big|_{\mathcal{G}=0} &= \frac{1}{\mathcal{F}}\frac{\alpha}{\pi}\frac{1}{m^2}\chi\Big\{\frac{15}{4}\zeta'(-2,\chi) - \chi\,\zeta'(-1,\chi) + \frac{1}{4}\chi^2\,\zeta'(0,\chi) - \frac{1}{6}\Big(3+3\chi-\frac{5}{2}\chi^2\Big)\chi\\
&\qquad + \Big(\frac{3}{2}\chi-\frac{5}{8}\Big)\chi\ln\chi + \Big(\frac{1}{12}-\chi^2\Big)\chi\,\psi(\chi) + \frac{1}{6}\chi^2\zeta(2,\chi) - \frac{1}{24}\Big\}.
\end{aligned}
\tag{2.112}
$$

Recall the definition $\chi = m^2/(2e\sqrt{2\mathcal{F}})$ introduced in the context of Eq. (2.71). Equation (2.112) in particular allows for closed-form analytical insights in the important cases of either a purely magnetic-like ($c_+ \neq 0$) or a electric-like ($c_- \neq 0$) field. It can be evaluated for arbitrary values of $\mathcal{F}$.

Using the exact series representations of the first derivative of the Hurwitz zeta function and the Digamma function for small arguments [43, 44] also the all-order strong field expansion of Eq. (2.112) can be worked out explicitly, yielding

$$
\begin{aligned}
h_T^{(2)+}\big|_{\mathcal{G}=0} &= \frac{\alpha}{\pi}\frac{1}{m^2}\chi\Big\{-18\zeta'(-2) + \Big[2\ln\chi - 24\zeta'(-1) - 1\Big]\chi + 3\Big[\ln\chi + \ln(2\pi) - \frac{5}{2}\Big]\chi^2 - 2\chi^3 \\
&\qquad + 12\sum_{j=0}^{\infty}(-1)^j\frac{j+1}{(j+2)(j+3)(j+4)}\zeta(j+2)\chi^{j+4}\Big\}, \\
h_T^{(2)-}\big|_{\mathcal{G}=0} &= \frac{\alpha}{\pi}\frac{1}{m^2}\chi\Big\{-\frac{27}{2}\zeta'(-2) - \frac{1}{4} + \Big[\frac{5}{4}\ln\chi - \frac{\gamma}{2} - 21\zeta'(-1) - \frac{5}{8}\Big]\chi \\
&\qquad + 3\Big[\ln\chi + \ln(2\pi) + \frac{\pi^2}{36} - \frac{19}{8}\Big]\chi^2 - \frac{1}{2}\Big[\frac{9}{2} + \zeta(3)\Big]\chi^3 \\
&\qquad + \frac{1}{2}\sum_{j=0}^{\infty}(-1)^j\Big[\frac{3(j^2+11j+10)}{(j+2)(j+3)(j+4)}\zeta(j+2) + \zeta(j+4)\Big]\chi^{j+4}\Big\}, \qquad (2.113) \\
h_{\bar{F}\bar{F}}^{(2)+}\big|_{\mathcal{G}=0} &= \frac{1}{\mathcal{F}}\frac{\alpha}{\pi}\frac{1}{m^2}\chi\Big\{3\zeta'(-2) - \frac{1}{12} - \Big[\ln(\tfrac{1}{2}\tfrac{m^2}{ec_+}) + \frac{\gamma}{3} - 8\zeta'(-1) + \frac{1}{6}\Big]\chi \\
&\qquad - \frac{1}{2}\Big[3\ln\chi + 3\ln(2\pi) - \frac{\pi^2}{6} - \frac{13}{2}\Big]\chi^2 + \frac{2}{3}\Big[2 - \zeta(3)\Big]\chi^3 \\
&\qquad - \sum_{j=0}^{\infty}(-1)^j\Big[\frac{2(j^2+6j+5)}{(j+2)(j+3)(j+4)}\zeta(j+2) - \frac{j+5}{6}\zeta(j+4)\Big]\chi^{j+4}\Big\}, \\
h_{\bar{F}\bar{F}}^{(2)-}\big|_{\mathcal{G}=0} &= \frac{1}{\mathcal{F}}\frac{\alpha}{\pi}\frac{1}{m^2}\chi\Big\{\frac{15}{4}\zeta'(-2) + \frac{1}{24} - \Big[\frac{5}{8}\ln\chi + \frac{\gamma}{12} - \frac{13}{2}\zeta'(-1) + \frac{3}{16}\Big]\chi \\
&\qquad - \frac{1}{2}\Big[3\ln\chi + 3\ln(2\pi) - \frac{\pi^2}{12} - \frac{45}{8}\Big]\chi^2 + \frac{1}{12}\Big[\frac{43}{2} - 5\zeta(3)\Big]\chi^3 \\
&\qquad - \frac{1}{4}\sum_{j=0}^{\infty}(-1)^j\Big[\frac{4j^3+35j^2+101j+70}{(j+2)(j+3)(j+4)}\zeta(j+2) - \frac{2j+7}{3}\zeta(j+4)\Big]\chi^{j+4}\Big\}.
\end{aligned}
$$

On the other hand, with the help of Eqs. (2.106) and (2.107), we infer the following weak field limits of the tensor structures in Eq. (2.102) for generic electromagnetic fields

$$
\begin{aligned}
(h_T^{(2)})^{\alpha\beta} &= -\frac{1}{15}\frac{\alpha}{\pi}\frac{1}{m^2}\Big[1 - \frac{4}{7}\Big(\frac{e}{m^2}\Big)^2\mathcal{F}\Big]g^{\alpha\beta} + \frac{1}{105}\frac{\alpha}{\pi}\frac{1}{m^2}\Big(\frac{e}{m^2}\Big)^2\bar{F}^{\alpha}{}_{\tau}\bar{F}^{\beta\tau} + O(\bar{F}^4), \\
(h_{\bar{F}\bar{F}}^{(2)})^{\alpha\beta} &= \frac{11}{315}\frac{\alpha}{\pi}\frac{1}{m^2}\Big(\frac{e}{m^2}\Big)^2 g^{\alpha\beta} + O(\bar{F}^2), \\
(h_{{}^*\bar{F}{}^*\bar{F}}^{(2)})^{\alpha\beta} &= \frac{4}{63}\frac{\alpha}{\pi}\frac{1}{m^2}\Big(\frac{e}{m^2}\Big)^2 g^{\alpha\beta} + O(\bar{F}^2), \\
(h_{{}^*\bar{F}\bar{F}}^{(2)})^{\alpha\beta} &= O(\bar{F}^2). \qquad (2.114)
\end{aligned}
$$

Upon plugging these results into Eq. (2.102) we obtain

$$\begin{aligned}\mathcal{L}_{\text{HE}}^{\text{1-loop}}\big|_{\sim\partial^2} = \frac{m^2}{240\pi^2}\Big(\frac{e}{m^2}\Big)^2 \partial_\alpha \bar{F}_{\mu\nu}\,\partial^\alpha \bar{F}^{\mu\nu} \\ - \frac{m^2}{12\pi^2}\Big(\frac{e}{m^2}\Big)^4\Big(\frac{1}{35}\partial_\alpha \bar{F}_{\mu\nu}\,\partial^\alpha \bar{F}^{\mu\nu}\,\mathcal{F} + \frac{1}{140}\partial_\alpha \bar{F}_{\mu\nu}\,\partial_\beta \bar{F}^{\mu\nu}\,\bar{F}^\alpha{}_\tau \bar{F}^{\beta\tau} \\ + \frac{11}{210}\partial_\alpha \mathcal{F}\partial^\alpha \mathcal{F} + \frac{2}{21}\partial_\alpha \mathcal{G}\partial^\alpha \mathcal{G}\Big) + O(\bar{F}^6)\,. \end{aligned} \tag{2.115}$$

A comparison with Eq. (2.65) unveils that, as to be expected, in the perturbative weak field regime the derivative operator is rendered dimensionless by the electron mass, which constitutes the only dimensionful physical scale of QED at zero external field. Correspondingly, in this parameter regime derivative corrections can be neglected if the typical frequency scale of variation of the external field is much smaller than the electron mass. It should be noted that the contribution to Eq. (2.115) which is quartic in the field strength can be expressed in terms of just four different tensor structures. Apart from contributions characterized by the same two structures which occur at zeroth order in the derivative expansion in Eq. (2.65) and the Minkowski indices of the two derivatives contracted with each other, also a new structure appears where the derivatives are contracted with field strength tensors in a non-trivial way. If desired, the dependences on the dual field strength tensor entering this expression via $\mathcal{G}$ can be completely eliminated with the help of the identity (A.3) in the Appendix A.1. We emphasize that the strategy employed here to determine derivative corrections to the Heisenberg-Euler effective action for QED in four space-time dimensions can be readily extended to QED in different space-time dimensions and other field theories, such as scalar QED.

The imaginary part of Eq. (2.102) is conveniently determined by first adopting the same transformation as leading from Eq. (2.56) to Eq. (2.57), and second, noting that the entire pole structure of the integrands in Eq. (2.110) on the real T axis can then be encoded in $\cot z'$ and derivatives thereof which are multiplied by functions of z' that are regular at $z' = n\pi$. In a third step, the imaginary parts of these contributions can be evaluated using Eq. (2.63). All expressions to be considered here are regular at $T = 0$ such that there is no pole at $n = 0$; cf. Eq. (2.106). A relatively straightforward but tedious calculation yields

$$\begin{aligned}\text{Im}\{h_T^{(2)-}\} = \frac{\alpha}{2}\frac{1}{ec_-}\frac{c_+^2 c_-^2}{(c_+^2+c_-^2)(c_+^2+4c_-^2)}\sum_{n=1}^{\infty}\mathrm{e}^{-\frac{m^2}{ec_-}n\pi}\Big\{-\frac{m^2}{ec_-}\frac{2c_+^2-c_-^2}{c_+^2}+\frac{3}{4}\Big(\frac{m^2}{ec_-}\Big)^2\frac{c_-}{c_+}\coth(\tfrac{c_+n\pi}{c_-}) \\ +\frac{3}{2}\frac{m^2}{ec_-}\frac{7c_+^2-2c_-^2}{4c_+^2+c_-^2}\coth^2(\tfrac{c_+n\pi}{c_-})+\frac{27}{2}\frac{c_+(c_+^2-c_-^2)}{(4c_+^2+c_-^2)c_-}\frac{\coth(\frac{c_+n\pi}{c_-})}{\sinh^2(\frac{c_+n\pi}{c_-})}\Big\}, \end{aligned} \tag{2.116}$$

$$\begin{aligned}\text{Im}\{h_T^{(2)+}\} = \frac{\alpha}{2}\frac{1}{ec_-}\frac{c_+^4 c_-^2}{(c_+^2+c_-^2)^2(c_+^2+4c_-^2)}\sum_{n=1}^{\infty}\mathrm{e}^{-\frac{m^2}{ec_-}n\pi}\Big\{-\frac{m^2}{ec_-}\frac{2c_+^2-c_-^2}{c_+^2}+\frac{3}{4}\Big(\frac{m^2}{ec_-}\Big)^2\frac{c_-}{c_+}\coth(\tfrac{c_+n\pi}{c_-}) \\ +\frac{3}{2}\frac{m^2}{ec_-}\frac{8c_+^4+3c_+^2c_-^2+4c_-^4}{(4c_+^2+c_-^2)c_+^2}\coth^2(\tfrac{c_+n\pi}{c_-})+9\frac{2c_+^4+c_+^2c_-^2+2c_-^4}{(4c_+^2+c_-^2)c_+c_-}\frac{\coth(\frac{c_+n\pi}{c_-})}{\sinh^2(\frac{c_+n\pi}{c_-})}\Big\}, \end{aligned} \tag{2.117}$$

$$\text{Im}\{h_\parallel^{(2)-}\} = \frac{\alpha}{2}\frac{1}{ec_-}\sum_{n=1}^{\infty}\mathrm{e}^{-\frac{m^2}{ec_-}n\pi}\Big\{\frac{m^2}{ec_-}\Big[\frac{3n\pi}{4}\frac{m^2}{ec_-}\frac{c_+^2}{c_-^2}-\frac{(c_+^2-5c_-^2)c_-^2}{(c_+^2+c_-^2)(c_+^2+4c_-^2)}\Big]$$

$$
\begin{aligned}
&-\frac{1}{4}\Big(\frac{m^2}{ec_-}\Big)^2\Big[n\pi\frac{m^2}{ec_-}\frac{c_+}{c_-}-\frac{(c_+^2-8c_-^2)c_-^3}{(c_+^2+c_-^2)(c_+^2+4c_-^2)c_+}\Big]\coth(\tfrac{c_+n\pi}{c_-})\\
&-\frac{1}{2}\frac{m^2}{ec_-}\Big[\frac{n\pi}{2}\frac{m^2}{ec_-}\frac{3c_+^2-2c_-^2}{c_-^2}-\frac{(5c_+^4-74c_+^2c_-^2-16c_-^4)c_-^2}{(c_+^2+c_-^2)(4c_+^2+c_-^2)(c_+^2+4c_-^2)}\Big]\coth^2(\tfrac{c_+n\pi}{c_-})\\
&-\frac{1}{2}\Big[n\pi\frac{m^2}{ec_-}\frac{c_+(3c_+^2-4c_-^2)}{c_-^3}-3\frac{c_+(c_+^4-43c_+^2c_-^2-8c_-^4)c_-}{(c_+^2+c_-^2)(4c_+^2+c_-^2)(c_+^2+4c_-^2)}\Big]\frac{\coth(\frac{c_+n\pi}{c_-})}{\sinh^2(\frac{c_+n\pi}{c_-})}\\
&-\frac{n\pi}{2}\frac{c_+^2(c_+^2-2c_-^2)}{c_-^4}\frac{1+2\cosh^2(\frac{c_+n\pi}{c_-})}{\sinh^4(\frac{c_+n\pi}{c_-})}\Big\},
\end{aligned}
\tag{2.118}
$$

$$
\begin{aligned}
\mathrm{Im}\{h_\parallel^{(2)+}\}=\frac{\alpha}{2}\frac{1}{ec_-}\frac{c_+^2}{c_+^2+c_-^2}\sum_{n=1}^{\infty}\mathrm{e}^{-\frac{m^2}{ec_-}n\pi}\Big\{&\frac{m^2}{ec_-}\Big[\frac{3n\pi}{4}\frac{m^2}{ec_-}\frac{c_+^2}{c_-^2}-2\frac{(c_+^4+2c_-^4)c_-^2}{(c_+^2+c_-^2)(c_+^2+4c_-^2)c_+^2}\Big]\\
&-\frac{1}{4}\Big(\frac{m^2}{ec_-}\Big)^2\Big[n\pi\frac{m^2}{ec_-}\frac{c_+}{c_-}-\frac{(3c_+^4+2c_+^2c_-^2+8c_-^2)c_-^3}{(c_+^2+c_-^2)(c_+^2+4c_-^2)c_+^3}\Big]\coth(\tfrac{c_+n\pi}{c_-})\\
&-\frac{1}{2}\frac{m^2}{ec_-}\Big[\frac{n\pi}{2}\frac{m^2}{ec_-}\frac{3c_+^4+2c_-^4}{c_+^2c_-^2}-\frac{(24c_+^6+25c_+^4c_-^2+80c_+^2c_-^4+16c_-^6)c_-^2}{(c_+^2+c_-^2)(4c_+^2+c_-^2)(c_+^2+4c_-^2)c_+^2}\Big]\coth^2(\tfrac{c_+n\pi}{c_-})\\
&-\Big[\frac{n\pi}{2}\frac{m^2}{ec_-}\frac{3c_+^4+4c_-^4}{c_+c_-^3}-3\frac{(6c_+^6+7c_+^4c_-^2+23c_+^2c_-^4+4c_-^6)c_-}{(c_+^2+c_-^2)(4c_+^2+c_-^2)(c_+^2+4c_-^2)c_+}\Big]\frac{\coth(\frac{c_+n\pi}{c_-})}{\sinh^2(\frac{c_+n\pi}{c_-})}\\
&-\frac{n\pi}{2}\frac{c_+^4+2c_-^4}{c_-^4}\frac{1+2\cosh^2(\frac{c_+n\pi}{c_-})}{\sinh^4(\frac{c_+n\pi}{c_-})}\Big\},
\end{aligned}
\tag{2.119}
$$

$$
\begin{aligned}
\mathrm{Im}\{h_\perp^{(2)-}\}=\frac{\alpha}{2}\frac{1}{ec_-}\sum_{n=1}^{\infty}\mathrm{e}^{-\frac{m^2}{ec_-}n\pi}\Big\{&\frac{m^2}{ec_-}\frac{(c_+^2-5c_-^2)c_-^2}{(c_+^2+c_-^2)(c_+^2+4c_-^2)}\\
&-\frac{3}{4}\Big(\frac{m^2}{ec_-}\Big)^2\frac{c_+c_-^3}{(c_+^2+c_-^2)(c_+^2+4c_-^2)}\coth(\tfrac{c_+n\pi}{c_-})\\
&-\frac{1}{2}\frac{m^2}{ec_-}\frac{(13c_+^4-40c_+^2c_-^2-8c_-^4)c_-^2}{(c_+^2+c_-^2)(4c_+^2+c_-^2)(c_+^2+4c_-^2)}\coth^2(\tfrac{c_+n\pi}{c_-})\\
&-\Big[n\pi\frac{m^2}{ec_-}\frac{c_+}{c_-}+\frac{3}{2}\frac{(5c_+^6-22c_+^4c_-^2+13c_+^2c_-^4+4c_-^6)c_-}{(c_+^2+c_-^2)(4c_+^2+c_-^2)(c_+^2+4c_-^2)c_+}\Big]\frac{\coth(\frac{c_+n\pi}{c_-})}{\sinh^2(\frac{c_+n\pi}{c_-})}\\
&-\frac{n\pi}{2}\frac{2c_+^2-c_-^2}{c_-^2}\frac{1+2\cosh^2(\frac{c_+n\pi}{c_-})}{\sinh^4(\frac{c_+n\pi}{c_-})}\Big\},
\end{aligned}
\tag{2.120}
$$

$$
\begin{aligned}
\mathrm{Im}\{h_\perp^{(2)+}\}=\frac{\alpha}{2}\frac{1}{ec_-}\frac{c_+^2}{c_+^2+c_-^2}\sum_{n=1}^{\infty}\mathrm{e}^{-\frac{m^2}{ec_-}n\pi}\Big\{&\frac{m^2}{ec_-}\frac{(c_+^2-5c_-^2)c_-^2}{(c_+^2+c_-^2)(c_+^2+4c_-^2)}\\
&-\frac{3}{4}\Big(\frac{m^2}{ec_-}\Big)^2\frac{c_+c_-^3}{(c_+^2+c_-^2)(c_+^2+4c_-^2)}\coth(\tfrac{c_+n\pi}{c_-})\\
&-\frac{1}{2}\frac{m^2}{ec_-}\frac{(16c_+^4-25c_+^2c_-^2+4c_-^4)c_-^2}{(c_+^2+c_-^2)(4c_+^2+c_-^2)(c_+^2+4c_-^2)}\coth^2(\tfrac{c_+n\pi}{c_-})\\
&-\Big[n\pi\frac{m^2}{ec_-}\frac{c_+}{c_-}+\frac{3}{2}\frac{(4c_+^8-32c_+^6c_-^2-17c_+^4c_-^4-21c_+^2c_-^6-4c_-^8)c_-}{(c_+^2+c_-^2)(4c_+^2+c_-^2)(c_+^2+4c_-^2)c_+^3}\Big]\frac{\coth(\frac{c_+n\pi}{c_-})}{\sinh^2(\frac{c_+n\pi}{c_-})}\\
&-\frac{n\pi}{2}\frac{2c_+^4+c_-^4}{c_+^2c_-^2}\frac{1+2\cosh^2(\frac{c_+n\pi}{c_-})}{\sinh^4(\frac{c_+n\pi}{c_-})}\Big\},
\end{aligned}
\tag{2.121}
$$

$$
\begin{aligned}
\mathrm{Im}\{h_Q^{(2)-}\} = \frac{\alpha}{2}\frac{1}{ec_-}\sum_{n=1}^{\infty}\mathrm{e}^{-\frac{m^2}{ec_-}n\pi}\Bigg\{&-\frac{m^2}{ec_-}\Bigg[\frac{3n\pi}{8}\frac{m^2}{ec_-}\frac{c_+}{c_-}-2\frac{(2c_+^2-c_-^2)c_-^3}{(c_+^2+c_-^2)(c_+^2+4c_-^2)c_+}\Bigg]\\
&-\frac{3}{2}\Big(\frac{m^2}{ec_-}\Big)^2\frac{c_-^4}{(c_+^2+c_-^2)(c_+^2+4c_-^2)}\coth(\tfrac{c_+n\pi}{c_-})\\
&+\frac{3}{4}\frac{m^2}{ec_-}\Bigg[\frac{n\pi}{2}\frac{m^2}{ec_-}\frac{c_+}{c_-}-\frac{(27c_+^4-13c_+^2c_-^2-4c_-^4)c_-^3}{(c_+^2+c_-^2)(4c_+^2+c_-^2)(c_+^2+4c_-^2)c_+}\Bigg]\coth^2(\tfrac{c_+n\pi}{c_-})\\
&+\frac{3}{4}\Bigg[n\pi\frac{m^2}{ec_-}\frac{2c_+^2-c_-^2}{c_-^2}-3\frac{(11c_+^4-17c_+^2c_-^2-4c_-^4)c_-^2}{(c_+^2+c_-^2)(4c_+^2+c_-^2)(c_+^2+4c_-^2)}\Bigg]\frac{\coth(\frac{c_+n\pi}{c_-})}{\sinh^2(\frac{c_+n\pi}{c_-})}\\
&+\frac{3n\pi}{4}\frac{c_+(c_+^2-c_-^2)}{c_-^3}\frac{1+2\cosh^2(\frac{c_+n\pi}{c_-})}{\sinh^4(\frac{c_+n\pi}{c_-})}\Bigg\},
\end{aligned}
\tag{2.122}
$$

$$
\begin{aligned}
\mathrm{Im}\{h_Q^{(2)+}\} = \frac{\alpha}{2}\frac{1}{ec_-}\frac{c_+^2}{c_+^2+c_-^2}\sum_{n=1}^{\infty}\mathrm{e}^{-\frac{m^2}{ec_-}n\pi}\Bigg\{&-\frac{1}{2}\frac{m^2}{ec_-}\Bigg[\frac{3n\pi}{4}\frac{m^2}{ec_-}\frac{c_+}{c_-}-\frac{(9c_+^4+c_+^2c_-^2+4c_-^4)c_-^3}{(c_+^2+c_-^2)(c_+^2+4c_-^2)c_+^3}\Bigg]\\
&-\frac{3}{2}\Big(\frac{m^2}{ec_-}\Big)^2\frac{c_-^4}{(c_+^2+c_-^2)(c_+^2+4c_-^2)}\coth(\tfrac{c_+n\pi}{c_-})\\
&+\frac{3}{4}\frac{m^2}{ec_-}\Bigg[\frac{n\pi}{2}\frac{m^2}{ec_-}\frac{c_+}{c_-}-\frac{32c_+^6+13c_+^4c_-^2+21c_+^2c_-^4+4c_-^6)c_-^3}{(c_+^2+c_-^2)(4c_+^2+c_-^2)(c_+^2+4c_-^2)c_+^3}\Bigg]\coth^2(\tfrac{c_+n\pi}{c_-})\\
&+\frac{3}{4}\Bigg[n\pi\frac{m^2}{ec_-}\frac{2c_+^4+c_-^4}{c_+^2c_-^2}-3\frac{(16c_+^6+9c_+^4c_-^2+21c_+^2c_-^4+4c_-^6)c_-^2}{(c_+^2+c_-^2)(4c_+^2+c_-^2)(c_+^2+4c_-^2)c_+^2}\Bigg]\frac{\coth(\frac{c_+n\pi}{c_-})}{\sinh^2(\frac{c_+n\pi}{c_-})}\\
&+\frac{3n\pi}{4}\frac{c_+^4+c_-^4}{c_+c_-^3}\frac{1+2\cosh^2(\frac{c_+n\pi}{c_-})}{\sinh^4(\frac{c_+n\pi}{c_-})}\Bigg\}.
\end{aligned}
\tag{2.123}
$$

These expressions constitute the imaginary part of Eq. (2.102) and result in corrections to Eq. (2.64) describing the decay of the quantum vacuum via electron-positron pair production in slowly-varying fields at one loop: the associated vacuum decay rate is $w = 2\,\mathrm{Im}\{\mathcal{L}_{\mathrm{HE}}\}$ [2, 4]; cf. also Refs. [11, 43, 45, 62] and references therein. As for the analogous result at zeroth order in the derivative expansion in Eq. (2.64), the characteristic feature of Eqs. (2.116)-(2.123) is the manifestly nonperturbative dependence on ec_- in the exponential. We emphasize the substantial increase in complexity of the leading derivative correction relative to the zeroth order result. For $c_+ = 0$, we recover the result for the imaginary part of $\mathcal{L}_{\mathrm{HE}}^{\text{1-loop}}\big|_{\partial^2}$ in a electric-like field derived in Ref. [59]. Derivatives acting on the external field can typically be considered as scaling as $\partial^\alpha \bar{F}^{\mu\nu} \sim \omega \bar{F}^{\mu\nu}$ where ω is the typical frequency scale of variation of the external field. Hence, Eqs. (2.116)-(2.123) allow us to infer that in order for the imaginary part at zeroth order in the derivative expansion to safely dominate the one at quadratic order in the parameter regime where $\{c_+, c_-\} \ll m^2/e$ and $\omega \ll m$ we have to ensure that $\omega \ll (ec_-)^2/m^3$. The latter criterion could not be inferred without an explicit calculation because it is *a priori* not clear which parameter sets the reference scale the frequency scale of variation of the external field is compared to for the manifestly non-perturbative imaginary part. Instead, one might have likely guessed it to be given by the electron mass as in Eq. (2.115).

Before closing this section, we note that along the same lines also higher order derivative contributions to $\mathcal{L}_{\mathrm{HE}}$ containing a fixed number $2n$, with $n \in \mathbb{N}$, of derivatives but accounting for arbitrary powers

of direct couplings to the field $\bar{F}^{\mu\nu}$ could be worked out. The contribution containing n first derivatives of the field could be extracted from the n-rank polarization tensor $\delta^n \Gamma^{\ell\text{-loop}}_{\text{HE}}[\bar{A}]/\delta\bar{A}^{\mu_1}\dots\delta\bar{A}^{\mu_n}$ evaluated in the homogeneous constant background field $\bar{F}^{\mu\nu}$. Its determination requires knowledge of the term scaling as $k^{2n} \sim k^{\sigma_1}\dots k^{\sigma_{2n}}$ of the n-rank polarization tensor. On the other hand, beyond the case of $n = 2$ considered explicitly here also contributions containing higher derivatives become relevant. For instance, at quartic order in the derivative expansion one also needs to evaluate the contributions which are characterized by the insertion of two second derivatives of the field in the charged particle loops of the constituting Feynman diagrams as well as those which contain two first derivatives and one second derivative. While, accounting for Eq. (2.22), the former can be extracted from the terms characterized by $\pi_p^{(4)}$ of the photon polarization tensor, the latter require the evaluation of the 3-rank polarization tensor up to $O(k^6)$. We emphasize that $\Pi^{\mu\nu}(k,k'|\bar{F})$ only provides access to symmetric contributions, namely those which mediate interactions between two same-order derivatives. Any asymmetric assignment of the derivatives to the two fields $\bar{f}^{\mu\nu}$ prior to the substitution $\bar{f}^{\mu\nu} \to \bar{F}^{\mu\nu}$ gives rise to inconsistencies: the possibility of partial integrations, which after this substitution also act on the factors of $\bar{F}^{\mu\nu}$ in the scalar functions $h^{(2n)}(\bar{F})$, renders different assignments inequivalent. In summary, the determination of the n-derivative contribution along these lines requires knowledge of the terms scaling as k^{2n} of the various j-rank polarization tensors with $j \leq n$. Aiming at the evaluation of the respective contribution in cases where the required j-rank polarization tensors in generic constant fields have not yet been determined, which is the case for $j > 2$, for the extraction of the nth order derivative expansion result it thus suffices to determine these tensors at an accuracy of order k^{2n}. See also Refs. [63, 64] for a related approach devised in a different context.

Finally, we highlight that Eq. (2.115) allows for the determination of the exact contribution to the one-loop photon polarization tensor in a generic inhomogeneous electromagnetic field at $O(k^4)$, i.e., the subleading correction to Eq. (2.80). In line with the discussion in the context of Eq. (2.75) and Sec. 2.3.2, this contribution is contained in $-(\delta^2/\delta\bar{A}^\mu\delta\bar{A}^\nu)\Gamma^{1\text{-loop}}_{\text{HE}}[\bar{A}]\big|_{\sim\partial^2}$. It is somewhat unexpected and amusing to note that, because Eq. (2.115) could be extracted from the contribution at $O(k^4)$ to the constant-field polarization tensor at one loop, it actually turns out that the full information about the exact contribution to $(\Pi^{1\text{-loop}}[\bar{A}])^{\mu\nu}(k,k')$ at $O(k^4)$ is already encoded in its constant-field analogue.

2.4 Explicit analytical insights beyond one loop

2.4.1 Two-loop Heisenberg-Euler effective Lagrangian

The Heisenberg-Euler effective action at two-loops (2.40) depicted in Fig. 2.3 is also known explicitly at zeroth order in a derivative expansion. As noted above, it decomposes into a 1PI and a 1PR contribution. The former can be worked out explicitly by contracting the two indices of the one-loop photon polarization tensor evaluated in a constant field (2.87) with a photon propagator (2.20) and integrating over all possible momentum transfers. This results in a rather unwieldy expression [33, 45]. In a notation following [33], but adopting the sequential substitutions $s' \to sv$, $s \to -\mathrm{i}T$ and a rotation of the integration contour, the on-shell renormalized effective Lagrangian associated with the 1PI contribution can be cast

in the following form,

$$\mathcal{L}_{\text{HE}}^{\text{2-loop}}\big|_{\text{1PI}} = \frac{\alpha}{\pi}\frac{1}{16\pi^2}\int_0^\infty \frac{\mathrm{d}T}{T^3}\,\mathrm{e}^{-m^2T}\int_0^1 \mathrm{d}\nu\left\{K(T,\nu) - \frac{K_0(T)}{\nu} + K_0(T)\left[\ln(m^2T) + \gamma - \frac{5}{6}\right]\right\}, \tag{2.124}$$

with

$$K_0(T) = (4m^2T + 2 - T\partial_T)\left[\frac{(ec_+T)(ec_-T)}{\tanh(ec_+T)\tan(ec_-T)} - 1 - \frac{(ec_+T)^2 - (ec_-T)^2}{3}\right] \tag{2.125}$$

and

$$\begin{aligned} K(T,\nu) = \mathrm{e}^{-\nu m^2T}\Bigg\{&\frac{(zz')^2}{P}[4m^2T(S+P)I_0 + 2I] \\ &- \frac{1}{\nu(1+\nu)}\left[4m^2T + \frac{2}{1+\nu} + \frac{z^2 - z'^2}{3}\left(2m^2T(2-\nu+2\nu^2) - \frac{5\nu}{1+\nu}\right)\right]\Bigg\}, \end{aligned} \tag{2.126}$$

which in turn is expressed in terms of

$$\begin{aligned} S &= \cosh z\cosh(\nu z)\cos z'\cos(\nu z')\,, \quad P = \sinh z\sinh(\nu z)\sin z'\sin(\nu z')\,, \\ I_0 &= \frac{1}{b-a}\ln\Big(\frac{b}{a}\Big), \quad I = \frac{1}{b-a}\left[(q-p)I_0 - \frac{q}{b} + \frac{p}{a}\right], \\ a &= z[\coth z + \coth(\nu z)]\,, \quad b = z'[\cot z' + \cot(\nu z')]\,, \\ p &= \frac{z^2\cos[(1-\nu)z']}{\sinh z\sinh(\nu z)}\,, \quad q = \frac{z'^2\cosh[(1-\nu)z]}{\sin z'\sin(\nu z')}\,. \end{aligned} \tag{2.127}$$

The proper time integration contour in Eq. (2.124) is assumed to lie slightly above the positive real T axis; see the paragraph below Eq. (2.57).

On the other hand, the 1PR contribution to the effective Lagrangian can be evaluated straightforwardly by inserting Eqs. (2.20) and (2.78) into the second expression in Eq. (2.40) and performing the momentum integrals using $[(2\pi)^4\delta(k)]^2 \to V^{(4)}(2\pi)^4\delta(k)$. This yields the compact representation [12]

$$\begin{aligned} \mathcal{L}_{\text{HE}}^{\text{2-loop}}\big|_{\text{1PR}} &= \frac{1}{2}\frac{\partial\mathcal{L}_{\text{HE}}^{\text{1-loop}}}{\partial\bar{F}_{\mu\nu}}\frac{\partial\mathcal{L}_{\text{HE}}^{\text{1-loop}}}{\partial\bar{F}^{\mu\nu}} = \frac{1}{4}\left[\left(\frac{\partial\mathcal{L}_{\text{HE}}^{\text{1-loop}}}{\partial c_+}\right)^2 - \left(\frac{\partial\mathcal{L}_{\text{HE}}^{\text{1-loop}}}{\partial c_-}\right)^2\right] \\ &= \frac{1}{2}\mathcal{F}\left[\left(\frac{\partial\mathcal{L}_{\text{HE}}^{\text{1-loop}}}{\partial\mathcal{F}}\right)^2 - \left(\frac{\partial\mathcal{L}_{\text{HE}}^{\text{1-loop}}}{\partial\mathcal{G}}\right)^2\right] + \mathcal{G}\frac{\partial\mathcal{L}_{\text{HE}}^{\text{1-loop}}}{\partial\mathcal{F}}\frac{\partial\mathcal{L}_{\text{HE}}^{\text{1-loop}}}{\partial\mathcal{G}}\,. \end{aligned} \tag{2.128}$$

Upon insertion of Eq. (2.61), we arrive at a rather compact double parameter integral representation.

Subsequently, we briefly study and compare the weak and strong field limits of Eqs. (2.124) and (2.128). A perturbative weak-field expansion of Eq. (2.124) results in

$$\mathcal{L}_{\text{HE}}^{\text{2-loop}}\big|_{\text{1PI}} = \frac{\alpha}{\pi}\frac{m^4}{360\pi^2}\left[\frac{5}{36}\Big(\frac{e}{m^2}\Big)^4(128\mathcal{F}^2+263\mathcal{G}^2) - \frac{1}{45}\Big(\frac{e}{m^2}\Big)^6\mathcal{F}(1219\mathcal{F}^2+2164\mathcal{G}^2) + O\Big(\big(\tfrac{e\bar{F}}{m^2}\big)^8\Big)\right]. \tag{2.129}$$

Apart from an overall suppression by the fine structure constant, Eq. (2.129) has the same structure as its one-loop analogue in the last line of Eq. (2.65). The leading term is an effective four-field interaction.

Conversely, the weak field expansion of Eq. (2.128),

$$\mathcal{L}_{\text{HE}}^{\text{2-loop}}\big|_{\text{1PR}} = \frac{\alpha}{\pi}\frac{m^4}{360\pi^2}\Big[\frac{1}{90}\Big(\frac{e}{m^2}\Big)^6\mathcal{F}(32\mathcal{F}^2+14\mathcal{G}^2)+O\Big(\big(\tfrac{e\bar{F}}{m^2}\big)^8\Big)\Big], \tag{2.130}$$

starts with a six-field interaction, and thus only contributes at subleading order. This can be easily understood by the fact that it arises from sewing together two lowest-order interactions at one-loop by a photon propagator. Because the lowest-order interaction couples four fields, this leaves three couplings to the external field for each loop.

As opposed to the situation at one loop, not even for $\mathcal{G}=0$ closed-form expressions for $\mathcal{L}_{\text{HE}}^{\text{2-loop}}\big|_{\text{1PI}}$ and its derivatives are available. A notable exception is the simplified case of self-dual fields [65]. The dominant contributions to $\mathcal{L}_{\text{HE}}^{\text{2-loop}}\big|_{\text{1PI}}$ in the limit of $|\mathcal{F}|\gg(m^2/e)^2$ and $|\mathcal{G}|\ll(m^2/e)^2$ hence have to be extracted from the double integral representation in Eq. (2.124). As detailed in the context of Eq. (2.66), independently of the sign of $\mathcal{F}$ for this it is sufficient to consider only the case of $c_+=\sqrt{2\mathcal{F}}$ and $|c_-|\ll|c_+|$. Aiming at extracting the respective asymptotics, it is convenient to first perform a transformation of the integration variable from T to dimensionless proper time $z=ec_+T$, and introduce the shorthand notation $\kappa=c_-/c_+$, which implies $z'=\kappa z$. In the considered limit, we obviously have $\chi=m^2/(2ec_+)\ll 1$ and $|\kappa|\ll 1$, which justifies expansions in both of these parameters; cf. also Eq. (2.67). Second, we note that because of the very mild overall exponential suppression of the integrand in Eq. (2.124) with $\exp\{-2\chi z\}$ the dominant contributions to $\mathcal{L}_{\text{HE}}^{\text{2-loop}}\big|_{\text{1PI}}$ in the limit of $\chi\to 0$ stem from large values of z; this can be easily checked by introducing a parameter Z fulfilling $Z\gg 1$ while $2\chi Z\ll 1$ which splits the proper time integration into two domains. In a next step, we infer

$$K_0(z)=z^3\Big\{-\partial_z\Big[\frac{\kappa}{\tanh z\tan(\kappa z)}-\frac{1}{z^2}-\frac{1-\kappa^2}{3}\Big]+O(\chi)\Big\} \tag{2.131}$$

and

$$Kz,\nu)=z^3\mathrm{e}^{-2\chi z\nu}\Big\{z\frac{\kappa^2}{P}2I-\frac{1}{z^3(1+\nu)^2}\Big[\frac{2}{\nu}-z^2\frac{5(1-\kappa^2)}{3}\Big]+O(\chi)\Big\}. \tag{2.132}$$

We emphasize that we have explicitly checked that the terms denoted by $O(\chi)$ in Eqs. (2.131) and (2.132) do not increase with z for $z\to\infty$, but scale at least as $O((\frac{1}{z})^0)$ at any given order in an expansion in $\kappa\to 0$. Moreover, note that at any fixed order in $\kappa\to 0$, we have $\lim_{z\to\infty}\big|z\frac{I}{P}\big|\sim z^l e^{-z(1+2\nu)}\to 0$, with $l\in\mathbb{Z}_0$. Herewith, we obtain

$$\int_0^\infty\frac{\mathrm{d}z}{z^3}\,\mathrm{e}^{-2\chi z}K_0(z)=O(\chi^0)\,O(\kappa^0), \tag{2.133}$$

and

$$\int_0^\infty\frac{\mathrm{d}z}{z^3}\,\mathrm{e}^{-2\chi z}\,K(z,\nu)=-\frac{5}{(1+\nu)^2}\frac{1-\kappa^2}{3}\ln\chi+O(\chi^0)\,O(\kappa^0)\,. \tag{2.134}$$

Apart from this, we need to consider the integral

$$\int_0^\infty\frac{\mathrm{d}z}{z^3}\,\mathrm{e}^{-2\chi z}\,K_0(z)\Big[\ln(2\chi z)+\gamma-\frac{5}{6}\Big]=\int_0^\infty\frac{\mathrm{d}z}{z}\,\mathrm{e}^{-2\chi z}\Big[\frac{\coth z}{z}-\frac{1}{z^2}-\frac{1}{3}\Big]$$

$$+\frac{\kappa^2}{3}\int_0^\infty \mathrm{d}z\,\mathrm{e}^{-2\chi z}\left[\frac{1}{z}-\coth z\right]+O(\chi^0)\,O(\kappa^0)+O(\kappa^4)\,. \quad (2.135)$$

In order to arrive at this result we have made use of Eq. (2.131) and performed an integration by parts. Thereafter, we have employed an expansion in $\kappa \to 0$, keeping only terms up to order κ^2. The integrals in Eq. (2.135) can be carried out with Eqs. (2.68) and (2.69), yielding

$$\begin{aligned}
&\int_0^\infty \frac{\mathrm{d}z}{z}\,e^{-2\chi z}\left[\frac{\coth z}{z}-\frac{1}{z^2}-\frac{1}{3}\right]=\left(\frac{1}{3}-2\chi+2\chi^2\right)\ln\chi+\frac{1}{3}-4\zeta'(-1,\chi)-\chi^2=\frac{1}{3}\ln\chi+O(\chi^0)\,,\\
&\int_0^\infty \mathrm{d}z\,\mathrm{e}^{-2\chi z}\left[\frac{1}{z}-\coth z\right]=\frac{1}{2}\chi^{-1}-\ln\chi+\psi(\chi)=-\frac{1}{2}\chi^{-1}-\ln\chi+O(\chi^0)\,. \quad (2.136)
\end{aligned}$$

Using these identities in Eq. (2.135), we infer

$$\int_0^\infty \frac{\mathrm{d}z}{z^3}\,\mathrm{e}^{-2\chi z}\,K_0(z)\left[\ln(2\chi z)+\gamma-\frac{5}{6}\right]=\frac{1}{3}\left[(1-\kappa^2)\ln\chi-\frac{1}{2}\chi^{-1}\kappa^2\right]+O(\chi^0)\,O(\kappa^0)+O(\kappa^4)\,. \quad (2.137)$$

Putting everything together, we hence have

$$\mathcal{L}_{\mathrm{HE}}^{\text{2-loop}}\big|_{\text{1PI}}=\frac{\alpha}{\pi}\frac{e^2\mathcal{F}}{16\pi^2}\left[(1-\kappa^2)\ln\chi^{-1}-\frac{1}{3}\chi^{-1}\kappa^2+O(\chi^0)\,O(\kappa^0)+O(\kappa^4)\right]. \quad (2.138)$$

which, using Eq. (2.67) can be written as

$$\mathcal{L}_{\mathrm{HE}}^{\text{2-loop}}\big|_{\text{1PI}}=\frac{\alpha}{\pi}\frac{1}{16\pi^2}\left\{e^2\mathcal{F}\left[\ln\chi^{-1}+O(\chi^0)\right]-\frac{1}{12}\frac{e^2\mathcal{G}^2}{\mathcal{F}}\left[\chi^{-1}+O(\chi^0)\right]\right\}+O(\mathcal{G}^4)\,. \quad (2.139)$$

Apart from the numeric coefficients and an overall factor of α/π, Eq. (2.139) has exactly the same form as its one-loop analogue in Eq. (2.74): the term $\sim\mathcal{F}$ starts contributing with a logarithm of χ and the one $\sim\mathcal{G}^2/\mathcal{F}$ with the inverse of χ. For completeness and as a consistency check, we note that the one-loop result (2.74) can alternatively be extracted from the parameter integral representation of the one-loop Heisenberg-Euler Lagrangian (2.61) along the same lines as presented here.

Finally we also extract the leading asymptotics of $\mathcal{L}_{\mathrm{HE}}^{\text{2-loop}}\big|_{\text{1PR}}$ in the same limit. The corresponding result can be readily obtained by plugging Eq. (2.66) into Eq. (2.128). Expressing the derivatives for $\mathcal{F}$ in terms of derivatives for $\chi=m^2/(2e\sqrt{2\mathcal{F}})$, this yields

$$\begin{aligned}
\mathcal{L}_{\mathrm{HE}}^{\text{2-loop}}\big|_{\text{1PR}}=\frac{1}{8}\mathcal{F}\Bigg((2-\chi\partial_\chi)\frac{\mathcal{L}_{\mathrm{HE}}^{\text{1-loop}}}{\mathcal{F}}\bigg|_{\mathcal{G}=0}\Bigg)^2-\frac{1}{8}\frac{\mathcal{G}^2}{\mathcal{F}}\Bigg[4\Bigg(\mathcal{F}\frac{\partial^2\mathcal{L}_{\mathrm{HE}}^{\text{1-loop}}}{\partial\mathcal{G}^2}\bigg|_{\mathcal{G}=0}\Bigg)^2\\
-(2-\chi\partial_\chi)\frac{\mathcal{L}_{\mathrm{HE}}^{\text{1-loop}}}{\mathcal{F}}\bigg|_{\mathcal{G}=0}(2-\chi\partial_\chi)\Bigg(\mathcal{F}\frac{\partial^2\mathcal{L}_{\mathrm{HE}}^{\text{1-loop}}}{\partial\mathcal{G}^2}\bigg|_{\mathcal{G}=0}\Bigg)\Bigg]+O(\mathcal{G}^4)\,, \quad (2.140)
\end{aligned}$$

where we divided $\mathcal{L}_{\mathrm{HE}}^{\text{1-loop}}\big|_{\mathcal{G}=0}$ by $\mathcal{F}$ and multiplied its second derivative for $\mathcal{G}$ by $\mathcal{F}$ such as to obtain dimensionless quantities fully parameterized by χ only; cf. also Eqs. (2.70)-(2.73). By employing Eqs. (2.72) and (2.73) in Eq. (2.140), we then find

$$\mathcal{L}_{\rm HE}^{\text{2-loop}}\big|_{\rm 1PR} = \frac{\alpha}{\pi}\frac{1}{24\pi^2}\bigg\{e^2\mathcal{F}\Big[\frac{1}{3}\ln^2\chi^{-1} + \Big(8\zeta'(-1) - \frac{1}{3}\Big)\ln\chi^{-1} + O(\chi^0)\Big] \\ - \frac{1}{4}\frac{e^2\mathcal{G}^2}{\mathcal{F}}\Big[\frac{1}{12}\chi^{-2} - \Big(\frac{1}{2}\ln\chi^{-1} - \frac{\gamma}{3} + 2\zeta'(-1) - \frac{1}{12}\Big)\chi^{-1} + O(\chi^0)\Big]\bigg\} + O(\mathcal{G}^4)\,. \quad (2.141)$$

Note that in the present context we count contributions scaling $\sim \ln\chi$ as $O(\chi^0)$. We emphasize that Eq. (2.141) has a different structure than the one-loop result (2.74) and the 1PI contribution at two loops (2.139). In comparison to these expressions the leading terms $\sim \mathcal{F}$ and $\sim \mathcal{G}^2/\mathcal{F}$ are enhanced: the former one by a factor of $\ln\chi^{-1}$ and the latter one by χ^{-1}. As $(e^2\mathcal{G}^2/\mathcal{F})\chi^{-2} = 8e^2\mathcal{G}\,(e^2\mathcal{G}/m^4)$, this in particular means that, in contrast to Eqs. (2.74) and (2.139), the leading term $\sim \mathcal{G}^2$ to the 1PR contribution at two loops is not parametrically suppressed by an inverse power of $\mathcal{F} \gg (m^2/e)^2$. Instead, one factor of $\mathcal{G}$ is rendered dimensionless by a quartic power of the electron mass. In summary, in the limit of $|\mathcal{F}| \gg (m^2/e)^2$ and $|\mathcal{G}| \ll (m^2/e)^2$ the leading contributions at one and two loops are related as

$$\frac{\mathcal{L}_{\rm HE}^{\text{2-loop}}\big|_{\rm 1PI}}{\mathcal{L}_{\rm HE}^{\text{1-loop}}} \simeq \frac{3}{4}\frac{\alpha}{\pi}\,, \qquad \frac{\mathcal{L}_{\rm HE}^{\text{2-loop}}\big|_{\rm 1PR}}{\mathcal{L}_{\rm HE}^{\text{2-loop}}\big|_{\rm 1PI}} \simeq \frac{2}{9}\ln\chi^{-1}\,, \quad (2.142)$$

while those $\sim \mathcal{G}^2$ fulfill

$$\frac{\partial\mathcal{L}_{\rm HE}^{\text{2-loop}}\big|_{\rm 1PI}}{\partial\mathcal{G}^2}\Big(\frac{\partial\mathcal{L}_{\rm HE}^{\text{1-loop}}}{\partial\mathcal{G}^2}\Big)^{-1} \simeq -\frac{1}{2}\frac{\alpha}{\pi}\,, \qquad \frac{\partial\mathcal{L}_{\rm HE}^{\text{2-loop}}\big|_{\rm 1PR}}{\partial\mathcal{G}^2}\Big(\frac{\partial\mathcal{L}_{\rm HE}^{\text{1-loop}}\big|_{\rm 1PI}}{\partial\mathcal{G}^2}\Big)^{-1} \simeq \frac{1}{6}\chi^{-1}\,. \quad (2.143)$$

Equations (2.142) and (2.143) imply that whereas the two-loop 1PI contribution remains suppressed relatively to the one loop result, the 1PR contribution at two loops can in principle even surpass the latter for exponentially large field field strengths $|\chi^{-1}| \geq \exp(6\pi/\alpha)$. On the other hand, with regard to the contribution $\sim \mathcal{G}^2$ the 1PR term becomes larger than the corresponding one-loop expression already for the much lower values of $|\chi^{-1}| \geq 12\pi/\alpha$.

2.4.2 Photon current and polarization tensor at two loops

For completeness, we note that the leading-order derivative expansion results for the photon current and polarization tensor at one loop given in Eqs. (2.75) and (2.80) can be readily generalized to higher loop orders. Recall, however, that $(\Pi^{\ell\text{-loop}}[\bar{A}])^{\mu\nu} \neq -\delta^2\Gamma_{\rm HE}[\bar{A}]/\delta\bar{A}^\mu\delta\bar{A}^\nu$ and $(j^{\ell\text{-loop}}[\bar{A}])^\mu \neq \delta\Gamma_{\rm HE}/\delta\bar{A}^\mu$ for $\ell > 1$. Instead, the explicit determination of $(\Pi[\bar{A}])^{\mu\nu}$ and $(j[\bar{A}])^\mu$ from $\Gamma_{\rm HE}[\bar{A}]$ at a given order n in the loop expansion requires solving Eq. (2.22). This can be done recursively: obviously the results for $(\Pi^{\ell\text{-loop}}[\bar{A}])^{\mu\nu}$ and $(j^{\ell\text{-loop}}[\bar{A}])^\mu$ with $\ell = n$ are fully determined by those for $1 \leq \ell \leq n-1$ as well as $\delta\Gamma_{\rm HE}^{n\text{-loop}}/\delta\bar{A}^\mu$ and $\delta^2\Gamma_{\rm HE}^{n\text{-loop}}[\bar{A}]/\delta\bar{A}^\mu\delta\bar{A}^\nu$. Equivalently, this means that they are attainable from the first and second functional derivatives of $\Gamma_{\rm HE}^{\ell\text{-loop}}[\bar{A}]$ for $1 \leq \ell \leq n$. Specifically at two loops we have

$$(\Pi^{\text{2-loop}}[\bar{A}])^{\mu\nu} = -\frac{\delta^2\Gamma_{\rm HE}^{\text{2-loop}}[\bar{A}]}{\delta\bar{A}_\mu\delta\bar{A}_\nu} + \iint(\Pi^{\text{1-loop}}[\bar{A}])^{\mu\alpha}D_{\alpha\beta}\,(\Pi^{\text{1-loop}}[\bar{A}])^{\beta\nu} \quad (2.144)$$

and

$$(j^{2\text{-loop}}[\bar{A}])^{\mu} = \frac{\delta\Gamma_{\text{HE}}^{2\text{-loop}}[\bar{A}]}{\delta\bar{A}_{\mu}} + \iint (j^{1\text{-loop}}[\bar{A}])^{\alpha} D_{\alpha\beta} (\Pi^{1\text{-loop}}[\bar{A}])^{\beta\mu} . \tag{2.145}$$

Hence, the consistent consideration of 1PR contributions, such as in Eqs. (2.144) and (2.145), constitutes an important step in the determination of the induced photon current and the photon polarization tensor for $\ell > 1$ loops from Eq. (2.22).

Aiming at the extraction of the low-energy expressions for $(\Pi^{\ell\text{-loop}}[\bar{A}])^{\mu\nu}$ and $(j^{\ell\text{-loop}}[\bar{A}])^{\mu}$ with $\ell > 1$ in a slowly-varying external field at zeroth order in a derivative expansion, these contributions can be determined in a convenient and unambiguous way by momentarily introducing labeled external fields. The procedure to work out a specific 1PR diagram to be accounted for is then as follows: First, one isolates the relevant diagrams together with the respective numerical prefactors. Second, instead of directly evaluating a given diagram included in this set, one eliminates its open indices and works out the formal expression for the resulting external-field vacuum diagram, with one important modification as compared to a standard QED calculations in a slowly-varying external electromagnetic field. Namely, the specific fermion loops featuring the open indices in the original diagram are now to be dressed by distinctly labelled slowly-varying external fields different from the one dressing the other fermion loops. By construction, this ensures the momentum transfer mediating between different 1PR structures to vanish identically. Third, a single functional derivative is taken for each of these fields to restores the open indices in the correct fermion loops. Fourth, the labels distinguishing the different external fields are removed. This yields the exact expression for the desired diagram at leading order in a derivative expansion, i.e., $(\Pi^{\ell\text{-loop}}[\bar{A}])^{\mu\nu}(k,k') \sim O(k^2)$ and $(j^{\ell\text{-loop}}[\bar{A}])^{\mu}(k) \sim O(k)$; cf. the corresponding discussion in the paragraph above Eq. (2.75).

We emphasize that this "trick" is advantageous over a seemingly more direct evaluation of these contributions by sewing together the corresponding low-energy effective vertices to obtain formal expressions for the diagrams with open indices. This is so because the latter approach requires additional assumptions. In order to obtain the correct results along these lines one has to carefully analyze the momentum structure of the contributing diagrams such that the zero momentum limit can be taken correctly. This involves for instance to invoke a specific order for performing the various momentum integrations.

Subsequently, we want to explicitly determine the photon polarization tensor at two loops in the soft-photon limit from Eq. (2.144). To this end, we first work out the 1PR term to be combined with the second derivative of $\Gamma_{\text{HE}}^{2\text{-loop}}[\bar{A}]$. Adopting the strategy laid out in the paragraph below Eq. (2.145) to evaluate such contributions, we find

$$\begin{aligned}\iint (\Pi^{1\text{-loop}}[\bar{A}])^{\mu\alpha} D_{\alpha\beta} (\Pi^{1\text{-loop}}[\bar{A}])^{\beta\nu}(k,k') &= (2\mathrm{i})^2 \int_x \mathrm{e}^{\mathrm{i}x(k+k')}\, k_{\alpha}\, \frac{\partial^2 \mathcal{L}_{\text{HE}}^{1\text{-loop}}}{\partial\bar{F}_{\alpha\mu}\partial\bar{F}_{\rho\sigma}} \frac{\partial^2 \mathcal{L}_{\text{HE}}^{1\text{-loop}}}{\partial\bar{F}^{\rho\sigma}\partial\bar{F}_{\beta\nu}}\, k'_{\beta} + O(k^4) \\ &= -\int_x \mathrm{e}^{\mathrm{i}x(k+k')} \sum_i p_i^{\mu\nu}(k,k')\, \Delta\pi_i^{2\text{-loop}}(\mathcal{F},\mathcal{G}) + O(k^4) ,\end{aligned} \tag{2.146}$$

where the sum is over $i \in \{T, \epsilon, \bar{F}\bar{F}, {}^{\star}\bar{F}{}^{\star}\bar{F}, {}^{\star}\bar{F}\bar{F}\}$ and the tensor structure is spanned by Eq. (2.81). The

explicit expressions for the coefficients are fully determined by $\mathcal{L}_{\text{HE}}^{\text{1-loop}}$ and read

$$\begin{aligned}
\Delta\pi_{T}^{\text{2-loop}} &= \frac{1}{2}\Big[(\partial_{\mathcal{F}}\mathcal{L}_{\text{HE}}^{\text{1-loop}})^2 - (\partial_{\mathcal{G}}\mathcal{L}_{\text{HE}}^{\text{1-loop}})^2\Big]\,,\\
\Delta\pi_{\epsilon}^{\text{2-loop}} &= \partial_{\mathcal{F}}\mathcal{L}_{\text{HE}}^{\text{1-loop}}\,\partial_{\mathcal{G}}\mathcal{L}_{\text{HE}}^{\text{1-loop}}\,,\\
\Delta\pi_{\bar{F}\bar{F}}^{\text{2-loop}} &= \partial_{\mathcal{F}}\mathcal{L}_{\text{HE}}^{\text{1-loop}}\,\partial_{\mathcal{F}}^2\mathcal{L}_{\text{HE}}^{\text{1-loop}} + \mathcal{F}\Big[(\partial_{\mathcal{F}}^2\mathcal{L}_{\text{HE}}^{\text{1-loop}})^2 - (\partial_{\mathcal{F}}\partial_{\mathcal{G}}\mathcal{L}_{\text{HE}}^{\text{1-loop}})^2\Big]\\
&\quad - \Big(\partial_{\mathcal{G}}\mathcal{L}_{\text{HE}}^{\text{1-loop}} - 2\mathcal{G}\,\partial_{\mathcal{F}}^2\mathcal{L}_{\text{HE}}^{\text{1-loop}}\Big)\partial_{\mathcal{F}}\partial_{\mathcal{G}}\mathcal{L}_{\text{HE}}^{\text{1-loop}}\,,\\
\Delta\pi_{\star\bar{F}\star\bar{F}}^{\text{2-loop}} &= \partial_{\mathcal{F}}\mathcal{L}_{\text{HE}}^{\text{1-loop}}\,\partial_{\mathcal{G}}^2\mathcal{L}_{\text{HE}}^{\text{1-loop}} - \mathcal{F}\Big[(\partial_{\mathcal{G}}^2\mathcal{L}_{\text{HE}}^{\text{1-loop}})^2 - (\partial_{\mathcal{F}}\partial_{\mathcal{G}}\mathcal{L}_{\text{HE}}^{\text{1-loop}})^2\Big]\\
&\quad + \Big(\partial_{\mathcal{G}}\mathcal{L}_{\text{HE}}^{\text{1-loop}} + 2\mathcal{G}\,\partial_{\mathcal{G}}^2\mathcal{L}_{\text{HE}}^{\text{1-loop}}\Big)\partial_{\mathcal{F}}\partial_{\mathcal{G}}\mathcal{L}_{\text{HE}}^{\text{1-loop}}\,,\\
\Delta\pi_{\star\bar{F}\bar{F}}^{\text{2-loop}} &= \frac{1}{2}\Big(\partial_{\mathcal{F}}^2\mathcal{L}_{\text{HE}}^{\text{1-loop}} - \partial_{\mathcal{G}}^2\mathcal{L}_{\text{HE}}^{\text{1-loop}}\Big)\Big(\partial_{\mathcal{G}}\mathcal{L}_{\text{HE}}^{\text{1-loop}} + 2\mathcal{F}\,\partial_{\mathcal{F}}\partial_{\mathcal{G}}\mathcal{L}_{\text{HE}}^{\text{1-loop}}\Big)\\
&\quad + \mathcal{G}\Big[\partial_{\mathcal{F}}^2\mathcal{L}_{\text{HE}}^{\text{1-loop}}\,\partial_{\mathcal{G}}^2\mathcal{L}_{\text{HE}}^{\text{1-loop}} + (\partial_{\mathcal{F}}\partial_{\mathcal{G}}\mathcal{L}_{\text{HE}}^{\text{1-loop}})^2\Big] + \partial_{\mathcal{F}}\mathcal{L}_{\text{HE}}^{\text{1-loop}}\,\partial_{\mathcal{F}}\partial_{\mathcal{G}}\mathcal{L}_{\text{HE}}^{\text{1-loop}}\,.
\end{aligned} \tag{2.147}$$

In order to allow for a compact notation, here we employed the shorthand notation $\partial_{\mathcal{F}} = \partial/\partial\mathcal{F}$, etc. To arrive at the representation in the second line of Eq. (2.146) we employed Eq. (A.10) in the Appendix A.3 to express the derivatives for the field strength tensor $\bar{F}^{\mu\nu}$ in terms of derivatives for the scalar invariants $\mathcal{F}$ and $\mathcal{G}$.

We highlight an important point here: in the context of Eqs. (2.80) and (2.81) we noted that the tensor structure $p_\epsilon^{\mu\nu}$, the coefficient of which encodes the full dependence of $(\Pi^{\text{1-loop}}[\bar{A}])^{\mu\nu}$ on $\partial_{\mathcal{G}}\mathcal{L}_{\text{HE}}^{\text{1-loop}}$, vanishes because of translational invariance in constant fields. This might suggest that in the calculation of processes in constant external fields involving the photon polarization tensor as building block, such as in particular the constant-field limit of Eq. (2.146), the contribution $\sim p_\epsilon^{\mu\nu}$ to the former can be omitted from the outset even in cases where $\mathcal{G} \neq 0$. However, the fact that all the functions in Eq. (2.147) depend on $\partial_{\mathcal{G}}\mathcal{L}_{\text{HE}}^{\text{1-loop}}$ clearly indicates that this is actually not permitted. In constant fields the integral in Eq. (2.146) yields a momentum conserving delta function which renders the contribution $p_\epsilon^{\mu\nu}\,\Delta\pi_\epsilon^{\text{2-loop}}$ zero, but all the other dependences on $\partial_{\mathcal{G}}\mathcal{L}_{\text{HE}}^{\text{1-loop}}$ persist. This apparent inconsistency is resolved by noting that when sewing together two polarization tensors by a photon propagator in the soft-photon limit a factor linear in the momentum is effectively removed from each of the two polarization tensors via $k^\alpha k^\beta/k^2 \to g^{\alpha\beta}/d$ in d space-time dimensions; cf. also Eq. (2.79) as well as the detailed discussion below Eq. (2.145). Thereby, each of the tensor structures $p_\epsilon^{\mu\nu}$ is effectively reduced from quadratic to linear order in the momentum. In turn, the argument $k_\alpha k_\beta \epsilon^{\mu\nu\alpha\beta} = 0$ invoked to render $p_\epsilon^{\mu\nu}$ zero for the photon polarization tensor considered as an isolated object does no longer apply when the latter appears as a subdiagram within a larger diagram. Here, always the full expression has to be accounted for. Similar apparent inconsistencies generically arise in sewing together more elementary building blocks to form larger Feynman diagrams. We emphasize that this illustrates once again that conclusions drawn by analyzing contributions considered as individual objects should never be taken over to composite ones without validation that these indeed remain justified. It specifically also applies to the determination of the full photon propagator in the presence of an external field from the polarization tensor; cf. Eqs. (2.19), (2.21) and (2.22).

On the other hand, the second derivative of $\Gamma_{\text{HE}}^{\text{2-loop}}[\bar{A}]$ for the external field $\bar{A}^\mu$ generically decomposes into 1PI and 1PR contributions. In the soft-photon limit these can be readily obtained from Eq. (2.80) by substituting $\mathcal{L}_{\text{HE}}^{\text{1-loop}} \to -\mathcal{L}_{\text{HE}}^{\text{2-loop}}\big|_{\text{1PI}}$ and $\mathcal{L}_{\text{HE}}^{\text{1-loop}} \to -\mathcal{L}_{\text{HE}}^{\text{2-loop}}\big|_{\text{1PR}}$, respectively. The minus signs arise because of $\Pi^{\text{1-loop}}[\bar{A}] = -\delta^2\Gamma_{\text{HE}}^{\text{1-loop}}[\bar{A}]/\delta\bar{A}\delta\bar{A}$. Equation (2.128) then in particular allows to represent the 1PR contribution directly in terms of derivatives of $\mathcal{L}_{\text{HE}}^{\text{1-loop}}$ for $\mathcal{F}$ and $\mathcal{G}$. The relevant derivatives determining Eq. (2.80) after the appropriate substitution can be expressed as

$$\begin{aligned}
\partial_{\mathcal{F}}\mathcal{L}_{\text{HE}}^{\text{2-loop}}\big|_{\text{1PR}} &= \pi_T^{\text{2-loop}}\big|_{\text{1PR}} + \Delta\pi_T^{\text{2-loop}}\,,\\
\partial_{\mathcal{G}}\mathcal{L}_{\text{HE}}^{\text{2-loop}}\big|_{\text{1PR}} &= \pi_\epsilon^{\text{2-loop}}\big|_{\text{1PR}} + \Delta\pi_\epsilon^{\text{2-loop}}\,,\\
\partial_{\mathcal{F}}^2\mathcal{L}_{\text{HE}}^{\text{2-loop}}\big|_{\text{1PR}} &= \pi_{\bar{F}\bar{F}}^{\text{2-loop}}\big|_{\text{1PR}} + \Delta\pi_{\bar{F}\bar{F}}^{\text{2-loop}}\,,\\
\partial_{\mathcal{G}}^2\mathcal{L}_{\text{HE}}^{\text{2-loop}}\big|_{\text{1PR}} &= \pi_{\star\bar{F}\star\bar{F}}^{\text{2-loop}}\big|_{\text{1PR}} + \Delta\pi_{\star\bar{F}\star\bar{F}}^{\text{2-loop}}\,,\\
\partial_{\mathcal{F}}\partial_{\mathcal{G}}\mathcal{L}_{\text{HE}}^{\text{2-loop}}\big|_{\text{1PR}} &= \pi_{\star\bar{F}\bar{F}}^{\text{2-loop}}\big|_{\text{1PR}} + \Delta\pi_{\star\bar{F}\bar{F}}^{\text{2-loop}}\,,
\end{aligned} \tag{2.148}$$

where we introduced

$$\begin{aligned}
\pi_T^{\text{2-loop}}\big|_{\text{1PR}} &= \left(\mathcal{F}\partial_{\mathcal{F}}\mathcal{L}_{\text{HE}}^{\text{1-loop}} + \mathcal{G}\partial_{\mathcal{G}}\mathcal{L}_{\text{HE}}^{\text{1-loop}}\right)\partial_{\mathcal{F}}^2\mathcal{L}_{\text{HE}}^{\text{1-loop}} + \left(\mathcal{G}\partial_{\mathcal{F}}\mathcal{L}_{\text{HE}}^{\text{1-loop}} - \mathcal{F}\partial_{\mathcal{G}}\mathcal{L}_{\text{HE}}^{\text{1-loop}}\right)\partial_{\mathcal{F}}\partial_{\mathcal{G}}\mathcal{L}_{\text{HE}}^{\text{1-loop}}\,,\\
\pi_\epsilon^{\text{2-loop}}\big|_{\text{1PR}} &= \left(\mathcal{F}\partial_{\mathcal{F}}\mathcal{L}_{\text{HE}}^{\text{1-loop}} + \mathcal{G}\partial_{\mathcal{G}}\mathcal{L}_{\text{HE}}^{\text{1-loop}}\right)\partial_{\mathcal{F}}\partial_{\mathcal{G}}\mathcal{L}_{\text{HE}}^{\text{1-loop}} + \left(\mathcal{G}\partial_{\mathcal{F}}\mathcal{L}_{\text{HE}}^{\text{1-loop}} - \mathcal{F}\partial_{\mathcal{G}}\mathcal{L}_{\text{HE}}^{\text{1-loop}}\right)\partial_{\mathcal{G}}^2\mathcal{L}_{\text{HE}}^{\text{1-loop}}\,,\\
\pi_{\bar{F}\bar{F}}^{\text{2-loop}}\big|_{\text{1PR}} &= \left(\mathcal{F}\partial_{\mathcal{F}}\mathcal{L}_{\text{HE}}^{\text{1-loop}} + \mathcal{G}\partial_{\mathcal{G}}\mathcal{L}_{\text{HE}}^{\text{1-loop}}\right)\partial_{\mathcal{F}}^3\mathcal{L}_{\text{HE}}^{\text{1-loop}} + \left(\mathcal{G}\partial_{\mathcal{F}}\mathcal{L}_{\text{HE}}^{\text{1-loop}} - \mathcal{F}\partial_{\mathcal{G}}\mathcal{L}_{\text{HE}}^{\text{1-loop}}\right)\partial_{\mathcal{F}}^2\partial_{\mathcal{G}}\mathcal{L}_{\text{HE}}^{\text{1-loop}}\\
&\quad + \partial_{\mathcal{F}}\mathcal{L}_{\text{HE}}^{\text{1-loop}}\,\partial_{\mathcal{F}}^2\mathcal{L}_{\text{HE}}^{\text{1-loop}} - \partial_{\mathcal{G}}\mathcal{L}_{\text{HE}}^{\text{1-loop}}\,\partial_{\mathcal{F}}\partial_{\mathcal{G}}\mathcal{L}_{\text{HE}}^{\text{1-loop}}\,,\\
\pi_{\star\bar{F}\star\bar{F}}^{\text{2-loop}}\big|_{\text{1PR}} &= \left(\mathcal{F}\partial_{\mathcal{F}}\mathcal{L}_{\text{HE}}^{\text{1-loop}} + \mathcal{G}\partial_{\mathcal{G}}\mathcal{L}_{\text{HE}}^{\text{1-loop}}\right)\partial_{\mathcal{F}}\partial_{\mathcal{G}}^2\mathcal{L}_{\text{HE}}^{\text{1-loop}} + \left(\mathcal{G}\partial_{\mathcal{F}}\mathcal{L}_{\text{HE}}^{\text{1-loop}} - \mathcal{F}\partial_{\mathcal{G}}\mathcal{L}_{\text{HE}}^{\text{1-loop}}\right)\partial_{\mathcal{G}}^3\mathcal{L}_{\text{HE}}^{\text{1-loop}}\\
&\quad + \partial_{\mathcal{F}}\mathcal{L}_{\text{HE}}^{\text{1-loop}}\,\partial_{\mathcal{G}}^2\mathcal{L}_{\text{HE}}^{\text{1-loop}} + \partial_{\mathcal{G}}\mathcal{L}_{\text{HE}}^{\text{1-loop}}\,\partial_{\mathcal{F}}\partial_{\mathcal{G}}\mathcal{L}_{\text{HE}}^{\text{1-loop}}\,,\\
\pi_{\star\bar{F}\bar{F}}^{\text{2-loop}}\big|_{\text{1PR}} &= \left(\mathcal{F}\partial_{\mathcal{F}}\mathcal{L}_{\text{HE}}^{\text{1-loop}} + \mathcal{G}\partial_{\mathcal{G}}\mathcal{L}_{\text{HE}}^{\text{1-loop}}\right)\partial_{\mathcal{F}}^2\partial_{\mathcal{G}}\mathcal{L}_{\text{HE}}^{\text{1-loop}} + \left(\mathcal{G}\partial_{\mathcal{F}}\mathcal{L}_{\text{HE}}^{\text{1-loop}} - \mathcal{F}\partial_{\mathcal{G}}\mathcal{L}_{\text{HE}}^{\text{1-loop}}\right)\partial_{\mathcal{F}}\partial_{\mathcal{G}}^2\mathcal{L}_{\text{HE}}^{\text{1-loop}}\\
&\quad + \partial_{\mathcal{F}}\mathcal{L}_{\text{HE}}^{\text{1-loop}}\,\partial_{\mathcal{F}}\partial_{\mathcal{G}}\mathcal{L}_{\text{HE}}^{\text{1-loop}} + \frac{1}{2}\left(\partial_{\mathcal{F}}^2\mathcal{L}_{\text{HE}}^{\text{1-loop}} - \partial_{\mathcal{G}}^2\mathcal{L}_{\text{HE}}^{\text{1-loop}}\right)\partial_{\mathcal{G}}\mathcal{L}_{\text{HE}}^{\text{1-loop}}\,.
\end{aligned} \tag{2.149}$$

For convenience, we also define the analogous quantities $\pi_i^{\text{2-loop}}\big|_{\text{1PI}}$ for the 1PI contributions. These follow from Eq. (2.148) by replacing the labels 1PR $\to$ 1PI and omitting the corrections $\Delta\pi_i^{\text{2-loop}}$. Their explicit expressions can be worked out straightforwardly from Eq. (2.124). However, as this results in rather unwieldy expressions we do not provide them here. Defining $\pi_i^{\text{2-loop}} = \pi_i^{\text{2-loop}}\big|_{\text{1PI}} + \pi_i^{\text{2-loop}}\big|_{\text{1PR}}$, the two-loop photon polarization tensor can then be represented compactly as

$$(\Pi^{\text{2-loop}}[\bar{A}])^{\mu\nu}(k,k') = \int_x \mathrm{e}^{\mathrm{i}x(k+k')}\sum_i p_i^{\mu\nu}(k,k')\,\pi_i^{\text{2-loop}}(\mathcal{F},\mathcal{G}) + O(k^4)\,. \tag{2.150}$$

Here, the coefficients $\pi_i^{\text{2-loop}}\big|_{\text{1PI}}$ encode the contributions due to the diagram depicted in Fig. 2.1 (left) and $\pi_i^{\text{2-loop}}\big|_{\text{1PR}}$ those associated with Fig. 2.1 (right). We in particular emphasize that all topologically inequivalent diagrams arising from the different possible insertions of the internal photon line in the left-hand diagram, and of the 1PR tadpole in the right-hand diagram, are consistently accounted for. As explicitly demonstrated by the above calculation, the diagrams which are 1PR with regard to the

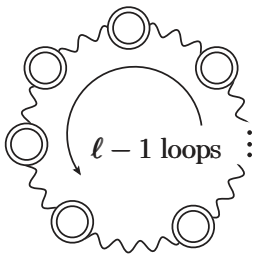

Figure 2.4: Feynman diagrams encoding the dominant strong-field behavior of $\mathcal{L}_{\text{HE}}^{\ell\text{-loop}}\big|_{\text{1PI}}$ for $\ell \geq 2$.

diagrammatic structure mediating between the two open indices in Eq. (2.146) are cancelled by an analogous contribution contained in $\delta^2\Gamma_{\text{HE}}^{\text{2-loop}}[\bar{A}]\big|_{\text{1PR}}/\delta\bar{A}\delta\bar{A}$. Equation (2.150) amounts to the result originally derived in Ref. [12] in a less formal way, namely by drawing all connected diagrams featuring two open photon lines at two loops and eliminating all those that correspond to iterations of more elementary ones. The analogous expression for the two-loop photon current in Eq. (2.145) can be derived exactly along the same lines. Because we do not need its explicit expression for the subsequent discussion, here we do not work out this result.

2.4.3 Higher-loop contributions

Beyond two loops relatively little is known about $\Gamma_{\text{HE}}[\bar{A}]$. Especially for the 1PI part so-far only an incomplete subset of contributions on the three-loop level has been evaluated explicitly in constant fields and 1+1 space-time dimensions [66, 67]. On the other hand, in 3+1 dimensions and constant fields the leading contributions of $\Gamma_{\text{HE}}[\bar{A}]\big|_{\text{1PI}}$ in the strong field limit characterized by $\mathcal{F} \gg (m^2/e)^2$ and $\mathcal{G} \ll (m^2/e)^2$ are known analytically at all loop orders. These were originally derived by Ritus [33] on the basis of the Callan-Symanzik equation [68, 69] and read

$$\begin{aligned}
\mathcal{L}_{\text{HE}}^{\text{1-loop}} &= e^2\mathcal{F}\,\frac{\beta_1}{4\pi}\ln\!\Big(\tfrac{e\sqrt{2\mathcal{F}}}{m^2}\Big)\Big[1+O\Big(\ln^{-1}\!\Big(\tfrac{e\sqrt{2\mathcal{F}}}{m^2}\Big)\Big)\Big]+O(\mathcal{G}^2) \quad \text{and} \\
\mathcal{L}_{\text{HE}}^{\ell\text{-loop}}\big|_{\text{1PI}} &= e^2\mathcal{F}\,\frac{\beta_1}{4\pi}\,\frac{\beta_2/\beta_1^2}{\ell-1}\Big(\alpha\beta_1\ln\!\Big(\tfrac{e\sqrt{2\mathcal{F}}}{m^2}\Big)\Big)^{\ell-1}\Big[1+O\Big(\ln^{-1}\!\Big(\tfrac{e\sqrt{2\mathcal{F}}}{m^2}\Big)\Big)\Big]+O(\mathcal{G}^2) \quad \text{for} \quad \ell\geq 2\,,
\end{aligned} \tag{2.151}$$

where $\beta_1 = 1/(3\pi)$ and $\beta_2 = 1/(4\pi^2)$ are the renormalization scheme independent coefficients of the QED β function,

$$\beta(\alpha(\mu^2)) = \frac{1}{\alpha(\mu^2)}\,\mu^2\frac{\partial}{\partial\mu^2}\alpha(\mu^2)\,, \quad \text{with} \quad \beta(\alpha) = \beta_1\alpha+\beta_2\alpha^2+O(\alpha^3)\,, \tag{2.152}$$

governing the running of the fine structure constant. They are the result of a close connection between the short-distance behaviour of renormalized Green's functions and the strong field limit of associated quantities calculated in prescribed background fields [33, 43, 45, 70–73] in the absence of zero modes [74]. Figure 2.4 depicts the ℓ-loop Feynman diagrams giving rise to the leading strong-field behavior of $\mathcal{L}_{\text{HE}}^{\ell\text{-loop}}\big|_{\text{1PI}}$ in Eq. (2.151) for $\ell \geq 2$ [75]. All these diagrams are generated by the last term in the first line of Eq. (2.39) [12]. For completeness, we note that the analogous results for scalar QED have

Figure 2.5: Diagrammatic representation of the 1PR part of the Heisenberg-Euler effective action at three loops. For the definition of the double line see Fig. 2.2.

exactly the same structure; in this case the coefficient β_1 and β_1 have of course to be replaced by those of the β function of scalar QED. See also Ref. [75] for a possible new approach to computations at higher loop order. One can easily verify that the result given for the ratio of the strong field limits of the 1PI contributions at two and one loops in Eq. (2.142) indeed equals $\alpha\beta_2/\beta_1$ as predicted by Eq. (2.151).

The situation is somewhat different for the 1PR part. In fact, all constant-field 1PR diagrams at three loops are known explicitly; see Fig. 2.5 for an illustration. The reason for this is that, similarly to the two-loop result Eq. (2.128), these are generated from lower-order 1PI diagrams by derivatives for the field strength tensor and appropriate contractions. In general, along these lines the ℓ-loop 1PR part of $\mathcal{L}_{\rm HE}$ in constant fields is fully determined by $\mathcal{L}_{\rm HE}^{n\text{-loop}}\big|_{\rm 1PI}$ with $n \in \{1, 2, \ldots, \ell - 1\}$. As detailed in Secs. 2.3.1 and 2.4.1 all diagrams relevant for this construction have been evaluated explicitly up to two loops. We note that a generalization of this procedure allowing to construct all possible 1PR contributions to a given quantity in constant electromagnetic fields from 1PI contributions of lower loop order is also available [17]. The latter was in particular used in Ref. [76] to determine the leading strong-field behavior of $\Gamma_{\rm HE}[\bar{A}]\big|_{\rm 1PR}$ at any loop order. The formal expression for the contribution depicted on the left-hand side of Fig. 2.5 can be readily obtained by expanding the expression given explicitly in the second line of Eq. (2.39) to three loops, yielding

$$\Gamma_{\rm HE}^{\text{3-loop}}[\bar{A}]\big|_{\rm 1PR}^{\rm (left)} = \frac{1}{2}\iiiint (S_\psi^{(1)}[\bar{A}])_\mu D^{\mu\alpha}(S_\psi^{(2)}[\bar{A}])_{\alpha\beta} D^{\beta\nu}(S_\psi^{(1)}[\bar{A}])_\nu \,. \tag{2.153}$$

With the help of Eqs. (2.20), (2.76) and (2.78), and the generalization of Eq. (2.79) to the product of four momenta in d space-time dimensions,

$$\int_k \frac{k^\alpha k^\beta k^\mu k^\nu}{(k^2)^2}(2\pi)^d \delta(k) = \frac{g^{\alpha\beta}g^{\mu\nu} + g^{\alpha\mu}g^{\beta\nu} + g^{\alpha\nu}g^{\beta\mu}}{d(d+2)} \,, \tag{2.154}$$

this expression can be readily evaluated explicitly. The associated Lagrangian be cast in the following form

$$\begin{aligned}\mathcal{L}_{\rm HE}^{\text{3-loop}}\big|_{\rm 1PR}^{\rm (left)} = \frac{1}{3}\Bigg[&\frac{\partial\mathcal{L}_{\rm HE}^{\text{1-loop}}}{\partial\bar{F}^{\mu\nu}}\frac{\partial^2\mathcal{L}_{\rm HE}^{\text{1-loop}}}{\partial\bar{F}_{\mu\nu}\partial\bar{F}_{\alpha\beta}}\frac{\partial\mathcal{L}_{\rm HE}^{\text{1-loop}}}{\partial\bar{F}^{\alpha\beta}} + \frac{\partial\mathcal{L}_{\rm HE}^{\text{1-loop}}}{\partial\bar{F}^{\mu\nu}}\frac{\partial^2\mathcal{L}_{\rm HE}^{\text{1-loop}}}{\partial\bar{F}_{\alpha\nu}\partial\bar{F}_{\mu\beta}}\frac{\partial\mathcal{L}_{\rm HE}^{\text{1-loop}}}{\partial\bar{F}^{\alpha\beta}} \\ &+ \frac{\partial\mathcal{L}_{\rm HE}^{\text{1-loop}}}{\partial\bar{F}^{\mu\nu}}\frac{\partial^2\mathcal{L}_{\rm HE}^{\text{1-loop}}}{\partial\bar{F}_{\alpha\nu}\partial\bar{F}^{\alpha\beta}}\frac{\partial\mathcal{L}_{\rm HE}^{\text{1-loop}}}{\partial\bar{F}_{\mu\beta}}\Bigg].\end{aligned} \tag{2.155}$$

The right-hand diagram in Fig. 2.5 is encoded in the contribution $\sim S_\psi^{(3)}$ in the last line of Eq. (2.39),

yielding the formal expression

$$\begin{aligned}\Gamma_{\text{HE}}^{\text{3-loop}}[\bar{A}]\big|_{\text{1PR}}^{(\text{right})} &= -\frac{\mathrm{i}}{2}\iiiint (S_\psi^{(1)}[\bar{A}])_\mu D^{\mu\alpha}(S_\psi^{(3)}[\bar{A}])_{\alpha\beta\gamma} D^{\beta\gamma} \\ &= \iint (S_\psi^{(1)}[\bar{A}])_\mu D^{\mu\alpha}\frac{\delta}{\delta\bar{A}^\alpha}\Gamma_{\text{HE}}^{\text{2-loop}}[\bar{A}]\big|_{\text{1PI}}\,,\end{aligned} \tag{2.156}$$

where we made use of Eqs. (2.30) and (2.40) to arrive at the representation given in the second line. The functional derivative of the two-loop 1PI contribution to $\Gamma_{\text{HE}}[\bar{A}]$ in a constant field in Eq. (2.156) can be rewritten in the same way as its one-loop analogue (2.75). Upon insertion of Eqs. (2.20) and (2.78), we then obtain

$$\mathcal{L}_{\text{HE}}^{\text{3-loop}}\big|_{\text{1PR}}^{(\text{right})} = \frac{\partial\mathcal{L}_{\text{HE}}^{\text{1-loop}}}{\partial\bar{F}_{\mu\nu}}\frac{\partial\mathcal{L}_{\text{HE}}^{\text{2-loop}}\big|_{\text{1PI}}}{\partial\bar{F}^{\mu\nu}}\,. \tag{2.157}$$

We reiterate that while expressions similar to Eqs. (2.155) and (2.157) can be written down for the 1PR contributions to $\mathcal{L}_{\text{HE}}$ at higher loops, these are not really of practical use as long as no explicit results are available for $\mathcal{L}_{\text{HE}}^{\ell\text{-loop}}\big|_{\text{1PI}}$ with $\ell \geq 3$.

However, note that at each loop order there is at least one 1PR diagram which can be expressed exclusively in terms of $\mathcal{L}_{\text{HE}}^{\text{1-loop}}$ and derivatives thereof. An ℓ-loop diagram of this type consists of ℓ charged particle loops that are coupled by photon propagators. The latter mediate only between different loops and a given pair of loops is coupled only once. The number of these diagrams grows with increasing loop order because higher-loop diagrams may contain a larger variety of effective soft-photon vertices (2.76). Particularly in the limit of $|\mathcal{F}| \gg (m^2/e)^2$ and $|\mathcal{G}| \ll (m^2/e)^2$ it can be shown that the dominant diagram of this type at ℓ loops is the one which can be expressed as the contraction of two first derivatives and $\ell - 2$ second derivatives of $\mathcal{L}_{\text{HE}}^{\text{1-loop}}$ for $\bar{F}^{\mu\nu}$.

To be specific, this follows from the fact that for $\mathcal{G} = 0$ we have $\partial/\partial\bar{F}^{\mu\nu} \sim \partial/\partial\sqrt{2\mathcal{F}}$, which implies $S_\psi^{(n)}[\bar{A}]\big|_{\mathcal{G}=0} \sim (\partial/\partial\sqrt{2\mathcal{F}})^n \mathcal{L}_{\text{HE}}^{\text{1-loop}}\big|_{\mathcal{G}=0}$ for the effective n soft-photon couplings (2.76) within 1PR tadpole structures [21]. With the help of the exact series representation of $\mathcal{L}_{\text{HE}}^{\text{1-loop}}\big|_{\mathcal{G}=0}$ in Eq. (2.72) it is then straightforward to infer that to leading order these effective couplings scales as

$$S_\psi^{(n)}[\bar{A}]\big|_{\mathcal{G}=0} \sim \alpha^{n/2}\,(e\sqrt{2\mathcal{F}})^{2-n}\begin{cases}\ln\!\left(\frac{e\sqrt{2\mathcal{F}}}{m^2}\right) & \text{for} \quad 0 \leq n \leq 2 \\ 1 & \text{for} \quad n \geq 3\end{cases} \tag{2.158}$$

with respect to the coupling $e \sim \alpha^{1/2}$ and the RG invariant combination $e\sqrt{2\mathcal{F}}$. This in particular means that the effective vertices with $n \geq 3$ go to zero for $|\mathcal{F}| \to \infty$, while those with $n \leq 2$ increase at least logarithmically with $\mathcal{F}$. If the logarithm in the first line of Eq. (2.158) would be absent, each 1PR compound $n \geq 2$ soft-photon coupling of generic loop order formed by the contraction of several $S_\psi^{(n')}[\bar{A}]$ by photon lines would again scale as $(\sqrt{2\mathcal{F}})^{2-n}$. In the presence of the logarithm this clearly remains only true for the 1PR effective couplings exclusively made up of effective vertices $S_\psi^{(n')}[\bar{A}]$ with $n' \geq 3$; couplings containing powers of $S_\psi^{(2)}[\bar{A}]$ are logarithmically enhanced. To obtain a scalar contribution each open photon coupling ultimately needs to be saturated with a current $S_\psi^{(1)}[\bar{A}]$. This implies that in this case all possible viable contributions to $\mathcal{L}_{\text{HE}}$ formed by sewing together 1-loop diagrams only to form 1PR structures would scale as $\sim 2\mathcal{F}$. With the logarithm present this scaling clearly can be

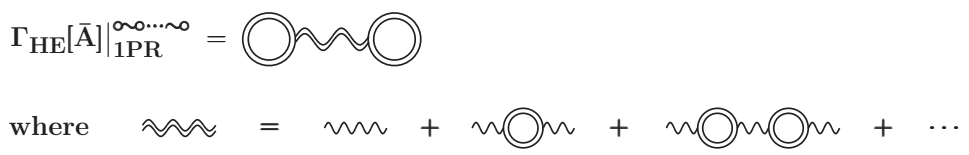

Figure 2.6: Diagrammatic representation of 1PR bubble chain contributions to the Heisenberg-Euler effective action at arbitrarily loops. The double wiggle line represents the photon propagator with arbitrarily many one-loop insertions. For the definition of the straight double line see Fig. 2.2.

enhanced at best to $2\mathcal{F}\ln^{\ell}\sqrt{2\mathcal{F}}$ for an ℓ-loop diagram. Clearly, the only ℓ-loop diagram scaling like this is the one made up of two currents $S^{(1)}_{\psi}[\bar{A}]$ connected by a chain of $\ell-2$ vacuum bubbles $S^{(2)}_{\psi}[\bar{A}]$. At the same time ℓ-loop diagrams with a different topology are relatively suppressed by at least a factor of $\ln^{-1}\sqrt{2\mathcal{F}}$.

Therefore, the diagrams constituting the leading contribution to $\mathcal{L}_{\rm HE}$ in the limit of $|\mathcal{F}| \gg (m^2/e)^2$ and $|\mathcal{G}| \ll (m^2/e)^2$ at a fixed loop order $\ell \geq 2$ for this specific subset of 1PR diagrams is encoded in the expression in the second line of Eq. (2.39),

$$\Gamma_{\rm HE}[\bar{A}]\big|^{\infty\circ\cdots\circ\infty}_{\rm 1PR} := \frac{1}{2}\iint (S^{(1)}_{\psi}[\bar{A}])_{\mu}[(D^{-1}-S^{(2)}_{\psi}[\bar{A}])^{-1}]^{\mu\nu}(S^{(1)}_{\psi}[\bar{A}])_{\nu}\,. \tag{2.159}$$

For a graphical representation of Eq. (2.159) see Fig. 2.6. The expression in the squared brackets in Eq. (2.159) amounts to the dressed, *one-loop bubble chain resummed* photon propagator. Aiming at an its explicit evaluation in the considered limit, we first note that in a constant field fulfilling $\mathcal{G}=0$ and $\mathcal{F}\geq 0$, the required two-point function $S^{(2)}_{\psi}[\bar{A}] = -\Pi^{\text{1-loop}}[\bar{A}]$ in the soft-photon limit following from Eq. (2.80) can be expressed as

$$\begin{aligned}(S^{(2)}[\bar{A}])^{\mu\nu}(k,k')\big|_{\mathcal{G}=0} = (2\pi)^4\delta(k+k')\Big\{&P_0^{\mu\nu}k^2\frac{\partial\mathcal{L}^{\text{1-loop}}_{\rm HE}}{\partial\mathcal{F}} + P_{\perp}^{\mu\nu}\Big(k^2\frac{\partial\mathcal{L}^{\text{1-loop}}_{\rm HE}}{\partial\mathcal{F}} + (k\bar{F})^2\frac{\partial^2\mathcal{L}^{\text{1-loop}}_{\rm HE}}{\partial\mathcal{F}^2}\Big)\\ &+ P_{\parallel}^{\mu\nu}\Big[k^2\Big(\frac{\partial\mathcal{L}^{\text{1-loop}}_{\rm HE}}{\partial\mathcal{F}} - 2\mathcal{F}\frac{\partial^2\mathcal{L}^{\text{1-loop}}_{\rm HE}}{\partial\mathcal{G}^2}\Big) + (k\bar{F})^2\frac{\partial^2\mathcal{L}^{\text{1-loop}}_{\rm HE}}{\partial\mathcal{G}^2}\Big] + O(k^4)\Big\}\Big|_{\mathcal{G}=0}\,,\end{aligned} \tag{2.160}$$

where we made use of the projectors defined in Eq. (2.88). Decomposing the transverse part of the (inverse) photon propagator (2.20) in terms of the same projectors (the longitudinal part can be dropped because the effective couplings $S^{(n)}_{\psi}[\bar{A}]$ fulfill the Ward identity) and using $(\sum_i c_i P_i^{\mu\nu})(\sum_i c_i^{-1}P_{i,\nu\rho}) = \delta^{\mu}_{\rho}$ with $i\in\{0,\parallel,\perp\}$, we obtain

$$\begin{aligned}[(D^{-1}-S^{(2)}_{\psi}[\bar{A}])^{-1}]^{\mu\nu}(k,k')\big|_{\mathcal{G}=0} = (2\pi)^4\delta(k+k')\Big\{&\frac{P_0^{\mu\nu}}{k^2(1-\partial_{\mathcal{F}}\mathcal{L}^{\text{1-loop}}_{\rm HE})} + \frac{P_{\perp}^{\mu\nu}}{k^2(1-\partial_{\mathcal{F}}\mathcal{L}^{\text{1-loop}}_{\rm HE}) - (k\bar{F})^2\partial^2_{\mathcal{F}}\mathcal{L}^{\text{1-loop}}_{\rm HE}}\\ &+ \frac{P_{\parallel}^{\mu\nu}}{k^2(1-\partial_{\mathcal{F}}\mathcal{L}^{\text{1-loop}}_{\rm HE}+2\mathcal{F}\partial^2_{\mathcal{G}}\mathcal{L}^{\text{1-loop}}_{\rm HE}) - (k\bar{F})^2\partial^2_{\mathcal{G}}\mathcal{L}^{\text{1-loop}}_{\rm HE}} + O(k^0)\Big\}\Big|_{\mathcal{G}=0}\,.\end{aligned} \tag{2.161}$$

For a diagrammatic representation of the photon propagator (2.161) dressed by one-loop vacuum bubbles

see Fig. 2.6. Because of $P_\parallel^{\mu\nu} \sim (k^\star\bar{F})^\mu(k^\star\bar{F})^\nu$ for $\mathcal{G}=0$, which immediately implies $P_\parallel^{\mu\nu}(S^{(1)}[\bar{A}])_\nu \sim \mathcal{G}$, upon insertion into Eq. (2.159) the term $\sim P_\parallel^{\mu\nu}$ in Eq. (2.161) does not contribute for $\mathcal{G}=0$. With the explicit expression for $S^{(1)}[\bar{A}]$ given in Eq. (2.78) we thus arrive at

$$\begin{aligned}\mathcal{L}_{\rm HE}\big|^{\infty\circ\cdots\circ\infty}_{\rm 1PR,\,\mathcal{G}=0} &= \frac{1}{2}\Big(\frac{\partial\mathcal{L}^{\text{1-loop}}_{\rm HE}}{\partial\mathcal{F}}\Big)^2\int_k(2\pi)^4\delta(k)\,\frac{(k\bar{F})^2}{k^2(1-\partial_\mathcal{F}\mathcal{L}^{\text{1-loop}}_{\rm HE})-(k\bar{F})^2\partial^2_\mathcal{F}\mathcal{L}^{\text{1-loop}}_{\rm HE}}\bigg|_{\mathcal{G}=0}\\ &= \frac{1}{2}\frac{(\partial_\mathcal{F}\mathcal{L}^{\text{1-loop}}_{\rm HE})^2}{1-\partial_\mathcal{F}\mathcal{L}^{\text{1-loop}}_{\rm HE}}\sum_{n=0}^{\infty}\bigg(\frac{\partial^2_\mathcal{F}\mathcal{L}^{\text{1-loop}}_{\rm HE}}{1-\partial_\mathcal{F}\mathcal{L}^{\text{1-loop}}_{\rm HE}}\bigg)^n\int_k(2\pi)^4\delta(k)\Big(\frac{(k\bar{F})^2}{k^2}\Big)^{n+1}\bigg|_{\mathcal{G}=0}.\end{aligned}\tag{2.162}$$

In the last step we need to evaluate the momentum integral. To perform this integral it is convenient to employ a Lorentz transformation to a reference system in which $\mathcal{F}$ amounts to a purely magnetic field. In this system we have $(k\bar{F})^2|_{\mathcal{G}=0} = 2\mathcal{F}k_\mu k_\nu g_\perp^{\mu\nu}$, with the metric $g_\perp^{\mu\nu}$ singling out the $d-2$ spatial components perpendicular to the magnetic field. Noting that the generalization of Eqs. (2.79) and (2.154) to $2n$ factors of k^μ in d space-time dimensions reads

$$\int_k\frac{k^{\sigma_1}\cdots k^{\sigma_{2n}}}{(k^2)^n}(2\pi)^d\delta(k) = \frac{g^{(\sigma_1\sigma_2}g^{\sigma_3\sigma_4}\cdots g^{\sigma_{2n-1}\sigma_{2n})}}{d(d+2)(d+4)\cdots(d+2n-2)}\,,\tag{2.163}$$

where we employed a normalized symmetrization in the numerator on the right-hand side, it is then obvious that the contraction of this numerator with $g_{\perp,\sigma_1\sigma_2}\cdots g_{\perp,\sigma_{2n-1}\sigma_{2n}}$ results in the factor in the nominator with $d\to d-2$. In turn, we find

$$\int_k\Big(\frac{(k\bar{F})^2}{k^2}\Big)^{n+1}\bigg|_{\mathcal{G}=0}(2\pi)^d\delta(k) = (2\mathcal{F})^{n+1}\frac{d-2}{d+2n}\xrightarrow{d=4}(2\mathcal{F})^{n+1}\frac{1}{n+2}\,,\tag{2.164}$$

such that, after performing the sum over n in the last line of Eq. (2.162) we obtain

$$\mathcal{L}_{\rm HE}\big|^{\infty\circ\cdots\circ\infty}_{\rm 1PR,\,\mathcal{G}=0} = \mathcal{F}\frac{(\partial_\mathcal{F}\mathcal{L}^{\text{1-loop}}_{\rm HE})^2}{1-\partial_\mathcal{F}\mathcal{L}^{\text{1-loop}}_{\rm HE}}\frac{-[\ln(1-\xi)+\xi]}{\xi^2}\bigg|_{\mathcal{G}=0},\quad\text{with}\quad\xi=\frac{2\mathcal{F}\partial^2_\mathcal{F}\mathcal{L}^{\text{1-loop}}_{\rm HE}}{1-\partial_\mathcal{F}\mathcal{L}^{\text{1-loop}}_{\rm HE}}\,.\tag{2.165}$$

On the other hand, with the help of the binomial theorem, the Cauchy product and Eq. (2.164), the last line of Eq. (2.162) can alternatively be represented as

$$\begin{aligned}&\mathcal{L}_{\rm HE}\big|^{\infty\circ\cdots\circ\infty}_{\rm 1PR,\,\mathcal{G}=0} = \sum_{n=0}^{\infty}\mathcal{L}^{(n+2)\text{-loop}}_{\rm HE}\big|^{\infty\circ\cdots\circ\infty}_{\rm 1PR,\,\mathcal{G}=0},\\ &\text{with}\quad\mathcal{L}^{(n+2)\text{-loop}}_{\rm HE}\big|^{\infty\circ\cdots\circ\infty}_{\rm 1PR,\,\mathcal{G}=0} = \mathcal{F}\sum_{j=0}^{n}\binom{n}{j}\frac{1}{n-j+2}\Big(\frac{\partial\mathcal{L}^{\text{1-loop}}_{\rm HE}}{\partial\mathcal{F}}\Big)^{j+2}\Big(2\mathcal{F}\frac{\partial^2\mathcal{L}^{\text{1-loop}}_{\rm HE}}{\partial\mathcal{F}^2}\Big)^{n-j}\bigg|_{\mathcal{G}=0}.\end{aligned}\tag{2.166}$$

One can easily check that exactly the same results are obtained also in the complementary parameter regime where $\mathcal{F}<0$. Note that Eqs. (2.128) and (2.155) considered above amount to the two- and three-loop representatives of this specific class of diagrams in a generic constant electromagnetic field. For $\mathcal{G}=0$ they give rise to the two lowest-order contributions to the infinite sum in the first line of Eq. (2.166). Because for $|\mathcal{F}|\gg(m^2/e)^2$ we have to leading order $\partial_\mathcal{F}\mathcal{L}^{\text{1-loop}}_{\rm HE}\big|_{\mathcal{G}=0}\sim\ln\sqrt{2\mathcal{F}}$ while $\partial^2_\mathcal{F}\mathcal{L}^{\text{1-loop}}_{\rm HE}\big|_{\mathcal{G}=0}\sim$

$1/(2\mathcal{F})$ (cf. also Eq. (2.158) above), the leading contribution in this limit at a given loop order is encoded in the term characterized by $j = n$ in the second line of Eq. (2.166), i.e.,

$$\begin{aligned}\Delta\mathcal{L}_{\text{HE}}^{\ell\text{-loop}}\big|_{\text{1PR},\,\mathcal{G}=0}^{\infty\text{-}\infty\cdots\infty} &:= \frac{1}{2}\,\mathcal{F}\left(\frac{\partial\mathcal{L}_{\text{HE}}^{\text{1-loop}}}{\partial\mathcal{F}}\right)^{\ell}\Bigg|_{\mathcal{G}=0} \\ &= \frac{1}{2}\,e^2\mathcal{F}\,\frac{\beta_1}{4\pi}\ln\!\left(\tfrac{e\sqrt{2\mathcal{F}}}{m^2}\right)\left(\alpha\beta_1\ln\!\left(\tfrac{e\sqrt{2\mathcal{F}}}{m^2}\right)\right)^{\ell-1}\left[1+\mathcal{O}\!\left(\ln^{-1}\!\left(\tfrac{e\sqrt{2\mathcal{F}}}{m^2}\right)\right)\right] \qquad (2.167)\end{aligned}$$

for $\ell \geq 2$. Here we made use of the first line of Eq. (2.151) to arrive at the explicit result given in the last step. As a consistency check we note that this result correctly reproduces the leading term in Eq. (2.141) for $\ell = 2$. Moreover, in line with Eqs. (2.151) and (2.167) the result given for the ratio of the strong field limits of the 1PR and 1PI contributions at two loops in Eq. (2.142) can be expressed as $\beta_1^2/(2\beta_2)\ln\chi^{-1}$. A comparison with Eq. (2.151) unveils that beyond one loop Eq. (2.167) is logarithmically enhanced and thus dominates the former at each loop order $\ell \geq 2$ in the strong field limit. Though we have not yet discussed the scaling of 1PR contributions containing also 1PI substructures, such as, e.g., the right-hand diagram in Fig. 2.5, this already implies that the 1PR sector dominates the 1PI one for $|\mathcal{F}| \gg (m^2/e)^2$ and $|\mathcal{G}| \ll (m^2/e)^2$. Resumming Eq. (2.167) to all loop orders fulfilling $\ell \geq 2$, we obtain

$$\begin{aligned}\Delta\mathcal{L}_{\text{HE}}\big|_{\text{1PR},\,\mathcal{G}=0}^{\infty\text{-}\infty\cdots\infty} &:= \frac{1}{2}\,\mathcal{F}\left(\frac{\partial\mathcal{L}_{\text{HE}}^{\text{1-loop}}}{\partial\mathcal{F}}\right)^{2}\frac{1}{1-\partial_{\mathcal{F}}\mathcal{L}_{\text{HE}}^{\text{1-loop}}}\Bigg|_{\mathcal{G}=0} \\ &= \frac{1}{2}\,e^2\mathcal{F}\,\frac{\beta_1}{4\pi}\,\alpha^{\text{1-loop}}(e\sqrt{2\mathcal{F}})\,\beta_1\ln^2\!\left(\tfrac{e\sqrt{2\mathcal{F}}}{m^2}\right)\left[1+\mathcal{O}\!\left(\ln^{-1}\!\left(\tfrac{e\sqrt{2\mathcal{F}}}{m^2}\right)\right)\right], \qquad (2.168)\end{aligned}$$

with the one-loop running of the fine structure given by

$$\alpha^{\text{1-loop}}(\mu^2) = \frac{\alpha}{1-\alpha\beta_1\ln(\frac{\mu^2}{m^2})}\,. \qquad (2.169)$$

In the strong field limit considered here we obviously have $\alpha^{\text{1-loop}}(e\sqrt{2\mathcal{F}}) \gg \alpha$.

Note, however, that Eq. (2.169) eventually diverges at the Landau pole $\mu^2 = m^2\exp\{1/(\alpha\beta_1)\}$, which signalizes the breakdown of a perturbative loop expansion of $\mathcal{L}_{\text{HE}}$ for exponentially large field strengths $|\sqrt{2\mathcal{F}}|$ approaching the value of $(m^2/e)\exp\{1/(\alpha\beta_1)\}$. For completeness, we also remark that this limiting value is by a factor of two smaller than the field strength for which $\mathcal{L}_{\text{HE}}^{\text{1-loop}}\big|_{\text{1PR}}$ formally surpasses $\mathcal{L}_{\text{HE}}^{\text{1-loop}}$ in the strong field limit; cf. the discussion in the context of Eq. (2.143) above. Of course, Eq. (2.168) can alternatively be extracted directly from Eq. (2.165) where it amounts to the limit of $\xi \to 0$.

A comparison of Eq. (2.168) with Eq. (2.128), which for $\mathcal{G} = 0$ reads

$$\mathcal{L}_{\text{HE}}\big|_{\text{1PR},\,\mathcal{G}=0}^{\text{2-loop}} = \frac{1}{2}\,\mathcal{F}\left(\frac{\partial\mathcal{L}_{\text{HE}}^{\text{1-loop}}}{\partial\mathcal{F}}\right)^{2}, \qquad (2.170)$$

unveils that in the limit of $|\mathcal{F}| \gg (m^2/e)^2$ the leading strong-field behavior of the former can be obtained by multiplying the analogous result for the latter by a factor of $\alpha^{\text{1-loop}}(e\sqrt{2\mathcal{F}})/\alpha$. This in particular implies that, when aiming at the determination of the strong-field behavior of a contribution to $\Gamma_{\text{HE}}[\bar{A}]$

in constant fields involving one-loop bubble chain resummed photon propagators connecting tadpole structures to the rest of the diagram, one can instead evaluate the strong field limit of the simpler diagram were these dressed photon propagators are replaced by bare ones. The result for the desired diagram is then obtained from this expression by replacing each factor of α coming with a bare photon propagator by $\alpha^{1\text{-loop}}(e\sqrt{2\mathcal{F}})$.

While we have now established that Eqs. (2.167) and (2.168) comprise the leading contributions in the 1PR sector formed exclusively by sewing together one-loop diagrams, a assessment of the relative importance of other 1PR diagrams is still missing here. It is, however, straightforward. To this end, we first note that higher-loop 1PI effective vertices mediating interactions among 1PR tadpole structures can be readily obtained from Eq. (2.76): the $\ell \geq 2$ loop 1PI effective coupling follows by the replacement $\mathcal{L}_{\text{HE}}^{1\text{-loop}} \to \mathcal{L}_{\text{HE}}^{\ell\text{-loop}}\big|_{\text{1PI}}$. With the same reasoning as adopted in the derivation of Eq. (2.158), one can then straightforwardly deduce that in constant fields fulfilling $|\mathcal{F}| \gg (m^2/e)^2$ and $\mathcal{G} = 0$ to leading order the corresponding $\ell \geq 2$ loop effective couplings scale as

$$S_{\psi}^{(n),\ell\text{-loop}}[\bar{A}]\big|_{\mathcal{G}=0} \sim \alpha^{n/2+\ell-1}\,(e\sqrt{2\mathcal{F}})^{2-n}\,\ln^{\ell-2}\Big(\tfrac{e\sqrt{2\mathcal{F}}}{m^2}\Big)\begin{cases}\ln\Big(\tfrac{e\sqrt{2\mathcal{F}}}{m^2}\Big) & \text{for} \quad 0 \leq n \leq 2\\ 1 & \text{for} \quad n \geq 3\end{cases}. \tag{2.171}$$

From these scalings it is obvious that for any given loop order indeed no other 1PR diagram can be formed that could potentially surpass Eq. (2.167): all possible ℓ-loop 1PR diagrams containing at least one 1PI effective coupling (2.171) with $\ell \geq 2$ are suppressed relatively to those given in the second line of Eq. (2.167) by at least a factor of $\ln^{-1}(e\sqrt{2\mathcal{F}}/m^2)$.

Hence, together with the Maxwell term $\mathcal{L}_{\text{MW}} = -\mathcal{F}$ amounting to the zero-loop contribution, the expressions in the first line of Eq. (2.151) and in the second line of Eq. (2.167) constitute the leading contributions to $\mathcal{L}_{\text{HE}}$ at any given order $\ell \geq 1$ in a perturbative loop expansion. Resumming these contributions to all loops with the help of Eq. (2.168), we arrive at

$$\mathcal{L}_{\text{HE}} = -\mathcal{F} + e^2\mathcal{F}\,\frac{\beta_1}{4\pi}\ln\Big(\tfrac{e\sqrt{2\mathcal{F}}}{m^2}\Big)\Big[1+\frac{1}{2}\alpha^{1\text{-loop}}(e\sqrt{2\mathcal{F}})\,\beta_1\ln\Big(\tfrac{e\sqrt{2\mathcal{F}}}{m^2}\Big)\Big]\Big[1+O\Big(\ln^{-1}\Big(\tfrac{e\sqrt{2\mathcal{F}}}{m^2}\Big)\Big)\Big]+O(\mathcal{G}^2)\,, \tag{2.172}$$

which constitutes the all-loop strong field limit of the Heisenberg-Euler effective Lagrangian at zeroth order in a derivative expansion. Equation (2.172) supersedes an analogous result originally obtained by Ritus [33] based on the resummation of the leading logarithms in the 1PI sector given in Eq. (2.151) while not accounting for any of the 1PR contributions which turn out to be dominant; cf. also Ref. [45]. It corresponds to the expression originally derived in Ref. [76] in a somewhat different way. We emphasize the structural similarity of Eq. (2.172) with the sum of the Maxwell term, the one-loop result (2.151) and the leading strong-field contribution in Eq. (2.141) which arises from the 1PR diagram at two loops depicted in Fig. 2.3. In fact, upon replacing $\alpha \to \alpha^{1\text{-loop}}(e\sqrt{2\mathcal{F}})$ in the sum of these three terms we recover Eq. (2.172). This structure is actually not too surprising: From an effective field theory point of view it is natural that the couplings are evaluated at the relevant momentum scale, which in the strong field limit $|\mathcal{F}| \gg (m^2/e)^2$, $|\mathcal{G}| \ll (m^2/e)^2$ and specifically at low momentum transfer $|k^\mu| \ll m$ amounts to the RG invariant combination $e\sqrt{2\mathcal{F}}$. Because of $\mathcal{L}_{\text{HE}}^{\ell\text{-loop}} \sim \alpha^{\ell-1}$ the leading explicit dependence on α occurs only at two-loop order.

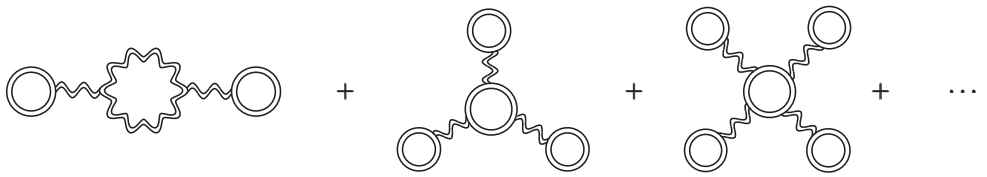

Figure 2.7: Contributions to $\mathcal{L}_{\text{HE}}$ scaling as $\sim e^2\mathcal{F}[\alpha^{\text{1-loop}}(e\sqrt{2\mathcal{F}})\beta_1\ln(e\sqrt{2\mathcal{F}}/m^2)]^n$ with $n \geq 2$ for $|\mathcal{F}| \gg (m^2/e)^2$ and $\mathcal{G} = 0$. For the definition of the double solid (wiggly) line see Fig. 2.2 (2.6).

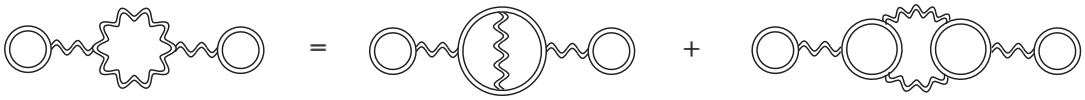

Figure 2.8: Decomposition of the leftmost diagram in Fig. 2.7 into topologically distinct building blocks.

It is then immediately clear that in the considered strong field limit the Feynman diagrams depicted in Fig. 2.7 should give rise to the leading contributions at quadratic order in $\alpha^{\text{1-loop}}(e\sqrt{2\mathcal{F}})$ and beyond as in these each power of $\alpha^{\text{1-loop}}(e\sqrt{2\mathcal{F}})$ comes in combination with a factor of $\ln(e\sqrt{2\mathcal{F}}/m^2)$; see Eq. (2.158). This results in contributions $\Delta\mathcal{L}^{(n)}_{\text{HE}}$ to $\mathcal{L}_{\text{HE}}$ scaling as

$$\Delta\mathcal{L}^{(n)}_{\text{HE}} \sim e^2\mathcal{F}\Big[\alpha^{\text{1-loop}}(e\sqrt{2\mathcal{F}})\beta_1\ln\Big(\tfrac{e\sqrt{2\mathcal{F}}}{m^2}\Big)\Big]^n \quad \text{with} \quad n \geq 2\,. \tag{2.173}$$

Here, we explicitly account for the factor of β_1 that effectively multiplies each logarithm; cf. Eq. (2.151). The first diagram in Fig. 2.7 actually accounts for two topologically distinct contributions: one where the two one-loop tadpoles couple to the same charged-particle loop within the bubble chain resummed photon propagator, and another one where they couple to two different loops. See Fig. 2.8 for an illustration. Apart from the first one, all diagrams in Fig. 2.7 can be readily obtained by sewing together only one-loop diagrams. To be specific, these contributions with $n \geq 3$ are obtained by connecting a one-loop n-photon vertex $S^{(n)}_\psi[\bar{A}]$ to n one-loop photon currents $S^{(1)}_\psi[\bar{A}]$ with one-loop bubble chain resummed photon propagators. As discussed in the context of Eq. (2.170) above, the corresponding expressions can be worked out by evaluating the depicted diagrams with the bare photon propagator and substituting $\alpha \to \alpha^{\text{1-loop}}(e\sqrt{2\mathcal{F}})$. Subleading contributions at a given order in $\alpha^{\text{1-loop}}(e\sqrt{2\mathcal{F}})$ feature at least one factor of the logarithm less. On the other hand, showing that the first diagram in Fig. 2.7 indeed reproduces the scaling in Eq. (2.173) for $n = 2$ is somewhat more elaborate. This is what will be done in the subsequent paragraph: first, the strong field limit of the one-loop diagram formed by the double wiggly line constituting a central building block this diagram evaluated. Second, this result is employed to extract the strong-field behavior of the leftmost diagram in Fig. 2.7.

As noted in the context of Eq. (2.151) above, the leading strong-field behavior of the 1PI sector of $\Gamma_{\text{HE}}[\bar{A}]$ in constant fields is arising from the Feynman diagrams depicted in Fig. 2.4. The last term in the first line of Eq. (2.39),

$$\Gamma^{\text{☆}}_{\text{HE}}[\bar{A}] := \quad = \frac{\mathrm{i}}{2}\ln\det(D^{-1} - S^{(2)}_\psi[\bar{A}])\,, \tag{2.174}$$

accounts for all these diagrams with $\ell \geq 2$ loops. For the definition of the wiggly double line in

Eq. (2.174), see Fig. 2.6. The leading contribution to the associated Lagrangian in the strong field limit $|\mathcal{F}| \gg (m^2/e)^2$, $|\mathcal{G}| \ll (m^2/e)^2$ can be readily obtained by resumming the ℓ-loop results in Eq. (2.151) for $\ell \geq 2$ [33, 45, 73]. This yields

$$\begin{aligned}\mathcal{L}_{\text{HE}}^{\text{☆}} &= e^2\mathcal{F}\frac{1}{4\pi}\frac{\beta_2}{\beta_1}\sum_{\ell=1}^{\infty}\frac{1}{\ell}\Big(\alpha\beta_1\ln\Big(\tfrac{e\sqrt{2\mathcal{F}}}{m^2}\Big)\Big)^{\ell}\left[1+O\Big(\ln^{-1}\Big(\tfrac{e\sqrt{2\mathcal{F}}}{m^2}\Big)\Big)\right]+O(\mathcal{G}^2)\\ &= e^2\mathcal{F}\frac{1}{4\pi}\frac{\beta_2}{\beta_1}\ln\left(\frac{\alpha^{\text{1-loop}}(e\sqrt{2\mathcal{F}})}{\alpha}\right)\left[1+O\Big(\ln^{-1}\Big(\tfrac{e\sqrt{2\mathcal{F}}}{m^2}\Big)\Big)\right]+O(\mathcal{G}^2)\,,\end{aligned} \tag{2.175}$$

where we employed the series representation of the logarithm, $\sum_{n=1}^{\infty}\chi^n/n = -\ln(1-\chi)$ for $|\chi|<1$, as well as Eq. (2.169) in the last step. In a next step, we note that the contribution of the first diagram in Fig. 2.7 to $\Gamma_{\text{HE}}[\bar{A}]$ can be formally expressed as

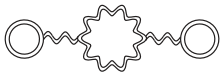

$$\begin{aligned}&= -\frac{\mathrm{i}}{4}\int\ldots\int\big[(D^{-1}-S_\psi^{(2)}[\bar{A}])^{-1}\big]_{\mu\alpha}\,(S_\psi^{(1)}[\bar{A}])^{\alpha}\,\big[(D^{-1}-S_\psi^{(2)}[\bar{A}])^{-1}\big]_{\nu\beta}\,(S_\psi^{(1)}[\bar{A}])^{\beta}\\ &\quad\times\Big\{(S_\psi^{(4)}[\bar{A}])^{\mu\nu\rho\sigma}\,\big[(D^{-1}-S_\psi^{(2)}[\bar{A}])^{-1}\big]_{\rho\sigma}\\ &\qquad+\iint(S_\psi^{(3)}[\bar{A}])^{\mu\rho\sigma}(S_\psi^{(3)}[\bar{A}])^{\nu\gamma\delta}\,\big[(D^{-1}-S_\psi^{(2)}[\bar{A}])^{-1}\big]_{\rho\gamma}\,\big[(D^{-1}-S_\psi^{(2)}[\bar{A}])^{-1}\big]_{\sigma\delta}\Big\}\,.\end{aligned} \tag{2.176}$$

Equation (2.176) can be extracted from the last line of Eq. (2.39) by straightforward but somewhat tedious manipulations. With the help of Eqs. (2.30) and (2.174) it can be identically rewritten as

$$= \frac{1}{2}\iint(S_\psi^{(1)}[\bar{A}])_{\alpha}\,\big[(D^{-1}-S_\psi^{(2)}[\bar{A}])^{-1}\big]^{\alpha\mu}\,\frac{\delta^2\Gamma_{\text{HE}}^{\text{☆}}[\bar{A}]}{\delta\bar{A}^{\mu}\delta\bar{A}^{\nu}}\,\big[(D^{-1}-S_\psi^{(2)}[\bar{A}])^{-1}\big]^{\nu\beta}\,(S_\psi^{(1)}[\bar{A}])_{\beta}\,, \tag{2.177}$$

the structure of which clearly resembles Eq. (2.153). In line with the above discussion, the result for the strong field limit of Eq. (2.177) can then be conveniently extracted from Eq. (2.155). It is encoded in

$$\begin{aligned}\to V^{(4)}\frac{1}{3}\Bigg[&\frac{\partial\mathcal{L}_{\text{HE}}^{\text{1-loop}}}{\partial\bar{F}^{\mu\nu}}\frac{\partial^2\mathcal{L}_{\text{HE}}^{\text{☆}}}{\partial\bar{F}_{\mu\nu}\partial\bar{F}_{\alpha\beta}}\frac{\partial\mathcal{L}_{\text{HE}}^{\text{1-loop}}}{\partial\bar{F}^{\alpha\beta}}+\frac{\partial\mathcal{L}_{\text{HE}}^{\text{1-loop}}}{\partial\bar{F}^{\mu\nu}}\frac{\partial^2\mathcal{L}_{\text{HE}}^{\text{☆}}}{\partial\bar{F}_{\alpha\nu}\partial\bar{F}_{\mu\beta}}\frac{\partial\mathcal{L}_{\text{HE}}^{\text{1-loop}}}{\partial\bar{F}^{\alpha\beta}}\\ &+\frac{\partial\mathcal{L}_{\text{HE}}^{\text{1-loop}}}{\partial\bar{F}^{\mu\nu}}\frac{\partial^2\mathcal{L}_{\text{HE}}^{\text{☆}}}{\partial\bar{F}_{\alpha\nu}\partial\bar{F}^{\alpha\beta}}\frac{\partial\mathcal{L}_{\text{HE}}^{\text{1-loop}}}{\partial\bar{F}_{\mu\beta}}\Bigg]\Big(\frac{\alpha^{\text{1-loop}}(e\sqrt{2\mathcal{F}})}{\alpha}\Big)^2\,,\end{aligned} \tag{2.178}$$

which in the relevant limit simplifies to

$$= V^{(4)}\frac{1}{2}\mathcal{F}\left(\frac{\partial\mathcal{L}_{\text{HE}}^{\text{1-loop}}}{\partial\mathcal{F}}\frac{\alpha^{\text{1-loop}}(e\sqrt{2\mathcal{F}})}{\alpha}\right)^2\left[\frac{\partial\mathcal{L}_{\text{HE}}^{\text{☆}}}{\partial\mathcal{F}}+\frac{4}{3}\mathcal{F}\frac{\partial^2\mathcal{L}_{\text{HE}}^{\text{☆}}}{\partial\mathcal{F}^2}\right]+O(\mathcal{G}^2)\,. \tag{2.179}$$

Upon insertion of Eqs. (2.151) and (2.175) and neglecting higher-order corrections in $\alpha^{\text{1-loop}}(e\sqrt{2\mathcal{F}})\beta_1$, we finally obtain

$$= V^{(4)}e^2\mathcal{F}\frac{1}{8\pi}\frac{\beta_2}{\beta_1}\ln\Big(\tfrac{\alpha^{\text{1-loop}}(e\sqrt{2\mathcal{F}})}{\alpha}\Big)\Big[\alpha^{\text{1-loop}}(e\sqrt{2\mathcal{F}})\beta_1\ln\Big(\tfrac{e\sqrt{2\mathcal{F}}}{m^2}\Big)\Big]^2\left[1+O\Big(\ln^{-1}\Big(\tfrac{e\sqrt{2\mathcal{F}}}{m^2}\Big)\Big)\right]+O(\mathcal{G}^2)\,, \tag{2.180}$$

which indeed agrees with the scaling in Eq. (2.174) for $n = 2$. It is worthwhile to recall and highlight in this context that the contribution linear in $\alpha^{\text{1-loop}}(e\sqrt{2\mathcal{F}})$ in Eq. (2.172) is not compatible with this scaling extended to $n = 1$. In comparison, this one is logarithmically enhanced and scales as $\Delta\mathcal{L}^{(1)}_{\text{HE}} \sim e^2\mathcal{F}[\alpha^{\text{1-loop}}(e\sqrt{2\mathcal{F}})\beta_1 \ln(e\sqrt{2\mathcal{F}}/m^2)]\beta_1 \ln(e\sqrt{2\mathcal{F}}/m^2)$. Taking into account that

$$\alpha^{\text{1-loop}}(e\sqrt{2\mathcal{F}})\beta_1 \ln\!\left(\tfrac{e\sqrt{2\mathcal{F}}}{m^2}\right) = \frac{l}{1-l}\,, \quad \text{where} \quad l = \alpha\beta_1 \ln\!\left(\tfrac{e\sqrt{2\mathcal{F}}}{m^2}\right), \tag{2.181}$$

the scaling of the contribution linear in $\alpha^{\text{1-loop}}(e\sqrt{2\mathcal{F}})$ as well as those with $n \geq 2$ in Eq. (2.173) can be alternatively represented as

$$\Delta\mathcal{L}^{(1)}_{\text{HE}} \sim e^2\mathcal{F}\left(\frac{l}{1-l}\right)\frac{l}{\alpha} \quad \text{and} \quad \Delta\mathcal{L}^{(n)}_{\text{HE}} \sim e^2\mathcal{F}\left(\frac{l}{1-l}\right)^n \quad \text{for} \quad n \geq 2\,. \tag{2.182}$$

This immediately implies that in the regime where the expansion parameter is smaller than unity, i.e., $l < 1/2$, the leading ($n = 1$) term is enhanced by a factor of $1/\alpha \simeq 137$ relatively to the other ones.

Finally, we briefly comment on the issue of convergence of this expansion. Equations (2.30), (2.36), (2.39), and (2.72) suggest that the resummation of the contributions in Eq. (2.182) should indeed be possible and even converge for $l < 1/2$. In line with this, for $|\mathcal{G}| \ll (m^2/e)^2$ the perturbative approach should thus grant access to field strengths $|\sqrt{2\mathcal{F}}| < (m^2/e)\exp\{1/(2\alpha\beta_1)\}$. Insights into the manifestly non-perturbative parameter regime where $l \geq 1/2$ require going beyond the perturbative loop expansion.

In this context, it should also be noted that due to the structure of the constituting Feynman diagrams the result in Eq. (2.172) can even be extracted from the leading contribution scaling as $\sim N$ to the Heisenberg-Euler effective Lagrangian for external-field QED with N degenerate-mass charged particle flavors in the 't Hooft limit [77] characterized by sending $N \to \infty$, while keeping both $N\alpha = \text{const.}$ and $e\bar{A}^\mu = \text{const.}$ [21, 76]. The same is true for the leading contributions beyond quadratic order in $\alpha^{\text{1-loop}}(e\sqrt{2\mathcal{F}})$ just discussed. A notable exception is the quadratic one: it scales only as $\sim N^0$ because of the double wiggly loop formed by identifying both ends of the bubble chain resummed photon propagator with each other; see the leftmost diagram in Fig. 2.7. This requires the number of charged-particle loop insertions and bare photon propagators in the loop to be the same and thus results in a suppression by a factor of $1/N$ relatively to the same diagram without the double wiggly loop.

Chapter 3

Photonic quantum vacuum signals

This chapter is concerned with the question of how the Heisenberg-Euler effective action $\Gamma_{\mathrm{HE}}[\bar{A}]$ introduced and detailed in Chapter 2 can be employed to reliably predict quantum vacuum signals in experimentally realistic field configurations. To this end, it focuses on the *vacuum emission picture* [16, 78] that encodes the nonlinear response of the quantum vacuum to strong electromagnetic fields in signal photons induced in the interaction region and assumed to be detected far outside. The theoretical foundations of this approach are outlined and in particular concise expressions allowing for quantitatively accurate predictions of prospective signals accessible with state-of-the-art technology are derived. This is explicitly demonstrated for the example of two head-on colliding laser beams. In this context also means to enhance the signal-to-background separation in experiment are highlighted.

3.1 Theoretical foundations

The basic idea of experiments aiming at the detection of quantum fluctuation induced corrections to the classical Maxwell theory is to apply strong macroscopic electromagnetic fields, such as provided by high-intensity laser pulses, and to measure a response which can be attributed to the latter. Even for the highest field strengths attainable in the laboratory with state-of-the-art and near-future high-intensity lasers this response is very small and can best be resolved and quantified in terms of single signal photons: high-intensity lasers comprising $O(10^{20})$ laser photons per pulse typically induce responses on the single photon level.

It turns out that such photonic signatures can be conveniently studied in the vacuum emission picture [16, 78]. In this approach, the initially applied macroscopically controlled fields are treated as classical fields, whereas the fluctuation-induced signal photons are dealt with on the level of the quantum Fock space. By definition, there are no signal photons in the initial state which thus amounts to the vacuum state containing zero signal photons $|0\rangle$. The signal photons are assumed to be detected far outside the interaction region V_{I}, where quantum vacuum nonlinearities play no role and can be safely neglected; cf. Sec. 2.1. It should also be noted that the vacuum emission picture considers all applied fields on an equal footing and a priori does not rely on a decomposition of the driving fields into pump and probe fields, typically underlying other approaches. Moreover, due to its inherent Fock space formulation, it does not

necessitate the somewhat tedious explicit use of Green's functions methods but gives direct access to the vacuum-to-signal amplitude, and thus the differential number of signal photons encoding the signature of quantum vacuum nonlinearity in experimentally realistic field configurations.

In the next step, we provide a concise summary of the theoretical foundations of the vacuum emission picture and detail how it allows to extract quantum vacuum signals from the Heisenberg-Euler effective action $\Gamma_{\rm HE}[\bar{A}]$. To this end, we first split the external field as $\bar{A}^\mu \to \bar{A}^\mu_{\rm in} + \bar{A}^\mu_{\rm signal}$ into an initially applied field and a signal photon field. However, to keep notations compact, throughout this chapter we actually use the shorthand notations $\bar{A}^\mu_{\rm in} \to \bar{A}^\mu$ and $\bar{A}^\mu_{\rm signal} \to a^\mu$. Then, the interaction part (2.14) $\tilde{\Gamma}_{\rm HE}[\bar{A}] = \Gamma_{\rm HE}[\bar{A}] - \Gamma_{\rm MW}[\bar{A}]$ of the effective action encoding quantum vacuum effects beyond classical Maxwell theory can be expanded as

$$\tilde{\Gamma}_{\rm HE}[\bar{A}+a] = \tilde{\Gamma}_{\rm HE}[\bar{A}] + \sum_{n=1}^{\infty} \frac{1}{n!} \int \dots \int (\tilde{\Gamma}^{(n)}_{\rm HE}[\bar{A}])^{\sigma_1 \dots \sigma_n} a_{\sigma_1} \dots a_{\sigma_n} \,, \tag{3.1}$$

where we employed the shorthand notation

$$(\tilde{\Gamma}^{(n)}_{\rm HE}[\bar{A}])^{\sigma_1 \dots \sigma_n} := \frac{\delta^n \tilde{\Gamma}_{\rm HE}[\bar{A}]}{\delta \bar{A}_{\sigma_1} \dots \delta \bar{A}_{\sigma_n}} \tag{3.2}$$

for the effective coupling of n signal photons. In turn, Eq. (3.1) acts as the generator of all effective interactions of the signal photon field in the presence of the initially applied field $\bar{A}^\mu$. Also note that Eq. (3.2) is fully non-perturbative in the applied classical field $\bar{A}$: for even (odd) values of n it accounts for couplings to arbitrary even (odd) orders of $\bar{A}$; cf. Sec. 2.2. As a consequence of the fact that the general result for $\Gamma_{\rm HE}[\bar{A}]$ contains the full information about all possible quantum-fluctuation-mediated interaction processes of an external field $\bar{A}^\mu$ involving arbitrary frequencies, the effective interactions (3.2) are generically nonlocal. Particularly in the weak-field $|\bar{F}^{\mu\nu}| \ll m^2/E$, low-frequency $\omega \ll m$ regime the nonlocality is controlled by the Compton wavelength.

As the signal photon fields a^μ (field strength tensor $f^{\mu\nu} = \partial^\mu a^\nu - \partial^\nu a^\mu$) are detected far outside $V_{\rm I}$ where quantum vacuum nonlinearities are absent, they are naturally to be considered as asymptotic outgoing on-shell fields that fulfill $k^2 = 0$ in momentum space. In line with that, we assume the signal photon field to be characterized by manifestly positive energy modes only. Correspondingly, in position-space it can be represented as

$$a^\mu(x) = \sum_p \int \frac{\mathrm{d}^3 k}{(2\pi)^3} \frac{1}{\sqrt{2k^0}} \epsilon^{*\mu}_{(p)}(\vec{k})\, \mathrm{e}^{-\mathrm{i}kx}\, a^\dagger_p(\vec{k}) \Big|_{k^0=|\vec{k}|} \,, \tag{3.3}$$

where the sum is over the two physical polarizations p transverse to $\vec{k}$, $\epsilon^\mu_{(p)}(\vec{k})$ are the associated polarization vectors, and $a^\dagger_p(\vec{k})$ is the creation operator for a signal photon of momentum $\vec{k}$ and polarization p. Our conventions are such that the single signal photon state is given by $a^\dagger_p(\vec{k})\,|0\rangle = |\gamma_p(\vec{k})\rangle$ and $\langle \gamma_p(\vec{k}) | \gamma'_p(\vec{k}')\rangle = \delta_{p,p'}\, \delta(\vec{k} - \vec{k}')$. We highlight that naively accounting for both positive and negative energy contributions in Eq. (3.3) would result in inconsistencies for processes coupling several signal photon fields beyond one-loop order: the contraction of $a_p(\vec{k})$ and $a^\dagger_{p'}(\vec{k}')$ would effectively generate in-

ternal (transverse) photon lines inconsistent with the external field concept and imply that contributions would be double counted.

The transition amplitude from the vacuum subjected to an initially applied field $\bar{A}^\mu$ to a state featuring n signal photons of momenta $\vec{k}_1, \ldots, \vec{k}_n$ and polarizations $p_1, \ldots, p_n$ can then be compactly expressed as

$$\mathcal{S}_{p_1,\ldots,p_n}(\vec{k}_1, \ldots, \vec{k}_n) = \langle \gamma_{p_1}(\vec{k}_1), \ldots, \gamma_{p_n}(\vec{k}_n) \big| \, \mathrm{e}^{\mathrm{i}\tilde{\Gamma}_{\mathrm{HE}}[\bar{A}+a]} \, \big| 0 \rangle \,. \tag{3.4}$$

Note that because the signal photons are asymptotic states and solve the source-free linear Maxwell equations $\partial_\mu f^{\mu\nu} = 0$ by definition, upon adopting the above splitting of the external field as $\bar{A}^\mu \to \bar{A}^\mu + a^\mu$ to the full Heisenberg-Euler effective action $\Gamma_{\mathrm{HE}}[\bar{A}]$, the contributions $\sim \bar{F}_{\mu\nu} f^{\mu\nu}$ and $\sim f_{\mu\nu} f^{\mu\nu}$ arising from $\Gamma_{\mathrm{MW}}[\bar{A} + a]$ vanish identically. Hence, in the present context we have $\Gamma_{\mathrm{HE}}[\bar{A} + a] \to \Gamma_{\mathrm{MW}}[\bar{A}] + \tilde{\Gamma}_{\mathrm{HE}}[\bar{A} + a]$.

The definition in Eq. (3.4) ensures that when not resolving any signal photon fields, i.e., setting $a^\mu \to 0$ (and accounting for the Maxwell term $\exp\{\mathrm{i}\Gamma_{\mathrm{MW}}[\bar{A}]\}$), the correct vacuum-to-vacuum transition amplitude in the presence of $\bar{A}^\mu$ as given in Eq. (2.23) is recovered. We emphasize that the limit $a^\mu \to 0$ immediately implies that the entire external field is treated classically and only the vacuum-to-vacuum term $\langle 0 \big| \, \mathrm{e}^{\mathrm{i}\tilde{\Gamma}_{\mathrm{HE}}[\bar{A}]} \, \big| 0 \rangle = \mathrm{e}^{\mathrm{i}\tilde{\Gamma}_{\mathrm{HE}}[\bar{A}]}$ in Eq. (3.4) can be nonvanishing. As a direct consequence of Eq. (3.3) being a manifestly positive energy field, no time-ordering is needed in the present context. The differential number of signal photons associated with the n signal photon emission process in Eq. (3.4) is given by

$$\mathrm{d}^{3n} N_{p_1,\ldots,p_n} = \frac{\mathrm{d}^3 k_1}{(2\pi)^3} \cdots \frac{\mathrm{d}^3 k_n}{(2\pi)^3} \left| \mathcal{S}_{p_1,\ldots,p_n}(\vec{k}_1, \ldots, \vec{k}_n) \right|^2 . \tag{3.5}$$

In passing, we note that along the same lines in principle also the inverse of signal photon emission, namely photon absorption by the quantum vacuum subjected to a classical electromagnetic field can be considered. To this end, one only needs to substitute the signal photon field in Eq. (3.3) by its hermitian conjugate and consider transitions from a state characterized by a given number of incident photons to the vacuum state in the presence of $\bar{A}^\mu$, i.e., essentially exchange the in- and out states in Eq. (3.4). The probability for a given incident multi-photon state to be completely absorbed by the vacuum in the classical field $\bar{A}^\mu$ then follows upon taking the modulus squared of this amplitude. However, in generic inhomogeneous electromagnetic fields $\bar{A}^\mu$ this effect is in general substantially suppressed in comparison to the associated signal photon emission process. The reason for this is that whereas a given incident photon state to be absorbed is typically characterized by a finite set of specific photon wave vectors, the phase space of the emission process typically spans a relatively wide range of possible signal photon energies and emission directions. This renders the isolated individual contribution of a particular signal photon wave vector essentially negligible; cf. also Eq. (3.5).

In particular, specializing Eq. (3.4) to the single signal photon state, which usually constitutes the dominant signal of quantum vacuum nonlinearity, we obtain

$$\mathcal{S}_p(\vec{k}) = \mathrm{e}^{\mathrm{i}\tilde{\Gamma}_{\mathrm{HE}}[\bar{A}]} \langle \gamma_p(\vec{k}) \big| \int \frac{\delta \tilde{\Gamma}_{\mathrm{HE}}[\bar{A}]}{\delta \bar{A}^\mu} \, a^\mu \big| 0 \rangle \,, \tag{3.6}$$

where we made use of the fact that only the term linear in a^μ gives rise to a nonvanishing transition amplitude. Upon insertion of Eq. (3.3), Eq. (3.6) can be expressed as

$$= \mathrm{e}^{\mathrm{i}\tilde{\Gamma}_{\mathrm{HE}}[\bar{A}]} \frac{\epsilon^{*\mu}_{(p)}(\vec{k})}{\sqrt{2\mathrm{k}}} \int_x \mathrm{e}^{-\mathrm{i}\mathrm{k}(\hat{k}x)} \frac{\delta\tilde{\Gamma}_{\mathrm{HE}}[\bar{A}]}{\delta\bar{A}^\mu(x)}\,, \tag{3.7}$$

with signal photon energy $\mathrm{k} = |\vec{k}|$ and normalized four wave vector $\hat{k}^\mu = (1, \vec{k}/\mathrm{k})$. Obviously, the quantity $\delta\tilde{\Gamma}_{\mathrm{HE}}[\bar{A}]/\delta\bar{A}^\mu$ constitutes the current sourcing the signal photon field at linear order. The differential number of signal photons of energy k emitted in the vicinity of the direction $\vec{k}/\mathrm{k}$ then follows from Eq. (3.5) as

$$\mathrm{d}^3N_p = \frac{\mathrm{d}^3k}{(2\pi)^3}\left|\mathcal{S}_p(\vec{k})\right|^2. \tag{3.8}$$

Alternatively, this result can also be derived within a classical electrodynamics approach resorting to Green's function methods [79]. One is often interested in extracting the particular quantum vacuum signal which is linear in a given subcomponent $\bar{\mathfrak{A}}^\mu$ of the applied field $\bar{A}^\mu \to \bar{A}^\mu + \bar{\mathfrak{A}}^\mu$. This is especially relevant for the signature of vacuum birefringence which can be understood and interpreted in terms of the scattering of photons associated with the coherent state underlying a specific external field $\bar{\mathfrak{A}}^\mu$ into a perpendicularly polarized mode assisted by another electromagnetic field $\bar{A}^\mu$. The corresponding single signal photon amplitude can obviously be expressed as

$$\mathcal{S}_p(\vec{k})\big|_{\sim\bar{\mathfrak{A}}} = \int \bar{\mathfrak{A}}^\nu \frac{\delta S_p(\vec{k})}{\delta\bar{A}^\nu}\,,$$

which upon insertion of Eq. (3.6) becomes

$$= \mathrm{e}^{\mathrm{i}\tilde{\Gamma}_{\mathrm{HE}}[\bar{A}]} \iint \bar{\mathfrak{A}}^\nu \left(\frac{\delta^2\tilde{\Gamma}_{\mathrm{HE}}[\bar{A}]}{\delta\bar{A}^\nu\delta\bar{A}^\mu} + \mathrm{i}\frac{\delta\tilde{\Gamma}_{\mathrm{HE}}[\bar{A}]}{\delta\bar{A}^\nu}\frac{\delta\tilde{\Gamma}_{\mathrm{HE}}[\bar{A}]}{\delta\bar{A}^\mu}\right)\langle\gamma_p(\vec{k})\big|a^\mu\big|0\rangle\,. \tag{3.9}$$

Equation (2.22) implies that at one-loop level the factor in the big round brackets in Eq. (3.9) equals $-(\Pi^{\text{1-loop}}[\bar{A}])^{\nu\mu}$. This is a direct consequence of the fact that only the first term contributes at this order. On the other hand, in the general case Eq. (2.19) allows to express this factor in terms of the full photon propagator in the external field $(\mathcal{D}[\bar{A}])^{\mu\nu}$ and the bare photon propagator $D^{\mu\nu}$. This results in the following representation

$$\mathcal{S}_p(\vec{k})\big|_{\sim\bar{\mathfrak{A}}} = -\mathrm{e}^{\mathrm{i}\tilde{\Gamma}_{\mathrm{HE}}[\bar{A}]} \iiiint \bar{\mathfrak{A}}^\nu (D^{-1})_{\nu\alpha}(\mathcal{D}[\bar{A}] - D)^{\alpha\beta}(D^{-1})_{\beta\mu}\,\langle\gamma_p(\vec{k})\big|a^\mu\big|0\rangle\,, \tag{3.10}$$

which, e.g., relates the birefringence phenomenon experienced by the photons constituting the macroscopic field $\bar{\mathfrak{A}}^\mu$ to the photon propagator in the presence of $\bar{A}^\mu$. As detailed in Sec. 2.1 the full photon propagator used here is normalized to the vacuum of sfQED: if instead a normalization to the field-free vacuum of QED is adopted, the overall factor of $\exp\{\mathrm{i}\tilde{\Gamma}_{\mathrm{HE}}[\bar{A}]\}$ in Eq. (3.10) is to be absorbed in the term $(\mathcal{D}[\bar{A}] - D)^{\alpha\beta}$ and thus does not show up explicitly. Hence, the quantum vacuum signal linear in both $\bar{\mathfrak{A}}^\mu$ and a^μ is fully determined by the full photon propagator. In turn, at least in principle, associated

phenomena like vacuum birefringence can be analyzed on the basis of the photon propagator without any explicit reference to $\Gamma_{\rm HE}[\bar{A}]$. This nicely illustrates the link between the present approach and traditional analyses of photon propagation effects in external fields, such as vacuum birefringence, based on the photon polarization tensor in constant or plane-wave fields at one loop. Studies of the latter type grant direct access to the parameter regime of large momentum transfers $|p^\mu| \gg m$ inaccessible by any finite-order derivative expansion.

For slowly varying electromagnetic fields, i.e., fields varying on spatial scales λ (temporal scales τ) much larger than the Compton wavelength $\lambda\!\!\!^{-}_{\rm C} = 1/m \simeq 3.9\times10^{-13}$ m (time $\tau_{\rm C} = \lambda\!\!\!^{-}_{\rm C}/c \simeq 1.3\times10^{-21}$ s) of the electron, further simplifications are possible. In this case, one can resort to a derivative expansion of the effective Lagrangian $\mathcal{L}_{\rm HE}$ and in essence restrict oneself to the terms depending only on $\bar{F}^{\mu\nu}$ and not on derivatives thereof. This is often also referred to as a *locally constant field approximation* (LCFA). Contributions to $\mathcal{L}_{\rm HE}$ containing derivatives of $\bar{F}^{\mu\nu}$ are parametrically suppressed by even powers of $\{\lambda\!\!\!^{-}_{\rm C}/\lambda, \tau_{\rm C}/\tau\} \ll 1$, or equivalently $(\omega/m)^2 \ll 1$, where ω denotes the typical frequency scales of variation of $\bar{F}^{\mu\nu}$; cf. Sec. 2.3.3. This approximation can be readily implemented in Eqs. (3.4) and (3.7) by substituting $\tilde{\Gamma}_{\rm HE}[\bar{A}] \to \int_x \tilde{\mathcal{L}}_{\rm HE}$, with the effective Lagrangian at zeroth-order in a derivative expansion $\tilde{\mathcal{L}}_{\rm HE} = \mathcal{L}_{\rm HE} - \mathcal{L}_{\rm MW}$ being a function of $\bar{F}^{\mu\nu}$ only. In turn, the functional derivatives (3.2) of $\tilde{\Gamma}_{\rm HE}[\bar{A}]$ determining the effective interactions of the signal photon field assume a particularly simple form, as

$$\frac{\delta\tilde{\Gamma}_{\rm HE}[\bar{A}]}{\delta\bar{A}_{\sigma_1}(x_1)} \to -2\frac{\partial}{\partial x_1^{\mu_1}}\int_x \frac{\partial\tilde{\mathcal{L}}_{\rm HE}}{\partial\bar{F}_{\mu_1\sigma_1}}(x)\,\delta(x-x_1)\,, \tag{3.11}$$

which can be readily extended to functional derivatives of nth order. In fact, though being somewhat more tedious because of the presence of additional derivatives acting on $\bar{F}^{\mu\nu}$, also generalizations accounting for *almost local* contributions arising from higher-orders in a derivative expansion of $\mathcal{L}_{\rm HE}$ can be straightforwardly accounted for and dealt with along the same lines.

Especially in the slowly varying field regime, quantum vacuum signals associated with signal photon states characterized by multiple photons are typically parametrically suppressed with powers of the induced signal photon frequencies $|\mathrm{k}_i^\mu| \ll m$ for $i \in \{1,\ldots,n\}$: because each signal photon field in Eq. (3.3) comes with an overall factor of $1/\sqrt{\mathrm{k}_i}$, $\mathrm{d}^3k_i \sim (\mathrm{k}_i)^3$, and the reference scale rendering these factors dimensionless is m, it is straightforward to show that in this limit Eq. (3.5) scales as $\mathrm{d}^{3n}N_{p_1,\ldots,p_n} \sim (\mathrm{k}_1/m)^2\times\ldots\times(\mathrm{k}_n/m)^2$ and thus $\mathrm{d}^{3n}N_{p_1,\ldots,p_n}/\mathrm{d}^{3n}N_{p_1,\ldots,p_{n+1}} \ll 1$. Particularly for weak quantum vacuum signals characterized by $|f^{\mu\nu}| \ll |\bar{F}^{\mu\nu}|$ it is moreover well-justified to describe the applied field configurations $\bar{A}^\mu$ which drives the signal photon emission process as a solution of the nonlinear Maxwell equations (2.15) initially generated by the source $\bar{J}^\mu = \bar{J}^\mu_{\rm in}$, and thereby to disregard the backreaction of the signal field a^μ on $\bar{A}^\mu$. In fact, given that the strength of the driving field fulfills $|\bar{F}^{\mu\nu}| \ll m^2/e$ and its typical frequency components $\omega \ll m$, a criterion which is met for essentially all macroscopic fields attainable in the laboratory, for the extraction of the leading effects it is even sufficient to completely neglect the response of quantum vacuum fluctuations on $\bar{A}^\mu$ and thus to model the latter by solutions of the linear Maxwell equations (2.11). As obvious from Eqs. (2.15), (2.65) and (2.97), in this limit the applied field is Maxwellian up to corrections of $O(\alpha)$ which are in addition parametrically

suppressed by powers of $(\omega/m)^2$ and $(e\bar{F}/m^2)^2$, respectively.

Equation (3.7) implies that the determination of the signal photon emission amplitude boils down to performing the Fourier transform of functional derivatives of $\Gamma_{\mathrm{HE}}[\bar{A}]$ for $\bar{A}^\mu$. Upon taking the modulus squared to determine the differential signal photon number, the overall factor of $\mathrm{e}^{\mathrm{i}\tilde{\Gamma}_{\mathrm{HE}}[\bar{A}]}$ results in a damping term $|\mathrm{e}^{\mathrm{i}\tilde{\Gamma}_{\mathrm{HE}}[\bar{A}]}|^2 = \mathrm{e}^{-2\mathrm{Im}\{\Gamma_{\mathrm{HE}}[\bar{A}]\}}$ for $\mathrm{Im}\{\Gamma_{\mathrm{HE}}[\bar{A}]\} > 0$, signalizing the principle possibility of the quantum vacuum to decay in an external field. However, for the typical field strengths attainable in the laboratory fulfilling $|\bar{F}^{\mu\nu}| \ll m^2/e$ this imaginary part is extremely small and can be safely neglected; cf. Eq. (2.64). As the overall exponential then amounts to a pure phase term, which plays no role in the determination of the signal photon number, it can be omitted and Eq. (3.7) reduces to the expression given in Eq. (5) of [80]. We note that the explicit expressions for the transition amplitudes to states with multiple signal photons are slightly more complicated: with increasing order of the Taylor expansion of $\mathrm{e}^{\mathrm{i}\tilde{\Gamma}_{\mathrm{HE}}[\bar{A}+a]}$ in a^μ more and more terms are generated because Eq. (3.1) appears as argument of the exponential. Therefore, in general no simple closed-form expressions are available. Nevertheless, especially for transitions to signal photon states containing few photons the corresponding results can be readily worked out from Eqs. (3.1)-(3.5). In this case, one has to perform Fourier transforms of polynomials involving products of different-order functional derivatives of $\tilde{\Gamma}_{\mathrm{HE}}[\bar{A}]$.

In Eq. (3.3) we adopted the conventional plane-wave decomposition of the signal photon field. For completeness, we note that one can, of course, also use other complete bases for its decomposition, such as orbital angular momentum eigenstates invoked to describe twisted photons [81, 82]. The corresponding modification of Eqs. (3.4)-(3.7) is straightforward. We emphasize that this would likely constitute the most convenient choice to study quantum vacuum processes involving twisted photons [83–85]. Outgoing signal photons with nontrivial orbital angular momentum are, for instance, to be expected in the collision of Laguerre-Gaussian laser beams involving modes with nonzero azimuthal index l. In this case, the vacuum-fluctuation-mediated effective interaction of several of such modes can in particular manifest itself in signal photons featuring orbital angular momentum quantum numbers different from the driving fields. Aside from a distinct propagation direction or polarization of the signal, this might constitute an additional clear signature allowing to discern optical signals of quantum vacuum nonlinearity in high-intensity laser experiments from the large background of the driving laser photons.

Finally, some clarifications are in order. While the approach just outlined can also be applied to macroscopic electromagnetic fields reaching critical or even supercritical field strengths, as well as high-frequency fields, one should be aware of the following caveats and limitations: first, if the condition $|f^{\mu\nu}| \ll |\bar{F}^{\mu\nu}|$ is no longer met the feedback of the signal field on the initially applied field needs to be properly accounted for. This requires a self-consistent solution of Eq. (2.15) in the full external field and is – at least in principle – possible; cf. also the detailed discussion in the context of Eq. (2.24). However, because a signal field $f^{\mu\nu}$ of the same order as the initially applied field $\bar{F}^{\mu\nu}$ inherently comes with a substantial modification of the latter, in this case a clear separation of the outgoing field into an induced signal and an applied component altered by the effective interaction with the former is typically inhibited. Second, for driving fields of sufficiently large strength or frequency real electron-positron pair production may become sizeable such that field-depletion and backreaction effects of the created charges on the external field can no longer be ignored. While pair-production effects are accounted for

in the present approach via the imaginary part of $\Gamma_{\rm HE}[\bar{A}]$, they essentially only manifest themselves as damping terms in the transition amplitude (3.4) which describe the decay of the quantum vacuum in any asymptotic pair state, but do not resolve the kinematics of the latter. This is fully consistent with the fact that by definition an approach based on $\Gamma_{\rm HE}[\bar{A}]$ does not account for the presence of real charged particles in the interaction region; cf. Sec. 2.1. These would in particular also modify the current in Eq. (2.15) and thus react back on the electromagnetic field. Correspondingly, the present approach may still be applied for the determination of the attainable signal photon numbers induced by quantum vacuum processes in cases where only few electrons and positrons are produced, the kinematics of which not resolved. However, one should be aware that it inevitably neglects secondary processes triggered by the presence of real electrons and positrons, such as their radiation field and annihilation processes into photons. In extreme parameter regimes, the fluxes of the latter may be as important as the original vacuum emission signals. A fully-consistent and proper treatment of all these effects will eventually require the use of non-equilibrium QFT methods.

3.2 Predictions for experiment

3.2.1 Quantum vacuum signals with state-of-the-art technology

The strongest macroscopic electromagnetic fields currently available in the laboratory are obtained in the foci of high-intensity lasers of the petawatt-class. These are slowly varying, i.e., their frequency scales of variation fulfill $\omega \ll m$, and reach electric and magnetic peak fields of $E = O(10^{14})\mathrm{V/m}$ and $B = O(10^{6})\mathrm{T}$ [86], much smaller than the QED reference field strengths $E_{\rm cr} = B_{\rm cr} = m^2/e$. The highest laser photon energy demonstrated in the laboratory at an x-ray free electron laser is $\omega = O(30)\,\mathrm{keV}$ [87]. Hence, aiming at providing accurate theoretical predictions for the quantum vacuum signals accessible in the laboratory with state-of-the-art technology it is usually sufficient to account only for the leading effective coupling between electromagnetic fields in the perturbative-weak-field and low-frequency limit [5, 88],

$$\tilde{\mathcal{L}}_{\rm HE} \simeq \frac{m^4}{360\pi^2}\Big(\frac{e}{m^2}\Big)^4 (c_a\,\mathcal{F}^2 + c_b\,\mathcal{G}^2)\,, \tag{3.12}$$

with numerical constants c_a and c_b. Up to two-loop accuracy, these can be read of Eqs. (2.65) and (2.129) and are given by

$$c_a \simeq 4\Big(1 + \frac{40}{9}\frac{\alpha}{\pi}\Big) \quad \text{and} \quad c_b = 7\Big(1 + \frac{1315}{252}\frac{\alpha}{\pi}\Big). \tag{3.13}$$

Equation (3.12) is quartic in $\bar{F}^{\mu\nu}$ and thus couples four electromagnetic fields. Corrections due to higher effective couplings of the electromagnetic field and derivative contributions are parametrically suppressed by powers of $(e\bar{F}/m^2)^2$ and $(\omega/m)^2$, respectively; cf. Sec. 2.2. Thus, for realistic scenarios of quantum vacuum experiments that can be envisioned based on current and near-future lasers the two-loop contribution $\sim \alpha$ already accounted for in Eq. (3.13) is expected to be the leading correction to Eq. (3.12) with $c_a = 4$ and $c_b = 7$. It obviously results in corrections of these one-loop values on the 10% level. The above discussion and Eqs. (3.7) and (3.11) then immediately imply that in this case the leading vacuum

to signal photon amplitude can be expressed as

$$\mathcal{S}_p(\vec{k}) = \mathrm{i}\sqrt{2\mathrm{k}}\,\epsilon^{*\mu}_{(p)}(\vec{k})\,\hat{k}^\nu \int_x \mathrm{e}^{-\mathrm{i}\mathrm{k}(\hat{k}x)}\,\frac{\partial\tilde{\mathcal{L}}_{\mathrm{HE}}}{\partial\bar{F}^{\mu\nu}}(x)\,.$$

Upon insertion of Eq. (3.12) this becomes

$$= \mathrm{i}\sqrt{2\mathrm{k}}\,\frac{m^4}{360\pi^2}\Big(\frac{e}{m^2}\Big)^4 \epsilon^{*\mu}_{(p)}(\vec{k})\,\hat{k}^\nu \int_x \mathrm{e}^{-\mathrm{i}\mathrm{k}(\hat{k}x)}\,(c_a\,\mathcal{F}\bar{F}_{\mu\nu} + c_b\,\mathcal{G}\,{}^\star\bar{F}_{\mu\nu})\,, \tag{3.14}$$

which scales cubic with the electromagnetic field. This cubic dependence is a direct consequence of the fact that the single signal photon amplitude is proportional to the current $\tilde{\Gamma}_{\mathrm{HE}}[\bar{A}]/\delta\bar{A}^\mu$; cf. also Eq. (3.7). In the determination of the latter, one of the couplings of $\tilde{\Gamma}_{\mathrm{HE}}[\bar{A}]$ to $\bar{A}^\mu$ is effectively promoted to an open index. For Eq. (3.12), which scales quartic in the field, this results in a cubic field dependence of the amplitude.

Equation (3.14) implies that in the considered limit an explicit evaluation of the signal photon amplitude only requires performing a Fourier transform of cubic powers of the applied electric and magnetic field components. Importantly, as noted in Sec. 3.1, practically without compromising the accuracy of a vacuum emission calculation based on Eq. (3.12), for macroscopic electromagnetic fields fulfilling $|e\bar{F}^{\mu\nu}| \ll m^2$ the latter can be modelled as solutions of the linear Maxwell equations (2.11); cf. the specification of the regime of validity of Eq. (3.12) given below Eq. (3.13). This makes the present approach ideally suited for the quantitatively accurate theoretical study of quantum vacuum signals in the strongest macroscopic fields available in the laboratory. Probably the most notable advantage is its flexibility concerning the driving fields in which signal photon emission can reliably and self-consistently be studied on a quantitative level: within the above constraints these are in essence all field configurations for which the linear Maxwell equations governing their dynamics can be solved (or their solution be sufficiently accurately approximated), in particular laser fields of generic space-time dependence.

In spherical momentum coordinates where $\vec{k} = \mathrm{k}(\cos\varphi\sin\vartheta, \sin\varphi\sin\vartheta, \cos\vartheta)$ it is easy to see that the unit vectors orthogonal to $\vec{k}$ can be parameterized by a single angle β as $\vec{e}_\perp(\beta) = \vec{e}_1(\vec{k})\cos\beta + \vec{e}_2(\vec{k})\sin\beta$, with orthonormal vectors $\vec{e}_1(\vec{k}) = (\cos\varphi\cos\vartheta, \sin\varphi\cos\vartheta, -\sin\vartheta)$ and $\vec{e}_2(\vec{k}) = (-\sin\varphi, \cos\varphi, 0)$. Correspondingly, the two vectors forming a linear polarization basis for signal photons of wave vector $\vec{k}$ can be parameterized as

$$\epsilon^\mu_{(p)}(\vec{k}) = (0, \vec{e}_\perp(\beta_p))\,, \quad \text{with} \quad \beta_p = \beta_0 + \frac{\pi}{2}(p-1) \quad \text{for} \quad p \in \{1,2\}\,, \tag{3.15}$$

and an angular offset β_0 which can be chosen freely, particularly also as a function of $\vec{k}/\mathrm{k}$. Explicitly accounting for β_0 is convenient as by adjusting it appropriately a given signal polarization can, for instance, immediately be chosen to coincide with the axis of a polarization filter. On the other hand, a circular polarization basis is spanned by $\epsilon^\mu_{(\pm)}(\vec{k}) = \mp(0, \vec{e}_1(\vec{k}) \pm \mathrm{i}\vec{e}_2(\vec{k}))/\sqrt{2}$, fulfilling $\epsilon_{(p)\mu}(\vec{k})\,\epsilon^{*\mu}_{(p')}(\vec{k}) = \delta_{p,p'}$. Here, the signs "+" and "−" refer to right and left hand circular polarization, respectively.

Adopting these conventions and a linear polarization basis (3.15) for the signal photons, the ampli-

tude in Eq. (3.14) can be represented as

$$\mathcal{S}_{(p)}(\vec{k}) = \frac{\mathrm{i}}{2\pi}\frac{m^2}{45}\sqrt{\frac{\alpha}{\pi}\frac{\mathrm{k}}{2}}\left(\frac{e}{m^2}\right)^3\left\{\cos\beta_p\left[\mathcal{I}_{11}(\vec{k})-\mathcal{I}_{22}(\vec{k})\right]+\sin\beta_p\left[\mathcal{I}_{12}(\vec{k})+\mathcal{I}_{21}(\vec{k})\right]\right\}, \tag{3.16}$$

where we made use of the definition

$$\mathcal{I}_{ij}(\vec{k}) = \int \mathrm{d}^4x\, \mathrm{e}^{-\mathrm{i}\mathrm{k}(\hat{k}x)}\,\vec{e}_i(\vec{k})\cdot\vec{U}_j\,, \tag{3.17}$$

with

$$\vec{U}_1 = c_a\mathcal{F}\vec{E} + c_b\mathcal{G}\vec{B} \quad \text{and} \quad \vec{U}_2 = c_a\mathcal{F}\vec{B} - c_b\mathcal{G}\vec{E}\,, \tag{3.18}$$

encoding the dependence on the electromagnetic fields driving the vacuum emission process. Note that $\vec{U}_1$ and $\vec{U}_2$ are directly proportional to the polarization and magnetization vectors of the quantum vacuum subjected to the prescribed external field configuration $\bar{F}^{\mu\nu}$, respectively [79]. The compact representation in Eqs. (3.16)-(3.18) is particularly suited for both analytical [16, 80] and numerical [89, 90] studies of quantum vacuum signals in experimentally realistic field configurations. It is obvious from Eqs. (3.14) and (3.18) that field configurations fulfilling $\mathcal{F} = \mathcal{G} = 0$ cannot induce a non-vanishing quantum vacuum signal in the considered parameter regime. Also note that due to the fact that Eq. (3.14) is linear in $\epsilon^{*\mu}_{(p)}(\vec{k})$ the analogous result for the transition amplitude to a circularly polarized signal can be essentially read off Eq. (3.16).

Having derived explicit formulas allowing to study quantum vacuum signals in generic laser fields, some additional comments concerning the isolation of different signal components are in order. The dominant quantum vacuum signals can typically be traced back to quasi-elastic scattering processes of photons originating from a specific source off the composite field generated by the other sources; recall also the corresponding discussion in the paragraph below Eq. (3.8) in Sec. 3.1. In field configurations $\bar{A}^\mu \to \bar{A}^\mu + \bar{\mathfrak{A}}^\mu$ involving at least one laser beam (gauge potential $\bar{\mathfrak{A}}^\mu$) which is collided with the field $\bar{A}^\mu$ generated by additional laser beams or other sources such as, e.g., magnets, one is therefore often interested in extracting the quasi-elastic scattering signal which can be clearly attributed to a given laser beam conventionally referred to as the *probe* (electric and magnetic fields $\vec{\mathfrak{E}}$, $\vec{\mathfrak{B}}$). In line with this, the other applied fields constitute the *pump* (electric and magnetic fields $\vec{E}$, $\vec{B}$). This specific signal is obviously encoded in the contribution to Eq. (3.16) which scales linearly with the field components of the probe beam; cf. also Sec. 3.1. In turn, it can be expressed in the same form as Eqs. (3.16) and (3.17) with the replacement $\vec{U}_{1,2} \to \vec{U}_{1,2}\big|_{\sim\bar{\mathfrak{A}}}$, where

$$\begin{aligned}
\vec{U}_1\big|_{\sim\bar{\mathfrak{A}}} &= c_a\left[\mathcal{F}\vec{\mathfrak{E}} + (\vec{B}\cdot\vec{\mathfrak{B}} - \vec{E}\cdot\vec{\mathfrak{E}})\vec{E}\right] + c_b\left[\mathcal{G}\vec{\mathfrak{B}} - (\vec{E}\cdot\vec{\mathfrak{B}} + \vec{B}\cdot\vec{\mathfrak{E}})\vec{B}\right],\\
\vec{U}_2\big|_{\sim\bar{\mathfrak{A}}} &= c_a\left[\mathcal{F}\vec{\mathfrak{B}} + (\vec{B}\cdot\vec{\mathfrak{B}} - \vec{E}\cdot\vec{\mathfrak{E}})\vec{B}\right] - c_b\left[\mathcal{G}\vec{\mathfrak{E}} - (\vec{E}\cdot\vec{\mathfrak{B}} + \vec{B}\cdot\vec{\mathfrak{E}})\vec{E}\right].
\end{aligned} \tag{3.19}$$

As a consistency check, utilizing the leading weak-field contribution to the polarization tensor in the slowly varying field limit worked out in Eq. (2.80), one can easily confirm that a direct evaluation of the linearized signal photon amplitude in Eq. (3.9) specialized to one loop, yields the same result.

3.2.2 Laser beam model

An analytical modeling of focused high-intensity laser beams is typically based on the paraxial approximation of the wave equation $\Box \bar{A}^\mu = 0$, which follows from the linear Maxwell equations (2.11) in vacuo presuming the Lorenz gauge condition $\partial_\mu \bar{A}^\mu = 0$ to hold [91–93]. This approximation assumes the complex gauge potential $\bar{A}^\mu(x)$ representing a given laser beam to have a time dependence of the form $\mathrm{e}^{\mathrm{i}\omega(\hat{k}x)}$ with $\hat{k}^\mu = (1, \hat{\vec{\kappa}})$ and to fulfill the condition $\vec{A} \cdot \hat{\vec{\kappa}} = 0$, where the unit vector $\hat{\vec{\kappa}}$ defines the direction of the beam axis of the beam constructed along these lines and ω denotes its oscillation frequency; the beam focus is supposed to be strationary and to be located at $\vec{x} = 0$. This approximation is valid for beams made up of plane waves (or equivalently, *laser photons*) with wave vectors $\vec{k}$ fulfilling $\sphericalangle(\vec{k}, \hat{\vec{\kappa}}) \ll 1$. The spatial coordinates parallel and perpendicular to $\hat{\vec{\kappa}}$ are then normalized by transverse w_0 and longitudinal $\mathrm{z_R} = \omega w_0^2/2$ reference scales*, respectively, and the envelope function multiplying $\mathrm{e}^{\mathrm{i}\omega(\hat{k}x)}$ is formally expanded in a power series in $\theta^2 \ll 1$, where $\theta := w_0/\mathrm{z_R}$. Upon insertion of this ansatz, the wave equation is iteratively solved order by order in θ^2. The conventional paraxial approximation amounts to truncating this expansion at $O(\theta^0)$, i.e., only accounts for the leading (or equivalently, zeroth order) contribution.

Coherent paraxial beams can be decomposed into an infinite sum of modes which are typically labeled by two integer indices. Two widely used bases are Laguerre-Gaussian and Hermite-Gaussian modes, both of which form a complete basis for coherent paraxial beams at $O(\theta^0)$ [94, 95]. The former is convenient for beams exhibiting a circular symmetry about the beam axis, and the latter for beams with a Cartesian transverse symmetry. In this work we only consider rotationally symmetric beams and thus employ Laguerre-Gaussian modes. At $O(\theta^0)$ the electric and magnetic fields characterizing the beam feature the same amplitude profile and are orthogonal to each other as well as to $\hat{\vec{\kappa}}$. In turn, the magnetic field can be expressed in terms of the electric field via $\vec{B} = \hat{\vec{\kappa}} \times \vec{E}$. To make the following considerations as transparent as possible, without loss of generality we assume the beam to propagate in z direction and use cylindrical coordinates (r, φ, z); these considerations can be readily generalized to arbitrary propagation directions by identifying $\mathrm{z} = \hat{\vec{\kappa}} \cdot \vec{x}$, $r^2 = \vec{x}^2 - (\hat{\vec{\kappa}} \cdot \vec{x})^2$ and letting φ parameterize rotations around $\hat{\vec{\kappa}}$. In these conventions, the electric field of a generic paraxial beam at $O(\theta^0)$ is characterized by a global polarization vector $\vec{\varepsilon}$ and can be expressed as

$$\vec{E} = \mathrm{e}^{-(\frac{\mathrm{z}-t}{\tau/2})^2} \frac{w_0}{w(\mathrm{z})} \mathrm{e}^{-(\frac{r}{w(\mathrm{z})})^2} \sum_{l,p} \mathcal{E}_{l,p} \left(\frac{\sqrt{2}r}{w(\mathrm{z})}\right)^{|l|} L_p^{|l|}\left(\tfrac{2r^2}{w^2(\mathrm{z})}\right) \mathrm{Re}\left\{\vec{\varepsilon}\, \mathrm{e}^{-\mathrm{i}\Phi_{l,p}(x)}\right\}, \tag{3.20}$$

where the sum runs over all the contributing modes labeled by an azimuthal index $l \in \mathbb{Z}$ and a radial index $p \in \mathbb{N}_0$. Here,

$$L_p^{|l|}\left(\tfrac{2r^2}{w^2(\mathrm{z})}\right) = \sum_{j=0}^{p} \frac{(-1)^j}{j!} \binom{p+|l|}{p-j} \left(\frac{2r^2}{w^2(\mathrm{z})}\right)^j \tag{3.21}$$

are generalized Laguerre polynomials, $w(\mathrm{z}) = w_0 \sqrt{1 + (\mathrm{z}/\mathrm{z_R})^2}$ is a radial length scale (cf. below) and $\mathcal{E}_{l,p}$ denotes the mode-specific field amplitudes. The first exponential factor in Eq. (3.20) supplements

*The identification of the longitudinal reference scale $\mathrm{z_R}$ with ωw_0^2 follows naturally from the form of the wave-equation at $O(\theta^0)$; the additional factor of $1/2$ is a convention.

the paraxial beam solution with a finite pulse duration τ[†], which is chosen such that the peak field is reached in the beam focus at $t = \mathrm{z} = 0$. The explicit expression for the mode-specific phase reads

$$\Phi_{l,p}(x) = \psi(x) + (|l| + 2p)\psi_{\mathrm{G}}(\mathrm{z}) + l\varphi + \psi_{l,p}\,, \tag{3.22}$$

where we separated off the $\{l, p\}$ independent part,

$$\psi(x) = \omega(t - \mathrm{z}) - \frac{\mathrm{z}}{\mathrm{z}_R}\left(\frac{r}{w(\mathrm{z})}\right)^2 + \psi_{\mathrm{G}}(\mathrm{z})\,, \tag{3.23}$$

with Guoy phase $\psi_{\mathrm{G}}(\mathrm{z}) = \arctan(\mathrm{z}/\mathrm{z}_{\mathrm{R}})$ and a mode specific constant phase offset $\psi_{l,p}$. The second term in Eq. (3.23) accounts for wavefront curvature effects. A mode with non-vanishing azimuthal index l amounts to an optical vortex of topological charge l. We emphasize that due to the dependence on the radial coordinate via $r/w(\mathrm{z})$ only, each of these modes does not change its transversal shape as a function of the longitudinal coordinate z. Also note that the beams constructed along these lines are essentially monochromatic with a small finite bandwidth arising due to the overall factor that implements the finite pulse duration. The associated $1/\mathrm{e}^2$ bandwidth with respect to intensity can be easily extracted from Eq. (3.20) with the help of a Fourier transform and is given by $\Delta\omega = 8/\tau$; the above pulsed beam prescription is applicable for $\Delta\omega/\omega \ll 1$. Correspondingly, for the quasi-monochromatic laser beams considered here the number of laser photons N constituting the beam can be related to the energy W put into the beam as $N \simeq W/\omega$. For the sake of completeness, in the present context we also note that a finite pulse duration could alternatively be implemented by the introduction of a finite bandwidth in frequency space, i.e., by appropriately superimposing copies of Eq. (3.20) with different oscillation frequencies ω. While this ensures that the pulses constructed along these lines fulfill the (considered order of the) paraxial approximation exactly and no additional restriction on $\tau\omega$ needs to be invoked, it typically comes to the price of an additional non-trivial integration over $\Delta\omega$ and thus a loss of analytical control; recall in particular the implicit dependence on ω encoded in the Rayleigh range. For this reason, here we exclusively stick to the above pulsed beam approximation which nicely aligns with the parameters of state-of-the-art high-intensity laser systems delivering pulses fulfilling $\tau\omega \gg 1$.

The conventional *(fundamental) Gaussian beam* solution follows from Eq. (3.20) upon restriction to the fundamental mode with $l = p = 0$; note that this term is typically used for modeling a focused laser beam solving the paraxial wave equation at $O(\theta^0)$. The radius of such a beam, or equivalently the $l = p = 0$ mode in Eq. (3.20), depends on the value of the longitudinal coordinate z and is given by $w(\mathrm{z})$; w_0 denotes the associated beam waist and z_{R} its Rayleigh range. The far-field divergence of this mode is defined as its radial opening angle and thus matches the above expansion parameter

$$\theta = \lim_{\mathrm{z}\to\infty} \arctan\left(\frac{w(\mathrm{z})}{\mathrm{z}}\right) = \frac{w_0}{\mathrm{z}_{\mathrm{R}}}\,. \tag{3.24}$$

This specific solution minimizes the product of the beam radius at focus and the far-field divergence.

[†]This factor acts as a regulator and augments the paraxial beam solution, which is recovered for $\tau \to \infty$, with a (Gaussian) temporal pulse envelope. For finite values of τ this *ad hoc* prescription implements a finite energy *pulsed beam* fulfilling the paraxial equation at $O(\theta^0)$ approximately. The neglected contributions are of $O(\frac{1}{\tau\omega})$ justifying the use of Eq. (3.19) for $\tau\omega \gg 1$.

Therefore, it often amounts to the desired output of a high-intensity laser system because it reaches the minimum beam waist and thus the maximum peak field strength for a given opening angle of the optics used to focus the beam and fixed other parameter. Nevertheless, for real high-intensity laser beams the description as a fundamental Gaussian beam is certainly an idealization, specifically also as typically rather flat-top-like transverse beam profiles are used in the amplification chain to distribute the intensity load equally and thus to minimize damages of the optics prior to focusing.

The polarization vectors of a linearly polarized beam can be parameterized as $\vec{\varepsilon} = (\cos\phi, \sin\phi, 0)$ by a single angle ϕ. Because $\vec{\varepsilon}$ is real-valued, the operator $\mathrm{Re}\{\cdot\}$ in Eq. (3.20) acts nontrivially only the exponential function in its argument. This results in an overall oscillation of the linearly polarized field with $\cos(\Phi_{l,p})$. On the other hand, circularly polarized beams follow upon identifying $\vec{\varepsilon} = \vec{e}_\mathrm{x} \pm \mathrm{i}\vec{e}_\mathrm{y}$ where the + (−) sign corresponds to right (left) hand polarization. Correspondingly, the complex-valued polarization vector implements a phase difference between the x and y components of the field such that $\mathrm{Re}\{\vec{\varepsilon}\,\mathrm{e}^{-\mathrm{i}\Phi_{l,p}}\} = (\cos\Phi_{l,p}, \pm\sin\Phi_{l,p}, 0)$. In this context, we emphasize that the use of real valued fields is absolutely essential for the consistent evaluation of nonlinear quantum vacuum signals because the unique mapping between complex and real valued fields clearly holds only for the linear theory. For linearly polarized beams the peak field amplitude $\mathcal{E}_{l,p}$ can be related to the energy put in a specific mode $W_{l,p}$ as [96]

$$\mathcal{E}_{l,p}^2 \simeq 8\sqrt{\frac{2}{\pi}}\frac{p!}{(|l|+p)!}\frac{W_{l,p}}{\pi w_0^2 \tau}\,, \tag{3.25}$$

where we neglected contributions $\sim \mathrm{e}^{-\#(\tau\omega)^2}$ with $\# > 0$ because these are anyhow less important than terms of $O(\frac{1}{\tau\omega})$ not accounted for in the employed approximation from the outset; cf. footnote † on page 68. Equation (3.25) follows straightforwardly upon integration of the z component of the Poynting vector $\vec{S} = \vec{E} \times \vec{B}$ at a fixed longitudinal coordinate z over the transverse coordinates and time. Alternatively, the expression given in Eq. (3.25) can be determined by integrating the cycle-averaged intensity profile $I(x) = \langle S_\mathrm{z}\rangle_t$ over r and t; here $\langle\cdot\rangle_t$ denotes time averaging over one oscillation period. Within the accuracy of the employed approximation the pulse envelope is not affected by this averaging procedure. In this case the exponentially suppressed corrections do not even show up. On the other hand, for circularly polarized beams the square of the peak field amplitude is smaller by a factor of two but otherwise agrees with Eq. (3.25) [97]. This can be easily understood by the fact that, as opposed to the case of a linearly polarized beam, for a circularly polarized beam the modulus of the field does not vary with $\omega(t - \mathrm{z})$ and accounting for $\langle\cos^2\Phi_{l,p}\rangle_t = 1/2$. The total energy put into the pulsed beam is $W = \sum_{l,p} W_{l,p}$.

For linearly polarized fundamental Gaussian beams also higher-order corrections in θ have been worked out analytically by means of the iterative procedure outlined above; up to $O(\theta^{11})$ in Ref. [93]. To this end, the solution at $O(\theta^0)$ is identified with the $l = p = 0$ mode. For a beam polarized along x on its beam axis the leading terms for the corresponding electric and magnetic fields can be expressed as

$$\begin{aligned}\vec{E} = \mathrm{e}^{-(\frac{\mathrm{z}-t}{\tau/2})^2}\mathcal{E}_0\,\frac{w_0}{w(\mathrm{z})}\,\mathrm{e}^{-(\frac{r}{w(\mathrm{z})})^2}\,\mathrm{Re}\Bigg\{\mathrm{e}^{-\mathrm{i}[\psi(x)+\psi_0]}\Bigg[\vec{e}_\mathrm{x} - \mathrm{i}\theta\,\mathrm{e}^{-\mathrm{i}\psi_\mathrm{G}(\mathrm{z})}\,\frac{\mathrm{x}}{w(\mathrm{z})}\,\vec{e}_\mathrm{z} \\ + (\theta\,\mathrm{e}^{-\mathrm{i}\psi_\mathrm{G}(\mathrm{z})})^2\Bigg[\Big(\frac{\mathrm{x}^2}{w^2(\mathrm{z})} - \frac{1}{4}\frac{r^4}{w^4(\mathrm{z})}\frac{w(\mathrm{z})}{w_0}\,\mathrm{e}^{-\mathrm{i}\psi_\mathrm{G}(\mathrm{z})}\Big)\vec{e}_\mathrm{x} + \frac{\mathrm{xy}}{w^2(\mathrm{z})}\,\vec{e}_\mathrm{y}\Bigg]\Bigg] + O(\theta^3)\Bigg\}\,,\end{aligned}$$

$$\vec{B} = \mathrm{e}^{-(\frac{z-t}{\tau/2})^2}\mathcal{E}_0\,\frac{w_0}{w(\mathrm{z})}\,\mathrm{e}^{-(\frac{r}{w(\mathrm{z})})^2}\,\mathrm{Re}\Big\{\mathrm{e}^{-\mathrm{i}[\psi(x)+\psi_0]}\Big[\vec{e}_\mathrm{y} - \mathrm{i}\theta\,\mathrm{e}^{-\mathrm{i}\psi_\mathrm{G}(\mathrm{z})}\,\frac{\mathrm{y}}{w(\mathrm{z})}\,\vec{e}_\mathrm{z} + (\theta\,\mathrm{e}^{-\mathrm{i}\psi_\mathrm{G}(\mathrm{z})})^2\frac{1}{2}\frac{r^2}{w^2(\mathrm{z})}\Big(1 - \frac{1}{2}\frac{r^2}{w^2(\mathrm{z})}\frac{w(\mathrm{z})}{w_0}\,\mathrm{e}^{-\mathrm{i}\psi_\mathrm{G}(\mathrm{z})}\Big)\vec{e}_\mathrm{y}\Big] + O(\theta^3)\Big\}, \tag{3.26}$$

where we identified $\mathcal{E}_0 := \mathcal{E}_{0,0}$ and $\psi_0 := \psi_{0,0}$ to simplify notations; also note the identity $\mathrm{e}^{-\mathrm{i}\psi_\mathrm{G}(\mathrm{z})} = \frac{w(\mathrm{z})}{w_0}\frac{1}{1+\mathrm{i}\mathrm{z}/\mathrm{z}_\mathrm{R}}$. The fields in Eq. (3.26) are transverse and linearly polarized only on the beam axis where $\mathrm{x} = \mathrm{y} = 0$. In this case an integration over the z component of the Poynting vector yields the following relation between the peak field amplitude and the energy W put into the pulsed laser beam,

$$\mathcal{E}_0^2 \simeq 8\sqrt{\frac{2}{\pi}}\frac{W}{\pi w_0^2\tau}\Big[1 - \Big(\frac{\theta}{2}\Big)^2 + O(\theta^4)\Big]. \tag{3.27}$$

where, as in Eq. (3.25), we neglected contributions which are exponentially suppressed with $(\tau\omega)^2$. At $O(\theta^0)$ Eqs. (3.26) and (3.27) clearly reduce to the $l = p = 0$ contributions in Eqs. (3.20) and (3.25). The explicit expressions for the scalar invariants (2.25) associated with Eq. (3.26) can be expressed as

$$\begin{aligned}\mathcal{F} &= -\Big(\theta\frac{w_0}{w(\mathrm{z})}\Big)^2\Big(\mathrm{e}^{-(\frac{z-t}{\tau/2})^2}\mathcal{E}_0\,\frac{w_0}{w(\mathrm{z})}\,\mathrm{e}^{-(\frac{r}{w(\mathrm{z})})^2}\Big)^2\,\frac{1}{2}\frac{\mathrm{x}^2-\mathrm{y}^2}{w^2(\mathrm{z})} + O(\theta^4)\,,\\ \mathcal{G} &= -\Big(\theta\frac{w_0}{w(\mathrm{z})}\Big)^2\Big(\mathrm{e}^{-(\frac{z-t}{\tau/2})^2}\mathcal{E}_0\,\frac{w_0}{w(\mathrm{z})}\,\mathrm{e}^{-(\frac{r}{w(\mathrm{z})})^2}\Big)^2\,\frac{\mathrm{x}\mathrm{y}}{w^2(\mathrm{z})} + O(\theta^4)\,,\end{aligned} \tag{3.28}$$

which illustrates that both $\mathcal{F}$ and $\mathcal{G}$ give rise to finite contributions at $O(\theta^2)$.

3.2.3 Single-beam signal emission

Equation (3.28) in particular implies that, though a single paraxial beam at $O(\theta^0)$ cannot induce a nonvanishing quantum vacuum signal because it fulfills $\mathcal{F} = \mathcal{G} = 0$, this should eventually become possible when accounting for higher-order corrections [89, 98]. However, due to the absence of a $O(\theta^0)$ contribution this signal is expected to be rather small. As shown explicitly in the current section, specifically at leading nonvanishing order, i.e., $O(\theta^2)$ on the level of the amplitude, this case is tractable analytically and closed form expressions for all relevant quantities can be worked out. Apart from providing insights into the effect of single-beam signal emission itself, this allows us to illustrate and benchmark convenient approximations allowing to extract simple analytical scalings describing the leading behavior of the studied quantities in experimentally relevant parameter regimes which can also be employed for scenarios envisioning the collision of multiple laser fields. Such scalings are very helpful to understand general trends [99] allowing, e.g., to put forward signal enhancement strategies in experiment [100], and to assist the interpretation of the phenomena observed in numerical simulations of quantum vacuum effects in electromagnetic fields which self-consistently fulfill the linear Maxwell equations [101].

Upon plugging the fields (3.26) at $O(\theta^0)$ and the expressions in Eq. (3.28) into Eq. (3.16), we obtain

$$\mathcal{S}_{(p)}(\vec{k}) = \theta^2(1-\cos\vartheta)\frac{\mathrm{i}}{2\pi}\frac{m^2}{45}\sqrt{\frac{\alpha}{\pi}\frac{\mathrm{k}}{2}}\Big(\frac{e}{m^2}\Big)^3\int \mathrm{d}^4x\,\mathrm{e}^{-\mathrm{i}\mathrm{k}(\hat{k}x)}\cos\Big(\psi(x)+\psi_0\Big)\Big(\frac{w_0}{w(\mathrm{z})}\Big)^2 \tag{3.29}$$

$$\times \left(\mathrm{e}^{-(\frac{z-t}{\tau/2})^2}\mathcal{E}_0\,\frac{w_0}{w(\mathrm{z})}\,\mathrm{e}^{-(\frac{r}{w(z)})^2}\right)^3\left[c_a\cos(\varphi-\beta_p)\frac{1}{2}\frac{\mathrm{x}^2-\mathrm{y}^2}{w^2(\mathrm{z})}+c_b\sin(\varphi-\beta_p)\frac{\mathrm{xy}}{w^2(\mathrm{z})}\right]+O(\theta^3)\,.$$

The integrations over the transverse coordinates and time can be readily performed: using parameter differentiations they can be reduced to standard Gaussian integrals. This results in

$$\begin{aligned}\mathcal{S}_{(p)}(\vec{k}) \simeq{}& \theta^2(1-\cos\vartheta)\sin^2\vartheta\,\frac{1}{2^6}\frac{\mathrm{i}\mathrm{e}^{-\mathrm{i}\psi_0}}{45}\sqrt{\frac{\alpha}{6}}\left(\frac{e\mathcal{E}_0}{m^2}\right)^3 w_0^4\,\mathrm{z_R}\tau\,m^2\,\mathrm{k}^{5/2}\,\mathrm{e}^{-\frac{\tau^2}{48}(\mathrm{k}-\omega)^2}\\ &\times\left[c_a\cos(\varphi-\beta_p)\cos(2\varphi)+c_b\sin(\varphi-\beta_p)\sin(2\varphi)\right]\\ &\times\int_{-\infty}^{\infty}\mathrm{d}\zeta\,\frac{1}{\zeta-\mathrm{i}}\,\frac{1}{(\zeta+3\mathrm{i})^3}\,\mathrm{e}^{\mathrm{i}z_\mathrm{R}\mathrm{k}(1-\cos\vartheta)\zeta-\mathrm{i}\frac{1}{4}w_0^2\mathrm{k}^2\sin^2\vartheta\frac{\zeta^2+1}{\zeta+3\mathrm{i}}}+O(\theta^3)\,,\end{aligned}\tag{3.30}$$

where we introduced the dimensionless variable $\zeta = \mathrm{z}/\mathrm{z_R}$ and once again neglected terms exponentially suppressed with $(\tau\omega)^2$; cf. also footnote † on page 68. The factor in the second line of Eq. (3.30) encodes the polarization dependence of the signal. Given that the condition

$$\frac{2(1-\cos\vartheta)}{\sin^2\vartheta}\geq\frac{\mathrm{k}w_0^2}{2\mathrm{z_R}}\tag{3.31}$$

is fulfilled, the integral over ζ can be easily evaluated with the help of the residue theorem by closing the integration contour at infinity such as to enclose the single pole at $\zeta = \mathrm{i}$, yielding

$$\int_{-\infty}^{\infty}\mathrm{d}\zeta\,\frac{1}{\zeta-\mathrm{i}}\,\frac{1}{(\zeta+3\mathrm{i})^3}\,\mathrm{e}^{\mathrm{i}z_\mathrm{R}\mathrm{k}(1-\cos\vartheta)\zeta-\mathrm{i}\frac{1}{4}w_0^2\mathrm{k}^2\sin^2\vartheta\frac{\zeta^2+1}{\zeta+3\mathrm{i}}}=-\frac{\pi}{32}\,\mathrm{e}^{-\mathrm{z_R}\mathrm{k}(1-\cos\vartheta)}\,.\tag{3.32}$$

The left-hand side of the condition (3.31) is equal or larger than one for all values $0 \leq \vartheta \leq \pi$ and monotonically increases with ϑ, ultimately going to infinity for $\vartheta \to \pi$. On the other hand, particularly for $\mathrm{k} \simeq \omega$ its right-hand side becomes equal to one. Note that the last exponential factor in the first line of Eq. (3.30) actually ensures the signal to be emitted at this frequency for $\tau \to \infty$. Hence, especially for large values of $\omega\tau \gg 1$, i.e., the limit where the employed pulsed beam approximation should be most reliable, the condition should be met. In this parameter regime we obtain the following result for the differential number of signal photons (3.8),

$$\begin{aligned}\frac{\mathrm{d}^3N_p}{\mathrm{dk}\,\mathrm{d}\varphi\,\mathrm{dcos}\,\vartheta}\simeq{}&\theta^4(1-\cos\vartheta)^2\sin^4\vartheta\,\frac{1}{2^{10}}\frac{\alpha^4}{6075\pi^2}\sqrt{\frac{2}{\pi}}\,\frac{1}{m}\left(\frac{W}{m}\right)^3\frac{(w_0\mathrm{z_R})^2m^3}{\tau}\left(\frac{\mathrm{k}}{m}\right)^7\mathrm{e}^{-\frac{\tau^2}{24}(\mathrm{k}-\omega)^2}\mathrm{e}^{-2\mathrm{z_R}\mathrm{k}(1-\cos\vartheta)}\\ &\times\left[c_a\cos(\varphi-\beta_p)\cos(2\varphi)+c_b\sin(\varphi-\beta_p)\sin(2\varphi)\right]^2+O(\theta^5)\,,\end{aligned}\tag{3.33}$$

where we employed Eq. (3.27) to express the peak field amplitude in terms of the energy put into the laser field.

Two commonly considered signals are the number of signal photons attainable in a polarization insensitive measurement $N_\mathrm{tot} = \sum_{p=1}^{2} N_p$ and the number of polarization-flipped signal photons $N_\perp$. In a theoretical idealization, $N_\perp$ is most appropriately defined in terms of signal photons polarized perpendicularly ($\perp$) to the driving laser fields far outside the interaction region where the former are to be discriminated from the photons constituting the latter in experiment. Due to the dependence of the

polarization vector governing the orientation of the electric field in Eq. (3.26) on the spatial position within the beam, in general this requires a different criterion and thus – with regard to an experimental realization – a differently oriented polarization filter for each far-field emission direction. We note that, especially with the aid of numerical methods, such a study is possible within the vacuum emission picture that accounts for the full polarization information of the signal as well as the driving fields and thus allows for direction resolved polarization analyses. Here, we instead consider the $\perp$-signal component to be defined as being polarized perpendicularly to the polarization direction $\vec{e}_\mathrm{x}$ of the driving beam on its beam axis. This results in the criterion $\vec{e}_\mathrm{x} \cdot \vec{e}_\perp(\beta_p) = 0 \;\leftrightarrow\; \beta_p = \arctan(\cot\varphi\cos\vartheta)$ for the polarization of the $\perp$-signal. In passing, we note that this mimics an experimental scenario involving a polarization filter transmitting only the component perpendicular to $\vec{e}_\mathrm{x}$ to analyze the initially applied and induced field components in the outgoing far field. As the components of the polarization vector of the driving field in directions other than $\vec{e}_\mathrm{x}$ are suppressed with powers of $\vartheta_\mathrm{x} \simeq \mathrm{x/z} \lesssim \theta \ll 1$ and $\vartheta_\mathrm{y} \simeq \mathrm{y/z} \lesssim \theta \ll 1$, which can be straightforwardly inferred from the far-field behavior of Eq. (3.26) for large values of z, the driving beam should indeed be predominantly polarized in x direction particularly also in the far field. One can therefore expect a substantial reduction of the laser-photon background in the $\perp$ mode relatively to the polarization-unresolved case. However, we emphasize that definite statements concerning the in-principle measurability of $N_\perp$ of course require a consistent quantitative assessment of the laser-photon background in the $\perp$ mode. Moreover, as no perfect polarization filters are available and these only come with a finite purity, there is always a residual background level in experiment which needs to be accounted for in order to facilitate reliable predictions of measurable signals.

Upon summation over two independent polarization modes to obtain the differential number of signal photons attainable in a polarization insensitive measurement, the factor in the second line of Eq. (3.33) becomes

$$[\cdot]^2 \;\to\; (c_a^2 - c_b^2)\cos^2(2\varphi) + c_b^2\,. \tag{3.34}$$

On the other hand, upon insertion of the above value of β_p defining the $\perp$-polarized signal component this factor becomes

$$[\cdot]^2 \;\to\; \frac{1}{2}\frac{\sin^2(2\varphi)}{1+u^2-(1-u^2)\cos(2\varphi)}\big[(c_a - c_b)(1+u)\cos(2\varphi) + c_b(1-u)\big]^2\,, \tag{3.35}$$

with $u = \cos\vartheta$. Remarkably, for both quantities the integrations over k, φ and $\cos\vartheta$ can be performed analytically, such that closed-form expressions for N_tot and $N_\perp$ as well as the respective single to triple differential quantities are available. However, these often turn out be quite unhandy and typically obscure the most relevant parameter dependences: for instance a direct integration over k naturally results in expressions containing the error function. Therefore, and as they can be readily worked out without any complications, we do not provide their explicit results here.

Instead, in the following we show that by adopting a set of well-justified approximations one can work out simple analytical scalings governing the leading behavior in the considered parameter regime: (i) As discussed already above, the Gaussian factor $\exp\{-\tau^2(\mathrm{k}-\omega)^2/24\}$ in Eq. (3.33) ensures that for $\tau\omega \gg 1$ the signal is predominantly emitted at a frequency of $\mathrm{k} \simeq \omega$. The other dependences of Eq. (3.33)

on k are slowly varying with k in comparison to this one; see also item (ii) below. Hence, it should amount to a good approximation to identify $\mathrm{k} = \omega$ everywhere apart from the Gaussian factor. Moreover, the integral over k can then to an excellent approximation be performed by formally extending its integration range from $-\infty$ to $+\infty$ resulting in an elementary Gaussian integral. (ii) For $\mathrm{k} = \omega$ the second exponential factor in Eq. (3.33) can be expressed as $\exp\{-4(1-u)/\theta^2\}$. Correspondingly, a sizable contribution to the signal can only be induced for $1 - u \lesssim \theta^2$, or equivalently, $\vartheta \lesssim \theta$. Because by definition $\theta \ll 1$ in the regime where the paraxial approximation is applicable, it should typically be well-justified to account for the leading non-vanishing contribution $1 - u \simeq \vartheta^2/2$ in this factor only. In line with that, also the trigonometric functions of ϑ in the prefactor multiplying the exponential functions can then be approximated such that only the leading non-vanishing dependence of the prefactor on ϑ is retained. Together with this approximation, the integration over ϑ can be most conveniently performed by formally extending its upper integration limit to $+\infty$. The exponential damping by the Gaussian factor $\exp\{-2(\vartheta/\theta)^2\}$ for large values of ϑ ensures that this practically does not impact the accuracy of the integration. We note that this factor exactly matches the far-field angular decay of the intensity profile, and thus also the associated photon distribution, of the fundamental Gaussian laser beam driving the effect. With the help of the approximations (i) and (ii) the expression given explicitly in Eq. (3.33) can be simplified to

$$\left\{ \begin{array}{c} \frac{\mathrm{d}^3 N_{\mathrm{tot}}}{\mathrm{dk}\,\mathrm{d}\varphi\,\vartheta\mathrm{d}\vartheta} \\ \frac{\mathrm{d}^3 N_{\perp}}{\mathrm{dk}\,\mathrm{d}\varphi\,\vartheta\mathrm{d}\vartheta} \end{array} \right\} \approx \theta^4\,\vartheta^8\,\frac{1}{2^{12}}\frac{\alpha^4}{6075\pi^2}\sqrt{\frac{2}{\pi}}\,\frac{1}{m}\Big(\frac{W}{m}\Big)^3\frac{(w_0 z_{\mathrm{R}})^2 m^3}{\tau}\Big(\frac{\omega}{m}\Big)^7 \mathrm{e}^{-\frac{\tau^2}{24}(\mathrm{k}-\omega)^2}\mathrm{e}^{-2(\vartheta/\theta)^2} \times \left\{ \begin{array}{c} (c_a^2 - c_b^2)\cos^2(2\varphi) + c_b^2 \\ \frac{1}{4}(c_a - c_b)^2 \sin^2(4\varphi) \end{array} \right\}. \tag{3.36}$$

The scaling of Eq. (3.36) with an overall factor of ϑ^8 immediately implies that no signal is induced along the forward beam axis and that the emission also remains highly suppressed in its surrounding. The physical reason for this is that only laser photons propagating along the beam axis and its vicinity can give rise to a sizable quantum vacuum signal in forward direction. However, precisely here the electric and magnetic fields (3.26) are essentially transverse and thus do not induce a signal. This results in relatively small signal photon numbers because sizable contributions can only be induced in the angular interval where $\vartheta > 0$ and $\frac{\mathrm{d}}{\mathrm{d}\vartheta}(\vartheta^8 \exp\{-2(\vartheta/\theta)^2\} \approx 0$, i.e., in the vicinity of $\vartheta \approx \sqrt{2}\theta$ where the exponential suppression is already pronounced. As a direct consequence of this behavior, approximation (ii) is expected to be less accurate in the present case relatively to situations where the prefactor of the exponential remains finite for $\vartheta \to 0$, which ensures the main contribution to the signal to arise from the smallest possible values of ϑ. In scenarios envisioning the collision of two or more laser fields on can always identify configurations that give rise to finite prefactors in this limit and therefore induce much larger quantum vacuum signals [99, 102]; cf. also Sec. 3.2.4 below.

Integrating Eq. (3.36) over the signal photon energy and the emission directions by formally extending the integration ranges for the k and ϑ integrals as discussed in the context of the approximations (i)

and (ii), we arrive at the following compact result for the signal photon numbers per laser shot [90],

$$\left\{ \begin{array}{c} N_{\text{tot}} \\ N_{\perp} \end{array} \right\} \approx \frac{\sqrt{3}\,\alpha^4}{4050\pi} \left(\frac{W}{m}\right)^3 \frac{1}{\tau^2 w_0^8} \frac{1}{(\omega m)^5} \left\{ \begin{array}{c} c_a^2 + c_b^2 \\ \frac{1}{4}(c_a - c_b)^2 \end{array} \right\} . \tag{3.37}$$

Note that $N_{\text{tot}}/N_{\perp} \simeq 4(c_a^2 + c_b^2)/(c_a - c_b)^2 \approx 28.9$ with the explicit values for the coefficients $c_{a,b}$ given in Eq. (3.13). We emphasize that the scaling $\{N_{\text{tot}}, N_{\perp}\} \sim 1/w_0^8$ of the self-emission signal from a single focused beam derived here is consistent with the outcome of numerical studies [89, 90, 103] modeling the driving beam with $\theta < 1$ as an exact solution of the linear Maxwell equations (2.11).

A comparison of the results for N_{tot} and $N_{\perp}$ obtained by a direct analytical integration of Eq. (3.33) using Eqs. (3.34) and (3.35) with the analytical scalings in Eq. (3.37) for a driving beam of wavelength $\lambda = 800\,\text{nm}$, corresponding to a photon energy of $\omega \simeq 1.55\,\text{eV}$, and a pulse duration of $\tau^{\text{FWHM}} = 25\,\text{fs}$[‡] unveils that, as to be expected from the above discussion, the relative deviations tend to decrease with growing w_0; note that $\tau\omega \simeq 100$ in this case. The waist w_0 of a fundamental Gaussian beam is determined by the f-number $f^{\#}$ of the focusing element as

$$w_0 = \frac{2\lambda f^{\#}}{\pi}\,, \tag{3.38}$$

such that the associated far-field divergence is given by $\theta = 1/(2f^{\#})$. Values of $f^{\#} \gtrsim 1$ can be achieved in experiment. For the wavelength and pulse duration specified above, which are representative for many currently available high-intensity laser systems, the relative deviations are 16% for $w_0 = 2\lambda/\pi$ ($\theta = 1/2$), 6% for $w_0 = \lambda$ ($\theta = 1/\pi$), less than 5% for $w_0 \gtrsim 1.1\lambda$ ($\theta \lesssim 0.29$), and less than 1% for $w_0 \gtrsim 2.4\lambda$ ($\theta \lesssim 0.14$).

We note that deviations of this size are completely acceptable for the present considerations and justify the use of Eqs. (3.36) and (3.37) for $f^{\#} \gtrsim 1$ because the results derived here on the basis of the paraxial approximation anyhow neglect corrections parametrically suppressed by just one additional power of θ; cf. Eq. (3.33). This can easily induce corrections of the same order or even larger than the error associated with approximations (i) and (ii). In fact, even the convergence behavior of the paraxial approximation, which corresponds to an asymptotic series [104], with increasing powers of θ is a prior unclear. However, numerical studies of the single-beam signal emission scenario discussed here [89] indicate a convergence behavior of the first few orders of the expansion for the example parameters adopted here already for $w_0 = \lambda$; cf. in particular Fig. 1 of [89].

For the above parameters and the minimal conceivable beam waist of $w_0 = 2\lambda/\pi$ Eq. (3.37) predicts $N_{\text{tot}} \approx 1.8 \times 10^{-8}\,(W/\text{J})^3$ which implies that a laser pulse energy as large as $W = O(500)\,\text{J}$ would be needed to induce just a single signal photon per shot; at the same time $N_{\perp} \simeq N_{\text{tot}}/28.9$. Clearly, such small signals at the frequency of the driving laser field would be absolutely background dominated. This lets us conclude that, as to be expected from the fact that the contribution at $O(\theta^0)$ vanishes identically for this case, a single (paraxial) laser beam does not provide us with a quantum vacuum signal measurable

[‡]In an experimental context, the duration of a laser pulse is typically specified in terms of its *full width at half maximum* (FWHM) τ^{FWHM} in temporal direction on the level of its cycle-averaged intensity. For Gaussian pulse envelopes as considered here this implies $\tau = \sqrt{2/\ln 2}\,\tau^{\text{FWHM}} \simeq 1.7\tau^{\text{FWHM}}$.

with current and near-future technology.

3.2.4 Quantum vacuum signals in laser beam collisions

In the next step, we study quantum vacuum signals induced in the collision of two laser beams [105–108]. Similarly as for the single-beam scenario discussed in the previous section, here we are mainly interested in understanding the dependence of the signal on the parameters characterizing the driving laser fields. To this end, we especially aim at extracting simple analytical scalings for the dominant signal components. These allow to identify the most prospective setup for experiment. Prior to an actual experimental implementation, the quantum vacuum signal for this setup is then to be studied in full detail in the experimentally realistic field configurations with the help of numerical techniques. This is necessary both to confirm the robustness of the signal under real-world experimental conditions, and to assist the measurement campaign by accurate predictions in the actually available field configurations.

As in Sec. 3.2.3 we limit our discussion to the leading non-vanishing contribution of the effect in a paraxial approximation of the driving laser beams and again focus exclusively on the signals attainable in a polarization insensitive measurement and those scattered into a $\perp$-polarized mode. However, now the leading signal in general arises at $O(\theta^0)$ and Eq. (3.16) needs to be evaluated in the composite electromagnetic field of two different laser beams. Because this signal photon amplitude is cubic in the field, for the case of two beams it naturally decomposes into two parts, each of which is linear in the field components of one of the beams and quartic in those of the complementary one. Upon restriction to the terms contributing at $O(\theta^0)$, Eq. (3.19) simplifies to

$$\begin{aligned}\vec{U}_1\big|_{\sim\mathfrak{F}} &= c_a\,(\vec{B}\cdot\vec{\mathfrak{B}} - \vec{E}\cdot\vec{\mathfrak{E}})\vec{E} - c_b\,(\vec{E}\cdot\vec{\mathfrak{B}} + \vec{B}\cdot\vec{\mathfrak{E}})\vec{B}\,,\\ \vec{U}_2\big|_{\sim\mathfrak{F}} &= c_a\,(\vec{B}\cdot\vec{\mathfrak{B}} - \vec{E}\cdot\vec{\mathfrak{E}})\vec{B} + c_b\,(\vec{E}\cdot\vec{\mathfrak{B}} + \vec{B}\cdot\vec{\mathfrak{E}})\vec{E}\,.\end{aligned} \tag{3.39}$$

Correspondingly, at $O(\theta^0)$ the signal photon amplitude for two colliding beams can be expressed in the form of Eqs. (3.16) and (3.17), with the vectors $\vec{U}_{1,2} \to \vec{U}_{1,2}\big|_{\sim\mathfrak{F}}$ given by Eq. (3.39) plus the analogous expression with the electric and magnetic fields of the two beams exchanged as $\vec{E} \leftrightarrow \vec{\mathfrak{E}}, \vec{B} \leftrightarrow \vec{\mathfrak{B}}$.

For simplicity, here we only consider linearly polarized laser fields, though the generalization to circularly polarized fields is straightforward; cf. the discussion in Sec. 3.2.2. Assuming the beam axes of the two lasers I and II without loss of generality to be confined to the xz plane, we parameterize their unit wave vectors and polarization vectors as $\hat{\vec{\kappa}}_I = \vec{e}_z$, $\vec{\epsilon}_I = (\cos\phi_I, \sin\phi_I, 0)$ and $\hat{\vec{\kappa}}_{II} = (\sin\vartheta_{\text{coll}}, 0, \cos\vartheta_{\text{coll}})$, $\vec{\epsilon}_{II} = (\cos\vartheta_{\text{coll}}\cos\phi_{II}, \sin\phi_{II}, -\sin\vartheta_{\text{coll}}\cos\phi_{II})$. The polarization directions of the beams are fixed by choosing the angles ϕ_I and ϕ_{II} appropriately. Finally, we introduce the field amplitude profiles $\mathcal{E}_b(x)$ of the beams $b \in \{I, II\}$ as $\vec{E} = \mathcal{E}_I(x)\,\vec{\epsilon}_I$, $\vec{\mathfrak{E}} = \mathcal{E}_{II}(x)\,\vec{\epsilon}_{II}$ and denote the associated peak field amplitudes by $\mathcal{E}_{0,b}$. Their oscillation frequencies and pulse durations are ω_b and τ_b, respectively. In the generic case, the amplitude profiles have the form of Eq. (3.20) with $\text{Re}\{\vec{\varepsilon}\,\mathrm{e}^{-\mathrm{i}\Phi_{l,p}(x)}\} \to \cos\Phi_{l,p}(x)$. With these definitions, the contribution to the signal photon amplitude linear in $\mathcal{E}_I$ can be compactly represented

as [80]

$$\mathcal{S}_{(p)}(\vec{k})\big|_{\sim\mathcal{E}_I} = (1-\cos\vartheta_{\text{coll}})\,\frac{(-\mathrm{i})}{2\pi}\,\frac{m^2}{45}\,\sqrt{\frac{\alpha}{\pi}\frac{\mathrm{k}}{2}}\left(\frac{e}{m^2}\right)^3 \int \mathrm{d}^4x\,\mathrm{e}^{-\mathrm{i}\mathrm{k}(\hat{k}x)}\,\mathcal{E}_I(x)\,\mathcal{E}_{II}^2(x)$$
$$\times\Big\{\big[\cos\varphi\,(1-\cos\vartheta\cos\vartheta_{\text{coll}})-\sin\vartheta\sin\vartheta_{\text{coll}}\big]\,h(\phi_I+\phi_{II},\beta_p+\phi_{II})$$
$$-\sin\varphi\,(\cos\vartheta-\cos\vartheta_{\text{coll}})\,h(\phi_I+\phi_{II},\beta_p+\phi_{II}-\tfrac{\pi}{2})\Big\}\,, \tag{3.40}$$

where we have made use of the shorthand notation

$$h(\mu,\nu) := c_a\cos\mu\cos\nu + c_b\sin\mu\sin\nu\,. \tag{3.41}$$

Note that, aside from a separate direct calculation, the complementary amplitude linear in $\mathcal{E}_{II}$ can be obtained from Eq. (3.40) by exchanging the labels I and II and transforming the coordinates and field vector orientations appropriately.

For sufficiently large pulse durations $\{\tau_I\omega_I, \tau_{II}\omega_{II}\} \gg 1$ as considered here, the energy spectra associated with the amplitude profiles $\mathcal{E}_{I,II}(x)$ show two pronounced peaks at the oscillation frequencies $\pm\omega_{I,II}$ and are compatible with zero at other energies; cf. also the discussion in the paragraph below Eq. (3.23). This immediately implies that the spectrum of $\mathcal{E}_{II}^2(x)$ exhibits similar peaks at $\pm 2\omega_{II}$ and 0, with the latter one being about twice as strong because both $\pm\omega_{II}\mp\omega_{II}$ result in this energy. Correspondingly, the specific amplitude $\sim\mathcal{E}_I$ in Eq. (3.40) can only induce sizeable signals with energies (a) $\mathrm{k}\approx\omega_I$ and (b) $\mathrm{k}\approx|\omega_I\pm 2\omega_{II}|$. On the other hand, in the regime of validity of the paraxial approximation we have $\theta \ll 1$, which implies that for the signal-photon momentum similar considerations as for its energy are possible; recall that on-shell signal photons fulfill $k^2 = \vec{k}^2 - \mathrm{k}^2 = 0$. These let us conclude that the wave vectors of the signals should fulfill (a) $|\vec{k}| \approx |\omega_I\hat{\vec{k}}_I| = \omega_I$ and (b) $|\vec{k}| \approx |\omega_I\hat{\vec{k}}_I \pm 2\omega_{II}\hat{\vec{k}}_{II}|$. Clearly, for $\hat{\vec{k}}_I \neq \hat{\vec{k}}_{II}$ only the energy and momentum conditions (a) are compatible with each other; no signal is induced for $\hat{\vec{k}}_I = \hat{\vec{k}}_{II}$ because in this limit $1-\cos\vartheta_{\text{coll}} = 0$ and Eq. (3.40) vanishes. In turn, in the considered two-beam case a sizable signal is only to be expected in the vicinity of (a) $\vec{k} = \omega_I\hat{\vec{k}}_I$. Applying exactly the same arguments to the amplitude linear in $\mathcal{E}_{II}$, we find that its signal should be predominantly emitted in the close surrounding of $\vec{k} = \omega_{II}\hat{\vec{k}}_{II}$.

Because these signals are independent of the oscillation frequency of the beam the field profile which enters the respective signal photon amplitude quadratically, in the determination of the dominant signal component one can safely neglect the terms encoding its dependence from the outset: it can be easily verified that this amounts to effectively replacing the quadratic dependence on the field amplitude profile by its cycle average [109]. For the signal photon amplitude $\sim\mathcal{E}_I$ in Eq. (3.40) this implies the replacement $\mathcal{E}_{II}^2(x) \to \langle\mathcal{E}_{II}^2(x)\rangle_t = I_{II}(x)$. Note once again that up to subleading corrections of $O(\frac{1}{\tau_{II}\omega_{II}})$, which are anyhow not accounted for by our simple pulsed beam model from the outset, the pulse envelope is not affected by this averaging procedure; cf. footnote † on page 68.

Moreover, for sufficiently different orientations of $\hat{\vec{k}}_I$ and $\hat{\vec{k}}_{II}$, or well-separated frequencies ω_I and ω_{II}, the interference term $2\mathrm{Re}\{\mathcal{S}_{(p)}(\vec{k})|_{\sim\mathcal{E}_I}\mathcal{S}^*_{(p)}(\vec{k})|_{\sim\mathcal{E}_{II}}\}$ can be safely neglected when taking the modulus squared of $\mathcal{S}_{(p)}(\vec{k})$ to obtain the differential number of signal photons (3.8). As a consequence, the signal

decomposes into two distinct contributions,

$$\mathrm{d}^3 N_{p,b} = \frac{\mathrm{d}^3 k}{(2\pi)^3} \left| \mathcal{S}_p(\vec{k}) \big|_{\sim \mathcal{E}_b} \right|^2 , \tag{3.42}$$

with $b \in \{I, II\}$. The above considerations in particular imply that the signal $N_{p,b}$ can be interpreted in terms of laser photons of beam b being quasi-elastically scattered at the cycle-averaged intensity profile of the other beam mediated by quantum vacuum fluctuations. In this sense, beam b can be considered as *probing* the quantum vacuum nonlinearity *pumped* by the other beam. Subsequently, we concentrate only on the signal $N_{p,I}$. As noted below Eq. (3.40), in general the result for $N_{p,II}$ can then be extracted therefrom with the help of a coordinate transformation and by mapping the parameters of beam I on beam II and vice versa.

With foresight, in Eq. (3.40) we have chosen $\hat{\vec{k}}_I = \vec{e}_\mathrm{z}$, such that, (in our conventions) the polar angle ϑ measures the deflection of the signal from the forward beam axis of beam I. Therefore, we can readily employ the approximations devised and detailed in Sec. 3.2.3 to simplify the prefactor of the Fourier integral, namely (i) identify $\mathrm{k} = \omega_I$ and (ii) account only for its leading contribution in the limit of $\vartheta \ll 1$. This yields the following expression,

$$\begin{aligned} \mathcal{S}_{(p)}(\vec{k})\big|_{\sim \mathcal{E}_I} \approx (1 - \cos\vartheta_\mathrm{coll})^2 \, \frac{(-\mathrm{i})}{2\pi} \frac{m^2}{45} \sqrt{\frac{\alpha}{\pi}\frac{\omega_I}{2}} \left(\frac{e}{m^2}\right)^3 \int \mathrm{d}^4 x \, \mathrm{e}^{-\mathrm{i}\mathrm{k}(\hat{k}x)} \, \mathcal{E}_I(x) \, \langle \mathcal{E}_{II}^2(x) \rangle_t \\ \times \Big[c_a \cos(\varphi + \beta_p + \phi_{II}) \cos(\phi_I + \phi_{II}) + c_b \sin(\varphi + \beta_p + \phi_{II}) \sin(\phi_I + \phi_{II}) \Big] , \end{aligned} \tag{3.43}$$

from which it is obvious that for focused laser beams (reaching their peak field at the same space-time coordinate) a collision angle of $\vartheta_\mathrm{coll} = \pi$ yields the maximum signal. We emphasize that this does not only follow from the overall factor of $(1 - \cos\vartheta_\mathrm{coll})^2$, but also from the Fourier integral to be performed over the field amplitude profiles: because the Rayleigh range $\mathrm{z_R}$ of a given beam is always larger than its focus diameter $2w_0$, the integral over the field amplitude profiles in Eq. (3.43) typically has the largest support for $\vartheta_\mathrm{coll} = \pi$ and thus becomes maximum in this limit; note that the genuine oscillatory behavior of the integrand as a function of x is approximately removed for $\mathrm{k} \simeq \omega_I$, such that the integral scales with the space-time volume where both field amplitude profiles overlap. This dependence of the signal motivates the use of collision angles $\pi/2 < \vartheta_\mathrm{coll} \leq \pi$ in prospective discovery experiments aiming at the verification of quantum vacuum nonlinearity. Also note that in this angle regime the orientations of $\hat{\vec{k}}_I$ and $\hat{\vec{k}}_{II}$ should indeed be sufficiently different to render the decomposition invoked to arrive at Eq. (3.42) well justified.

As in Sec. 3.2.3, here we focus exclusively on the number of signal photons attainable in a polarization insensitive measurement $N_{\mathrm{tot},I}$ and the number of signal photons scattered in a $\perp$-polarized mode $N_{\perp,I}$. Because the signal $N_{p,I}$ is predominantly emitted in the vicinity of the forward cone of beam I constituting the background from which it is to be distinguished in the far-field, it is natural to identify $N_{\perp,I}$ with the component fulfilling $\vec{\epsilon}_I \cdot \vec{e}_\perp(\beta_p) = 0 \;\leftrightarrow\; \beta_p = \arctan\{\cot(\varphi - \phi_I)\cos\vartheta\}$. For $\vartheta \ll 1$ as considered here, this simplifies to $\beta_p \simeq \frac{\pi}{2} - (\varphi - \phi_I)$. Employing these definitions and once again (i) and (ii) to write $\mathrm{d}^3 k \approx \omega_I^2 \mathrm{dk}\,\mathrm{d}\varphi\,\vartheta\mathrm{d}\vartheta$, the differential number of signal photons (3.42) associated with

Eq. (3.43) can be compactly expressed as

$$\left\{ \begin{array}{c} \frac{\mathrm{d}^3 N_{\mathrm{tot},I}}{\mathrm{dk}\,\mathrm{d}\varphi\,\vartheta\mathrm{d}\vartheta} \\ \frac{\mathrm{d}^3 N_{\perp,I}}{\mathrm{dk}\,\mathrm{d}\varphi\,\vartheta\mathrm{d}\vartheta} \end{array} \right\} \approx (1-\cos\vartheta_{\mathrm{coll}})^4\,\omega_I^3 m^4 \frac{1}{(2\pi)^6}\frac{\alpha}{2025}\left(\frac{e}{m^2}\right)^6 \left|\mathcal{M}_I(\vec{k})\right|^2 \left\{ \begin{array}{c} (c_a^2-c_b^2)\cos^2(\Delta\phi)+c_b^2 \\ \frac{1}{4}(c_a-c_b)^2\sin^2(2\Delta\phi) \end{array} \right\}, \quad (3.44)$$

where we introduced the shorthand notation

$$\mathcal{M}_I(\vec{k}) = \int \mathrm{d}^4 x\, \mathrm{e}^{-\mathrm{ik}(\hat{k}x)}\,\mathcal{E}_I(x)\,\langle \mathcal{E}_{II}^2(x)\rangle_t\,, \quad (3.45)$$

and $\Delta\phi = \phi_I + \phi_{II}$ encodes the full dependence of the signal on the polarization directions of the driving laser beams. Even though in our conventions the polarization vector $\vec{\epsilon}_{II}$ of beam II naturally also depends on $\vartheta_{\mathrm{coll}}$, in Eq. (3.44) this dependence factorizes. This allows choosing optimal beam polarizations that maximize the signal photon numbers independently of the collision angle. As $c_a^2 - c_b^2 < 0$, the result for $N_{\mathrm{tot},I}$ becomes maximum for $\Delta\phi = \pi/2$. On the other hand, for $N_{\perp,I}$ the best choice is clearly $\Delta\phi = \pi/4$. The ratio of maximum attainable values for $N_{\mathrm{tot},I}$ and $N_{\perp,I}$ is $N_{\mathrm{tot},I}|_{\Delta\phi=\frac{\pi}{2}}/(N_{\perp,I}|_{\Delta\phi=\frac{\pi}{4}}) = [2c_b/(c_a-c_b)]^2 \simeq 21.8$ [110]. For completeness, we also note that the signal $N_{\parallel,I} = N_{\mathrm{tot},I} - N_{\perp,I}$ polarized parallel to beam I is again maximized by $\Delta\phi = \pi/2$. For this particular choice we have $N_{\perp,I} = 0$ and thus $N_{\parallel,I} = N_{\mathrm{tot},I}$.

Subsequently we adopt the choice $\vartheta_{\mathrm{coll}} = \pi$, i.e., focus on counter-propagating laser beams. As argued above, this results in the maximal signal photon yield. At the same time, it simplifies the calculation considerably due to the factorization of the transverse and longitudinal coordinate dependences of both beams in the integral to be performed in Eq. (3.44). Especially for collisions at zero impact parameter, the resulting field configuration features a rotational symmetry around the common beam axis. From the form of Eq. (3.20) it is immediately obvious that in the counter-propagating geometry the integrations over the temporal and the transverse coordinates can be readily carried out analytically for generic field amplitude profiles; they boil down to simple Gaussian integrals. Only the integration over the longitudinal coordinate z remains in general analytically intractable. Also note that in this case $\Delta\phi$ directly measures the angle between the polarization vectors of the two colliding laser beams.

Another important feature of Eq. (3.44) is that it scales linearly with the number of laser photons N_I constituting the probe beam and with a positive power of its frequency ω_I. Note that Eq. (3.27) implies $\mathcal{E}_{0,I}^2 \sim W_I \simeq N_I\omega_I$, and hence $\mathrm{d}^3N_{p,I}/\mathrm{dk}\mathrm{d}\varphi\,\vartheta\mathrm{d}\vartheta|_{\vartheta=0} \sim \omega_I^4 N_I$. On the other hand, the signals in Eq. (3.44) scale quadratic with the pulse energy of the pump $W_{II} \simeq N_{II}\omega_{II}$. Taking into account $\int \mathrm{d}\vartheta\,\vartheta \sim \theta_I^2 \sim 1/\omega_I^2$, the full integrated signal is thus expected to scale as $N_{p,I} \sim (\omega_I\omega_{II})^2 N_I N_{II}^2$; cf. also Eq. (3.60) below. Among other possibilities, this suggests using a brilliant x-ray probe such as provided by an x-ray free-electron laser (XFEL) for quantum vacuum experiments based on two laser beams [109, 111–116]. By reaching a similar order of magnitude for the combined parameter $\omega_I^2 N_I$, an x-ray photon energy ω_I in the keV range should then compensate the typically smaller number of probe photons N_I per pulse provided by XFELs relatively to a petawatt-class near-infrared laser probe in the attainable signal. At the same time one could benefit from the higher detection efficiencies for photons in the x-ray regime. Therefore, we specialize our subsequent considerations to an x-ray probe counter-propagating a near-infrared high-intensity laser beam. For completeness, we also note that in this specific case the

quasi-elastic signal $N_{II,p} \sim (\omega_I \omega_{II})^2 N_I^2 N_{II}$ in the complementary channel is considerably suppressed relatively to $N_{I,p}$ because of $N_I \ll N_{II}$.

3.2.4.1 Collisions of fundamental Gaussian beams

To keep the discussion transparent and easy to follow, in a first step we model both the pump and the probe laser fields as fundamental Gaussian beams. Moreover, to allow for the investigation of the behavior of the signal for non-optimal collisions, in this scenario we account for a finite spatial offset $\vec{x}_0$ between the foci of both beams as well as a temporal detuning t_0; see the explicit field amplitude profiles in Eqs. (3.46) and (3.47) below.

An additional advantage of the scenario involving an x-ray and a near-infrared laser beam is that it allows for further simplifications of the calculation of the Fourier integral in Eq. (3.44) arising from the fact that x-ray beams with photon energies $\omega_I \gtrsim 5\,\mathrm{keV}$ as considered in the following cannot be focused even close to their diffraction limit without substantial losses with present technology. Accessible waists fulfill $w_{0,I} \gtrsim 50\,\mathrm{nm}$, which for the above photon energies translates into Rayleigh ranges $\mathrm{z}_{\mathrm{R},I} \gtrsim 30\,\mu\mathrm{m}$. Note that the Rayleigh range $\mathrm{z}_{\mathrm{R},II}$ of an near-infrared laser with wavelength $\lambda_{II} = 800\,\mathrm{nm}$ is smaller than this value if it is focused down to $w_{0,II} \lesssim 3\,\mu\mathrm{m}$, which is precisely the waist regime targeted in experiment to reach the largest peak field strengths with high-intensity lasers. Hence, especially for pump and probe waists of the same order, $w_{0,I} \sim w_{0,II}$, we have $\mathrm{z}_{\mathrm{R},I} \gg \mathrm{z}_{\mathrm{R},II}$ such that the widening of beam I as a function of the longitudinal coordinate z can be safely neglected in the interaction region with beam II for longitudinal offsets z_0 between the beam foci fulfilling $\mathrm{z}_0 \ll \mathrm{z}_{\mathrm{R},I}$ without compromising the accuracy of the calculation. This *infinite Rayleigh range approximation* [80, 117] for beam I is equivalent to formally sending $\mathrm{z}_{\mathrm{R},I} \to \infty$ while keeping $w_I(\mathrm{z}) \to w_{0,I}$ constant and will be adopted below. We emphasize that this approximation is certainly only justified in the interaction region and will be exclusively employed there. When discussing features of the beam in the far field, i.e., for $\mathrm{z} \gg \mathrm{z}_{\mathrm{R},II}$, its widening with z inevitably has to be accounted for. For completeness, we note that the same approximation with $w_I(\mathrm{z}) \to w_I(\mathrm{z}_0)$ can be used also for finite longitudinal offsets z_0 between the beam foci in the parameter regime where $\mathrm{z}_0 \lesssim \mathrm{z}_{\mathrm{R},I}$, and given that the transverse offset $r_0 = (\mathrm{x}_0^2 + \mathrm{y}_0^2)^{1/2}$ is sufficiently small such that the criterion $r_0 \ll w_{0,I}$ holds even for $\mathrm{z}_0 > \mathrm{z}_{\mathrm{R},I}$. Otherwise, wave-front curvature of the probe need to be consistently accounted for [118, 119]. However, as to be expected, for longitudinal offsets of the order of $\mathrm{z}_{\mathrm{R},I}$ the attainable quantum vacuum signals are substantially suppressed in comparison to the regime of primary interest to us characterized by $\mathrm{z}_0 \ll \mathrm{z}_{\mathrm{R},I}$.

In line with the above discussion, we choose the field amplitude profiles entering Eq. (3.45) as

$$\mathcal{E}_I(x) = \mathcal{E}_{0,I}\, \mathrm{e}^{-\left(\frac{(\mathrm{z}-\mathrm{z}_0)-(t-t_0)}{\tau_I/2}\right)^2} \mathrm{e}^{-\left(\frac{r-r_0}{w_I}\right)^2} \cos\Big(\omega_I[(\mathrm{z}-\mathrm{z}_0)-(t-t_0)] - \psi_0\Big)\,, \tag{3.46}$$

and

$$\langle \mathcal{E}_{II}^2(x)\rangle_t = \frac{1}{2}\,\mathcal{E}_{0,II}^2\, \mathrm{e}^{-2\left(\frac{\mathrm{z}+t}{\tau_{II}/2}\right)^2} \left(\frac{w_{0,II}}{w_{II}(\mathrm{z})}\right)^2 \mathrm{e}^{-2\left(\frac{r}{w_{II}(\mathrm{z})}\right)^2}\,, \tag{3.47}$$

with $w_I := w_{0,I}$ and $w_{II}(\mathrm{z}) = w_{0,II}\sqrt{1+(\mathrm{z}/\mathrm{z}_{\mathrm{R},II})^2}$. Upon insertion of Eqs. (3.46) and (3.47) into Eq. (3.45), the integrations over time and the transverse coordinates can be performed right away, yield-

ing the following expression for the modulus of Eq. (3.45),

$$\left|\mathcal{M}_I(\vec{k})\right| \simeq \mathcal{E}_{0,I}\,\mathcal{E}_{0,II}^2\,\frac{1}{4}\Big(\frac{\pi}{2}\Big)^{\frac{3}{2}}\frac{\tau_{II}\,\mathrm{z}_{\mathrm{R},II}}{\sqrt{1+\frac{1}{2}(\frac{\tau_{II}}{\tau_I})^2}}\,\mathrm{e}^{-\frac{2}{1+\frac{1}{2}(\frac{\tau_{II}}{\tau_I})^2}\left[\tau_{II}^2(\frac{\omega_I-\mathrm{k}}{8})^2+2(\frac{\mathrm{z}_0-t_0}{\tau_I})^2\right]}$$
$$\times\left|\int \mathrm{d}\zeta\,\frac{w_{0,II}^2 w_I^2}{w_{II}^2(\zeta)+2w_I^2}\,\mathrm{e}^{-\frac{2r_0^2}{w_{II}^2(\zeta)+2w_I^2}-\frac{1}{4}\frac{w_{II}^2(\zeta)w_I^2(\mathrm{k}\sin\vartheta)^2}{w_{II}^2(\zeta)+2w_I^2}}\,\mathrm{e}^{-\left(\frac{4\mathrm{z}_{\mathrm{R},II}}{\tau_I}\right)^2\frac{\zeta^2-\frac{\mathrm{z}_0-t_0}{\mathrm{z}_{\mathrm{R},II}}\zeta}{1+\frac{1}{2}(\frac{\tau_{II}}{\tau_I})^2}}\,\mathrm{e}^{\mathrm{i}\mathrm{z}_{\mathrm{R},II}\left[\frac{2(\omega_I-\mathrm{k})}{1+\frac{1}{2}(\frac{\tau_{II}}{\tau_I})^2}+\mathrm{k}(1-\cos\vartheta)\right]\zeta}\right|. \quad (3.48)$$

Here, we introduced a dimensionless longitudinal coordinate $\zeta = \mathrm{z}/\mathrm{z}_{\mathrm{R},II}$ and $w_{II}(\zeta) = w_{0,II}\sqrt{1+\zeta^2}$. Moreover, in accordance with the employed pulsed beam approximation, we neglected a contribution $\sim \mathrm{e}^{-\#(\tau_I\omega_I)^2}$ with $\# > 0$; cf. Eq. (3.25) and footnote † on page 68. Accounting for the approximations (i) and (ii) already adopted to simplify the prefactor of the Fourier integral in Eq. (3.43), in a next step we identify $\mathrm{k} = \omega_I$ in the slowly varying terms in Eq. (3.48) and restrict ourselves to the leading contribution in $\vartheta \ll 1$ in the exponential; note that in the present context we have $\theta_I = 2/(\omega_I w_I) \ll 1$ and $\vartheta/\theta_I \lesssim 1$ such that the term scaling with $\vartheta^2/\theta_I \ll 1$ can be safely neglected. This results in the approximation

$$\left|\mathcal{M}_I(\vec{k})\right| \approx \mathcal{E}_{0,I}\,\mathcal{E}_{0,II}^2\,\frac{1}{4}\Big(\frac{\pi}{2}\Big)^{\frac{3}{2}}\frac{\tau_{II}\,\mathrm{z}_{\mathrm{R},II}}{\sqrt{1+\frac{1}{2}(\frac{\tau_{II}}{\tau_I})^2}}\,\mathrm{e}^{-\frac{2}{1+\frac{1}{2}(\frac{\tau_{II}}{\tau_I})^2}\left[\tau_{II}^2(\frac{\omega_I-\mathrm{k}}{8})^2+2(\frac{\mathrm{z}_0-t_0}{\tau_I})^2\right]}$$
$$\times\left|\int \mathrm{d}\zeta\,\frac{w_{0,II}^2 w_I^2}{w_{II}^2(\zeta)+2w_I^2}\,\mathrm{e}^{-\frac{2r_0^2}{w_{II}^2(\zeta)+2w_I^2}-\frac{w_{II}^2(\zeta)}{w_{II}^2(\zeta)+2w_I^2}(\vartheta/\theta_I)^2}\,\mathrm{e}^{-\left(\frac{4\mathrm{z}_{\mathrm{R},II}}{\tau_I}\right)^2\frac{\zeta^2-\frac{\mathrm{z}_0-t_0}{\mathrm{z}_{\mathrm{R},II}}\zeta}{1+\frac{1}{2}(\frac{\tau_{II}}{\tau_I})^2}}\,\mathrm{e}^{\mathrm{i}\frac{2\mathrm{z}_{\mathrm{R},II}(\omega_I-\mathrm{k})}{1+\frac{1}{2}(\frac{\tau_{II}}{\tau_I})^2}\zeta}\right|, \quad (3.49)$$

which is well-behaved and can be straightforwardly evaluated numerically for arbitrary parameters. For the special case of $r_0 = \vartheta = 0$, the integral over ζ can even be performed analytically. Resorting to the following identity for $a > 0$ and $A \geq 0$,

$$\int \mathrm{d}\zeta\,\frac{1}{a^2+\zeta^2}\,\mathrm{e}^{-A\zeta^2+(B+\mathrm{i}C)\zeta} = \frac{1}{a}\frac{\pi}{2}\,\mathrm{e}^{a^2A}\sum_{s=\pm1}\mathrm{e}^{sa(C-\mathrm{i}B)}\,\mathrm{erfc}\Big(a\sqrt{A}+\tfrac{s}{2}\tfrac{C-\mathrm{i}B}{\sqrt{A}}\Big), \quad (3.50)$$

it can be expressed in terms of the complementary error function $\mathrm{erfc}(\cdot)$. The latter is related to the error function by $\mathrm{erf}(\cdot) = 1 - \mathrm{erfc}(\cdot)$.

Also note that if we had replaced $w_{II}(\mathrm{z})$ in the exponential of Eq. (3.47) by an z independent *effective waist* $\bar{w}_{II} \geq w_{0,II}$ while correctly accounting for the longitudinal localization of the field profile $\sim 1/[1 + (\mathrm{z}/\mathrm{z}_{\mathrm{R},II})^2]$ encoded in its prefactor and had otherwise employed exactly the same approximations as invoked above we would have arrived at an expression very similar to Eq. (3.49): the corresponding result follows from Eq. (3.49) by identifying all occurrences of $w_{II}(\zeta)$ with $\bar{w}_{II} = \text{const.}$ and taking into account an additional factor of $(\bar{w}_{II}/w_{II}(\zeta))^2$ in the integrand of the ζ integral; this defines $|\bar{\mathcal{M}}_I(\vec{k})|$. Clearly, the integration to be performed in this case has the structure of the one in Eq. (3.49) in the limit of $r_0 = \vartheta = 0$ and thus can also be carried out explicitly. The effective waist $\bar{w}_{II}$ can be interpreted as an average beam radius governing the radial decay of beam II in the interaction region where the quantum vacuum signal is induced. Making use of this fact, further analytical insights are possible. Namely,

we can determine the signal photon amplitude for generic parameters by resorting to the effective waist approximation and in a second step fix the effective waist by demanding the expressions for $\int \mathrm{dk}\,|\mathcal{M}_I(\vec{k})|^2$ and $\int \mathrm{dk}\,|\bar{\mathcal{M}}_I(\vec{k})|^2$ to agree with each other for $r_0 = \vartheta = 0$; recall that in line with (ii) the integral over k can be extended to the entire k axis without compromising the accuracy of the approximation because it rapidly decays to zero away from $\mathrm{k} \simeq \omega_I$. This yields an excellent approximation in a wide range of parameters and allows for the derivation of simple analytical scalings [99] that can be employed to identify the most prospective choices of parameters in experiment [100]; see [99] for a generalization to elliptical probe beam profiles. An explicit evaluation results in

$$\int \mathrm{dk}\,\big|\mathcal{M}_I(\vec{k})\big|^2\Big|_{r_0=\vartheta=0} \approx \frac{1}{2}\sqrt{\frac{3}{2}}\left(\frac{\pi}{4}\right)^5 \mathcal{E}_{0,I}^2\,\mathcal{E}_{0,II}^4\,\frac{\tau_I\tau_{II}^2 w_I^4}{[1+2(\frac{w_I}{w_{0,II}})^2]^2}\,F\!\left(\frac{4\mathrm{z_{R,}}_{II}\sqrt{1+2(\frac{w_I}{w_{0,II}})^2}}{\sqrt{\tau_I^2+\frac{1}{2}\tau_{II}^2}},\frac{2(\mathrm{z}_0-t_0)}{\sqrt{\tau_I^2+\frac{1}{2}\tau_{II}^2}},\frac{\tau_I}{\tau_{II}}\right), \quad (3.51)$$

and

$$\int \mathrm{dk}\,\big|\bar{\mathcal{M}}_I(\vec{k})\big|^2 \approx \frac{1}{2}\sqrt{\frac{3}{2}}\left(\frac{\pi}{4}\right)^5 \mathcal{E}_{0,I}^2\,\mathcal{E}_{0,II}^4\,\frac{\tau_I\tau_{II}^2 w_I^4}{[1+2(\frac{w_I}{\bar{w}_{II}})^2]^2}\,F\!\left(\frac{4\mathrm{z_{R,}}_{II}}{\sqrt{\tau_I^2+\frac{1}{2}\tau_{II}^2}},\frac{2(\mathrm{z}_0-t_0)}{\sqrt{\tau_I^2+\frac{1}{2}\tau_{II}^2}},\frac{\tau_I}{\tau_{II}}\right) \times \mathrm{e}^{-\frac{4r_0^2}{\bar{w}_{II}^2+2w_I^2}-\frac{2\bar{w}_{II}^2}{\bar{w}_{II}^2+2w_I^2}\left(\frac{\vartheta}{\theta_I}\right)^2}, \quad (3.52)$$

where we made use of the definition

$$F(\chi,\chi_0,\rho) := \sqrt{\frac{1+2\rho^2}{3}}\,\chi^2\,\mathrm{e}^{2(\chi^2-\chi_0^2)}\int_{-\infty}^{\infty}\mathrm{d}K\,\mathrm{e}^{-K^2}\left|\sum_{s=\pm1}\mathrm{e}^{2s(\rho K-\mathrm{i}\chi_0)\chi}\,\mathrm{erfc}\Big(s(\rho K-\mathrm{i}\chi_0)+\chi\Big)\right|^2. \quad (3.53)$$

Equating Eqs. (3.51) and (3.52) evaluated for $r_0 = \vartheta = 0$, we obtain a defining equation for the effective waist $\bar{w}_{II}$ [100],

$$\left(\frac{1+2(\frac{w_I}{\bar{w}_{II}})^2}{1+2(\frac{w_I}{w_{0,II}})^2}\right)^2 = \frac{F(0)}{F(\frac{w_I}{w_{0,II}})} \leq 1\,, \quad (3.54)$$

where, for convenience, we introduced the shorthand notation

$$F(b) := F\!\left(\frac{4\mathrm{z_{R,}}_{II}\sqrt{1+2b^2}}{\sqrt{\tau_I^2+\frac{1}{2}\tau_{II}^2}},\frac{2(\mathrm{z}_0-t_0)}{\sqrt{\tau_I^2+\frac{1}{2}\tau_{II}^2}},\frac{\tau_I}{\tau_{II}}\right), \quad (3.55)$$

suppressing the dependences on the laser and collision parameters τ_I, τ_{II}, $\mathrm{z_{R,}}_{II}$ and z_0-t_0. Equation (3.54) implies that for $w_I/w_{0,II} \to 0$ the effective waist $\bar{w}_{II}$ matches $w_{0,II}$. This is in line with expectations because in this limit the transverse extent of the interaction region should be determined by $w_I \ll w_{0,II}$ and thus be essentially insensitive to deviations of the radius of beam II from $w_{0,II}$. Even though Eq. (3.55) can be easily evaluated numerically in all relevant parameter regimes, it is also worthwhile to briefly highlight the immediate analytic insights available in various limits, namely (cf. also [99])

$$F(b)\big|_{\mathrm{z_{R,}}_{II}\to\infty} \simeq \frac{4}{\sqrt{3\pi}}\,,$$

$$
\begin{aligned}
F(b)\big|_{(\tau_I=\tau_{II})\to\infty} &\simeq \frac{2}{3}\sqrt{\pi}\Big(\frac{8\mathrm{z}_{\mathrm{R},II}}{\tau_I}\Big)^2(1+2b^2)\,,\\
F(b)\big|_{\tau_I\to\infty} &\simeq \sqrt{\frac{2\pi}{3}}\,\frac{\tau_{II}}{\tau_I}\Big(\frac{8\mathrm{z}_{\mathrm{R},II}}{\tau_{II}}\Big)^2(1+2b^2)\,\mathrm{e}^{\left(\frac{8\mathrm{z}_{\mathrm{R},II}}{\tau_{II}}\right)^2(1+2b^2)}\,\mathrm{erfc}\Big(\tfrac{8\mathrm{z}_{\mathrm{R},II}}{\tau_{II}}\sqrt{1+2b^2}\Big)\,,\\
F(b)\big|_{\tau_{II}\to\infty} &\simeq 2\sqrt{\frac{\pi}{3}}\Big(\frac{8\mathrm{z}_{\mathrm{R},II}}{\tau_{II}}\Big)^2(1+2b^2)\,.
\end{aligned}
\tag{3.56}
$$

Each of these expressions should constitute a reasonable approximation to $F(b)$ if the parameter formally sent to infinity is much larger than the others out of the set $\{\mathrm{z}_{\mathrm{R},II},\tau_I,\tau_{II},\mathrm{z}_0-t_0\}$ determining the argument of Eq. (3.55). All the limiting values given in Eq. (3.56) are independent of the longitudinal offset z_0-t_0. The fact that $F(b)|_{\mathrm{z}_{\mathrm{R},II}\to\infty}$ does not depend on b immediately implies $\bar{w}_{II}=w_{0,II}$ in this limit; cf. Eq. (3.54). This matches the expected behavior of an infinite Rayleigh range approximation [80, 117] for beam II; cf. also the corresponding discussion in the introductory paragraph of the present section.

In a next step, we use Eq. (3.25) to express the peak field amplitudes via the pulse energies of the driving laser beams. Adopting the *effective waist approximation* (3.52) as well as Eq. (3.54), the angular distribution of the signal photons can then be approximated as

$$
\begin{aligned}
\left\{\begin{array}{c}\frac{\mathrm{d}^2N_{\mathrm{tot},I}}{\mathrm{d}\varphi\,\vartheta\mathrm{d}\vartheta}\\[2pt]\frac{\mathrm{d}^2N_{\perp,I}}{\mathrm{d}\varphi\,\vartheta\mathrm{d}\vartheta}\end{array}\right\} \approx\;& \sqrt{\frac{3}{\pi}}\frac{8\alpha^4}{2025\pi^2}\frac{W_IW_{II}^2}{m^3}\Big(\frac{\omega_I}{m}\Big)^3\frac{1}{(mw_{0,II})^2}\left\{\begin{array}{c}(c_a^2-c_b^2)\cos^2(\Delta\phi)+c_b^2\\[2pt]\frac{1}{4}(c_a-c_b)^2\sin^2(2\Delta\phi)\end{array}\right\}\\
&\times\frac{(\frac{w_I}{w_{0,II}})^2}{[1+2(\frac{w_I}{w_{0,II}})^2]^2}\,F\big(\tfrac{w_I}{w_{0,II}}\big)\,\mathrm{e}^{-\frac{4r_0^2}{\bar{w}_{II}^2+2w_I^2}}\,\mathrm{e}^{-\frac{2\bar{w}_{II}^2}{\bar{w}_{II}^2+2w_I^2}\left(\frac{\vartheta}{\theta_I}\right)^2}\,,
\end{aligned}
\tag{3.57}
$$

where only the exponential factors depends on $\bar{w}_{II}$. To be specific, this result follows from Eq. (3.44) specialized to $\vartheta_{\mathrm{coll}}=\pi$ upon substitution of $\mathcal{M}_I(\vec{k})\to\bar{\mathcal{M}}_I(\vec{k})$ and integration over the signal photon energy. With the help of Eq. (3.54) the residual explicit dependence of Eq. (3.57) on $\bar{w}_{II}$ can be readily eliminated. However, because the resulting expression is not particularly instructive, we refrain from doing this here. A particular advantage of the approximation (3.57) is that it allows to extract an analytic result for the far-field angular divergence of the signal, namely

$$
\theta_{\mathrm{signal},I}\simeq\theta_I\sqrt{1+2\Big(\frac{w_I}{\bar{w}_{II}}\Big)^2}=\theta_I\sqrt{1+2\Big(\frac{w_I}{w_{0,II}}\Big)^2}\Big(\frac{F(0)}{F(\frac{w_I}{w_{0,II}})}\Big)^{\frac{1}{4}}\,;
\tag{3.58}
$$

recall the definition of the divergence of a fundamental Gaussian beam in Eq. (3.24). From the first expression in Eq. (3.58) it is obvious that the divergence of the signal surpasses the divergence θ_I of beam I for generic choices of the beam waists. Only in the limit of $w_I/w_{0,II}\to 0$ we have $\theta_{\mathrm{signal},I}\simeq\theta_I$. Another key feature of Eq. (3.57) is that it makes explicit the exponential decay of the signal as a function of the impact parameter r_0,

$$
\sim\exp\Big\{-\frac{4r_0^2}{\bar{w}_{II}^2+2w_I^2}\Big\}=\exp\Big\{-2\Big(\frac{r_0}{w_I}\Big)^2\Big(1-\frac{w_{0,II}^2}{w_{0,II}^2+2w_I^2}\sqrt{\frac{F(\frac{w_I}{w_{0,II}})}{F(0)}}\Big)\Big\}\,.
\tag{3.59}
$$

For later reference, we note that for $w_I/w_{0,II}\to 0$ Eq. (3.59) reduces to $\exp\{-4(r_0/w_{0,II})^2\}$. Finally, we

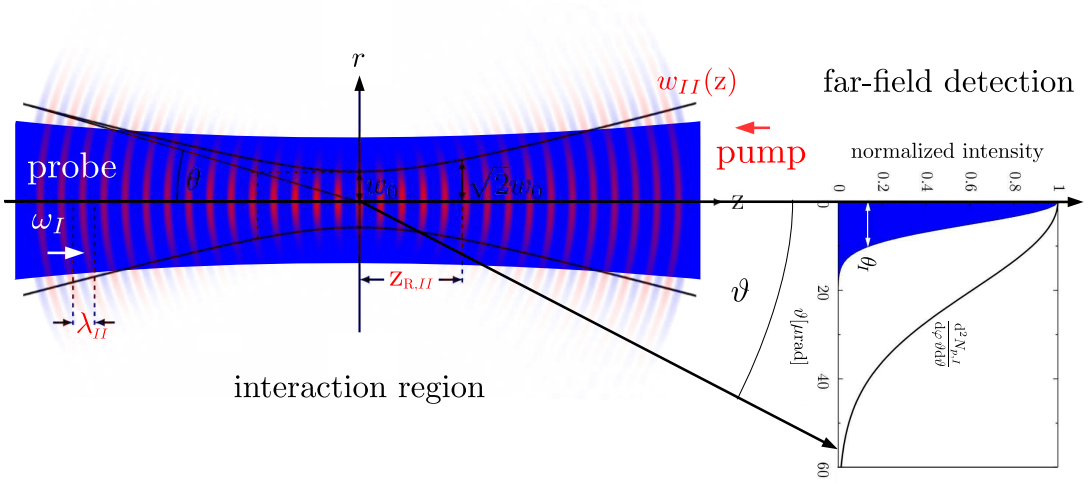

Figure 3.1: Schematic layout of the collision scenario considered here for $x_0^\mu = 0$. In general, the far-field angular decay of the signal photons $N_{p,I}$ differs from that of the laser photons N_I constituting the probe (blue shaded curve). Typically, the signal photons become discernible for sufficiently large values of ϑ.

highlight that Eq. (3.57) can be straightforwardly integrated over all possible emission angles, yielding

$$\left\{ \begin{array}{c} N_{\text{tot},I} \\ N_{\perp,I} \end{array} \right\} \approx N_I \sqrt{\frac{3}{\pi}} \frac{16\alpha^4}{2025\pi} \left(\frac{W_{II}}{m}\frac{\omega_I}{m}\right)^2 \frac{1}{(m w_{0,II})^4} \left\{ \begin{array}{c} (c_a^2 - c_b^2)\cos^2(\Delta\phi) + c_b^2 \\ \frac{1}{4}(c_a - c_b)^2 \sin^2(2\Delta\phi) \end{array} \right\}$$
$$\times \frac{1}{1 + 2(\frac{w_I}{w_{0,II}})^2} \sqrt{F(0)F(\tfrac{w_I}{w_{0,II}})}\, \mathrm{e}^{-\frac{4r_0^2}{w_{II}^2 + 2w_I^2}}, \tag{3.60}$$

where we have expressed the pulse energy W_I in terms of the number of laser photons contained in the pulse given by $N_I \simeq W_I/\omega_I$. Obviously, the ratio of the number of signal to driving laser photons $N_{p,I}/N_I$ then scales with the square of the photon energy ω_I. Using Eq. (3.54) it is straightforward to see that when considering w_I as a free parameter to be adjusted while keeping the other parameters fixed the integrated signal photon numbers in Eq. (3.60) become maximum for $w_I \ll w_{0,II}$. We recall that this is precisely the limit in which the far-field divergences of the signal $\theta_{\text{signal},I}$ and the background θ_I approximately coincide.

An important criterion to assess if a quantum vacuum signal is accessible in experiment with reasonable efforts and not completely background dominated is the signal-to-background separation. This can typically be formulated in terms of a *discernibility criterion*, which in the present context is of the form

$$\frac{\mathrm{d}^3 N_{p,I}}{\mathrm{d}^3 k} \geq \mathcal{P}_p \frac{\mathrm{d}^3 N_I}{\mathrm{d}^3 k}, \tag{3.61}$$

where $\mathcal{P}_p \geq 0$ quantifies the performance or purity of the photon detection system used for the measurement of the p-polarized signal component. In general, $\mathcal{P}_p$ depends on the energy k and the emission direction (φ, ϑ) of the photons to be detected. Signal components which fulfill Eq. (3.61) are *discernible* from the background of the driving laser photons. For simplicity and for illustration purposes, in this work

we assume $\mathcal{P}_p$ to be independent of $\vec{k}$, i.e., $\mathcal{P}_p = \text{const}$. In this case, Eq. (3.61) can be simply integrated over all possible photon energies and emission directions, and the analogous criterion for the integrated number of p-polarized signal photons to be discernible from the number of the driving laser photons N_I traversing the interaction region essentially without modification reads $N_{p,I} \geq \mathcal{P}_p N_I$. Here, the quantity on the right-hand side amounts to the number of background photons registered by the detector. The latter condition is typically not met for the parameters available in experiment with state-of-the-art technology. However, the fact that the divergence of the signal (3.58) fulfills $\theta_{\text{signal},I} > \theta_I$ for finite w_I and $w_{0,II}$ implies that even in situations where $N_{p,I}/N_I < \mathcal{P}_p$, and thus also $(\mathrm{d}N_{p,I}/\vartheta\mathrm{d}\vartheta)\,(\mathrm{d}N_I/\vartheta\mathrm{d}\vartheta)^{-1}|_{\vartheta=0} < \mathcal{P}_p$, the signal will eventually become discernible from a certain polar angle ϑ_p^{dis} onwards, i.e., for $\vartheta \geq \vartheta_p^{\text{dis}}$. See Fig. 3.1 for an illustration. The far-field angular decay of the number N_I of laser photons constituting the fundamental Gaussian beam I with ϑ is given by

$$\frac{\mathrm{d}N_I}{\vartheta\mathrm{d}\vartheta} \simeq N_I \Big(\frac{2}{\theta_I}\Big)^2 \mathrm{e}^{-2\left(\frac{\vartheta}{\theta_I}\right)^2} . \tag{3.62}$$

Hence, for the two different signals $N_{p,I}$ with $p \in \{\text{tot}, \perp\}$ considered here we can easily determine an analytical expression for ϑ_p^{dis}. Using Eqs. (3.57) and (3.62), we obtain

$$\Big(\frac{\vartheta_p^{\text{dis}}}{\theta_I}\Big)^2 = -\frac{\kappa}{2} \ln\left\{\frac{\kappa-1}{\kappa}\frac{1}{\mathcal{P}_p}\frac{N_{p,I}}{N_I}\bigg|_{r_0=0}\right\} + \Big(\frac{r_0}{w_I}\Big)^2 , \tag{3.63}$$

with

$$\kappa := \frac{\bar{w}_{II}^2 + 2w_I^2}{2w_I^2} = \frac{1 + 2(\frac{w_I}{w_{0,II}})^2}{1 + 2(\frac{w_I}{w_{0,II}})^2 - \sqrt{F(\frac{w_I}{w_{0,II}})/F(0)}} > 1 . \tag{3.64}$$

Also note that the last definition relates the effective waist of beam II and the waist of beam I as $\bar{w}_{II} = \sqrt{2(\kappa-1)}\, w_I$. Upon integration of Eq. (3.57) over the full azimuthal angle φ and $\vartheta \geq \vartheta_p^{\text{dis}}$, we arrive at a closed-form expression for the numbers of discernible signal photons,

$$N_{p,I}^{\text{dis}} \approx \mathcal{P}_p N_I \frac{\kappa}{\kappa-1}\left(\frac{\kappa-1}{\kappa}\frac{1}{\mathcal{P}_p}\frac{N_{p,I}}{N_I}\bigg|_{r_0=0}\right)^{\kappa} \mathrm{e}^{-2\left(\frac{r_0}{w_I}\right)^2} . \tag{3.65}$$

On the other hand, the number of laser photons propagating into the same angular regime follows straightforwardly from Eq. (3.62). Upon multiplication with $\mathcal{P}_p$ it constitutes the background against which the discernible signal is to be compared to and can be cast in the following form,

$$N_{p,I}^{\text{bgr}} \simeq \mathcal{P}_p N_I \left(\frac{\kappa-1}{\kappa}\frac{1}{\mathcal{P}_p}\frac{N_{p,I}}{N_I}\bigg|_{r_0=0}\right)^{\kappa} \mathrm{e}^{-2\left(\frac{r_0}{w_I}\right)^2} . \tag{3.66}$$

We emphasize that the ratio of Eqs. (3.65) and (3.66) is $N_{p,I}^{\text{dis}}/N_{p,I}^{\text{bgr}} \simeq \kappa/(\kappa-1) > 1$ independent of the signal polarization. It is fully determined by the waists w_I, $w_{0,II}$ of the colliding lasers and the effective waist $\bar{w}_{II}$; cf. Eq. (3.64). The discernible signal in Eq. (3.65) still scales linearly with N_I. At the same time, its scaling with the energy of beam II is increased to $W_{II}^{2\kappa}$ in comparison to the full signal (3.60) which is proportional to W_{II}^2. Similarly, the overall scaling of $N_{p,I}/N_I \sim \omega_I^2$ is enhanced to $N_{p,I}^{\text{dis}}/N_I \sim \omega_I^{2\kappa}$.

In this context it is particularly interesting to note that with the help of Eq. (3.64), the total signal photon numbers in Eq. (3.60) can be compactly represented as

$$\left\{ \begin{array}{c} N_{\mathrm{tot},I} \\ N_{\perp,I} \end{array} \right\} \approx N_I \, \frac{\kappa - 1}{\kappa} \sqrt{\frac{3}{\pi}} \frac{16\alpha^4}{2025\pi} \left(\frac{W_{II}}{m} \frac{\omega_I}{m} \right)^2 \frac{F(0)}{(m w_{0,II})^4} \left\{ \begin{array}{c} (c_a^2 - c_b^2)\cos^2(\Delta\phi) + c_b^2 \\ \frac{1}{4}(c_a - c_b)^2 \sin^2(2\Delta\phi) \end{array} \right\} \mathrm{e}^{-2\left(\frac{r_0}{w_I\sqrt{\kappa}}\right)^2} , \quad (3.67)$$

such that for $r_0 = 0$ the entire dependence of Eqs. (3.65) and (3.67) on w_I is fully encoded in the parameter κ. Hence, the probe waist w_I which yields the maximum discernible signal for $r_0 = 0$ and given other parameters can be conveniently extracted by first determining the value of κ that maximizes the discernible signal and thereafter plugging this value into Eq. (3.64), which is then solved for w_I. For $N_{p,I}^{\mathrm{dis}}$ the corresponding condition on κ reads

$$\frac{1}{\mathcal{P}_p} \frac{N_{p,I}}{N_I}\bigg|_{r_0=0} = \frac{\kappa}{\kappa - 1} \exp\left\{ -\frac{1}{\kappa}\left(2 + \frac{1}{\kappa - 1} \right) \right\} , \quad (3.68)$$

which cannot be solved analytical for κ.

In the next step, we aim at illustrating the size of the quantum vacuum signals attainable in the collision of XFEL and high-intensity laser pulses in a counter-propagating geometry for a specific set of example parameters to become available at the *Helmholtz International Beamline for Extreme Fields* (HIBEF) at the European XFEL. For the high-intensity laser pump we adopt the parameters of the 300 TW *Relativistic Laser at XFEL* (ReLaX) system installed at HIBEF, providing pulses of energy $W_{II} = 10\,\mathrm{J}$ and duration $\tau_{II}^{\mathrm{FWHM}} = 25\,\mathrm{fs}$ at a wavelength of $\lambda_{II} = 800\,\mathrm{nm}$ with a repetition rate of 1 Hz [120]. We envision these to be focused to a waist of $w_{0,II} = 1\,\mu\mathrm{m}$ with a $f^{\#} = 2$ focusing optics; cf. Eq. (3.38). On the other hand, for the x-ray probe we assume a photon energy of $\omega_I = 12914\,\mathrm{eV}$. For this value the possibility of high-definition polarimetry was successfully demonstrated in experiment using multiple Bragg reflections in a pair of silicon channel cuts [121] acting as polarizer and analyzer, respectively, and the present polarization purity record of $\mathcal{P}_\perp = 1.4 \times 10^{-11}$ was achieved with four reflections per channel cut [122]. Neglecting losses due to focusing optics and the limited acceptance of polarizer and analyzer but accounting for the increase of the initial XFEL pulse duration by the four reflections in the polarizer prior to the interaction with the high-intensity pump along the lines of [123,124] (cf. Ref. [102] for the detailed procedure), at this photon energy the European XFEL is expected to deliver pulses of $N_I = 8.26 \times 10^{11}$ photons at a pulse duration of $\tau_I^{\mathrm{FWHM}} = 129\,\mathrm{fs}$ in the interaction region [100, 125]. For simplicity, we keep these values for N_I and τ_I also when considering the signal $N_{\mathrm{tot},I}^{\mathrm{dis}}$ in a polarization insensitive measurement. However, in this case we set $\mathcal{P}_{\mathrm{tot}} = 1$. Being primarily interested in the maximum achievable signal, in line with the discussion below Eq. (3.45), here we choose $\Delta\phi = \pi/2$ for $N_{\mathrm{tot},I}^{\mathrm{dis}}$ and $\Delta\phi = \pi/4$ for $N_{\perp,I}^{\mathrm{dis}}$. Moreover, we limit ourselves to ideal collisions with $r_0 = \mathrm{z}_0 = t_0 = 0$. Finally, the waist of the x-ray beam w_I is considered as a free parameter which is chosen to fulfill Eq. (3.68) and thus to maximize the discernible signals. Upon evaluation of Eq. (3.65) for these parameters we find the maximum numbers of discernible signal photons per shot to be given by

$$N_{\mathrm{tot},I}^{\mathrm{dis}} \approx 0.226 \quad \text{for} \quad \kappa \simeq 1.03 \quad \rightarrow \quad w_I \simeq 5.3 w_{0,II} \,, \; \bar{w}_{II} \simeq 1.37 w_{0,II} \,,$$

$$N^{\rm dis}_{\perp,I} \approx 0.045 \quad \text{for} \quad \kappa \simeq 1.19 \quad \rightarrow \quad w_I \simeq 2.1 w_{0,II}\,,\ \bar{w}_{II} \simeq 1.30 w_{0,II}\,, \tag{3.69}$$

where in addition to the value of the parameter κ for which the maximum value is reached we also provide the corresponding probe waist w_I and the effective waist $\bar{w}_{II}$ of the pump. For the repetition rate of 1 Hz of the high-intensity laser pump mentioned above this amounts to $N^{\rm dis}_{{\rm tot},I} \approx 814$ and $N^{\rm dis}_{{\rm tot},I} \approx 161$ discernible signal photons per hour. The associated signal-to-background ratios are $N^{\rm dis}_{{\rm tot},I}/N^{\rm bgr}_{{\rm tot},I} \simeq 31$ and $N^{\rm dis}_{\perp,I}/N^{\rm bgr}_{\perp,I} \simeq 6$, respectively. For comparison, we note that keeping all other parameters fixed but presuming $w_I \ll w_{0,II}$, which results in the largest values for $N_{p,I}$, the signal-to-background ratios for the photon numbers integrated over all possible emission directions are $N_{{\rm tot},I}/(\mathcal{P}_{\rm tot}N_I) \simeq 2.41 \times 10^{-11}$ and $N_{\perp,I}/(\mathcal{P}_\perp N_I) \simeq 0.079$. Hence, in particular with regard to a polarization insensitive measurement, it is obvious that there is no hope for a successful experimental measurement of the quantum vacuum signal without using angular cuts or other selection criteria. On the other hand, in both cases considered in Eq. (3.69) we have $w_I > w_{0,II}$. As to be expected, for the larger value of w_I also $\bar{w}_{II}$ is larger: the widening of the transverse extent of the interaction region of the two beams inherently comes with an increase in longitudinal direction. This manifests itself in a larger value of the average beam radius $\bar{w}_{II}$. We emphasize that because Eq. (3.65) depends on $\mathcal{P}_p$ via $(1/\mathcal{P}_p)^{\kappa-1}$ and $\kappa = 1 + \delta\kappa$ with $0 < \delta\kappa \ll 1$ in Eq. (3.69), the gain in the number of discernible signal photons by achieving $\mathcal{P}_p \ll 1$ is much smaller than one may have naively expected. Remarkably, even the value of $\mathcal{P}_\perp$ on the 10^{-11} level quoted above eventually only contributes a factor of $(1/\mathcal{P}_p)^{\kappa-1} \simeq 115$ to $N^{\rm dis}_{\perp,I}$ in Eq. (3.69).

It is especially interesting and relevant to assess how many optimal laser pulse collisions n are required to achieve the measurement of a given quantum vacuum signal consisting of $N_{\rm signal}$ signal photons per shot with a specified significance of C sigma. Assuming a normal distribution of the data, this requires the signal over n collisions $nN_{\rm signal}$ to surpass the standard deviation of the background $\sigma = \sqrt{nN_{\rm bgr}}$, with $N_{\rm bgr}$ background photons registered by the detector per shot, and thus results in the following stringent criterion,

$$nN_{\rm signal} > C\sqrt{nN_{\rm bgr}} \quad \leftrightarrow \quad n > \frac{C^2}{N_{\rm signal}}\left(\frac{N_{\rm signal}}{N_{\rm bgr}}\right)^{-1}. \tag{3.70}$$

Demanding a measurement of the signals in Eq. (3.69) that maximize the discernible signal photon numbers for the presumed laser parameters with a significance of 5σ, and invoking the highly idealized assumption that the full discernible signal can be collected on a detector we find that just $n > 3$ optimal collisions are required for the signal attainable in a polarization insensitive measurement, and $n > 89$ for the $\perp$-polarized signal component. These values follow from Eq. (3.70) upon insertion of the signal photon numbers in Eq. (3.69) and the associated signal-to-background ratios given in the text below this equation. On the other hand, a 5σ confirmation of the signals integrated over all possible emission directions and $w_I \ll w_{0,II}$ would require $n > 5.21 \times 10^{10}$ optimal shots for $N_{{\rm tot},I}$ and $n > 346$ for $N_{\perp,I}$. Recall that in the limit of $w_I \ll w_{0,II}$ implied here for $N_{p,I}$ the divergence of the signal (3.58) matches the divergence of the original probe beam and can thus be collected by the same optics as the probe laser photons traversing the interaction region without interaction. As noted above, in the present scenario the latter constitute the background against which the signal is to be discriminated via $N_{\rm bgr} = \mathcal{P}_p N_I$. It is worthwhile to emphasize that in an actual experiment the signals $N_{p,I}$ are expected to be substantially

reduced even for optimal laser pulse collisions because the tighter the focusing of the x-ray beam, i.e., the smaller its waist w_I, generically the larger the losses associated with the lens used to focus it down to this value of w_I in experiment. This losses become particularly pronounced for $w_I \ll 1\,\mu\text{m}$. While this leaves the ratio of $N_{\text{signal}}/N_{\text{bgr}}$ in Eq. (3.70) unaffected, the additional overall dependence on $1/N_{\text{signal}}$ immediately implies an increase in the number of required shots. Also note that in the parameter regime where they become maximal, i.e., for $w_I \ll w_{0,II}$, these signals $N_{p,I}$ decrease by a factor of $1/\text{e}^2$ for $r_0 \simeq w_{0,II}/\sqrt{2} \approx 0.7 w_{0,II}$ relative to their peak values at $r_0 = 0$; cf. Eq. (3.59). Conversely, the discernible signals (3.67) decay by the same factor for $r_0 = w_I\sqrt{\kappa}$: especially those in Eq. (3.69) maximizing the signal yield are thus reduced by $1/\text{e}^2$ for $r_0 \approx 5.4 w_{0,II}$ in case of $N^{\text{dis}}_{\text{tot},I}$, and $r_0 \approx 2.3 w_{0,II}$ in case of $N^{\text{dis}}_{\perp,I}$. This immediately implies that the latter signals are much less sensitive to a finite transverse impact parameter r_0 than the former. This constitutes another important advantage in favor of the discernible signals apart from the reduced number of shots required for the measurement of the effect with a given significance. Collisions with finite impact parameters are inevitable in experiment due to the presence of shot-to-shot fluctuations. Finally, we remark that as $\kappa = O(1)$ in Eq. (3.69), an effective reduction in the number of photons N_I available for probing due to a loss as large as 99% could be compensated by changing the parameters of the pump beam such that $W_{II}/w^2_{0,II} \to 10\, W_{II}/w^2_{0,II}$. This follows from Eqs. (3.66) and (3.67). Especially presuming the availability of a focusing optics with $f^{\#} = 1$ instead of $f^{\#} = 2$ in the case of such a severe loss an increase in the pump pulse energy W_{II} by only a factor of 2.5 would be needed to retain the values of the signal photon numbers given above.

What is certainly unsatisfactory is that the angular cuts required here for the extraction of the discernible signal are precisely cutting out the main signal component consisting of photons that are quasi-elastically scattered in the forward cone of beam I with polar angles $\vartheta \lesssim \theta_I$. As detailed above, here the quantum vacuum signal is typically dominated by the background of the driving laser photons. Besides the comparably wide angular spread of the discernible signals typically comes with large demands on the optics needed to collect the full discernible signal on the detector. However, what is likely even more critical with regard to an actual experimental implementation is that for the selection of the discernible signals the analysis presented here explicitly makes use of the highly idealized assumption that the probe laser beam amounts to a fundamental Gaussian beam. In the far field where the induced quantum vacuum signals are to be discerned from the laser photons contained in this beam, the transverse field profile of the latter thus exhibits a perfect Gaussian decay with ϑ. Correspondingly, any deviation from this idealization in experiment will immediately impact the discernible signal photon numbers and slightly different beam profiles in the far-field will inevitably come with profile-specific and hence even laser-shot-specific discernibility angles $\vartheta_p^{\text{dis}}(\varphi)$. This motivates the search for strategies allowing to diminish the background in the main propagation direction of the signal while essentially not reducing the latter, and for detection schemes that are essentially insensitive to the precise details of the probe laser fields in the far-field where the quantum vacuum signals are to be detected. At the same time, it should be emphasized that the scattering phenomenon out of the forward cone of the driving laser beams studied in detail in this section is generic and thus persists for arbitrary laser fields. In fact, the dependencies of the quantum vacuum signal on the various parameters of the driving laser beams derived above are sufficiently general to allow inferring the characteristic properties of the signal and relevant signal en-

hancement strategies also beyond fundamental Gaussian beams.

Before concluding this section we moreover emphasize that, though resorting to an infinite Rayleigh range approximation $z_{R,I} \to \infty$ for the probe, the explicit results of this section even allow for reasonable estimates of the quasi-elastic quantum vacuum signals induced in the collision of two optical high-intensity lasers with Rayleigh ranges $z_{R,I} \geq z_{R,II}$ in a counter-propagation geometry. The reason for this is that the finite Rayleigh length $z_{R,II}$ of the pump beam, consistently accounted for in the above calculation, strongly localizes the strong field region in longitudinal direction to the vicinity of its focus at $z = 0$ via a factor $\sim 1/[1 + (z/z_{R,II})^2]$ on the level of its intensity profile. Because the signal photon number scales with the square of the pump intensity and linearly with that of the probe, the impact of the Rayleigh range of the latter is less relevant and hence can be neglected for qualitative estimates. However, the less pronounced localization of the composite field of pump and probe tends to somewhat overestimate the associated quantum vacuum signals in this case.

3.2.4.2 Collisions involving an annular probe beam

An interesting perspective is to consider essentially the same collision scenario as in the previous section 3.2.4.1 but to replace the fundamental Gaussian probe by an annular probe beam which features a field-free shadow in the converging (expanding) beam before (after) focus but retains a pronounced peak in its focus [126]. When choosing the pump and probe waists appropriately, this should give rise to a quasi-elastic scattering signal at the probe frequency in the shadow where they can be detected essentially without background. Experimentally, this annular beam approach was pioneered by [127, 128] for the detection of weak non-linear optics signals in the presence of strong fields. As detailed below, this approach can prospectively solve both issues highlighted in the last paragraph of the previous section, namely give rise to a directed discernible quantum vacuum signal that is basically insensitive to the precise details of the far-field profile of the probe beam because it can be spatially separated from the latter by setting up an appropriate filter and imaging system. To construct laser fields with these properties we make use of Eq. (3.20) with $l = 0$ which forms a full basis for rotationally symmetric beams without topological charge at zeroth order in the paraxial approximation. The field amplitude profile of a linearly polarized laser beam of this type propagating in positive z direction then be decomposed as

$$\mathcal{E}(x) = \mathrm{e}^{-(\frac{z-t}{\tau/2})^2} \frac{w_0}{w(z)} \mathrm{e}^{-(\frac{r}{w(z)})^2} \sum_p \mathcal{E}_p \, L_p\Big(\tfrac{2r^2}{w^2(z)}\Big) \cos\Big(\psi(x) + 2p\,\psi_G(z) + \psi_p\Big), \tag{3.71}$$

with Laguerre polynomials $L_p(\cdot) = L_p^0(\cdot)$, and the phase $\psi(x)$ defined in Eq. (3.23). The mode-specific peak field amplitude $\mathcal{E}_p \equiv \mathcal{E}_{0,p}$ is related to the energy $W_p \equiv W_{0,p}$ put into this mode via Eq. (3.25) specialized to $l = 0$. For later reference we also note that the cycle-averaged intensity profile $I(x) = \langle \mathcal{E}^2(x) \rangle_t$ associated with Eq. (3.71) reads

$$I(x) = \frac{1}{2} \mathrm{e}^{-2(\frac{z-t}{\tau/2})^2} \Big(\frac{w_0}{w(z)}\Big)^2 \mathrm{e}^{-2(\frac{r}{w(z)})^2} \sum_{p,p'} \mathcal{E}_p \, \mathcal{E}_{p'} L_p\Big(\tfrac{2r^2}{w^2(z)}\Big) L_{p'}\Big(\tfrac{2r^2}{w^2(z)}\Big) \cos\Big(2(p-p')\,\psi_G(z) + \psi_p - \psi_{p'}\Big). \tag{3.72}$$

Therewith it is straightforward to implement a specified transverse beam profile at a given value of the longitudinal coordinate $z = z_0$. To this end, one first needs to expand it in terms of Laguerre polynomials and second choose the mode-specific field amplitudes $\mathcal{E}_p$ and phases φ_p in Eq. (3.71) accordingly. Because Eq. (3.71) fulfills the paraxial wave equation at $\mathcal{O}(\theta^0)$ by construction, this single input profile defines an entire paraxial beam. In particular, note that the function

$$\frac{\Gamma(\mathcal{N}+1,(\frac{r}{w(z_0)})^2)}{\Gamma(\mathcal{N}+1)} = \mathrm{e}^{-(\frac{r}{w(z_0)})^2}\sum_{n=0}^{\mathcal{N}}\frac{1}{n!}\Big(\frac{r}{w(z_0)}\Big)^{2n}, \tag{3.73}$$

referred to as *flattened Gaussian* (FG) of order $\mathcal{N}$ in Ref. [129] is peaked around $r = 0$ where it reaches its maximum value of one; $\Gamma(\mathcal{N}+1) = \mathcal{N}!$ and $\Gamma(\cdot,\cdot)$ is the incomplete gamma function. For sufficiently large values of $\mathcal{N}$ it exhibits a flat plateau which increases in width with growing $\mathcal{N}$ [129, 130]. This makes it an ideal candidate to construct an annular transverse profile at $z = z_0$ by the subtraction of two such FG profiles characterized by different values of $\mathcal{N}$ and $\mathcal{N}'$ [126]. Equation (3.73) has the following expansion in Laguerre polynomials,

$$\frac{\Gamma(\mathcal{N}+1,(\frac{r}{w(z_0)})^2)}{\Gamma(\mathcal{N}+1)} = \mathrm{e}^{-(\frac{r}{w(z_0)})^2}\sum_{p=0}^{\mathcal{N}}(-1)^p\,c_{p,\mathcal{N}}\,L_p\Big(\tfrac{2r^2}{w^2(z_0)}\Big), \quad \text{with} \quad c_{p,\mathcal{N}} = \sum_{j=p}^{\mathcal{N}}\frac{1}{2^j}\binom{j}{p}. \tag{3.74}$$

An explicit representation of the expansion coefficients $c_{p,\mathcal{N}}$ in the limit of $\mathcal{N} \gg 1$ is derived in Appendix A.6; cf. specifically Eq. (A.44).

In a first step, we implement a beam of pulse energy W featuring the transverse profile (3.73) at $z = z_0$. To this end, we restrict the sums over the radial indices in Eqs. (3.71) and (3.72) to run from 0 to $\mathcal{N}$ and identify

$$\psi_p = p[\pi - 2\psi_\mathrm{G}(z_0)] + \tilde{\psi}_0\,, \tag{3.75}$$

such as to accommodate for the $(-1)^p$ term from Eq. (3.74); $\tilde{\psi}_0$ denotes a common constant phase offset. On the other hand, the coefficients $c_{p,\mathcal{N}}$ have to be accounted for in the field amplitudes $\mathcal{E}_p$. The total energy put into the beam can be expressed as $W = \sum_{p=0}^{\mathcal{N}} W_p$ with mode energies $W_p \sim \mathcal{E}_p^2$; cf. Eq. (3.25). In order to keep the beam energy to be given by W we thus have to choose [110]

$$W_p = \Big(\frac{c_{p,\mathcal{N}}}{C_\mathcal{N}}\Big)^2 W\,, \quad \text{where} \quad C_\mathcal{N}^2 = \sum_{p=0}^{\mathcal{N}} c_{p,\mathcal{N}}^2\,. \tag{3.76}$$

The explicit expressions for the field amplitude and cycle-averaged intensity profile of such a beam following upon plugging Eqs. (3.75) and (3.76) into Eqs. (3.71) and (3.72) hence read

$$\mathcal{E}_\mathcal{N}^{z_0}(x) = \mathcal{E}\,\mathrm{e}^{-(\frac{z-t}{\tau/2})^2}\frac{w_0}{w(z)}\,\mathrm{e}^{-(\frac{r}{w(z)})^2}\sum_{p=0}^{\mathcal{N}}(-1)^p\frac{c_{p,\mathcal{N}}}{C_\mathcal{N}}\,L_p\Big(\tfrac{2r^2}{w^2(z)}\Big)\,\cos\Big(\psi(x) + 2p[\psi_\mathrm{G}(z) - \psi_\mathrm{G}(z_0)] + \tilde{\psi}_0\Big),$$

$$I_\mathcal{N}^{z_0}(x) = \frac{1}{2}\,\mathcal{E}^2\,\mathrm{e}^{-2(\frac{z-t}{\tau/2})^2}\Big(\frac{w_0}{w(z)}\Big)^2\,\mathrm{e}^{-2(\frac{r}{w(z)})^2}\sum_{p=0}^{\mathcal{N}}\sum_{p'=0}^{\mathcal{N}}(-1)^{p-p'}\frac{c_{p,\mathcal{N}}}{C_\mathcal{N}}\,\frac{c_{p',\mathcal{N}}}{C_\mathcal{N}}\,L_p\Big(\tfrac{2r^2}{w^2(z)}\Big)\,L_{p'}\Big(\tfrac{2r^2}{w^2(z)}\Big)$$

$$\times \cos\Big(2(p-p')[\psi_{\mathrm{G}}(\mathrm{z})-\psi_{\mathrm{G}}(\mathrm{z}_0)]\Big)\,, \tag{3.77}$$

with

$$\mathcal{E}^2 = 8\sqrt{\frac{2}{\pi}}\frac{W}{\pi w_0^2 \tau}\,. \tag{3.78}$$

For convenience, in Eq. (3.77) we introduced labels: the upper one refers to the longitudinal coordinate z_0 where the FG transverse profile is implemented and the lower one to its order $\mathcal{N}$. From the structure of Eq. (3.77) the transverse $\mathrm{FG}_{\mathcal{N}}$ profile at $\mathrm{z} = \mathrm{z}_0$ is evident: for this particular value of z the cosine no longer depends on p, p' and the identity (3.74) can be employed to perform the sums. Obviously, Eq. (3.77) can be immediately generalized to exhibit an annular transverse profile at $\mathrm{z} = \mathrm{z}_0$ formed by the subtraction of an $\mathrm{FG}_{\mathcal{N}'}$ profile with $\mathcal{N}' < \mathcal{N}$ from an $\mathrm{FG}_{\mathcal{N}}$ profile; in the remainder of this work, we refer to the resulting beam profile at $\mathrm{z} = \mathrm{z}_0$ as an $\mathrm{FG}^{\circledcirc}_{\mathcal{N},\mathcal{N}'}$ profile. This only requires modifying the expansion coefficients $c_{p,\mathcal{N}}$ as

$$c_{p,\mathcal{N}} \to c_{p,\mathcal{N},\mathcal{N}'} := c_{p,\mathcal{N}} - \Theta(\mathcal{N}' - p + 0^+)\, c_{p,\mathcal{N}'}\,, \tag{3.79}$$

while keeping $C_{\mathcal{N}}$ fixed; here $\Theta(\cdot)$ denotes Heaviside function. In line with this, the pulse energy contained in the resulting beam featuring an $\mathrm{FG}^{\circledcirc}_{\mathcal{N},\mathcal{N}'}$ profile at $\mathrm{z} = \mathrm{z}_0$ can be expressed as sum over the W_p in Eq. (3.76) with the substitution (3.79) and is, of course, smaller than W. Note, however, that its direct evaluation from the intensity profile at $\mathrm{z} = \mathrm{z}_0$ employing Eqs. (3.73) and (3.74) typically yields a more compact representation for the pulse energy of this beam.

For completeness, we remark that in the explicit example discussed below employing such an annular beam the pulse energy provided by the laser system supposed to create it is always assumed to match the energy W of the full beam without the central shadow. This is so because in experiment we envision the latter to be created with the help of an obstacle acting as beamstop and shading part of the cross section of the initial beam at $\mathrm{z} = \mathrm{z}_0$. This inherently comes with a loss in pulse energy. In this context, we also note that while a physical beamstop will inevitably come with diffraction effects, these naturally and consistently do not arise in our (idealized) theoretical modeling. The reason for this is that, by construction, we enforce the beam with the desired transverse beam profile at $\mathrm{z} = \mathrm{z}_0$ to approximately solve the linear Maxwell equations in vacuo in the absence of any real matter, i.e., Eq. (2.11) with $\bar{J}^\mu = 0$. We emphasize that we expect such diffraction effects to leave our predictions of the peak-field driven quantum vacuum signals essentially unmodified. However, they will certainly affect the background level in experiment and thus ultimately need to be accounted for; cf. also the discussion starting in the second paragraph below Eq. (3.123) where the size of such background effects in the shadow is extracted from an experimental measurement.

Furthermore, it is obvious that the transverse intensity profile of the beam in Eq. (3.77) should closely resemble the one in its focus at $\mathrm{z} = 0$ as long as $|\mathrm{z}| \ll \mathrm{z}_{\mathrm{R}}/\mathcal{N}$ because in this case the term $2(p-p')\psi_{\mathrm{G}}(\mathrm{z})$ in the phase of the cosine is close to zero for all possible values of p, p'. We emphasize that this criterion also holds for beams featuring an annular transverse profile at $\mathrm{z} = \mathrm{z}_0$ because this construction only affects the expansion coefficients $c_{p,\mathcal{N}}$ in Eq. (3.77). On the other hand, the Rayleigh range z_{R} associated

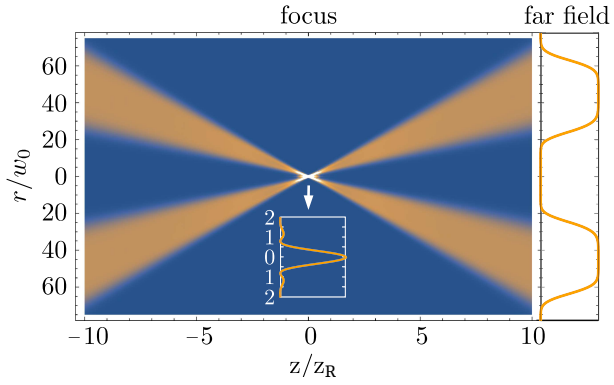

Figure 3.2: Intensity profile $I^{\infty}_{50,5}(x)$ as a function of the longitudinal and radial beam coordinates measured in units of the Rayleigh range z_R and the waist w_0 of the fundamental Gaussian mode, respectively. The pulse duration is very large and fulfills $\tau \gg z_R$. The local value of the intensity is encoded in the color scale: the larger its value, the brighter the color. Its maximum is reached in the beam focus at $z = r = 0$. The transverse intensity profile in the focus (far field) is shown in the inset (on the right).

with the fundamental mode in Eq. (3.77) still amounts to the longitudinal reference scale separating the near $|z| \ll z_R$ and the far $|z| \gg z_R$ field, respectively.

Subsequently, we exclusively focus on a far-field implementation of the $\mathrm{FG}_{\mathcal{N}}$ profile at $z_0 \gg z_R$. This is equivalent to formally sending $z_0/z_R \to \infty$ and $\psi_G(z_0) \to \pi/2$. Note that symmetry implies that for $z_0/z_R \to -\infty$ the same result is obtained and the forward and backward far fields agree with each other. In this limit, Eq. (3.77) can be represented in the compact form

$$\mathcal{E}^{\infty}_{\mathcal{N}}(x) = \mathcal{E}\, \mathrm{e}^{-(\frac{z-t}{\tau/2})^2} \frac{w_0}{w(z)}\, \mathrm{e}^{-(\frac{r}{w(z)})^2} \sum_{p=0}^{\mathcal{N}} \frac{c_{p,\mathcal{N}}}{C_{\mathcal{N}}} L_p\Big(\tfrac{2r^2}{w^2(z)}\Big) \cos\Big(\psi(x) + 2p\,\psi_G(z) + \tilde{\psi}_0\Big), \tag{3.80}$$

$$I^{\infty}_{\mathcal{N}}(x) = \frac{1}{2}\mathcal{E}^2\, \mathrm{e}^{-2(\frac{z-t}{\tau/2})^2} \Big(\frac{w_0}{w(z)}\Big)^2 \mathrm{e}^{-2(\frac{r}{w(z)})^2} \sum_{p=0}^{\mathcal{N}} \sum_{p'=0}^{\mathcal{N}} \frac{c_{p,\mathcal{N}}}{C_{\mathcal{N}}} \frac{c_{p',\mathcal{N}}}{C_{\mathcal{N}}} L_p\Big(\tfrac{2r^2}{w^2(z)}\Big) L_{p'}\Big(\tfrac{2r^2}{w^2(z)}\Big) \cos\Big(2(p-p')\,\psi_G(z)\Big).$$

Note that precisely this choice for z_0 results in the maximum peak field in the beam focus attainable with a beam featuring an $\mathrm{FG}_{\mathcal{N}}$ profile for given parameters: the phases in the intensity profile are such that the coefficients are added with maximum amplitude at $z = 0$; cf. Eqs. (3.77) and (3.80). In this limit, the peak field reached for $z = t = r = \tilde{\psi} = 0$ becomes identical to $\mathcal{E}\sum_{p=0}^{\mathcal{N}} c_{p,\mathcal{N}}/C_{\mathcal{N}}$. Clearly, the field amplitude profile of a beam with an $\mathrm{FG}^{\circledcirc}_{\mathcal{N},\mathcal{N}'}$ profile in the far field and the corresponding cycle-averaged intensity profile are given by

$$\mathcal{E}^{\infty}_{\mathcal{N},\mathcal{N}'}(x) = \mathcal{E}^{\infty}_{\mathcal{N}}(x)\Big|_{c_{p,\mathcal{N}} \to c_{p,\mathcal{N},\mathcal{N}'}} \quad \text{and} \quad I^{\infty}_{\mathcal{N},\mathcal{N}'}(x) = I^{\infty}_{\mathcal{N}}(x)\Big|_{c_{p,\mathcal{N}} \to c_{p,\mathcal{N},\mathcal{N}'}}, \tag{3.81}$$

where the substitution is implicitly assumed to affect both $c_{p,\mathcal{N}}$ and $c_{p',\mathcal{N}}$ in case of the intensity profile. In Fig. 3.2 we depict the intensity profile of such an annular beam for the case of $\mathcal{N} = 50$ and $\mathcal{N}' = 5$ [126]. In the remainder of this section, we are primarily interested in the case of $\mathcal{N} \gtrsim \mathcal{N}' \gg 1$ where the $\mathrm{FG}_{\mathcal{N}}$ and $\mathrm{FG}_{\mathcal{N}'}$ far-field profiles of the beams to be subtracted to form the annular beam are flat-top-like. This

results in an macroscopically extended, completely field-free region in the $\mathrm{FG}^{\circledcirc}_{\mathcal{N},\mathcal{N}'}$ far-field profile of the resulting beam; cf. Eq. (3.90) below.

Equation (3.80) is parameterized in terms of the waist of the fundamental Gaussian mode w_0. However, for a beam made up of many modes this parameter does not have an immediate physical interpretation and is hard to access in experiment. Hence, it is beneficial to trade w_0 for the physical waist $w_{\mathcal{N}}$ of the resulting beam to be measured and manipulated in experiment. We define the latter as the $1/\mathrm{e}^2$ radius of the intensity profile $I^{\infty}_{\mathcal{N}}(x)|_{\mathrm{z}=0}$ in the beam focus, which results in the defining equation

$$\sum_{p=0}^{\mathcal{N}} c_{p,\mathcal{N}} L_p(2s^2_{\mathcal{N}}) = \mathrm{e}^{s^2_{\mathcal{N}}-1} \sum_{p=0}^{\mathcal{N}} c_{p,\mathcal{N}}\,, \tag{3.82}$$

where the scaling parameter $s_{\mathcal{N}} = w_{\mathcal{N}}/w_0$ measures $w_{\mathcal{N}}$ in units of w_0. For the present scenario, where the $\mathrm{FG}_{\mathcal{N}}$ profile is implemented in the far field, the widening of the $\mathrm{FG}_{\mathcal{N}}$ profile with $\mathcal{N}$ results in an increase of the physical divergence of the beam. As the divergence and the waist size are indirectly proportional to each other, this implies $w_{\mathcal{N}+1} < w_{\mathcal{N}}$, and thus $s_{\mathcal{N}} < 1$ for $\mathcal{N} \geq 1$. Expanding the above defining equation up to quadratic order in $s_{\mathcal{N}} < 1$, we obtain the estimate [126]

$$s^2_{\mathcal{N}} \approx \frac{(1-\mathrm{e}^{-1})\sum_{p=0}^{\mathcal{N}} c_{p,\mathcal{N}}}{\sum_{p=0}^{\mathcal{N}}(2p+\mathrm{e}^{-1})\,c_{p,\mathcal{N}}} \quad \text{for} \quad \mathcal{N} \geq 1\,. \tag{3.83}$$

Upon insertion of the finite-sum representation of the expansion coefficients given in Eq. (3.74), the sums in Eqs. (3.83) can be performed explicitly, yielding

$$\sum_{p=0}^{\mathcal{N}} c_{p,\mathcal{N}} = \mathcal{N}+1\,, \quad \sum_{p=0}^{\mathcal{N}} p\, c_{p,\mathcal{N}} = \frac{1}{4}\mathcal{N}(\mathcal{N}+1)\,. \tag{3.84}$$

This results in $s^2_{\mathcal{N}} \approx 2(1-\mathrm{e}^{-1})/(\mathcal{N}+2\mathrm{e}^{-1})$ and correspondingly $s_{\mathcal{N}} \ll 1$ for sufficiently large values of $\mathcal{N}$. The analogous result for a beam with an $\mathrm{FG}^{\circledcirc}_{\mathcal{N},\mathcal{N}'}$ far-field profile and a physical waist $w_{\mathcal{N},\mathcal{N}'} = s_{\mathcal{N},\mathcal{N}'}\, w_0$ follows from Eq. (3.83) upon insertion of Eq. (3.79) and using Eq. (3.84): $s^2_{\mathcal{N},\mathcal{N}'} \approx 2(1-\mathrm{e}^{-1})/(\mathcal{N}+\mathcal{N}'+1+2\mathrm{e}^{-1})$. In particular for $\mathcal{N}+\mathcal{N}' \gg 1$ we hence have

$$w_{\mathcal{N},\mathcal{N}'} \simeq w_0 \sqrt{\frac{2(1-\mathrm{e}^{-1})}{\mathcal{N}+\mathcal{N}'}} \quad \text{and} \quad w_{\mathcal{N}} = w_{\mathcal{N},0}\,. \tag{3.85}$$

Note that an $\mathrm{FG}^{\circledcirc}_{\mathcal{N},\mathcal{N}'}$ profile with $\mathcal{N}' = 0$ amounts to a $\mathrm{FG}_{\mathcal{N}}$ profile and $\sqrt{2(1-\mathrm{e}^{-1})} \approx 1.1$. Subsequently we stick to the identification in Eq. (3.85). However, we emphasize here that though the $1/\mathrm{e}^2$ radius given in Eq. (3.85) obviously amounts to an approximation, if desired, results derived on its basis for given values of $\mathcal{N}$ and $\mathcal{N}'$ can always be readjusted to the exact value (3.82) by rescaling the parameter $w_{\mathcal{N},\mathcal{N}'}$ fixed by the identification in Eq. (3.85) accordingly. In this context, we also highlight that, because of $\mathrm{z_R} \sim w_0^2$, for beams featuring an $\mathrm{FG}^{\circledcirc}_{\mathcal{N},\mathcal{N}'}$ far-field profile and a physical waist given by Eq. (3.85) the above condition $|\mathrm{z}| \ll \mathrm{z_R}/\mathcal{N}$ on the longitudinal coordinates for which the transverse beam profile closely resembles its focus profile can actually be rephrased as $|\mathrm{z}| \ll \mathrm{z_R}|_{w_0 \to w_{\mathcal{N},\mathcal{N}'}}$.

In the forward far field $\mathrm{z} \gg \mathrm{z}_\mathrm{R}$, we have $r/w(\mathrm{z}) \to r/(\theta\,\mathrm{z}) \simeq \vartheta/\theta$, where the polar angle ϑ is measured with respect to the forward beam axis. Taking into account $N \simeq W/\omega$ and $W = \int_0^\infty \mathrm{d}r r \int_0^{2\pi} \mathrm{d}\varphi \int_{-\infty}^{\infty} \mathrm{d}t\, I(x)$, the far-field angular decay of the number of laser photons N contained in a beam with $\mathrm{FG}_\mathcal{N}$ far-field profile (3.80) as a function of ϑ can thus be expressed as

$$\frac{\mathrm{d}N}{\vartheta\,\mathrm{d}\vartheta} \simeq \frac{N}{C_\mathcal{N}^2}\left(\frac{2}{\theta}\right)^2\left(\mathrm{e}^{-(\frac{\vartheta}{\theta})^2}\sum_{p=0}^{\mathcal{N}}(-1)^p\, c_{p,\mathcal{N}}\, L_p\Big(\tfrac{2\vartheta^2}{\theta^2}\Big)\right)^2 = \frac{N}{C_\mathcal{N}^2}\left(\frac{2}{\theta}\right)^2\left(\frac{\Gamma(\mathcal{N}+1,(\frac{\vartheta}{\theta})^2)}{\Gamma(\mathcal{N}+1)}\right)^2, \tag{3.86}$$

where we made use of Eq. (3.74) in the last step; θ is the far-field divergence of the fundamental Gaussian mode (3.24). Because of $r \sim \vartheta$ this quantity is directly proportional to the transverse intensity profile of the beam in its far field; integrations over the azimuthal angle φ and time t only affect its amplitude by an overall factor. The analogous result for a beam with $\mathrm{FG}^{\circledcirc}_{\mathcal{N},\mathcal{N}'}$ far-field profile follows by substituting $c_{p,\mathcal{N}} \to c_{p,\mathcal{N},\mathcal{N}'}$, which yields

$$\frac{\mathrm{d}N^{\circledcirc}}{\vartheta\,\mathrm{d}\vartheta} \simeq \frac{N}{C_\mathcal{N}^2}\left(\frac{2}{\theta}\right)^2\left(\frac{\Gamma(\mathcal{N}+1,(\frac{\vartheta}{\theta})^2)}{\Gamma(\mathcal{N}+1)} - \frac{\Gamma(\mathcal{N}'+1,(\frac{\vartheta}{\theta})^2)}{\Gamma(\mathcal{N}'+1)}\right)^2, \tag{3.87}$$

where $N^{\circledcirc} < N$ denotes the number of photons contained in this annular beam. On the other hand, for such a beam and $\mathcal{N}+\mathcal{N}' \gg 1$, using Eqs. (3.24) and (3.85) we can write

$$\theta \simeq \frac{2}{\omega w_{\mathcal{N},\mathcal{N}'}}\sqrt{\frac{2(1-\mathrm{e}^{-1})}{\mathcal{N}+\mathcal{N}'}}\,. \tag{3.88}$$

Also note that, as shown in the Appendix A.4, the following identity holds

$$\lim_{\mathcal{N}\to\infty}\frac{\Gamma(\mathcal{N}+1,\mathcal{N}\chi^2)}{\Gamma(\mathcal{N}+1)} = \Theta(1-\chi) \quad \text{for} \quad \chi \geq 0\,. \tag{3.89}$$

Employing Eq. (3.89) in Eq. (3.86) and performing the integration over ϑ, we can determine an explict expression for the factor $C_\mathcal{N}$ in the limit of $\mathcal{N} \gg 1$, namely $C_\mathcal{N} \simeq \sqrt{2\mathcal{N}}$. In the limit of $\mathcal{N} \gtrsim \mathcal{N}' \gg 1$ the far-field angular decay of the laser photons contained in the annular beam (3.87) can thus be compactly represented as

$$\frac{\mathrm{d}N^{\circledcirc}}{\vartheta\,\mathrm{d}\vartheta} \simeq N\,\frac{\omega^2 w_{\mathcal{N},\mathcal{N}'}^2}{4(1-\mathrm{e}^{-1})}\Big(1+\frac{\mathcal{N}'}{\mathcal{N}}\Big)\Big(\Theta(\theta_\mathrm{out}-\vartheta)-\Theta(\theta_\mathrm{in}-\vartheta)\Big), \tag{3.90}$$

with the inner and outer divergences of the beam given by

$$\theta_\mathrm{out} = \frac{2}{\omega w_{\mathcal{N},\mathcal{N}'}}\sqrt{\frac{2(1-\mathrm{e}^{-1})}{1+\frac{\mathcal{N}'}{\mathcal{N}}}} \quad \text{and} \quad \theta_\mathrm{in} = \theta_\mathrm{out}\sqrt{\frac{\mathcal{N}'}{\mathcal{N}}}\,. \tag{3.91}$$

The analogous result for a beam with $\mathrm{FG}_\mathcal{N}$ far-field profile and $\mathcal{N} \gg 1$ follows from Eq. (3.90) upon setting $\mathcal{N}' = 0$. Because the energy put into the beam is proportional to its cross-sectional area and the total cross section of the beam in the far field (including the shadow) scales as $\sim \theta_\mathrm{out}^2$, while that of the central shadow scales as $\sim \theta_\mathrm{in}^2$, we can readily infer from Eq. (3.91) that for $\mathcal{N} \gtrsim \mathcal{N}' \gg 1$ the beamstop

envisioned to create the (perfect rectangular) shadow in experiment is supposed to block a fraction

$$\frac{\Delta W}{W} = \left(\frac{\theta_{\text{in}}}{\theta_{\text{out}}}\right)^2 = \frac{\mathcal{N}'}{\mathcal{N}} \tag{3.92}$$

of the total energy W put into the original beam featuring a $\text{FG}_{\mathcal{N}}$ far-field profile with $\mathcal{N} \gg 1$; ΔW is the energy blocked by the beamstop. For completeness, we remark that a steep discontinuous far-field profile as implemented in Eq. (3.90) generically comes with a smooth focus profile; cf. also Eq. (3.99) and Fig. 3.3 below. This in particular implies a smooth beam profile in the interaction region, which thus does not at all challenge the slowly varying field approximation invoked in Sec. 3.2.1 for experimentally realistic laser beam parameters.

Building on these preparations, we can now study quantum vacuum signals in laser beam collisions utilizing a much more advanced laser beam model than provided by fundamental Gaussian beams. At the same time, mainly by considering the limit of $\mathcal{N} \gtrsim \mathcal{N}' \gg 1$ which implements ideal flat-top transverse profiles in the far field for both the original beam and the resulting annular beam featuring a field-free central shadow, we retain full analytical control; cf. also below. We highlight that this limit aligns well with experimental capabilities, where such beam profiles are often used prior to focusing. In our explicit example detailed below we focus on the head-on collision of an x-ray probe featuring a $\text{FG}^{\circledcirc}_{\mathcal{N},\mathcal{N}'}$ far-field profile fulfilling $\mathcal{N} \gtrsim \mathcal{N}' \gg 1$ with a fundamental Gaussian high-intensity pump in a counter-propagation geometry, i.e., revisit the scenario discussed in Sec. 3.2.4.1 with an annular probe beam. To this end, we return to Eqs. (3.44) and (3.45) and essentially repeat the same calculation for a different probe amplitude profile $\mathcal{E}_I(x)$. The pump field profile $\mathcal{E}_{II}(x)$ remains to be given by Eq. (3.47). We emphasize that for simplicity and not to obscure the impact of the much more involved probe beam structure on the quantum vacuum signal by additional technicalities, in our explicit calculations accounting for the details of the full probe beam profile we limit ourselves exclusively to optimal collisions at vanishing impact parameter $x_0^\mu = 0$. Note, however, that it will turn out that the results on the finite impact dependence inferred for the head-on collision of two fundamental Gaussian beams in Sec. 3.2.4.1 can also be invoked to reliably estimate the reduction of the signal photon numbers to be detected in the present scenario; cf. in particular Eq. (3.119) below.

Recall, that we have already established that the transverse profile of the x-ray probe with $\text{FG}^{\circledcirc}_{\mathcal{N},\mathcal{N}'}$ far-field profile and physical waist Eq. (3.85) closely resembles its focus profile for $|\text{z}| \ll \text{z}_\text{R}|_{w_0 \to w_{\mathcal{N},\mathcal{N}'}}$. Because of $\text{z}_\text{R}|_{w_0 \to w_{\mathcal{N},\mathcal{N}'}} \ll \text{z}_\text{R}$, in this regime also the field profile in longitudinal direction is insensitive to effects arising from the finiteness of z_R. This immediately implies that particularly for an x-ray waist $w_{\mathcal{N},\mathcal{N}'}$ of the same order as that of the near-infrared pump $w_{0,II}$, we have $\text{z}_\text{R}|_{w_0 \to w_{\mathcal{N},\mathcal{N}'}} \gg \text{z}_{\text{R},II}$. In turn, the longitudinal extent of the interaction region is controlled by $\text{z}_{\text{R},II}$ and similarly to the fundamental beam case in Sec. 3.2.4.1 an infinite Rayleigh range approximation can be adopted for the probe beam in the interaction region. Correspondingly, in particular for $\mathcal{N} + \mathcal{N}' \gg 1$ which ensures that the physical waist of the beam is well-approximated by Eq. (3.85), in the interaction region the field amplitude of the

probe beam should be well-described by

$$\mathcal{E}_I(x) = \mathcal{E}_{0,I}\sqrt{\frac{2(1-1/\mathrm{e})}{\mathcal{N}+\mathcal{N}'}}\,\mathrm{e}^{-(\frac{z-t}{\tau_I/2})^2}\,\mathrm{e}^{-(\frac{r}{w_I})^2\frac{2(1-1/\mathrm{e})}{\mathcal{N}+\mathcal{N}'}}\sum_{p=0}^{\mathcal{N}}\frac{c_{p,\mathcal{N},\mathcal{N}'}}{C_{\mathcal{N}}}\,L_p\Big(\tfrac{2r^2}{w_I^2}\tfrac{2(1-1/\mathrm{e})}{\mathcal{N}+\mathcal{N}'}\Big)\cos\Big(\omega_I(\mathrm{z}-t)-\tilde{\psi}_0\Big)\,, \quad (3.93)$$

where we have identified $w_I := w_{\mathcal{N},\mathcal{N}'}$ such that, similarly as for the fundamental Gaussian probe in Eq. (3.46), w_I amounts to the physical waist of the beam. Moreover, here the field amplitude $\mathcal{E}_{0,I}$ is defined in a way that it is related to the energy W_I put into the full beam prior to implementing the central shadow as

$$\mathcal{E}_{0,I}^2 = 8\sqrt{\frac{2}{\pi}}\frac{W_I}{\pi w_I^2\tau_I}\,, \quad (3.94)$$

and thus matches the analogous relation for a fundamental Gaussian beam. To arrive at these expressions we made use of Eq. (3.78) as well as Eqs. (3.80) and (3.85). At the same time, the number of laser photons $N_I^{\circledcirc}$ contained in the probe beam with $\mathrm{FG}^{\circledcirc}_{\mathcal{N},\mathcal{N}'}$ far-field profile and their angular decay in the outgoing far field follow from Eq. (3.90) with the replacements $N \to N_I$, $\omega \to \omega_I$ and $w_{\mathcal{N},\mathcal{N}'} \to w_I$. This immediately implies that only $N_I^{\circledcirc} = (1-\mathcal{N}'/\mathcal{N})N_I$ out of the N_I laser photons constituting the original probe beam prior to implementing the central shadow reach the interaction region and thus can potentially participate in the effective interaction with the pump laser beam. Also note that using Eqs. (3.79) and (3.84) we can immediately derive an explicit expression for the peak field amplitude obtained by setting $\mathrm{z} = t = r = \tilde{\psi}_0 = 0$ in Eq. (3.93). The latter is given by

$$\mathcal{E}_I^{\mathrm{peak}} = \sqrt{2(1-1/\mathrm{e})}\,\frac{\mathcal{N}-\mathcal{N}'}{C_{\mathcal{N}}\sqrt{\mathcal{N}+\mathcal{N}'}}\,\mathcal{E}_{0,I} \xrightarrow{\mathcal{N}\gg 1} \sqrt{\frac{1-1/\mathrm{e}}{1+\frac{\mathcal{N}'}{\mathcal{N}}}}\Big(1-\frac{\mathcal{N}'}{\mathcal{N}}\Big)\mathcal{E}_{0,I}\,, \quad (3.95)$$

where we made use of the fact that for large values of $\mathcal{N}$ we have $C_{\mathcal{N}} \simeq \sqrt{2\mathcal{N}}$. From this result we can in particular infer that $\mathcal{E}_I^{\mathrm{peak}} \leq \sqrt{1-1/\mathrm{e}}\,\mathcal{E}_{0,I}$ for $\mathcal{N} \gg 1$, with the upper limit reached for a beam without central shadow, i.e., for $\mathcal{N}' = 0$. For completeness, we emphasize once again that even though the identification of the beam waist with the approximate expression (3.85) employed in Eq. (3.93) is clearly motivated only for $\mathcal{N}+\mathcal{N}' \gg 1$, Eq. (3.93) can still be adopted for the study of beams parameterized by generic values of $\mathcal{N} > \mathcal{N}'$, the only caveat being that for $\mathcal{N}$ and $\mathcal{N}'$ not fulfilling the criterion $\mathcal{N}+\mathcal{N}' \gg 1$ the waist w_I no longer amounts to the physical waist of the beam and has to be rescaled accordingly depending on the specific values of $\mathcal{N}$ and $\mathcal{N}'$; cf. also the comment below Eq. (3.85).

In a next step, we highlight that for beams with either an $\mathrm{FG}_{\mathcal{N}}$ far-field profile with $\mathcal{N} \gg 1$ or an $\mathrm{FG}^{\circledcirc}_{\mathcal{N},\mathcal{N}'}$ far-field profile with $\mathcal{N} \gtrsim \mathcal{N}' \gg 1$ additional simplifications are possible. These even allow for a closed-form representation of the field amplitude profile (3.93) of the probe beam in the interaction region. Using the sum representation of the Laguerre polynomials in Eq. (A.27) it is easy to show that

$$\begin{aligned} L_p(x/\mathcal{N}) &= 1-\frac{p}{\mathcal{N}}x+\sum_{j=2}^{p}\frac{(-1)^j}{(j!)^2}\Big(\frac{p}{\mathcal{N}}x\Big)^j\Big(1+O(\tfrac{1}{p})\Big) \\ &= 1-\frac{p}{\mathcal{N}}x+\sum_{j=2}^{\infty}\frac{(-1)^j}{(j!)^2}\Big(\frac{p}{\mathcal{N}}x\Big)^j\Big(1+O(\tfrac{1}{p})\Big)+\frac{1}{[(p+1)!]^2}\,O((\tfrac{p}{\mathcal{N}}x)^{p+1})\,. \end{aligned} \quad (3.96)$$

For the terms written explicitly in the second line of this equation the sum can even be performed, yielding the closed-form result $J_0(2\sqrt{xp/\mathcal{N}})$, where $J_a(\cdot)$ is the a Bessel function of the first kind of order a. For later reference we note that $J_0(2\sqrt{-xp/\mathcal{N}}) = I_0(2\sqrt{xp/\mathcal{N}})$ with modified Bessel function of the first kind $I_0(\cdot)$. Together with Eq. (A.47) the expression given in Eq. (3.96) implies that for $\mathcal{N} \gg 1$ we have

$$\sum_{p=0}^{\mathcal{N}} c_{p,\mathcal{N}}\, L_p(x/\mathcal{N}) = \mathcal{N} \sum_{j=0}^{\infty} \frac{(-1)^j}{(j+1)!\,j!}\Big(\frac{x}{2}\Big)^j\Big(1+O(\tfrac{1}{\mathcal{N}})\Big) = 2\mathcal{N}\,\frac{J_1(\sqrt{2x})}{\sqrt{2x}}\Big(1+O(\tfrac{1}{\mathcal{N}})\Big). \tag{3.97}$$

With the help of Eq. (A.48) we can analogously infer that for $\mathcal{N} \gtrsim \mathcal{N}' \gg 1$ the following identity holds,

$$\sum_{p=0}^{\mathcal{N}} c_{p,\mathcal{N},\mathcal{N}'}\, L_p(x/\mathcal{N}) = 2\mathcal{N}\left[\frac{J_1(\sqrt{2x})}{\sqrt{2x}} - \frac{\mathcal{N}'}{\mathcal{N}}\,\frac{J_1(\sqrt{2(\mathcal{N}'/\mathcal{N})x})}{\sqrt{2(\mathcal{N}'/\mathcal{N})x}}\right]\Big(1+O(\tfrac{1}{\mathcal{N}})\Big), \tag{3.98}$$

where we count $O(1/\mathcal{N}') = O(1/\mathcal{N})$. Hence, in cases where either $\mathcal{N} \gtrsim \mathcal{N}' \gg 1$ or $\mathcal{N} \gg 1$ and simultaneously $\mathcal{N}' = 0$, Eq. (3.93) can be compactly represented as

$$\begin{aligned}\mathcal{E}_I(x) = 2\,\mathcal{E}_{0,I}\sqrt{\frac{1-1/\mathrm{e}}{1+\frac{\mathcal{N}'}{\mathcal{N}}}}\,\mathrm{e}^{-(\frac{z-t}{\tau_I/2})^2} \\ \times\left[\frac{J_1\Big(\sqrt{\frac{2(1-1/\mathrm{e})}{1+\frac{\mathcal{N}'}{\mathcal{N}}}}\,\frac{2r}{w_I}\Big)}{\sqrt{\frac{2(1-1/\mathrm{e})}{1+\frac{\mathcal{N}'}{\mathcal{N}}}}\,\frac{2r}{w_I}} - \frac{\mathcal{N}'}{\mathcal{N}}\,\frac{J_1\Big(\sqrt{\frac{2(1-1/\mathrm{e})}{1+\frac{\mathcal{N}'}{\mathcal{N}}}\,\frac{\mathcal{N}'}{\mathcal{N}}}\,\frac{2r}{w_I}\Big)}{\sqrt{\frac{2(1-1/\mathrm{e})}{1+\frac{\mathcal{N}'}{\mathcal{N}}}\,\frac{\mathcal{N}'}{\mathcal{N}}}\,\frac{2r}{w_I}}\right]\cos\Big(\omega_I(\mathrm{z}-t)-\tilde{\psi}_0\Big),\end{aligned} \tag{3.99}$$

where we set $\exp\{-(\frac{r}{w_I})^2\frac{2(1-1/\mathrm{e})}{\mathcal{N}+\mathcal{N}'}\} \to 1$. This is well-justified because in the considered limit the expression containing the Bessel functions ensure the field to decay with r/w_I. Note, that the transverse intensity profile associated with Eq. (3.99) precisely matches the Airy pattern arising as the Fraunhofer diffraction pattern of a circular aperture. This is in line with expectations because the far-field profile which gives rise to Eq. (3.99) describing the field in the vicinity of the beam focus amounts to a step function; cf. Eq. (3.90). One can easily check that the $1/\mathrm{e}$ radius of the pronounced central peak characteristic for this field profile is well-approximated by w_I for generic choices of the parameter $0 \leq \mathcal{N}'/\mathcal{N} < 1$, which thus confirms the validity of the approximation (3.85) invoked in its construction. Correspondingly, aiming at capturing exclusively the effect of the central peak that typically dominates the transverse field profile of the beam, one can adopt the following Gaussian approximation to Eq. (3.99),

$$\mathcal{E}_I(x) = \mathcal{E}_I^{\mathrm{peak}}\,\mathrm{e}^{-(\frac{z-t}{\tau_I/2})^2}\mathrm{e}^{-(\frac{r}{w_I})^2}\cos\Big(\omega_I(\mathrm{z}-t)-\tilde{\psi}_0\Big), \tag{3.100}$$

with the peak field amplitude given by Eq. (3.95) in the limit of $\mathcal{N} \gg 1$. See Fig. 3.3 for an illustration of the associated focus intensity profiles together with the corresponding far-field intensity profiles for different values of the ratio $\mathcal{N}'/\mathcal{N}$. In this figure we also confront Eq. (3.99) with its Gaussian approximation (3.100). As Eq. (3.100) is precisely of the form of Eq. (3.46) at vanishing spatio-

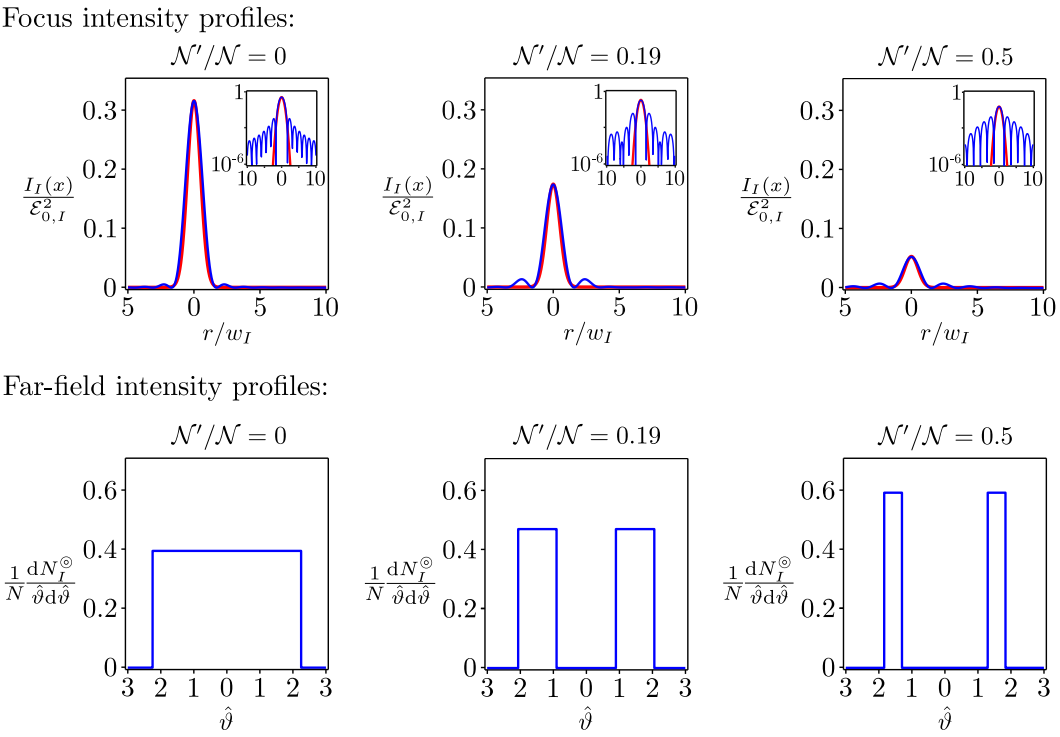

Figure 3.3: Focus and far-field transverse intensity profiles of laser beams featuring ideal flat-top profiles in the far field characterized by different representative values of the blocking fraction $\mathcal{N}'/\mathcal{N}$ in Eq. (3.92). Upper panel: The curves accounting for the Airy ring structure (blue) are obtained from Eq. (3.99) via cycle-averaging as $I_I(x) = \langle \mathcal{E}_I^2(x)\rangle_t$ and setting $t = 0$. Analogously, the Gaussian curves (red) follow from Eq. (3.100). The insets show the same results on a logarithmic intensity scale. Lower panel: Far-field distributions of the laser photons constituting the beam extracted from Eq. (3.90). Here, $\hat{\vartheta} := \omega_I w_I \vartheta$ is an appropriately rescaled polar angle.

temporal offset $x_0^\mu = 0$, the quantum vacuum signals induced by the central peak in the transverse field profile alone ignoring the Airy rings follows readily from the results worked out in Sec. 3.2.4.1. In fact, only the peak field of the probe has to be adjusted accordingly, resulting in an overall factor of $(1 - 1/\mathrm{e})(1 - \mathcal{N}'/\mathcal{N})^2/(1 + \mathcal{N}'/\mathcal{N})$ to be accounted for on the level of the (differential) signal photon numbers; cf. Eq. (3.95). While this may constitute a very good approximation for determining the dominant signal in certain parameter regimes, it has to be taken with caution because its quality is certainly not universal: in the focus the information about the actual far-field profile of a given laser beam is encoded in the Airy ring structure. Analogously also the far-field distribution of the signal depends decisively on the details of the focus profiles of the driving laser fields. Hence, in particular if only the central Gaussian peak (3.100) of the probe focus profile is accounted for in the determination of the associated signal photon distribution in the present scenario, this signal will feature a Gaussian profile by definition. Especially in cases where the probe is focused to a waist much smaller than that of the pump, which implies a sizable fraction of the Airy ring structure of the probe to be illuminated by the pump, significant deviations from the true signal photon distribution are to be expected; cf. also the detailed discussion in the context of Eq. (3.111) below.

In a next step, we note that making use of parameter differentiations Eq. (3.93) can be expressed as

$$\mathcal{E}_I(x) = \sqrt{\frac{2(1-1/\mathrm{e})}{\mathcal{N}+\mathcal{N}'}} \sum_{p=0}^{\mathcal{N}} \frac{c_{p,\mathcal{N},\mathcal{N}'}}{C_{\mathcal{N}}} L_p(-2\partial_\chi) \underbrace{\mathcal{E}_{0,I}\, \mathrm{e}^{-(\frac{z-t}{\tau_I/2})^2}\, \mathrm{e}^{-\chi(\frac{r}{w_I})^2 \frac{2(1-1/\mathrm{e})}{\mathcal{N}+\mathcal{N}'}}\, \cos\!\big(\omega_I(\mathrm{z}-t)-\tilde{\psi}_0\big)}_{=\text{Eq. (3.46)}|_{x_0^\mu=0,\, w_I^2\to\frac{1}{\chi}w_I^2\frac{\mathcal{N}+\mathcal{N}'}{2(1-1/\mathrm{e})},\, \psi_0\to\tilde{\psi}_0}} \Big|_{\chi=1} . \tag{3.101}$$

In turn, the integrations over the spacetime coordinates necessary for the explicit evaluation of the amplitude (3.45), which is linear in $\mathcal{E}_I(x)$, reduce to those required for the collision of two fundamental Gaussian beams in Sec. 3.2.4.1. As the arguments invoked between Eqs. (3.48) and (3.49) to simplify the expression of the corresponding amplitude remain valid also in the present case, we can employ Eq. (3.101) directly to the appropriately simplified result given in Eq. (3.49). Note that it is easy to see that for the case of $x_0^\mu = 0$ and $\psi_0 \to \tilde{\psi}_0$ considered here the modulus of the amplitude in Eqs. (3.48) and (3.49) is related to the amplitude as $\mathcal{M}_I(\vec{k}) = \big|\mathcal{M}_I(\vec{k})\big|\, \mathrm{e}^{-\mathrm{i}\tilde{\psi}_0}$; cf. also Ref. [109]. Hence, for the specific scenario studied here the result for the differential number of signal photons can be obtained from Eq. (3.44) with the relevant amplitude now given by

$$\begin{aligned}\mathcal{M}_I(\vec{k}) \approx{}& \mathcal{E}_{0,I}\, \mathcal{E}_{0,II}^2\, \frac{1}{4}\Big(\frac{\pi}{2}\Big)^{\frac{3}{2}} \sqrt{\frac{2(1-1/\mathrm{e})}{\mathcal{N}+\mathcal{N}'}}\, \frac{\tau_{II}\, \mathrm{z}_{\mathrm{R},II}\, w_{0,II}^2}{\sqrt{1+\frac{1}{2}(\frac{\tau_{II}}{\tau_I})^2}}\, \mathrm{e}^{-\frac{2}{1+\frac{1}{2}(\frac{\tau_{II}}{\tau_I})^2}\tau_{II}^2(\frac{\omega_I-\mathrm{k}}{8})^2}\, \mathrm{e}^{-\mathrm{i}\tilde{\psi}_0} \\ &\times \sum_{p=0}^{\mathcal{N}} \frac{c_{p,\mathcal{N},\mathcal{N}'}}{C_{\mathcal{N}}} L_p(-2\partial_\chi) \int \mathrm{d}\zeta\, \frac{1}{2+\chi v^2(\zeta)}\, \mathrm{e}^{-\frac{w_{II}^2(\zeta)}{4[2+\chi v^2(\zeta)]}\omega_I^2\vartheta^2}\, \mathrm{e}^{-(\frac{4\mathrm{z}_{\mathrm{R},II}}{\tau_I})^2 \frac{\zeta^2}{1+\frac{1}{2}(\frac{\tau_{II}}{\tau_I})^2}}\, \mathrm{e}^{\mathrm{i}\frac{2\mathrm{z}_{\mathrm{R},II}(\omega_I-\mathrm{k})}{1+\frac{1}{2}(\frac{\tau_{II}}{\tau_I})^2}\zeta} \Big|_{\chi=1} ,\end{aligned} \tag{3.102}$$

where we introduced the shorthand notation

$$v(\zeta) := \frac{w_{II}(\zeta)}{w_I} \sqrt{\frac{2(1-1/\mathrm{e})}{\mathcal{N}+\mathcal{N}'}} . \tag{3.103}$$

With the help of Eq. (A.21) in the Appendix the parameter differentiations in Eq. (3.102) can be carried out explicitly. This results in the relatively compact expression

$$\begin{aligned}\mathcal{M}_I(\vec{k}) \approx{}& \mathcal{E}_{0,I}\, \mathcal{E}_{0,II}^2\, \frac{1}{4}\Big(\frac{\pi}{2}\Big)^{\frac{3}{2}} \sqrt{\frac{2(1-1/\mathrm{e})}{\mathcal{N}+\mathcal{N}'}}\, \frac{\tau_{II}\, \mathrm{z}_{\mathrm{R},II}\, w_{0,II}^2}{\sqrt{1+\frac{1}{2}(\frac{\tau_{II}}{\tau_I})^2}}\, \mathrm{e}^{-\frac{2}{1+\frac{1}{2}(\frac{\tau_{II}}{\tau_I})^2}\tau_{II}^2(\frac{\omega_I-\mathrm{k}}{8})^2}\, \mathrm{e}^{-\mathrm{i}\tilde{\psi}_0} \sum_{p=0}^{\mathcal{N}} \frac{c_{p,\mathcal{N},\mathcal{N}'}}{C_{\mathcal{N}}} \\ &\times \int \mathrm{d}\zeta\, \frac{[2-v^2(\zeta)]^p}{[2+v^2(\zeta)]^{p+1}}\, L_p\Big(\frac{v^2(\zeta)\, w_{II}^2(\zeta)\, \omega_I^2\vartheta^2}{2[v^4(\zeta)-4]}\Big)\, \mathrm{e}^{-\frac{w_{II}^2(\zeta)}{4[2+v^2(\zeta)]}\omega_I^2\vartheta^2}\, \mathrm{e}^{-(\frac{4\mathrm{z}_{\mathrm{R},II}}{\tau_I})^2 \frac{\zeta^2}{1+\frac{1}{2}(\frac{\tau_{II}}{\tau_I})^2}}\, \mathrm{e}^{\mathrm{i}\frac{2\mathrm{z}_{\mathrm{R},II}(\omega_I-\mathrm{k})}{1+\frac{1}{2}(\frac{\tau_{II}}{\tau_I})^2}\zeta} .\end{aligned} \tag{3.104}$$

Equation (3.104) can be considered as the analogue and generalization of Eq. (3.49) to the case of a probe with $\mathrm{FG}_{\mathcal{N}}$ or $\mathrm{FG}^{\circledcirc}_{\mathcal{N},\mathcal{N}'}$ far-field profile. It can in particular be evaluated numerically for generic choices of $\mathcal{N}$ and $\mathcal{N}'$ (when accounting for an appropriate $\mathcal{N}$ and $\mathcal{N}'$ dependent rescaling of w_I for those values not fulfilling $\mathcal{N}+\mathcal{N}' \gg 1$; cf. the corresponding comment in the paragraph below Eq. (3.95)).

For either $\mathcal{N} \gtrsim \mathcal{N}' \gg 1$ or $\mathcal{N} \gg 1$ and at the same time $\mathcal{N}' = 0$, i.e., probe beams featuring an ideal flat-top profile, additional simplifications of Eq. (3.104) are possible. Utilizing Eq. (A.44), the following

identity,

$$\frac{[2-(x/\sqrt{\mathcal{N}})^2]^p}{[2+(x/\sqrt{\mathcal{N}})^2]^{p+1}} = \frac{1}{2}\sum_{j=0}^{\infty}\frac{1}{j!}\Big(-\frac{p}{\mathcal{N}}x^2\Big)^j\Big(1+O(\tfrac{1}{p})\Big) = \frac{1}{2}\,\mathrm{e}^{-\frac{p}{\mathcal{N}}x^2}\Big(1+O(\tfrac{1}{p})\Big), \tag{3.105}$$

and accounting for Eq. (3.96), in a first step we obtain

$$\begin{aligned}\big|\mathcal{M}_I(\vec{k})\big| \approx{}& \mathcal{E}_{0,I}\,\mathcal{E}_{0,II}^2\,\frac{1}{4}\Big(\frac{\pi}{2}\Big)^{\frac{3}{2}}\sqrt{\frac{1-1/\mathrm{e}}{(\mathcal{N}+\mathcal{N}')\mathcal{N}}}\,\frac{\tau_{II}\,\mathrm{z}_{\mathrm{R},II}\,w_{0,II}^2}{\sqrt{1+\frac{1}{2}(\frac{\tau_{II}}{\tau_I})^2}}\,\mathrm{e}^{-\frac{2}{1+\frac{1}{2}(\frac{\tau_{II}}{\tau_I})^2}\tau_{II}^2(\frac{\omega_I-\mathrm{k}}{8})^2}\\
&\times\Bigg|\sum_{p=\mathcal{N}'/2}^{\mathcal{N}/2}\int\mathrm{d}\zeta\,I_0\Big(\sqrt{\tfrac{1}{2}\tfrac{p}{\mathcal{N}}}\,r(\zeta)\,w_{II}(\zeta)\,\omega_I\,\vartheta\Big)\,\mathrm{e}^{-\frac{p}{\mathcal{N}}r^2(\zeta)-\frac{1}{8}w_{II}^2(\zeta)\,\omega_I^2\,\vartheta^2}\,\mathrm{e}^{-(\frac{4\mathrm{z}_{\mathrm{R},II}}{\tau_I})^2\frac{\zeta^2}{1+\frac{1}{2}(\frac{\tau_{II}}{\tau_I})^2}}\,\mathrm{e}^{\mathrm{i}\frac{2\mathrm{z}_{\mathrm{R},II}(\omega_I-\mathrm{k})}{1+\frac{1}{2}(\frac{\tau_{II}}{\tau_I})^2}\zeta}\Bigg|,\end{aligned} \tag{3.106}$$

where

$$r(\zeta) := \sqrt{\mathcal{N}v^2(\zeta)} = \frac{w_{II}(\zeta)}{w_I}\sqrt{\frac{2(1-1/\mathrm{e})}{1+\frac{\mathcal{N}'}{\mathcal{N}}}}\,. \tag{3.107}$$

To arrive at the result in Eq. (3.106), we moreover made use of the fact that $v(\zeta) \ll 1$ for $\mathcal{N}+\mathcal{N}' \gg 1$ to simply the arguments of the Legendre polynomials as well as the exponential function in Eq. (3.104) and completely omitted subleading corrections suppressed by inverse powers of $\mathcal{N}$ and $\mathcal{N}'$. Finally, because the dependence of the summands on the ratio $p/\mathcal{N}$ is manifest in Eq. (3.106), in the considered limit we can rewrite the sum over p in terms of an integral. To this end, we identify $P = 2p/\mathcal{N}$ and thus obtain the manifestly finite expression

$$\begin{aligned}\big|\mathcal{M}_I(\vec{k})\big| \approx{}& \mathcal{E}_{0,I}\,\mathcal{E}_{0,II}^2\,\frac{1}{8}\Big(\frac{\pi}{2}\Big)^{\frac{3}{2}}\sqrt{\frac{1-1/\mathrm{e}}{1+\frac{\mathcal{N}'}{\mathcal{N}}}}\,\frac{\tau_{II}\,\mathrm{z}_{\mathrm{R},II}\,w_{0,II}^2}{\sqrt{1+\frac{1}{2}(\frac{\tau_{II}}{\tau_I})^2}}\,\mathrm{e}^{-\frac{2}{1+\frac{1}{2}(\frac{\tau_{II}}{\tau_I})^2}\tau_{II}^2(\frac{\omega_I-\mathrm{k}}{8})^2}\\
&\times\Bigg|\int_{\frac{\mathcal{N}'}{\mathcal{N}}}^1\mathrm{d}P\int\mathrm{d}\zeta\,I_0\Big(\tfrac{1}{2}\sqrt{P}\,r(\zeta)\,w_{II}(\zeta)\,\omega_I\,\vartheta\Big)\,\mathrm{e}^{-\frac{1}{2}Pr^2(\zeta)-\frac{1}{8}w_{II}^2(\zeta)\,\omega_I^2\,\vartheta^2}\,\mathrm{e}^{-(\frac{4\mathrm{z}_{\mathrm{R},II}}{\tau_I})^2\frac{\zeta^2}{1+\frac{1}{2}(\frac{\tau_{II}}{\tau_I})^2}}\,\mathrm{e}^{\mathrm{i}\frac{2\mathrm{z}_{\mathrm{R},II}(\omega_I-\mathrm{k})}{1+\frac{1}{2}(\frac{\tau_{II}}{\tau_I})^2}\zeta}\Bigg|\end{aligned} \tag{3.108}$$

for the modulus of the amplitude. Equation (3.108) does not depend individually on $\mathcal{N}$ and $\mathcal{N}'$ but only on the ratio $0 \leq \mathcal{N}'/\mathcal{N} < 1$ that measures the fraction of the far-field cross-sectional area, or equivalently the beam energy, blocked by the obstacle implementing the central shadow; cf. Eq. (3.92). It can be readily evaluated numerically for generic parameters. In particular, note that the first two terms in the integrand in the second line of Eq. (3.108) are of the structure $I_0(2\sqrt{ab})\,\mathrm{e}^{-a-b}$, which makes the finiteness of Eq. (3.108) for arbitrary parameters manifest.

To obtain further analytical insights, in a next step we utilize an effective waist approximation for the high-intensity pump as already employed in Sec. 3.2.4.1 for the collision scenario involving two fundamental Gaussian beams. This amounts to identifying all occurrences of $w_{II}(\zeta)$ in Eq. (3.108) with $\bar{w}_{II} = \text{const.}$ while accounting for an additional factor of $(\bar{w}_{II}/w_{II}(\zeta))^2$ in the integrand of the integral over ζ. As in Sec. 3.2.4.1 we denote the corresponding amplitude by $\bar{\mathcal{M}}_I(\vec{k})$. It should be noted that because the defining equation (3.54) for the effective waist devised for the collision scenario of two fundamental Gaussian beams depends only on the probe pulse duration τ_I, the probe waist w_I and pump laser parameters, all of which play exactly the same role also in the present collision scenario, we can adopt

this definition here also. Resorting to this approximation the integration over ζ can then be performed with Eq. (3.50), yielding

$$\begin{aligned}\left|\bar{\mathcal{M}}_I(\vec{k})\right| \approx \mathcal{E}_{0,I}\,\mathcal{E}_{0,II}^2\,\frac{1}{8}\Big(\frac{\pi}{2}\Big)^{\frac{5}{2}}\sqrt{\frac{1-1/\mathrm{e}}{1+\frac{\mathcal{N}'}{\mathcal{N}}}}\,\frac{\tau_{II}\,\mathrm{z}_{\mathrm{R},II}\,\bar{w}_{II}^2}{\sqrt{1+\frac{1}{2}(\frac{\tau_{II}}{\tau_I})^2}}\,\mathrm{e}^{(\frac{4\mathrm{z}_{\mathrm{R},II}}{\tau_I})^2\frac{1}{1+\frac{1}{2}(\frac{\tau_{II}}{\tau_I})^2}} \\ \times\,\mathrm{e}^{-\frac{2}{1+\frac{1}{2}(\frac{\tau_{II}}{\tau_I})^2}\tau_{II}^2(\frac{\omega_I-\mathrm{k}}{8})^2}\sum_{s=\pm1}\mathrm{e}^{2s\frac{\mathrm{z}_{\mathrm{R},II}(\omega_I-\mathrm{k})}{1+\frac{1}{2}(\frac{\tau_{II}}{\tau_I})^2}}\,\mathrm{erfc}\Bigg(\frac{s\tau_I\frac{\omega_I-\mathrm{k}}{4}+\frac{4\mathrm{z}_{\mathrm{R},II}}{\tau_I}}{\sqrt{1+\frac{1}{2}(\frac{\tau_{II}}{\tau_I})^2}}\Bigg) \\ \times\int_{\frac{\mathcal{N}'}{\mathcal{N}}}^1\mathrm{d}P\,I_0\Big(\sqrt{\tfrac{(1-1/\mathrm{e})P}{2(1+\frac{\mathcal{N}'}{\mathcal{N}})}}\,\tfrac{\bar{w}_{II}}{w_I}\,\bar{w}_{II}\,\omega_I\,\vartheta\Big)\,\mathrm{e}^{-\frac{(1-1/\mathrm{e})P}{1+\frac{\mathcal{N}'}{\mathcal{N}}}(\frac{\bar{w}_{II}}{w_I})^2-\frac{1}{8}(\bar{w}_{II}\,\omega_I\,\vartheta)^2}\,. \end{aligned}\tag{3.109}$$

With the help of Eq. (3.53) the square of Eq. (3.109) integrated over the signal photon energies can in turn be compactly expressed as

$$\begin{aligned}\int\mathrm{d}\mathrm{k}\left|\bar{\mathcal{M}}_I(\vec{k})\right|^2 \approx \frac{1}{8}\sqrt{\frac{3}{2}}\Big(\frac{\pi}{4}\Big)^5\frac{1-1/\mathrm{e}}{1+\frac{\mathcal{N}'}{\mathcal{N}}}\,\mathcal{E}_{0,I}^2\,\mathcal{E}_{0,II}^4\,\tau_I\,\tau_{II}^2\,\bar{w}_{II}^4\,F\Bigg(\frac{4\mathrm{z}_{\mathrm{R},II}}{\sqrt{\tau_I^2+\frac{1}{2}\tau_{II}^2}},0,\frac{\tau_I}{\tau_{II}}\Bigg) \\ \times\Bigg(\int_{\frac{\mathcal{N}'}{\mathcal{N}}}^1\mathrm{d}P\,I_0\Big(\sqrt{\tfrac{(1-1/\mathrm{e})P}{2(1+\frac{\mathcal{N}'}{\mathcal{N}})}}\,\tfrac{\bar{w}_{II}}{w_I}\,\bar{w}_{II}\,\omega_I\,\vartheta\Big)\,\mathrm{e}^{-\frac{(1-1/\mathrm{e})P}{1+\frac{\mathcal{N}'}{\mathcal{N}}}(\frac{\bar{w}_{II}}{w_I})^2-\frac{1}{8}(\bar{w}_{II}\,\omega_I\,\vartheta)^2}\Bigg)^2\,. \end{aligned}\tag{3.110}$$

Upon substituting $\mathcal{M}_I(\vec{k})\to\bar{\mathcal{M}}_I(\vec{k})$ in Eq. (3.44), integrating it over all possible signal photon energies k and inserting Eq. (3.110), we finally arrive at a compact result for the directional emission characteristics of the dominant quasi-elastic scattering signal $\mathrm{d}^2N_{p,I}/\mathrm{d}\varphi\,\vartheta\mathrm{d}\vartheta$. The resulting expression can be easily evaluated numerically and analyzed for generic choices of the parameters of the driving laser beams. However, in the remainder of this section we rather demonstrate that, especially when invoking a single additional well-founded condition on the far-field angular decay of the induced quantum vacuum signals, further simplifications are possible. This will in particular allow us to obtain essentially analytic expressions for the signals scattered into the central shadow in the outgoing probe beam that are as simple as those derived for the collision of two fundamental Gaussian beams in Sec. 3.2.4.1.

In order to ensure that the signal is peaked in forward direction and falls off slowly with increasing ϑ we demand the second derivative of Eq. (3.110), or equivalently Eq. (3.109), for ϑ to vanish identically [131]. This results in the following relation between the probe waist w_I, the effective waist of the pump $\bar{w}_{II}$ and the ratio $\nu:=\mathcal{N}'/\mathcal{N}$ corresponding to the blocking fraction introduced in Eq. (3.92),

$$\Big(\frac{\bar{w}_{II}}{w_I}\Big)^2\simeq-\frac{1}{1-1/\mathrm{e}}\,\frac{1+\nu}{1-\nu}\ln\nu\,.\tag{3.111}$$

As will be clear below, using this constraint guarantees the possibility of an analytic treatment of the integral still to be performed in Eq. (3.110) and thereby helps to substantially simplify the subsequent calculation. At the same time the choice (3.111) is expected to approximately give rise to the maximum number of signal photons scattered into the shadow. This follows form the following reasoning: In the context of Eq. (3.100) we argued that the central peak dominating the transverse field profile of the probe in the focus is well approximated by a Gaussian of waist w_I. Hence, especially for $w_I\gtrsim\bar{w}_{II}/\sqrt{2}$ the

far-field angular decay of the signal with ϑ should be accurately described by the last exponential factor in Eq. (3.57) derived for the collision of two fundamental Gaussian beams, implying a Gaussian decay of the signal with ϑ.[§] In this regime it moreover holds true that the larger w_I for given $\bar{w}_{II}$, the wider the divergence of the signal (3.58) and thus generically the smaller the signal in the shadow. On the other hand, when decreasing the probe waist to $w_I \lesssim \bar{w}_{II}/\sqrt{2}$ the overlap of the side peaks of the probe profile with the strong pump field increases. As these in particular encode the information about the shadow in the far-field profile of the probe, this shadow starts to get imprinted also in the far-field distribution of the signal induced in the interaction region of the two beams, leading to a local minimum of the signal photon distribution at ϑ for $w_I \lesssim \bar{w}_{II}/\sqrt{2}$ which gets increasingly pronounced when further decreasing towards $w_I \ll \bar{w}_{II}$. Because both of these behaviors effectively tend to decrease the signal in the shadow, we expect this signal to become maximum when tuning the ratio of the waists $w_I/\bar{w}_{II}$ to the inflection point between them. Therefore, we adopt the choice (3.111) in all our subsequent considerations. We emphasize that Eq. (3.111) does not immediately fix the ratio of w_I and $\bar{w}_{II}$ to a numeric constant, but instead expresses it in terms of the blocking fraction $0 \leq \nu \leq 1$ which controls the details of the Airy pattern associated with the probe beam focus in Eq. (3.99) and amounts to a free parameter to be adjusted at will. However, when choosing ν such as to maximize the signal photon number in the shadow we indeed find a value of $w_I/\bar{w}_{II}$ close to the naive estimate of $1/\sqrt{2}$; see Eq. (3.118) below. Upon plugging Eq. (3.111) into Eq. (3.110) we arrive at

$$\int \mathrm{d}k \left|\bar{\mathcal{M}}_I(\vec{k})\right|^2 \approx \frac{1}{8}\sqrt{\frac{3}{2}}\left(\frac{\pi}{4}\right)^5 \frac{1-1/\mathrm{e}}{1+\nu}\,\mathcal{E}_{0,I}^2\,\mathcal{E}_{0,II}^4\,\tau_I\,\tau_{II}^2\,\bar{w}_{II}^4\,F\!\left(\frac{4z_{\mathrm{R},II}}{\sqrt{\tau_I^2+\frac{1}{2}\tau_{II}^2}},0,\frac{\tau_I}{\tau_{II}}\right) \times\left(\int_\nu^1 \mathrm{d}P\, I_0\!\left(\sqrt{-\tfrac{\ln\nu}{1-\nu}\tfrac{P}{2}}\,\bar{w}_{II}\,\omega_I\,\vartheta\right)\mathrm{e}^{\frac{\ln\nu}{1-\nu}P-\frac{1}{8}(\bar{w}_{II}\,\omega_I\,\vartheta)^2}\right)^2, \quad (3.112)$$

where we expressed each occurrence of w_I in terms of $\bar{w}_{II}$. Next, we note that for $\vartheta \leq \theta_{\mathrm{in}}$, with θ_{in} as defined in Eq. (3.91), which in the present context (i.e., after substituting $\omega \to \omega_I$ and $w_{\mathcal{N},\mathcal{N}'} \to w_I$) and accounting for Eq. (3.111) reads

$$\theta_{\mathrm{in}} = \frac{2}{\omega_I \bar{w}_{II}}\sqrt{-\frac{2\nu\ln\nu}{1-\nu}}\,, \quad (3.113)$$

the argument of the Bessel function in Eq. (3.112) fulfills

$$0 \leq \sqrt{-\frac{\ln\nu}{1-\nu}\frac{P}{2}}\,\bar{w}_{II}\,\omega_I\,\vartheta \leq 2\,. \quad (3.114)$$

This immediately implies that for the evaluation of the signal component scattered into the central shadow in the probe beam it is sufficient to expand the Bessel function $I_0(\cdot)$ up to quartic order in its argument. Making use of this approximation, the integral over P in Eq. (3.112) can be performed analytically, yielding

[§]The factor of $\sqrt{2}$ accounted for here originates in the fact that the quantum vacuum signal under consideration scales linearly in the probe (I) and quadratic in the pump (II) field.

$$\int \mathrm{d}\mathrm{k}\,\big|\bar{\mathcal{M}}_I(\vec{k})\big|^2 \approx \frac{1}{8}\sqrt{\frac{3}{2}}\Big(\frac{\pi}{4}\Big)^5 \frac{1-1/\mathrm{e}}{1+\nu}\,\mathcal{E}_{0,I}^2\,\mathcal{E}_{0,II}^4\,\tau_I\,\tau_{II}^2\,\bar{w}_{II}^4\,F\Big(\tfrac{4z_{\mathrm{R},II}}{\sqrt{\tau_I^2+\frac{1}{2}\tau_{II}^2}},0,\tfrac{\tau_I}{\tau_{II}}\Big)\,\mathrm{e}^{-\frac{1}{4}(\bar{w}_{II}\,\omega_I\,\vartheta)^2}$$
$$\times\left\{-\frac{(1-\nu)^2\,\nu^{\frac{\nu}{1-\nu}}}{\ln\nu}\Big[1+\frac{1}{8}\,(\bar{w}_{II}\omega_I\vartheta)^2+\frac{1}{128}\,(\bar{w}_{II}\omega_I\vartheta)^4\Big]+\frac{\nu^{\frac{1}{1-\nu}}\ln\nu}{256}\,(\bar{w}_{II}\omega_I\vartheta)^4\right\}^2. \quad (3.115)$$

From Eq. (3.44) with $\mathcal{M}_I(\vec{k}) \to \bar{\mathcal{M}}_I(\vec{k})$ the number of signal photons scattered into the central shadow $N^{\bullet}_{p,I}$ then follows upon integration over the full azimuthal angle φ and over the polar angle ϑ from 0 to θ_{in} given in Eq. (3.113). For the counter-propagating laser fields considered here, this results in

$$\left\{\begin{array}{c} N^{\bullet}_{\mathrm{tot},I} \\ N^{\bullet}_{\perp,I}\end{array}\right\} \approx N_I\,\frac{1}{4}\sqrt{\frac{3}{\pi}}\,\frac{\alpha^4}{2025\pi}\Big(\frac{W_{II}}{m}\frac{\omega_I}{m}\Big)^2\frac{1}{(mw_{0,II})^4}\left\{\begin{array}{c}(c_a^2-c_b^2)\cos^2(\Delta\phi)+c_b^2 \\ \frac{1}{4}(c_a-c_b)^2\sin^2(2\Delta\phi)\end{array}\right\}F\Big(\tfrac{4z_{\mathrm{R},II}}{\sqrt{\tau_I^2+\frac{1}{2}\tau_{II}^2}},0,\tfrac{\tau_I}{\tau_{II}}\Big)$$
$$\times\left\{132\Big(1-\nu^{-\frac{2\nu}{1-\nu}}\Big)\frac{(1-\nu)^3}{\ln\nu}\,\nu^{\frac{4\nu}{1-\nu}}-200(1-\nu)^2\,\nu^{\frac{1+3\nu}{1-\nu}}-8\Big[4\Big(1-\nu^{-\frac{2\nu}{1-\nu}}\Big)-17\nu\Big]\nu^{\frac{1+3\nu}{1-\nu}}(1-\nu)\ln\nu\right.$$
$$+16(4-3\nu)\,\nu^{\frac{2(1+\nu)}{1-\nu}}\ln^2\nu+\Big[3\Big(1-\nu^{-\frac{2\nu}{1-\nu}}\Big)-8\nu\,(8-\nu)\Big]\frac{\ln^3\nu}{1-\nu}\,\nu^{\frac{2(1+\nu)}{1-\nu}}$$
$$\left.-(6-32\nu)\frac{\ln^4\nu}{(1-\nu)^2}\,\nu^{\frac{3+\nu}{1-\nu}}+(6-8\nu)\frac{\ln^5\nu}{(1-\nu)^3}\,\nu^{\frac{4}{1-\nu}}-4\frac{\ln^6\nu}{(1-\nu)^4}\,\nu^{\frac{5-\nu}{1-\nu}}+2\frac{\ln^7\nu}{(1-\nu)^5}\,\nu^{\frac{2(3-\nu)}{1-\nu}}\right\}, \quad (3.116)$$

where $N_I \simeq W_I/\omega_I$ and we expressed the electric field amplitudes in terms of the laser pulse energies via Eqs. (3.25) and (3.94). We emphasize that using the particular condition in Eq. (3.111) on the far-field angular decay behavior of the signal photons we could eventually also eliminate any explicit reference of the signal photon numbers in Eq. (3.116) on the effective pump waist $\bar{w}_{II}$. Recall, however, that choosing a specific value of ν is now equivalent to fixing the ratio $\bar{w}_{II}/w_I$, which in turn is related to the ratio $w_{0,II}/w_I$ directly accessible in experiment via Eq. (3.54). One can easily check that the expression in the curly brackets in Eq. (3.116) becomes maximum for $\nu = \mathcal{N}'/\mathcal{N} \simeq 0.19$. For this choice of ν we have $\{\cdot\} \simeq 3.59$, such that

$$\left\{\begin{array}{c} N^{\bullet}_{\mathrm{tot},I} \\ N^{\bullet}_{\perp,I}\end{array}\right\} \approx N_I\,\frac{3.59}{4}\sqrt{\frac{3}{\pi}}\,\frac{\alpha^4}{2025\pi}\Big(\frac{W_{II}}{m}\frac{\omega_I}{m}\Big)^2\frac{1}{(mw_{0,II})^4}\left\{\begin{array}{c}(c_a^2-c_b^2)\cos^2(\Delta\phi)+c_b^2 \\ \frac{1}{4}(c_a-c_b)^2\sin^2(2\Delta\phi)\end{array}\right\}$$
$$\times F\Big(\tfrac{4z_{\mathrm{R},II}}{\sqrt{\tau_I^2+\frac{1}{2}\tau_{II}^2}},0,\tfrac{\tau_I}{\tau_{II}}\Big). \quad (3.117)$$

Using $\nu \simeq 0.19$, which implies that 19% of the energy put in the original beam are to be blocked by the obstacle creating the shadow in the beam [cf. Eq. (3.92)], in Eqs. (3.111) and (3.54) we moreover find

$$\frac{w_I}{\bar{w}_{II}} \simeq 0.51 \quad \leftrightarrow \quad \frac{w_I}{w_{0,II}} \simeq 0.60\,. \quad (3.118)$$

The focus and far-field transverse intensity profiles for a probe beam with precisely this value of the blocking fraction ν are depicted in the middle panel in Fig. 3.3. Also note that the value of $w_I/\bar{w}_{II}$ maximizing the signal in the shadow given in Eq. (3.118) is indeed reasonably close to the naive estimate of $\approx 1/\sqrt{2} \simeq 0.7$ based on Gaussian transverse beam profiles; cf. the paragraph below Eq. (3.111)

elaborating on this.

On the other hand, using the central-peak approximation (3.100) for the probe beam the number of signal photons scattered into the shadow can be readily extracted from the results derived in Sec. 3.2.4.1. To this end, one has to multiply Eq. (3.57) by the rescaling factor identified in the paragraph below Eq. (3.100) and limit the integration over the polar angle to $\vartheta \leq \theta_{\text{in}}$ with θ_{in} defined in Eq. (3.91). Recall, that in the present context $\omega \to \omega_I$ and $w_{\mathcal{N},\mathcal{N}'} \to w_I$. This yields the following approximate result for the signal photon numbers scattered into the central shadow imprinted into the probe beam,

$$\begin{aligned}\left\{ \begin{array}{c} N^{\bullet}_{\text{tot},I} \\ N^{\bullet}_{\perp,I} \end{array} \right\} \approx N_I \, \frac{(1-\nu)^2}{1+\nu} \sqrt{\frac{3}{\pi}} \frac{16\alpha^4}{2025\pi} \left(\frac{W_{II}}{m}\frac{\omega_I}{m}\right)^2 \frac{1}{(m w_{0,II})^4} \left\{ \begin{array}{c} (c_a^2 - c_b^2)\cos^2(\Delta\phi) + c_b^2 \\ \frac{1}{4}(c_a - c_b)^2 \sin^2(2\Delta\phi) \end{array} \right\} \\ \times \, \frac{1-1/\mathrm{e}}{1+2(\frac{w_I}{\bar{w}_{II}})^2} \left(1 - \mathrm{e}^{-4(1-1/\mathrm{e})\frac{\nu}{1+\nu}[1+2(\frac{w_I}{\bar{w}_{II}})^2]^{-1}}\right) \mathrm{e}^{-\frac{4r_0^2}{\bar{w}_{II}^2+2w_I^2}} \, F\!\left(\frac{4z_{\text{R},II}}{\sqrt{\tau_I^2+\frac{1}{2}\tau_{II}^2}}, \frac{2(z_0-t_0)}{\sqrt{\tau_I^2+\frac{1}{2}\tau_{II}^2}}, \frac{\tau_I}{\tau_{II}}\right), \end{aligned} \tag{3.119}$$

which should hold for probe waists fulfilling

$$w_I \gtrsim \bar{w}_{II} \sqrt{-\frac{1-1/\mathrm{e}}{\ln\nu}\,\frac{1-\nu}{1+\nu}}\,. \tag{3.120}$$

This criterion follows readily from Eq. (3.111), the value of which delimits the regime of probe waists for which a fundamental Gaussian approximation should allow for trustworthy insights from below. Notably, Eq. (3.119) even accounts for the possibility of a finite spatio-temporal offset x_0^μ between the foci of the two colliding laser beams and thus allows to estimate its impact on the attainable signal photon numbers. However, as it only accounts for a single central peak in the transverse focus intensity profile of the probe which is supposed to dominate the latter, by construction this approximation is insensitive to the oscillatory behavior of the signal as a function of the transverse impact parameter r_0 induced by the Airy ring structure in its focus, that is to be encountered for transverse offsets $r_0 \gtrsim w_I$. In turn, it is even expected to overestimate the drop of the signal with growing r_0 to a certain degree.

Specializing Eq. (3.119) to a vanishing spatio-temporal offset and choosing $\nu \simeq 0.19$ and $w_I/\bar{w}_{II} \simeq 0.51$ such as in Eq. (3.118), apart from an overall multiplicative factor of ≈ 0.95 we retain the result given in Eq. (3.117) that consistently accounts for all the relevant details of the transverse probe profile (3.99). This clearly confirms that the quantum vacuum signals studied here can be predominantly traced back to probe laser photons that originate in the central peak dominating the transverse field profile of the probe in the interaction region. At the same time, there are distinct differences in the angular decay of the full and the approximate signal photon distributions with ϑ. These can thus be attributed to the subleading peaks giving rise to the Airy rings in the transverse probe field profile. For a graphical representation of the far-field distribution of the signal as well as the background as a function of an appropriately normalized polar angle ϑ at zero impact parameter, see Fig. 3.4. Note, that for the specific parameters adopted here, the divergence of the signal is well-characterized by the Gaussian approximation in Eq. (3.58), which yields $\theta_{\text{signal},I} \simeq 2.44$. This is in line with the above observation that the signal photon numbers inferred from a calculation approximating the actual probe beam featuring an $\text{FG}^{\circledcirc}_{\mathcal{N},\mathcal{N}'}$ far-field profile as a fundamental Gaussian beam are in good agreement with the results of a full calculation for the

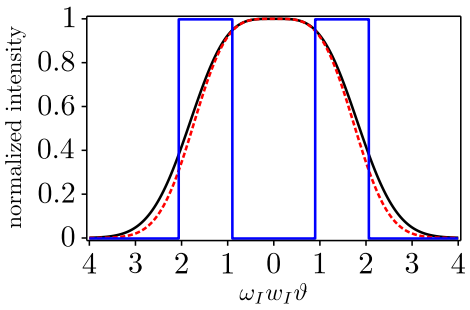

Figure 3.4: Far-field angular decay of signal and background for a blocking fraction of $\nu = 0.19$. The solid blue (discontinuous) curve depicts the background of the probe laser photons; cf. the middle bottom panel in Fig. 3.3. The solid black (continuous) curve shows the exact decay of the signal predicted by Eq. (3.112) and the dashed red one the result of the approximation (3.115). By construction, in the central shadow in the probe beam this approximation is in excellent agreement with the exact result.

parameters considered here. The latter clearly meet the criterion (3.120).

Moreover, a comparison of Eq. (3.117) and Eq. (3.60) unveils that for laser pulse collisions in a counter-propagation geometry at zero impact parameter the numbers of signal photons scattered into the field free shadow for $\nu \simeq 0.19$ is reduced by a factor of $\simeq (3.59/4)/16 \approx 0.056$ in comparison to the analogous signals integrated over all possible emission angles induced in the collision of ordinary fundamental Gaussian beams in the limit of $w_I \to 0$. We recall that the latter signal photon numbers amount to the best result in principle attainable for given parameters of the fundamental Gaussian beams and considering the x-ray waste w_I as free parameter to be adjusted at will. These signals are, however, typically background dominated. On the other hand, in the scenario involving an annular probe beam the background in the shadow in its forward far-field, where the detection is assumed to take place, should be substantially reduced. In the ideal case considered here the shadow is even completely field free. Hence, this essentially means that under ideal conditions a fraction of $\approx 5.6\%$ of the maximum quantum vacuum signal that can be in principle induced with fundamental Gaussian beams should become directly accessible in experiment with the dark field setup put forward here.

In particular for an angle of $\Delta\phi = \pi/4$ between the polarization vectors of the linearly polarized colliding beams Eq. (3.117) can be compactly expressed as

$$\left\{ \begin{array}{c} N^{\bullet}_{\parallel,I} \\ N^{\bullet}_{\perp,I} \end{array} \right\}\Bigg|_{\Delta\phi=\frac{\pi}{4}} \approx N_I \, \frac{3.59}{16} \sqrt{\frac{3}{\pi}} \, \frac{\alpha^4}{2025\pi} \left(\frac{W_{II}}{m}\frac{\omega_I}{m}\right)^2 \frac{1}{(m w_{0,II})^4} \left\{ \begin{array}{c} (c_a+c_b)^2 \\ (c_a-c_b)^2 \end{array} \right\} F\left(\frac{4 z_{\mathrm{R},II}}{\sqrt{\tau_I^2+\frac{1}{2}\tau_{II}^2}}, 0, \frac{\tau_I}{\tau_{II}}\right), \quad (3.121)$$

where the $\parallel$ and $\perp$-polarized components are proportional to $(c_a + c_b)^2$ and $(c_a - c_b)^2$, respectively. An important point is that the shadow in the probe beam should make both polarization components accessible in experiment. It is especially interesting to note that the ratio

$$\frac{N^{\bullet}_{I,\perp}}{N^{\bullet}_{I,\parallel}}\Bigg|_{\Delta\phi=\frac{\pi}{4}} \simeq \left(\frac{c_a - c_b}{c_a + c_b}\right)^2 = \frac{9}{121}\left(1 + \frac{\alpha}{\pi}\frac{260}{99} + \cdots\right) \quad (3.122)$$

does not depend on intensity and thus is insensitive to fluctuations in experimental parameters such as

spatio-temporal jitter or intensity fluctuations. These typically limit the achievable precision in experiments requiring the overlap of pump and probe foci. Also note that it is obvious from the discussion in the paragraph below Eq. (3.45) that the maximum attainable result for the number of signal photons scattered into the shadow is given by $N^{\bullet}_{\mathrm{tot},I}|_{\Delta\phi=\frac{\pi}{2}} = [2c_b/(c_a - c_b)]^2\, N^{\bullet}_{\perp,I}|_{\Delta\phi=\frac{\pi}{4}} \approx 21.8\, N^{\bullet}_{\perp,I}|_{\Delta\phi=\frac{\pi}{4}}$.

Adopting the same parameters as in Sec. 3.2.4.1 for the high-intensity laser pump modelled after the ReLax laser system at HIBEF, i.e., $\lambda_{II} = 800\,\mathrm{nm}$, $W_{II} = 10\,\mathrm{J}$, $\tau_{II}^{\mathrm{FWHM}} = 25\,\mathrm{fs}$, $w_{0,II} = 1\,\mu\mathrm{m}$, and $N_I = 8.26 \times 10^{11}$, $\omega_I = 12914\,\mathrm{eV}$, $\tau_I^{\mathrm{FWHM}} = 129\,\mathrm{fs}$ for the XFEL probe, Eq. (3.121) which implicitly assumes a blocking fraction of $\nu \simeq 19\%$ and a probe waist of $w_I \simeq 0.6 w_{0,II}$, predicts

$$\left.\left\{ \begin{array}{c} N^{\bullet}_{\parallel,I} \\ N^{\bullet}_{\perp,I} \end{array} \right\}\right|_{\Delta\phi=\frac{\pi}{4}} \approx \left\{ \begin{array}{c} 0.689 \\ 0.051 \end{array} \right\} \tag{3.123}$$

signal photons to be scattered into the central shadow in the probe beam. For completeness, we note that with the help of Eq. (3.112) we find at the same time that the integrated numbers of signal photons scattered beyond the outside divergence of the probe beam, i.e., to $\vartheta > \theta_{\mathrm{out}}$, exceed the values quoted in Eq. (3.123) by a factor of $\simeq 1.13$. Figure 3.4 clearly demonstrates that these signals are roughly limited to $\vartheta < 4/(w_I\omega_I)$, which implies that they are scattered into a solid angle interval that is ≈ 15 times larger than the one associated with the central shadow [126]. Correspondingly, in the central shadow $\vartheta < \theta_{\mathrm{in}}$ the number of signal photons per solid angle surpasses the one in the outside area of the probe beam $\theta_{\mathrm{out}} < \vartheta < 4/(w_I\omega_I)$ by a factor of ≈ 13. In any case, in the present context we focus exclusively on the signals scattered into the central shadow because the realization of a very efficient and robust background suppression scheme allowing to measure precisely this signal component is experimentally conceivable. See also the discussion of aspects of the experimental concept sketched in Fig. 3.5 below.

An elementary test setup recently demonstrated a level of $\mathfrak{S} = (3 \pm 1.7) \times 10^{-8}$ of the primary beam intensity in the shadow [131], a value which is expected to be substantially improved by the use of apertures and a properly set up imaging system. Taking into account that the initial XFEL beam features an inherent polarization purity on the $\mathcal{P}_\perp = 10^{-6}$ level [132], for the $\perp$-polarized signal component the background in the shadow can thus be conservatively estimated as $N_{\mathrm{bgr}} = \mathfrak{S}\mathcal{P}_\perp N_I \simeq (3 \times 10^{-8}) \times 10^{-6}\, N_I = 3 \times 10^{-14}\, N_I$. In turn, Eq. (3.70) predicts that for the laser parameters adopted in the present work $n > 238$ optimal laser pulse collisions are needed to confirm the $\perp$-component of the quantum vacuum signal with a significance of 5σ. We note that by combining the annular probe scheme with high-precision polarimetry it should be possible to reduce the required number of shots even further. Analogously, estimating the background for the $\parallel$-component to be given by $N_{\mathrm{bgr}} = \mathfrak{S}N_I \simeq 3 \times 10^{-8} N_I$, we find that $n > 1.30 \times 10^6$ optimal shots would be required for a 5σ signal based on the above estimate for $\mathfrak{S}$. On the other hand, one can easily infer from Eq. (3.70) that in order for the latter component to reach a 5σ significance for the number of shots $n > 238$ just obtained for the $\perp$-component the quoted conservative value of $\mathfrak{S}$ needs to be improved by about four orders of magnitude to $\mathfrak{S} \simeq 5.5 \times 10^{-12}$. Such an improvement should indeed be possible by setting up an appropriate imaging system using lenses and apertures to block the direct optical path of parasitic scattering signals to the detector, but is yet to be set up and confirmed in a dedicated benchmark experiment. Based on the approximate result (3.119)

and employing the values in Eq. (3.118) we moreover find that for the parameters considered here one can expect the signal photon yield to be reduced by a factor of $1/\mathrm{e}^2$ for $r_0 \approx 1.0 w_0$ independent of the considered polarization component.

A comparison with the signal photon numbers determined in Sec. 3.2.4.1 for same laser parameters unveils that the number of $n > 238$ optimal shots required for a 5σ measurement of the $\perp$-component $N^{\bullet}_{\perp,I}$ of the quantum vacuum signal utilizing an annular probe beam determined here is somewhat larger than the threshold value of $n > 89$ found for the optimal discernible signal $N^{\mathrm{dis}}_{\perp,I}$ consisting of $\perp$-polarized signal photons scattered out of the forward cone of a fundamental Gaussian probe laser beam and smaller than the value of $n > 346$ obtained for a measurement of the full $\perp$-signal $N_{\perp,I}$ attainable with a fundamental Gaussian probe in the limit of $w_I \ll w_{0,II}$. In summary, we find that the lower threshold for the numbers of optimal shots n required for a 5σ detection of the different signals $N^{\mathrm{dis}}_{\perp,I}$, $N^{\bullet}_{\perp,I}$ and $N_{\perp,I}$ roughly scale as $1 : 3 : 4$. Note however, that while all the different cases of laser beam collisions discussed in this work employ exactly the same pump laser field, the probe laser energy assumed to be put into the central focus peak of waist w_I in Sec. 3.2.4.1 differs notably from the scenario studied here. Already for a beam featuring a flat-top far-field profile without shadow, i.e., for $\nu = \mathcal{N}' = 0$, the energy put into the central focus peak of radius w_I is reduced by a factor of $(1 - 1/\mathrm{e}) \simeq 0.63$ relatively to that of a fundamental Gaussian featuring a single peak in its beam focus; cf. Eq. (3.95). For the optimal blocking fraction of $\nu \simeq 19\%$ inferred for the laser parameters adopted in the present work, Eq. (3.95) predicts this energy to be reduced even further by an additional factor of $(1 - \nu)^2/(1 + \nu) \simeq 0.55$. Hence, in the specific scenario studied here the energy put into the central focus peak of radius w_I of the annular probe amounts to just ≈ 0.35 of the fundamental Gaussian beam value. In fact, the scaling of the number of shots (3.70) required to measure the discernible signal $N^{\mathrm{dis}}_{p,I}$ in the fundamental Gaussian beam case with a specified significance as $n \sim 1/(N^{\mathrm{dis}}_{p,I}) \sim W_I^{-1}$ [cf. Eqs. (3.65) and (3.66)] implies that a reduction of the probe pulse energy W_I by this value would increase the required number of shots by a factor of ≈ 3. In turn, for a given energy put into the central focus peak of radius w_I a similar number of shots would be required for the detection of the two distinct signals $N^{\mathrm{dis}}_{\perp,I}$ and $N^{\bullet}_{\perp,I}$ with a given significance.

At this point, we furthermore emphasize once again that the explicit predictions for the signal photon numbers $N^{\bullet}_{p,I}$ scattered into the central shadow of the annular beam given here are based on a conservative estimate for the shadow quantity $\Subset$. This value can likely be improved by several orders of magnitude with a properly set up imaging system. This is in sharp contrast to the signals $N_{\perp,I}$ and $N^{\mathrm{dis}}_{\perp,I}$ that depend critically on the polarization purity $\mathcal{P}_\perp$ which is limited by the divergence of the source. As argued in Ref. [133], the current limit that is possible to realize under ideal experimental conditions is a polarization purity of $\mathcal{P}_\perp = 2 \times 10^{-12}$ at XFELs with a divergence of 1 μrad. This limiting value just implies the possibility of an improvement by a factor of 7 relatively to the currently realized polarization purity record of $\mathcal{P}_\perp = 1.4 \times 10^{-11}$ on which the explicit results for the signals $N_{\perp,I}$ and $N^{\mathrm{dis}}_{\perp,I}$ determined in Sec. 3.2.4.1 are based on. Another important point in favor of the annular probe beam concept put forwards here is that it should not be very sensitive to the precise details of the employed probe beam. The key features to be imprinted into the probe beam are a pronounced on-axis peak in its focus and a essentially field-free shadow in its far field profile. Clearly, the details of the outside decay of its transverse intensity profile around $\vartheta \gtrsim \theta_{\mathrm{out}}$ should essentially not affect the signal in the shadow. At the

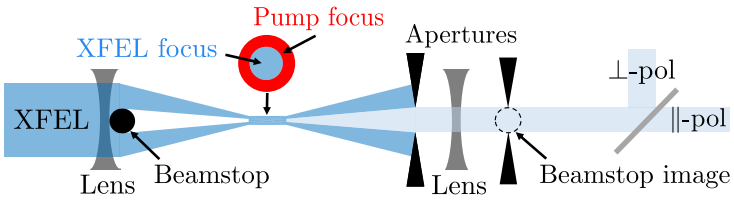

Figure 3.5: Schematic layout of an experiment using an annular probe beam. The XFEL is focused to a spot with a beamstop creating a central shadow in the beam on both sides of the focus while retaining a central intensity peak in the focus. X-ray optics image the beamstop to a matched aperture plane. The interaction with the pump results in signal photons scattered into the central shadow. The $\perp$, $\parallel$-polarized signal components are directed to separate detectors using a crystal polarizer.

same time, also the specifics of the decay of its transverse intensity profile from the annulus containing the majority of the laser photons of the probe in the far field into the central shadow should not be too critical with regard to an experimental implementation. This becomes clear from the experimental arrangement involving several apertures to select the specific far field region to be imaged on the detector envisioned in Fig. 3.5; cf. also Ref. [131]. In fact, one should always come very close to the scenario theoretically modeled with a hard shadow even for cases where the decay of the laser photons into the shadow is smooth and rather slow: if there was a finite decay width over which the background photons leaked into the shadow, one could always choose the area selected by the apertures as smaller until one effectively cut out a region of radial divergence $\theta_{\text{ap}} \lesssim \theta_{\text{in}}$ where the background is sufficiently suppressed. In the worst case this leads to a somewhat increased integration time required to measure the quantum vacuum signal with a given significance. Because the differential signal photon number depicted in Fig. 3.4 remains practically constant throughout the shadow, the signal to be measured per shot is then reduced by a factor of $\approx (\theta_{\text{ap}}/\theta_{\text{in}})^2$. In turn, the number of shots required to reach a specified significance for a given shadow quality $\mathfrak{S}$ increases by $\approx (\theta_{\text{ap}}/\theta_{\text{in}})^{-4}$; cf. Eq. (3.70). We note that this is different for the signal scattered outside θ_{out} in Fig. 3.4 briefly mentioned above: first this signal decays quite rapidly with ϑ, and second it depends critically on the decay of the background for $\vartheta \gtrsim \theta_{\text{out}}$ which is not improved by imaging and filtering techniques in the setup devised in Fig. 3.5.

Finally, it should also be noted that in experiment it may be more convenient to implement a rectangular shadow in the probe beam by blocking a part of the incident far-field of the beam with a wire. While the corresponding calculation is outside the scope of this work, we remark that it can be straightforwardly performed along the same lines as the one for the annular probe beam presented here. The central difference is that to model this scenario appropriately one rather needs to decompose the amplitude profile of the beam to be subtracted from the rotationally symmetric one featuring an FG_N far-field profile in Hermite-Gaussian modes. This then allows to implement a rectangular-shaped flattened-Gaussian far-field profile in the latter and thereby to imprint a rectangular shadow into the far-field profile of the probe beam.

Chapter 4

Conclusions and Outlook

In this work we studied quantum vacuum nonlinearities in strong electromagnetic fields, covering a wide range of subtopics: from the fundamentals of the underlying theory, via controlled approximations and assumptions to the phenomenological implications, namely quantitative predictions of signatures of quantum vacuum signals accessible in experiment with state-of-the-art technology. A key topic on the fundamental side was the emergence of one-particle reducible contributions to the Heisenberg-Euler effective action beyond one loop and their relevance in the limit of strong quasi-constant magnetic- or electric-like fields. With regard to phenomenology, we mainly concentrated on the prospective quantum vacuum signals induced in the collision of a brilliant XFEL probe with a near-infrared high-intensity laser pump, such as will become possible at the recently inaugurated Helmholtz International Beamline for Extreme Fields at the European XFEL.

In Chapter 2, we focused on the fundamentals and provided a detailed account of the present knowledge of the Heisenberg-Euler effective action governing the physics of macroscopic electromagnetic fields in the QED vacuum. After detailing and clarifying its emergence from the underlying microscopic theory of QED, we explicitly rederived the one-loop result in slowly varying quasi-constant electromagnetic fields originally worked out by Heisenberg, Euler and Weisskopf in their seminal papers [2, 3] in a rather pedagogical and easy to understand way. To this end, we resorted to Schwinger's proper time representation [4]. Subsequently, we introduced the photon polarization tensor in the presence of an external electromagnetic field and used the one-loop constant-field result first derived by Batalin and Shabad [34] to determine the leading derivative corrections to the effective action at one loop. This constitutes an alternative and complementary route to the results originally obtained by Gusynin and Shovkovy [58, 61]. One of our new results in this context is an explicit expression for the imaginary part of the corresponding effective Lagrangian in general electromagnetic fields. This allowed us to infer the leading derivative correction to Nikishov's generalization [36] of the renowned Schwinger-formula [4] describing the decay of the quantum vacuum via electron-positron pair production in generic slowly-varying field configurations at zeroth order in a derivative expansion. Thereafter, we discussed higher-loop contributions to the effective action. At two loops we briefly reviewed the result of Ritus for the one-particle irreducible contribution [33, 71] and worked out its strong-field behavior. This expression is confronted with the one-particle reducible contribution of the same loop order, the relevance of which was only recently dis-

covered [12]. Moreover, we explicitly derived the low-energy limit of the photon polarization tensor in slowly-varying fields at two loops. We concluded this chapter with a detailed discussion of contributions of arbitrary loop order. Here, we put special attention on the one-particle reducible sector of the theory and showed that it dominates the one-particle reducible one in the strong field limit. We in particular worked out the all-loop strong field limit of the Heisenberg-Euler effective Lagrangian at zeroth order in a derivative expansion by means of an explicit calculation, i.e., without resorting to the iterative algebraic construction procedure [17] invoked for its first derivation in Ref. [76]. This expression involves contributions scaling at most linearly with $\alpha^{\text{1-loop}}(e\sqrt{2\mathcal{F}})$. As a new result, we then identified the contributions to the effective action giving rise to the leading strong-field behavior at any order in $\alpha^{\text{1-loop}}(e\sqrt{2\mathcal{F}})$. This specifically allowed us to explicitly determined the parameter regime where such an expansion is systematic in the sense that the higher-loop corrections are dominated by the term linear in $\alpha^{\text{1-loop}}(e\sqrt{2\mathcal{F}})$ and higher-order contributions with regard to this parameter become less and less relevant.

On the other hand, in Chapter 3 we switched to the phenomenologically relevant question of how photonic signals of quantum vacuum nonlinearities can be conveniently extracted from the Heisenberg-Euler effective action discussed in detail in the preceding chapter. Here we presented the theoretical foundations and the regime of applicability of the vacuum emission picture [16, 78] which corresponds to our approach of choice for the evaluation of photonic quantum vacuum signals in unprecedented detail. Aiming at providing accurate predictions for such signals that should be accessible with state-of-the-art and near-future technology, in a next step we limited ourselves to the leading vacuum-fluctuation-mediated nonlinear interaction between electromagnetic fields in the perturbative-weak-field and low-frequency limit. To this end, we moreover briefly reviewed a convenient laser beam model based on an approximate solution of the paraxial wave equation allowing for an analytical evaluation of prospective quantum vacuum signals induced in the collision of pulsed laser beams. Resorting to this description, as a simple introductory example we determined the emission characteristics of the dominant signal component induced by a single focused paraxial laser beam in vacuo. In this context, we in particular introduced several convenient approximations allowing to arrive at simple analytical scalings of the signal photon numbers and their emission characteristics with the different parameters characterizing the driving laser field. In the remainder of the chapter, we then switched to the collision of two laser beams and discussed two different scenarios in full detail. Here, also means to enhance the signal-to-background separation in experiment were highlighted. To be specific, the two-beam collision scenarios studied here were: first, the collision of two fundamental Gaussian beams [99, 100], and second the collision of an annular probe beam with a fundamental Gaussian pump [126, 131] in a counter-propagation geometry. In these cases we moreover envisioned the probe to amount to an XFEL and the pump to a near-infrared high-intensity laser beam. This allows for additional simplifying assumptions for the probe beam and thereby facilitates a controlled analytical treatment of these scenarios. In the present work special emphasis was put on the annular probe case, which was discussed in full breadth: starting from a probe beam with flattened-Gaussian transverse profile of finite order $\mathcal{N}$ [129], in particular the limit of $\mathcal{N} \to \infty$ yielding a top-hat-like far-field profile was worked out explicitly for the first time. The annular probe beam constructed by superposing two such beams was then collided with a fundamental Gaussian pump. This allowed for essentially analytical predictions of the quantum vacuum signals scattered into the cen-

tral shadow in the outgoing far field of the annular probe beam. Interestingly, the corresponding results account for all the relevant details of the driving laser beams, but at the same time do not require the additional simplifications invoked in Ref. [131].

The present work provides many impulses for future research activities and directions. With regard to the fundamentals these concern, for instance, the role of finite-temperature corrections to the Heisenberg-Euler effective action in the strong field limit discussed in Chapter 2. In fact, from the detailed discussion in Sec. 2.4.3 it is already obvious that especially for temperatures T well below the electron mass the leading finite-temperature correction $\sim T^4$ to the effective action will follow by dressing the two-loop contribution scaling as $\sim T^4$ derived in [134] with zero-temperature tadpoles [17]. This will effectively generate one-particle reducible contributions to the effective action of arbitrary loop order [76]. Upon extracting the leading strong-field behavior at any given loop order and resumming it along the same lines as in Sec. 2.4.3, one should then be able to extract a closed-form all-loop strong field result reminiscent of Eq. (2.172) for the finite temperature correction $\sim T^4$. Another important aspect for future research on the fundamental side will be insights into the manifestly non-perturbative strong field limit of the theory beyond a perturbative loop expansion. As clear from Chapter 2, so far no manifestly non-perturbative results for the Heisenberg-Euler effective action are available. While it is presently completely unclear how to obtain controlled insights into this parameter regime for ordinary external-field QED, such insights should be possible for a particular deformation of ordinary external-field QED, namely its generalization to N generations of electrons and positrons featuring the same mass and charge and considering an appropriate large N limit [77], characterized by sending $N \to \infty$, while keeping $N\alpha$ as well as $e\bar{A}^\mu$ constant [21]. We are convinced that external-field QED in the large N limit constitutes an interesting deformation of standard external-field QED and strongly believe that its study will also have a large feedback on the latter and be of high relevance for it. In any case, it will facilitate unprecedented comparisons with perturbative results for the effective action and unveil useful information about their convergence properties.

With regard to questions of phenomenological relevance a both natural and important next step will be the extension of the annular probe scheme to account for rectangular-shaped shadows in the transverse beam profile. The latter are likely to be more straightforwardly implemented in experiment, essentially by using wires as beamstop. In addition, it would certainly also be interesting to adopt similar analytical approximation strategies as detailed and put forward in Chapter 3 of this work to prospective scenarios for quantum vacuum experiments envisioning the collision of more than two [84, 117, 135–138] or multicolor [90, 101] laser fields. We are absolutely convinced that controlled analytical approximations are extremely helpful for identifying the most prospective scenario and optimal parameters for quantum vacuum experiments. The outcomes of such studies can then serve as a convenient starting point and valuable input for in-depth numerical studies in experimentally realistic field configurations which self-consistently fulfill the Maxwell equations in vacuo and eventually set the stage for the actual experiment.

Acknowledgements

I would like to express my deepest gratitude to everyone I had the pleasure to collaborate with in the past years. Special thanks go to Holger Gies, Elena A. Mosman, Antonin Sainte-Marie, Rashid Shaisultanov, Chantal Sundqvist, Daniel Ullmann and Matt Zepf for a very enjoyable collaboration on the topics presented in this work. Moreover, I would like to thank all my colleagues at the Helmholtz Institute Jena, the Institute for Theoretical Physics and the Institute of Optics of the Friedrich Schiller University Jena, as well as the members of the DFG Research Unit FOR 2783 "Probing the Quantum Vacuum at the High-Intensity Frontier" for the very nice, stimulating and collegial working environment. I am especially indebted to Holger Gies for bringing me both to Jena and to the interesting research field of strong-field QED. I would also like to thank him as well as Stephan Fritzsche, Barbara Kirchner and Thomas Stöhlker for their continuous support resulting in the unique possibility of a long-term employment at the Helmholtz Institute Jena over the past years. Finally, I am more than grateful to my family for both the wonderful support as well as the very important and valuable distractions provided by them.

Chapter 5

Bibliography

[1] H. B. G. Casimir. On the Attraction Between Two Perfectly Conducting Plates. *Indag. Math.*, 10:261–263, 1948. 2

[2] W. Heisenberg and H. Euler. Consequences of Dirac's theory of positrons. *Z. Phys.*, 98(11-12):714–732, 1936. 2, 3, 6, 8, 20, 21, 24, 40, 109

[3] V. Weisskopf. The electrodynamics of the vacuum based on the quantum theory of the electron. *Kong. Dan. Vid. Sel. Mat. Fys. Med.*, 14N6:1–39, 1936. 3, 20, 21, 109

[4] Julian S. Schwinger. On gauge invariance and vacuum polarization. *Phys. Rev.*, 82:664–679, 1951. 3, 14, 20, 21, 24, 29, 40, 109

[5] H. Euler and B. Kockel. The scattering of light by light in Dirac's theory. *Naturwiss.*, 23(15):246–247, 1935. 3, 65

[6] Robert Karplus and Maurice Neuman. Non-Linear Interactions between Electromagnetic Fields. *Phys. Rev.*, 80:380–385, 1950. 3

[7] Robert Karplus and Maurice Neuman. The scattering of light by light. *Phys. Rev.*, 83:776–784, 1951. 3

[8] John Sampson Toll. *The Dispersion relation for light and its application to problems involving electron pairs*. Phd thesis (unpublished), Princeton University, 1952. 3

[9] V. Costantini, B. De Tollis, and G. Pistoni. Nonlinear effects in quantum electrodynamics. *Nuovo Cim. A*, 2(3):733–787, 1971. 3

[10] B. De Tollis. The scattering of photons by photons. *Nuovo Cim.*, 35(4):1182–1193, 1965. 3

[11] A. Fedotov, A. Ilderton, F. Karbstein, B. King, D. Seipt, H. Taya, and G. Torgrimsson. Advances in QED with intense background fields. *Phys. Rept.*, 1010:1–138, 2023. 4, 11, 40

[12] Holger Gies and Felix Karbstein. An Addendum to the Heisenberg-Euler effective action beyond one loop. *JHEP*, 03, 2016. 6, 12, 13, 20, 27, 28, 42, 49, 110

[13] L.D. Faddeev and V.N. Popov. Feynman diagrams for the yang-mills field. *Physics Letters B*, 25(1):29–30, 1967. 7

[14] John Clive Ward. An Identity in Quantum Electrodynamics. *Phys. Rev.*, 78:182, 1950. 8, 28

[15] Felix Karbstein. Vacuum Birefringence at the Gamma Factory. *Annalen Phys.*, 534(3):2100137, 2022. 10

[16] Felix Karbstein and Rashid Shaisultanov. Stimulated photon emission from the vacuum. *Phys. Rev. D*, 91(11):113002, 2015. 11, 59, 67, 110

[17] Felix Karbstein. Tadpole diagrams in constant electromagnetic fields. *JHEP*, 10:075, 2017. 13, 28, 32, 50, 110, 111

[18] Francesco Pegoraro and Sergei Bulanov. Nonlinear waves in a dispersive vacuum described with a high order derivative electromagnetic Lagrangian. *Phys. Rev. D*, 103(9):096012, 2021. 14

[19] W. Dittrich and H. Gies. *Probing the quantum vacuum. Perturbative effective action approach in quantum electrodynamics and its application*, volume 166. Springer Tracts in Modern Physics, 2000. 14, 29, 30

[20] W. H. Furry. A Symmetry Theorem in the Positron Theory. *Phys. Rev.*, 51:125–129, 1937. 14, 16

[21] Felix Karbstein. Large N external-field quantum electrodynamics. *JHEP*, 01:057, 2022. 19, 51, 58, 111

[22] R. Pausch, M. Thies, and V. L. Dolman. Solving the Gross-Neveu model with relativistic many body methods. *Z. Phys. A*, 338:441–453, 1991. 19

[23] R. L. Stratonovich. A method for the. computation of quantum distribution functions. *Dokl. Akad. Nauk SSSR*, 115:1097–1100, 1957. 19

[24] J. Hubbard. Calculation of partition functions. *Phys. Rev. Lett.*, 3:77–80, 1959. 19

[25] V. Fock. Proper time in classical and quantum mechanics. *Phys. Z. Sowjetunion*, 12:404–425, 1937. 20

[26] Christian Schubert. Perturbative quantum field theory in the string inspired formalism. *Phys. Rept.*, 355:73–234, 2001. 20

[27] N. B. Narozhnyi and A. I. Nikishov. The Simplist processes in the pair creating electric field. *Yad. Fiz.*, 11:1072, 1970. 20

[28] S. G. Mamaev, V. M. Mostepanenko, and Michael I. Eides. The effective action for a non-stationary electromagnetic field. *Sov. J. Nucl. Phys.*, 33(4):569–572, 1981. [Yad. Fiz. **33**, 1075–1082 (1981)]. 20, 33

[29] Daniel Cangemi, Eric D'Hoker, and Gerald V. Dunne. Effective energy for QED in (2+1)-dimensions with semilocalized magnetic fields: A Solvable model. *Phys. Rev. D*, 52:R3163–R3167, 1995. 20

[30] Gerald V. Dunne and Theodore M. Hall. An exact (3+1)-dimensional QED effective action. *Phys. Lett. B*, 419:322–325, 1998. 20

[31] Gerald V. Dunne and Theodore Hall. On the QED effective action in time dependent electric backgrounds. *Phys. Rev. D*, 58:105022, 1998. 20

[32] Sang Pyo Kim, Hyun Kyu Lee, and Yongsung Yoon. Effective Action of QED in Electric Field Backgrounds II. Spatially Localized Fields. *Phys. Rev. D*, 82:025015, 2010. 20

[33] Vladimir I. Ritus. Lagrangian of an intense electromagnetic field and quantum electrodynamics at short distances. *J. Exp. Theor. Phys.*, 42(5):774–782, 1975. [Zh. Eksp. Teor. Fiz. **69**, 1517–1535 (1975)]. 20, 23, 29, 41, 49, 55, 57, 109

[34] I. A. Batalin and A. E. Shabad. Photon green function in a stationary homogeneous field of the most general form. *Sov. Phys. JETP*, 33(3):483–486, 1971. [Zh. Eksp. Teor. Fiz. **60**, 894–900 (1971)]. 20, 29, 109

[35] Ulrich D. Jentschura, Holger Gies, Sree Ram Valluri, Darrell R. Lamm, and Ernst Joachim Weniger. QED effective action revisited. *Can. J. Phys.*, 80:267–284, 2002. 23

[36] A. I. Nikishov. Pair production by a constant external field. *Sov. Phys. JETP*, 30(4):660–662, 1970. [Zh. Eksp. Teor. Fiz. **57**, 1210–1216 (1969)]. 25, 109

[37] I. S. Gradshteyn and I. M. Ryzhik. *Table of Integrals, Series, and Products*. Academic Press, fifth edition, 1994. 25, 26

[38] George B Arfken and Hans J Weber. *Mathematical methods for physicists; 4th ed.* Academic Press, San Diego, CA, fifth edition, 2001. 25

[39] Jeremy S. Heyl and Lars Hernquist. An Analytic form for the effective Lagrangian of QED and its application to pair production and photon splitting. *Phys. Rev. D*, 55:2449–2454, 1997. 25, 26

[40] Felix Karbstein and Rashid Shaisultanov. Photon propagation in slowly varying inhomogeneous electromagnetic fields. *Phys. Rev. D*, 91(8):085027, 2015. 25, 26

[41] Chul Min Kim and Sang Pyo Kim. Vacuum birefringence at one-loop in a supercritical magnetic field superposed with a weak electric field and application to pulsar magnetosphere. *Eur. Phys. J. C*, 83(2):104, 2023. 26

[42] W. Dittrich. One Loop Effective Potentials in QED. *J. Phys. A*, 9:1171, 1976. 26

[43] Gerald V. Dunne. *Heisenberg-Euler effective Lagrangians: Basics and extensions*, pages 445–522. World Scientific, 6 2004. 26, 37, 40, 49

[44] J. S. Dowker. Computation of the derivative of the Hurwitz zeta-function and the higher Kinkelin constants. arXiv : 1506.01819 [math.NT], 6 2015. 26, 37

[45] W. Dittrich and M. Reuter. *Effective Lagrangians in Quantum Electrodynamics*, volume 220. Lect. Notes Phys. (Springer), 1985. 29, 40, 41, 49, 55, 57

[46] G. K. Artimov and Vladimir I. Ritus. Fermion and boson mass shifts in an electric field: relation to quantum electrodynamics at short distances. *J. Exp. Theor. Phys.*, 63(3):476–483, 1986. [Zh. Eksp. Teor. Fiz. **90**, 816–828 (1986)]. 29

[47] E. S. Fradkin, D. M. Gitman, and Sh. M. Shvartsman. *Quantum electrodynamics with unstable vacuum*. Springer Series in Nuclear and Particle Physics, 1991. 29

[48] N. B. Narozhny. Propagation of plane electromagnetic waves in a constant field. *Sov. Phys. JETP*, 28(2):371–374, 1969. [Zh. Eksp. Teor. Fiz. **55**, 714–721 (1968)]. 29

[49] V. N. Baier, V. M. Katkov, and V. M. Strakhovenko. Operator approach to quantum electrodynamics in an external field. Electron loops. *Sov. Phys. JETP*, 41(2):198–204, 1975. [Zh. Eksp. Teor. Fiz. **68**, 405–420 (1975)]. 29

[50] L. F. Urrutia. Vacuum Polarization in Parallel Homogeneous Electric and Magnetic Fields. *Phys. Rev. D*, 17:1977, 1978. 29

[51] W. Dittrich and R. Shaisultanov. Vacuum polarization in QED with worldline methods. *Phys. Rev. D*, 62:045024, 2000. 29

[52] Christian Schubert. Vacuum polarization tensors in constant electromagnetic fields. Part 1. *Nucl. Phys. B*, 585:407–428, 2000. 29

[53] V. N. Baier, A. I. Milshtein, and V. M. Strakhovenko. Interaction Between a Photon and a High Intensity Electromagnetic Wave. *Sov. Phys. JETP*, 42(6):961–965, 1975. [Zh. Eksp. Teor. Fiz. **69**, 1893–1904 (1975)]. 29

[54] W. Becker and H. Mitter. Vacuum polarization in laser fields. *J. Phys. A*, 8(10):1638–1657, 1975. 29

[55] S. Meuren, C. H. Keitel, and A. Di Piazza. Polarization operator for plane-wave background fields. *Phys. Rev. D*, 88(1):013007, 2013. 29

[56] D. M. Wolkow. Uber eine Klasse von Losungen der Diracschen Gleichung. *Z. Phys.*, 94:250–260, 1935. 29

[57] Felix Karbstein. Photon polarization tensor in a homogeneous magnetic or electric field. *Phys. Rev. D*, 88(8):085033, 2013. 31

[58] V. P. Gusynin and I. A. Shovkovy. Derivative expansion of the effective action for QED in (2+1)-dimensions and (3+1)-dimensions. *J. Math. Phys.*, 40:5406–5439, 1999. 33, 109

[59] Felix Karbstein. Derivative corrections to the Heisenberg-Euler effective action. *JHEP*, 09:070, 2021. 33, 36, 40

[60] H. W. Lee, P. Y. Pac, and H. K. Shin. Derivative expansions in quantum electrodynamics. *Phys. Rev. D*, 40:4202–4205, 1989. 33

[61] V. P. Gusynin and I. A. Shovkovy. Derivative expansion for the one loop effective Lagrangian in QED. *Can. J. Phys.*, 74:282–289, 1996. 33, 109

[62] Thomas D. Cohen and David A. McGady. The Schwinger mechanism revisited. *Phys. Rev. D*, 78:036008, 2008. 40

[63] Felix Karbstein and Michael Thies. Integrating out the Dirac sea: Effective field theory approach to exactly solvable four-fermion models. *Phys. Rev. D*, 77:025008, 2008. 41

[64] Felix Karbstein. Integrating out the Dirac sea in the Walecka model. *Phys. Rev. C*, 81:045206, 2010. 41

[65] Gerald V. Dunne and Christian Schubert. Closed form two loop Euler-Heisenberg Lagrangian in a selfdual background. *Phys. Lett. B*, 526:55–60, 2002. 43

[66] Idrish Huet, Michel Rausch de Traubenberg, and Christian Schubert. Asymptotic Behaviour of the QED Perturbation Series. *Adv. High Energy Phys.*, 2017:6214341, 2017. 49

[67] Idrish Huet, Michel Rausch De Traubenberg, and Christian Schubert. Three-loop Euler-Heisenberg Lagrangian in 1+1 QED, part 1: single fermion-loop part. *JHEP*, 03:167, 2019. 49

[68] Curtis G. Callan, Jr. Broken scale invariance in scalar field theory. *Phys. Rev. D*, 2:1541–1547, 1970. 49

[69] K. Symanzik. Small distance behavior in field theory and power counting. *Commun. Math. Phys.*, 18:227–246, 1970. 49

[70] Sidney R. Coleman and Erick J. Weinberg. Radiative Corrections as the Origin of Spontaneous Symmetry Breaking. *Phys. Rev. D*, 7:1888–1910, 1973. 49

[71] Vladimir I. Ritus. Connection between strong-field quantum electrodynamics with short-distance quantum electrodynamics. *J. Exp. Theor. Phys.*, 46(3):423–430, 1977. [Zh. Eksp. Teor. Fiz. **73**, 807–821 (1977)]. 49, 109

[72] Sergei G. Matinyan and G. K. Savvidy. Vacuum Polarization Induced by the Intense Gauge Field. *Nucl. Phys. B*, 134:539–545, 1978. 49

[73] V. I. Ritus. Effective Lagrange function of intense electromagnetic field in QED. In *Workshop on Frontier Tests of Quantum Electrodynamics and Physics of the Vacuum*, pages 11–28, 6 1998. 49, 57

[74] Gerald V. Dunne, Holger Gies, and Christian Schubert. Zero modes, beta functions and IR / UV interplay in higher loop QED. *JHEP*, 11:032, 2002. 49

[75] Gerald V. Dunne and Zachary Harris. Higher-loop Euler-Heisenberg transseries structure. *Phys. Rev. D*, 103(6):065015, 2021. 49, 50

[76] Felix Karbstein. All-Loop Result for the Strong Magnetic Field Limit of the Heisenberg-Euler Effective Lagrangian. *Phys. Rev. Lett.*, 122(21):211602, 2019. 50, 55, 58, 110, 111

[77] Gerard 't Hooft. A Planar Diagram Theory for Strong Interactions. *Nucl. Phys. B*, 72:461, 1974. 58, 111

[78] D. Galtsov and V. Skobelev. Photons creation by an external field. *Physics Letters B*, 36(3):238–240, 1971. 59, 110

[79] Felix Karbstein. Probing vacuum polarization effects with high-intensity lasers. *Particles*, 3(1):39–61, 2020. 62, 67

[80] Holger Gies, Felix Karbstein, and Christian Kohlfürst. All-optical signatures of Strong-Field QED in the vacuum emission picture. *Phys. Rev. D*, 97(3):036022, 2018. 64, 67, 77, 80, 83

[81] M. Babiker and D. L. Andrews. *Quantum Electrodynamics, angular momentum and chirality*, pages 246–264. Cambridge University Press, 2012. 64

[82] O. V. Bogdanov, P. O. Kazinski, and G. Yu. Lazarenko. Probability of radiation of twisted photons by classical currents. *Phys. Rev. A*, 97(3):033837, 2018. 64

[83] J. T. Mendonça. Emission of twisted photons from quantum vacuum. *Eur. Phys. Lett.*, 120(6):61001, 2017. 64

[84] Aboushelbaya, R. and Glize, K. and Savin, A. F. and Mayr, M. and Spiers, B. and Wang, R. and Collier, J. and Marklund, M. and Trines, R. M. G. M. and Bingham, R. and Norreys, P. A. Orbital angular momentum coupling in elastic photon-photon scattering. *Phys. Rev. Lett.*, 123(11):113604, 2019. 64, 111

[85] Cesim K. Dumlu, Yoshihide Nakamiya, and Kazuo A. Tanaka. QED vacuum nonlinearity in Laguerre-Gauss beams. *Phys. Rev. D*, 106(11):116001, 2022. 64

[86] Colin N. Danson, Constantin Haefner, Jake Bromage, Thomas Butcher, Jean-Christophe F. Chanteloup, Enam A. Chowdhury, Almantas Galvanauskas, Leonida A. Gizzi, Joachim Hein, David I. Hillier, and et al. Petawatt and exawatt class lasers worldwide. *High Power Laser Science and Engineering*, 7:e54, 2019. 65

[87] Y. Chen, F. Brinker, W. Decking, M. Scholz, L. Winkelmann, and Z.H. Zhu. Virtual Commissioning of the European XFEL for Advanced User Experiments at Photon Energies Beyond 25 keV Using Low-Emittance Electron Beams. In *Proc. 13th International Particle Accelerator Conference (IPAC'22)*, number 13 in International Particle Accelerator Conference, pages 1018–1021. JACoW Publishing, Geneva, Switzerland, 07 2022. 65

[88] Hans Euler. On the scattering of light by light according to Dirac's theory. *Annalen Phys.*, 26(5):398–448, 1936. 65

[89] Alexander Blinne, Holger Gies, Felix Karbstein, Christian Kohlfürst, and Matt Zepf. All-optical signatures of quantum vacuum nonlinearities in generic laser fields. *Phys. Rev. D*, 99(1):016006, 2019. 67, 71, 75

[90] Antonin Sainte-Marie, Luca Fedeli, Neïl Zaïm, Felix Karbstein, and Henri Vincenti. Quantum vacuum processes in the extremely intense light of relativistic plasma mirror sources. *New J. Phys.*, 24(6):065005, 2022. 67, 75, 111

[91] L. W. Davis. Theory of electromagnetic beams. *Phys. Rev. A*, 19:1177–1179, Mar 1979. 68

[92] J. P. Barton and D. R. Alexander. Fifth-order corrected electromagnetic field components for a fundamental gaussian beam. *Journal of Applied Physics*, 66(7):2800–2802, 1989. 68

[93] Y. I. Salamin. Fields of a gaussian beam beyond the paraxial approximation. *Applied Physics B*, 86(2):319–326, Jan 2007. 68, 70

[94] Anthony E. Siegman. *Lasers*. University Science Books, 1986. 68

[95] Bahaa EA Saleh and Malvin Carl Teich. *Fundamentals of Photonics*. John Wiley & Sons, 1991. 68

[96] Felix Karbstein and Elena A. Mosman. Photon polarization tensor in pulsed Hermite- and Laguerre-Gaussian beams. *Phys. Rev. D*, 96(11):116004, 2017. 70

[97] Felix Karbstein and Elena A. Mosman. Photon polarization tensor in circularly polarized Hermite- and Laguerre-Gaussian beams. *Mod. Phys. Lett. A*, 33(07n08):1850044, 2018. 70

[98] Y. Monden and R. Kodama. Enhancement of laser interaction with vacuum for a large angular aperture. *Phys. Rev. Lett.*, 107:073602, Aug 2011. 71

[99] Felix Karbstein. Vacuum birefringence in the head-on collision of x-ray free-electron laser and optical high-intensity laser pulses. *Phys. Rev. D*, 98(5):056010, 2018. 71, 74, 82, 110

[100] Elena A. Mosman and Felix Karbstein. Vacuum birefringence and diffraction at an x-ray free-electron laser: From analytical estimates to optimal parameters. *Phys. Rev. D*, 104(1):013006, 2021. 71, 82, 86, 110

[101] Felix Karbstein, Alexander Blinne, Holger Gies, and Matt Zepf. Boosting quantum vacuum signatures by coherent harmonic focusing. *Phys. Rev. Lett.*, 123(9):091802, 2019. 71, 111

[102] Felix Karbstein, Chantal Sundqvist, Kai S. Schulze, Ingo Uschmann, Holger Gies, and Gerhard G. Paulus. Vacuum birefringence at x-ray free-electron lasers. *New J. Phys.*, 23(9):095001, 2021. 74, 86

[103] Alexander Blinne, Holger Gies, Felix Karbstein, Christian Kohlfürst, and Matt Zepf. The Vacuum Emission Picture Beyond Paraxial Approximation. *J. Phys. Conf. Ser.*, 1206(1):012017, 2019. 75

[104] A. Wünsche. Transition from the paraxial approximation to exact solutions of the wave equation and application to gaussian beams. *J. Opt. Soc. Am. A*, 9(5):765–774, May 1992. 75

[105] J. McKenna and P. M. Platzman. Nonlinear interaction of light in a vacuum. *Phys. Rev.*, 129:2354–2360, Mar 1963. 76

[106] F. Moulin, Denis Bernard, and F. Amiranoff. Photon-photon elastic scattering in the visible domain. *Z. Phys. C*, 72:607–611, 1996. 76

[107] Daniele Tommasini and Humberto Michinel. Light by light diffraction in vacuum. *Phys. Rev. A*, 82:011803, 2010. 76

[108] B. King and C. H. Keitel. Photon-photon scattering in collisions of laser pulses. *New J. Phys.*, 14:103002, 2012. 76

[109] Felix Karbstein and Chantal Sundqvist. Probing vacuum birefringence using x-ray free electron and optical high-intensity lasers. *Phys. Rev. D*, 94(1):013004, 2016. 77, 79, 99

[110] Felix Karbstein and Elena A. Mosman. X-ray photon scattering at a focused high-intensity laser pulse. *Phys. Rev. D*, 100(3):033002, 2019. 79, 90

[111] E. B. Aleksandrov, A. A. Ansel'm, and A. N. Moskalev. Vacuum birefringence in an intense laser radiation field. *Sov. Phys. JETP*, 62(4):680–684, 1985. [Zh. Eksp. Teor. Fiz. **89**, 1181–1189 (1985)]. 79

[112] Thomas Heinzl, Ben Liesfeld, Kay-Uwe Amthor, Heinrich Schwoerer, Roland Sauerbrey, and Andreas Wipf. On the observation of vacuum birefringence. *Opt. Commun.*, 267:318–321, 2006. 79

[113] Victor Dinu, Tom Heinzl, Anton Ilderton, Mattias Marklund, and Greger Torgrimsson. Vacuum refractive indices and helicity flip in strong-field QED. *Phys. Rev. D*, 89(12):125003, 2014. 79

[114] Victor Dinu, Tom Heinzl, Anton Ilderton, Mattias Marklund, and Greger Torgrimsson. Photon polarization in light-by-light scattering: Finite size effects. *Phys. Rev. D*, 90(4):045025, 2014. 79

[115] Felix Karbstein, Holger Gies, Maria Reuter, and Matt Zepf. Vacuum birefringence in strong inhomogeneous electromagnetic fields. *Phys. Rev. D*, 92(7):071301, 2015. 79

[116] Hans-Peter Schlenvoigt, Tom Heinzl, Ulrich Schramm, Thomas E. Cowan, and Roland Sauerbrey. Detecting vacuum birefringence with x-ray free electron lasers and high-power optical lasers: a feasibility study. *Phys. Scripta*, 91(2):023010, 2016. 79

[117] B. King, H. Hu, and B. Shen. Three-pulse photon-photon scattering. *Phys. Rev. A*, 98(2):023817, 2018. 80, 83, 111

[118] Y. Seino, T. Inada, T. Yamazaki, T. Namba, and S. Asai. New estimation of the curvature effect for the X-ray vacuum diffraction induced by an intense laser field. *PTEP*, 2020(7):073C02, 2020. 80

[119] Felix Karbstein and Ricardo R. Q. P. T. Oude Weernink. X-ray vacuum diffraction at finite spatiotemporal offset. *Phys. Rev. D*, 104(7):076015, 2021. 80

[120] A. Laso Garcia, H. Höppner, A. Pelka, C. Bähtz, E. Brambrink, S. Di Dio Cafiso, J. Dreyer, S. Göde, M. Hassan, T. Kluge, and et al. Relax: the helmholtz international beamline for extreme fields high-intensity short-pulse laser driver for relativistic laserâĂŞmatter interaction and strong-field science using the high energy density instrument at the european x-ray free electron laser facility. *High Power Laser Science and Engineering*, 9:e59, 2021. 86

[121] B. Marx, K. S. Schulze, I. Uschmann, T. Kämpfer, R. Lötzsch, O. Wehrhan, W. Wagner, C. Detlefs, T. Roth, J. Härtwig, E. Förster, T. Stöhlker, and G. G. Paulus. High-precision x-ray polarimetry. *Phys. Rev. Lett.*, 110:254801, Jun 2013. 86

[122] B. Marx-Glowna, B. Grabiger, R. Lötzsch, I. Uschmann, A. T. Schmitt, K.S. Schulze, A. Last, T. Roth, S. Antipov, H.-P. Schlenvoigt, I. Sergueev, O. Leupold, R. Röhlsberger, and G. G. Paulus. Scanning high-sensitive x-ray polarization microscopy. *New Journal of Physics*, 24(5):053051, may 2022. 86

[123] R. R. Lindberg and Yu. V. Shvyd'ko. Time dependence of bragg forward scattering and self-seeding of hard x-ray free-electron lasers. *Phys. Rev. ST Accel. Beams*, 15:050706, May 2012. 86

[124] Yuri Shvyd'ko and Ryan Lindberg. Spatiotemporal response of crystals in x-ray bragg diffraction. *Phys. Rev. ST Accel. Beams*, 15:100702, Oct 2012. 86

[125] E. A. Schneidmiller and M. V. Yurkov. Photon beam properties at the European XFEL. *Technical Report*, 2011. 86

[126] Felix Karbstein and Elena A. Mosman. Enhancing quantum vacuum signatures with tailored laser beams. *Phys. Rev. D*, 101(11):113002, 2020. 89, 90, 92, 93, 106, 110

[127] J. Peatross, J. L. Chaloupka, and D. D. Meyerhofer. High-order harmonic generation with an annular laser beam. *Opt. Lett.*, 19(13):942–944, Jul 1994. 89

[128] M. Zepf, G. D. Tsakiris, G. Pretzler, I. Watts, D. M. Chambers, P. A. Norreys, U. Andiel, A. E. Dangor, K. Eidmann, C. Gahn, A. Machacek, J. S. Wark, and K. Witte. Role of the plasma scale length in the harmonic generation from solid targets. *Phys. Rev. E*, 58:R5253–R5256, Nov 1998. 89

[129] F. Gori. Flattened gaussian beams. *Optics Communications*, 107(5):335–341, 1994. 90, 110

[130] C. Palma and V. Bagini. Propagation of super-gaussian beams. *Optics Communications*, 111(1):6–10, 1994. 90

[131] Felix Karbstein, Daniel Ullmann, Elena A. Mosman, and Matt Zepf. Direct Accessibility of the Fundamental Constants Governing Light-by-Light Scattering. *Phys. Rev. Lett.*, 129(6):061802, 2022. 101, 106, 108, 110, 111

[132] Gianluca Geloni, Vitali Kocharyan, and Evgeni Saldin. Theoretical computation of the polarization characteristics of an X-ray Free-Electron Laser with planar undulator. *Opt. Commun.*, 356:435, 2015. 106

[133] K. S. Schulze. Fundamental limitations of the polarization purity of x rays. *APL Photonics*, 3(12):126106, 2018. 107

[134] Holger Gies. QED effective action at finite temperature: Two loop dominance. *Phys. Rev. D*, 61:085021, 2000. 111

[135] A. A. Varfolomeev. Induced scattering of light by light. *Sov. Phys. JETP*, 23(4):681–688, 1966. [Zh. Eksp. Teor. Fiz. **50**, 1024–1035 (1966)]. 111

[136] F. Moulin and D. Bernard. Four-wave interaction in gas and vacuum. Definition of a third order nonlinear effective susceptibility in vacuum: $\chi^{(3)}_{\text{vacuum}}$. *Opt. Commun.*, 164:137–144, 1999. 111

[137] E. Lundstrom, G. Brodin, J. Lundin, M. Marklund, R. Bingham, J. Collier, J. T. Mendonca, and P. Norreys. Using high-power lasers for detection of elastic photon-photon scattering. *Phys. Rev. Lett.*, 96:083602, 2006. 111

[138] Holger Gies, Felix Karbstein, Christian Kohlfürst, and Nico Seegert. Photon-photon scattering at the high-intensity frontier. *Phys. Rev. D*, 97(7):076002, 2018. 111

[139] The Mathematical Functions Site. Laguerre polynomials: Summation (formula 05.02.23.0003) `http://functions.wolfram.com/05.02.23.0003.01`. Visited on 2023-02-13. 126

Appendix A

Supplementary material

A.1 Elimination of the dual field strength tensor

Starting from the identity ${}^\star\bar{F}^{\mu\alpha}\bar{F}^{\nu}{}_{\alpha} = \mathcal{G}g^{\mu\nu}$ it can be easily shown that $\mathcal{G}^2$ can be expressed in terms of the field strength tensor alone, without resorting to the dual field strength tensor or expressions involving the Levi-Civita symbol, respectively. More specifically, we have

$$\mathcal{G}^2 = \frac{1}{4}({}^\star F_{\mu\alpha}\bar{F}^{\nu\alpha})(\bar{F}_{\nu\beta}{}^\star F^{\mu\beta}) = -\frac{1}{8}(\bar{F}_{\rho\sigma}\bar{F}^{\rho\sigma}\bar{F}_{\beta\nu}\bar{F}^{\beta\nu} - 2\bar{F}_{\rho\sigma}\bar{F}^{\rho\nu}\bar{F}_{\beta\nu}\bar{F}^{\beta\sigma})\,. \tag{A.1}$$

The last identity follows straightforwardly upon plugging in the definition of the dual field strength tensor and making use of the fact that

$$\epsilon^{\mu\alpha\rho\sigma}\epsilon_{\mu\beta\kappa\lambda} = -(\delta^\alpha_\beta\delta^\rho_\kappa\delta^\sigma_\lambda + \delta^\alpha_\kappa\delta^\rho_\lambda\delta^\sigma_\beta + \delta^\alpha_\lambda\delta^\rho_\beta\delta^\sigma_\kappa - \delta^\alpha_\kappa\delta^\rho_\beta\delta^\sigma_\lambda - \delta^\alpha_\beta\delta^\rho_\lambda\delta^\sigma_\kappa - \delta^\alpha_\lambda\delta^\rho_\kappa\delta^\sigma_\beta)\,. \tag{A.2}$$

Along the same lines, we can express the scalar quantity $\partial_\rho\mathcal{G}\partial^\rho\mathcal{G}$ as

$$\begin{aligned}\partial_\rho\mathcal{G}\partial^\rho\mathcal{G} &= \frac{1}{4}\partial_\rho({}^\star\bar{F}_{\mu\alpha}\bar{F}^{\nu\alpha})\,\partial^\rho(\bar{F}_{\nu\beta}{}^\star\bar{F}^{\mu\beta}) \\ &= \bar{F}_{\rho\mu}\bar{F}^{\sigma\mu}\partial_\alpha\bar{F}_{\sigma\nu}\partial^\alpha\bar{F}^{\rho\nu} - \frac{1}{4}\bar{F}_{\mu\nu}\bar{F}^{\mu\nu}\partial_\alpha\bar{F}_{\rho\sigma}\partial^\alpha\bar{F}^{\rho\sigma} - \frac{1}{4}\bar{F}_{\mu\nu}\partial_\alpha\bar{F}^{\mu\nu}\bar{F}_{\rho\sigma}\partial^\alpha\bar{F}^{\rho\sigma}\,.\end{aligned} \tag{A.3}$$

in terms of the field strength tensor and derivatives thereof without any reference to the dual field strength tensor.

A.2 Scalar QED

The microscopic Lagrangian defining scalar quantum electrodynamics (sQED) reads

$$\mathcal{L}_{\text{sQED}} = -(D_\mu[A]\Phi)^*(D^\mu[A]\Phi) - m^2\Phi^*\Phi - \frac{1}{4}F_{\mu\nu}F^{\mu\nu}\,, \tag{A.4}$$

with complex scalar field Φ. Employing the substitution $S_\psi \to S_\Phi$, with

$$\mathrm{e}^{\mathrm{i}S_\Phi[A]} = \int \mathcal{D}\Phi^* \int \mathcal{D}\Phi\, \mathrm{e}^{\,\mathrm{i}\int \Phi^*(D^2[A]-m^2)\Phi} = \det{}^{-1/2}(-D^2[A]+m^2)\,, \tag{A.5}$$

in the partition function (2.3) and in the subsequent considerations, essentially all results derived for spinor QED in the main text can be readily, and with only minor modifications, transferred to sQED also. In the present case, we obviously have $\ln\det(\cdot) = \mathrm{tr}\ln\{\cdot\}$. Equation (A.5) in particular implies that upon subtracting the zero-field contribution, we have

$$S_\Phi[A] = \frac{\mathrm{i}}{2}\mathrm{tr}\ln(-D^2[A]+m^2) - \frac{\mathrm{i}}{2}\mathrm{tr}\ln(-\partial^2+m^2)\,, \tag{A.6}$$

which closely resembles the analogous expression for spinor QED given in Eq. (2.45): apart from an overall minus sign and the additional Dirac trace, the spinor result only features the extra term $\frac{e}{2}F_{\mu\nu}\sigma^{\mu\nu}$ in the argument of the logarithm.

A.3 Low-order derivatives for the field strength

As detailed in the main text, at leading order in a derivative expansion with respect to the strength $\bar{F}^{\mu\nu}$ of the external field the effective Lagrangian $\mathcal{L}_{\mathrm{HE}}$ is a function of the scalar invariants of the electromagnetic field $\mathcal{F}$ and $\mathcal{G}^2$ only. This holds at arbitrary orders ℓ in the loop expansion $\mathcal{L}_{\mathrm{HE}}^{\ell\text{-loop}}$. Correspondingly, it is convenient to express derivatives for the field strength tensor $\bar{F}^{\mu\nu}$ in terms of derivatives for $\mathcal{F}$ and $\mathcal{G}$. The explicit expressions for these transformations for $\mathcal{L} = \mathcal{L}(\mathcal{F},\mathcal{G})$ up to cubic order in the derivative for $\bar{F}^{\mu\nu}$ are

$$\frac{\partial\mathcal{L}}{\partial\bar{F}^{\mu\nu}} = \frac{1}{2}\Big(\bar{F}_{\mu\nu}\frac{\partial\mathcal{L}}{\partial\mathcal{F}} + {}^\star\bar{F}_{\mu\nu}\frac{\partial\mathcal{L}}{\partial\mathcal{G}}\Big), \tag{A.7}$$

$$\begin{aligned}\frac{\partial^2\mathcal{L}}{\partial\bar{F}^{\alpha\beta}\partial\bar{F}^{\mu\nu}} = \frac{1}{4}\Big[&(g_{\alpha\mu}g_{\beta\nu}-g_{\alpha\nu}g_{\beta\mu})\frac{\partial\mathcal{L}}{\partial\mathcal{F}} + \epsilon_{\mu\nu\alpha\beta}\frac{\partial\mathcal{L}}{\partial\mathcal{G}} + \bar{F}_{\alpha\beta}\bar{F}_{\mu\nu}\frac{\partial^2\mathcal{L}}{\partial\mathcal{F}^2} + {}^\star\bar{F}_{\alpha\beta}{}^\star\bar{F}_{\mu\nu}\frac{\partial^2\mathcal{L}}{\partial\mathcal{G}^2}\\ &+ ({}^\star\bar{F}_{\alpha\beta}\bar{F}_{\mu\nu} + \bar{F}_{\alpha\beta}{}^\star\bar{F}_{\mu\nu})\frac{\partial^2\mathcal{L}}{\partial\mathcal{F}\,\partial\mathcal{G}}\Big],\end{aligned} \tag{A.8}$$

and

$$\begin{aligned}\frac{\partial^3\mathcal{L}}{\partial\bar{F}^{\rho\sigma}\partial\bar{F}^{\alpha\beta}\partial\bar{F}^{\mu\nu}} = \frac{1}{8}\Big\{&\bar{F}_{\rho\sigma}\bar{F}_{\alpha\beta}\bar{F}_{\mu\nu}\frac{\partial^3\mathcal{L}}{\partial\mathcal{F}^3} + {}^\star\bar{F}_{\rho\sigma}{}^\star\bar{F}_{\alpha\beta}{}^\star\bar{F}_{\mu\nu}\frac{\partial^3\mathcal{L}}{\partial\mathcal{G}^3}\\ &+ (\bar{F}_{\rho\sigma}{}^\star\bar{F}_{\alpha\beta}\bar{F}_{\mu\nu} + \bar{F}_{\rho\sigma}\bar{F}_{\alpha\beta}{}^\star\bar{F}_{\mu\nu} + {}^\star\bar{F}_{\rho\sigma}\bar{F}_{\alpha\beta}\bar{F}_{\mu\nu})\frac{\partial^3\mathcal{L}}{\partial\mathcal{F}^2\partial\mathcal{G}}\\ &+ ({}^\star\bar{F}_{\rho\sigma}{}^\star\bar{F}_{\alpha\beta}\bar{F}_{\mu\nu} + {}^\star\bar{F}_{\rho\sigma}\bar{F}_{\alpha\beta}{}^\star\bar{F}_{\mu\nu} + \bar{F}_{\rho\sigma}{}^\star\bar{F}_{\alpha\beta}{}^\star\bar{F}_{\mu\nu})\frac{\partial^3\mathcal{L}}{\partial\mathcal{F}\,\partial\mathcal{G}^2}\\ &+ \Big[(g_{\alpha\mu}g_{\beta\nu}-g_{\alpha\nu}g_{\beta\mu})\bar{F}_{\rho\sigma} + (g_{\rho\mu}g_{\sigma\nu}-g_{\rho\nu}g_{\sigma\mu})\bar{F}_{\alpha\beta} + (g_{\rho\alpha}g_{\sigma\beta}-g_{\rho\beta}g_{\sigma\alpha})\bar{F}_{\mu\nu}\Big]\frac{\partial^2\mathcal{L}}{\partial\mathcal{F}^2}\end{aligned}$$

$$+ (\epsilon_{\mu\nu\alpha\beta}\,{}^\star\bar{F}_{\rho\sigma} + \epsilon_{\mu\nu\rho\sigma}\,{}^\star\bar{F}_{\alpha\beta} + \epsilon_{\alpha\beta\rho\sigma}\,{}^\star\bar{F}_{\mu\nu})\frac{\partial^2\mathcal{L}}{\partial\mathcal{G}^2}$$
$$+ \Big[(\epsilon_{\mu\nu\alpha\beta}\bar{F}_{\rho\sigma} + \epsilon_{\mu\nu\rho\sigma}\bar{F}_{\alpha\beta} + \epsilon_{\alpha\beta\rho\sigma}\bar{F}_{\mu\nu}) + (g_{\alpha\mu}g_{\beta\nu} - g_{\alpha\nu}g_{\beta\mu})\,{}^\star\bar{F}_{\rho\sigma}$$
$$+ (g_{\rho\mu}g_{\sigma\nu} - g_{\rho\nu}g_{\sigma\mu})\,{}^\star\bar{F}_{\alpha\beta} + (g_{\rho\alpha}g_{\sigma\beta} - g_{\rho\beta}g_{\sigma\alpha})\,{}^\star\bar{F}_{\mu\nu}\Big]\frac{\partial^2\mathcal{L}}{\partial\mathcal{F}\,\partial\mathcal{G}}\Bigg\}. \quad \text{(A.9)}$$

In all these expressions we have explicitly ensured that the antisymmetry under the exchange of the Lorentz indices of a given field strength tensor is preserved.

Moreover, we give the result for the contraction of two second-order derivatives of the effective Lagrangian for $\bar{F}^{\mu\nu}$, which is relevant for the extraction of the low-energy limit of the photon polarization tensor at two loops,

$$\frac{\partial^2\mathcal{L}}{\partial\bar{F}^{\alpha\beta}\partial\bar{F}_{\rho\sigma}}\frac{\partial^2\mathcal{L}}{\partial\bar{F}^{\rho\sigma}\partial\bar{F}^{\mu\nu}} = \frac{1}{4}\Bigg\{(g_{\alpha\mu}g_{\beta\nu} - g_{\alpha\nu}g_{\beta\mu})\,\frac{1}{2}\Bigg[\Big(\frac{\partial\mathcal{L}}{\partial\mathcal{F}}\Big)^2 - \Big(\frac{\partial\mathcal{L}}{\partial\mathcal{G}}\Big)^2\Bigg] + \epsilon_{\mu\nu\alpha\beta}\,\frac{\partial\mathcal{L}}{\partial\mathcal{F}}\frac{\partial\mathcal{L}}{\partial\mathcal{G}}$$
$$+ \bar{F}_{\alpha\beta}\bar{F}_{\mu\nu}\left[\frac{\partial\mathcal{L}}{\partial\mathcal{F}}\frac{\partial^2\mathcal{L}}{\partial\mathcal{F}^2} + \mathcal{F}\Bigg[\Big(\frac{\partial^2\mathcal{L}}{\partial\mathcal{F}^2}\Big)^2 - \Big(\frac{\partial^2\mathcal{L}}{\partial\mathcal{F}\,\partial\mathcal{G}}\Big)^2\Bigg] - \Big(\frac{\partial\mathcal{L}}{\partial\mathcal{G}} - 2\mathcal{G}\frac{\partial^2\mathcal{L}}{\partial\mathcal{F}^2}\Big)\frac{\partial^2\mathcal{L}}{\partial\mathcal{F}\,\partial\mathcal{G}}\right]$$
$$+ {}^\star\bar{F}_{\alpha\beta}\,{}^\star\bar{F}_{\mu\nu}\left[\frac{\partial\mathcal{L}}{\partial\mathcal{F}}\frac{\partial^2\mathcal{L}}{\partial\mathcal{G}^2} - \mathcal{F}\Bigg[\Big(\frac{\partial^2\mathcal{L}}{\partial\mathcal{G}^2}\Big)^2 - \Big(\frac{\partial^2\mathcal{L}}{\partial\mathcal{F}\,\partial\mathcal{G}}\Big)^2\Bigg] + \Big(\frac{\partial\mathcal{L}}{\partial\mathcal{G}} + 2\mathcal{G}\frac{\partial^2\mathcal{L}}{\partial\mathcal{G}^2}\Big)\frac{\partial^2\mathcal{L}}{\partial\mathcal{F}\,\partial\mathcal{G}}\right]$$
$$+ ({}^\star\bar{F}_{\alpha\beta}\bar{F}_{\mu\nu} + \bar{F}_{\alpha\beta}\,{}^\star\bar{F}_{\mu\nu})\,\frac{1}{2}\Bigg[\Big(\frac{\partial^2\mathcal{L}}{\partial\mathcal{F}^2} - \frac{\partial^2\mathcal{L}}{\partial\mathcal{G}^2}\Big)\Big(\frac{\partial\mathcal{L}}{\partial\mathcal{G}} + 2\mathcal{F}\frac{\partial^2\mathcal{L}}{\partial\mathcal{F}\,\partial\mathcal{G}}\Big)$$
$$+ 2\mathcal{G}\Bigg[\frac{\partial^2\mathcal{L}}{\partial\mathcal{F}^2}\frac{\partial^2\mathcal{L}}{\partial\mathcal{G}^2} + \Big(\frac{\partial^2\mathcal{L}}{\partial\mathcal{F}\,\partial\mathcal{G}}\Big)^2\Bigg] + 2\frac{\partial\mathcal{L}}{\partial\mathcal{F}}\frac{\partial^2\mathcal{L}}{\partial\mathcal{F}\,\partial\mathcal{G}}\Bigg]\Bigg\}. \quad \text{(A.10)}$$

We note that this expression is spanned by the same tensor structures as Eq. (A.8).

A.4 Gamma function representation of the Heaviside function

Here, we show that the following identity (3.89) holds

$$\lim_{\mathcal{N}\to\infty}\frac{\Gamma(\mathcal{N}+1,\mathcal{N}\chi^2)}{\Gamma(\mathcal{N}+1)} = \Theta(1-\chi) \quad \text{for} \quad \chi \geq 0\,. \quad \text{(A.11)}$$

To this end, we first note that Eq. (3.73) implies

$$\frac{\Gamma(\mathcal{N}+1,\mathcal{N}\chi^2)}{\Gamma(\mathcal{N}+1)} = \mathrm{e}^{-\mathcal{N}\chi^2}\sum_{n=0}^{\mathcal{N}}\frac{1}{n!}(\mathcal{N}\chi^2)^n\,. \quad \text{(A.12)}$$

This is the representation used for the subsequent analysis. For $\chi \geq 0$ Eq. (A.12) clearly is non-negative and reaches its maximum of one for $\chi = 0$, such that

$$0 \leq \frac{\Gamma(\mathcal{N}+1,\mathcal{N}\chi^2)}{\Gamma(\mathcal{N}+1)} \leq 1\,. \quad \text{(A.13)}$$

With Eq. (A.13) it is easy to show that

$$\frac{\partial}{\partial\chi^2}\frac{\Gamma(\mathcal{N}+1,\mathcal{N}\chi^2)}{\Gamma(\mathcal{N}+1)} = -\frac{\mathcal{N}(\mathcal{N}\chi^2\,\mathrm{e}^{-\chi^2})^{\mathcal{N}}}{\Gamma(\mathcal{N}+1)}\,, \tag{A.14}$$

which, employing Stirling's formula $\mathcal{N}! = \sqrt{2\pi\mathcal{N}}\,(\frac{\mathcal{N}}{\mathrm{e}})^{\mathcal{N}}(1+O(\frac{1}{\mathcal{N}}))$, becomes

$$= -\frac{\sqrt{\mathcal{N}}(\chi^2\,\mathrm{e}^{1-\chi^2})^{\mathcal{N}}}{\sqrt{2\pi}}\left(1+O(\tfrac{1}{\mathcal{N}})\right). \tag{A.15}$$

Taking into account that $\chi^2\,\mathrm{e}^{1-\chi^2} < 1$ for all $\chi \geq 0$ apart from $\chi = 1$, we can hence infer that

$$\lim_{\mathcal{N}\to\infty}\frac{\partial}{\partial\chi^2}\frac{\Gamma(\mathcal{N}+1,\mathcal{N}\chi^2)}{\Gamma(\mathcal{N}+1)} = 0 \quad \text{for} \quad \chi\in\mathbb{R}_0^+\setminus\{1\}\,. \tag{A.16}$$

Due to the fact that Eq. (A.12) equals one for $\chi = 0$, Eq. (A.16) immediately implies that

$$\lim_{\mathcal{N}\to\infty}\frac{\Gamma(\mathcal{N}+1,\mathcal{N}\chi^2)}{\Gamma(\mathcal{N}+1)} = 1 \quad \text{for} \quad 0\leq\chi<1\,. \tag{A.17}$$

On the other hand for $\chi > 1$, we can use $\chi^n \leq \chi^{\mathcal{N}}$ for $0 \leq n \leq \mathcal{N}$ to obtain

$$\frac{\Gamma(\mathcal{N}+1,\mathcal{N}\chi^2)}{\Gamma(\mathcal{N}+1)} \leq \mathrm{e}^{-\mathcal{N}\chi^2}\sum_{n=0}^{\mathcal{N}}\frac{1}{n!}\mathcal{N}^n\chi^{2\mathcal{N}} = \left(\chi^2\,\mathrm{e}^{1-\chi^2}\right)^{\mathcal{N}}. \tag{A.18}$$

With $\chi^2\,\mathrm{e}^{1-\chi^2} < 1$ for $\chi > 1$, we thus have

$$\lim_{\mathcal{N}\to\infty}\frac{\Gamma(\mathcal{N}+1,\mathcal{N}\chi^2)}{\Gamma(\mathcal{N}+1)} \leq 0\,, \tag{A.19}$$

and together with Eq. (A.13),

$$\lim_{\mathcal{N}\to\infty}\frac{\Gamma(\mathcal{N}+1,\mathcal{N}\chi^2)}{\Gamma(\mathcal{N}+1)} = 0 \quad \text{for} \quad \chi>1\,. \tag{A.20}$$

Combining Eqs. (A.17) and (A.20) we arrive at Eq. (A.11) and the desired identity is shown to hold.

A.5 Laguerre derivative identity

Here, we show that the following identity holds true,

$$L_p(-2\partial_\chi)\,\frac{1}{2+\chi r^2}\,\mathrm{e}^{-\frac{a}{2+\chi r^2}}\bigg|_{\chi=1} = \mathrm{e}^{-\frac{a}{2+r^2}}\,\frac{(2-r^2)^p}{(2+r^2)^{p+1}}\,L_p\Big(\tfrac{-2ar^2}{4-r^4}\Big)\,. \tag{A.21}$$

To this end, we first write

$$\frac{1}{2+\chi r^2}\,\mathrm{e}^{-\frac{a}{2+\chi r^2}} = \mathrm{e}^{-\frac{a}{2+r^2}} \sum_{j=0}^{\infty} \frac{1}{j!} \frac{(ar^2)^j}{(2+r^2)^j} \frac{(\chi-1)^j}{(2+\chi r^2)^{j+1}}\,, \tag{A.22}$$

which allows us to infer that

$$(-2\partial_\chi)^k \frac{1}{2+\chi r^2}\,\mathrm{e}^{-\frac{a}{2+\chi r^2}}\bigg|_{\chi=1} = \mathrm{e}^{-\frac{a}{2+r^2}} \sum_{j=0}^{\infty} \frac{1}{j!} \frac{(ar^2)^j}{(2+r^2)^j} (-2\partial_c)^k \frac{c^j}{(2+r^2+cr^2)^{j+1}}\bigg|_{c=0}\,. \tag{A.23}$$

Using the general Leibniz rule, we obtain

$$\partial_c^k \frac{c^j}{(2+r^2+cr^2)^{j+1}} = \sum_{l=0}^{k} \binom{k}{l} \partial_c^l c^j\, \partial_c^{k-l} \frac{1}{(2+r^2+cr^2)^{j+1}}\,, \tag{A.24}$$

which immediately implies

$$\begin{aligned} \partial_c^k \frac{c^j}{(2+r^2+cr^2)^{j+1}}\bigg|_{c=0} &= \sum_{l=0}^{k} \binom{k}{l} j!\,\delta_{l,j}\, \partial_c^{k-l} \frac{1}{(2+r^2+cr^2)^{j+1}}\bigg|_{c=0} \\ &= \sum_{l=0}^{k} \binom{k}{j} k!\,\delta_{l,j}\, \frac{(-r^2)^{k-j}}{(2+r^2)^{1+k}}\,, \end{aligned} \tag{A.25}$$

with Kronecker delta $\delta_{l,j}$. Upon insertion of Eq. (A.25) into Eq. (A.23) we arrive at

$$\begin{aligned} (-2\partial_\chi)^k \frac{1}{2+\chi r^2}\,\mathrm{e}^{-\frac{a}{2+\chi r^2}}\bigg|_{\chi=1} &= \mathrm{e}^{-\frac{a}{2+r^2}}\, k!\, \frac{(2r^2)^k}{(2+r^2)^{k+1}} \sum_{j=0}^{k} \binom{k}{j} \frac{(-1)^j}{j!} \left(\frac{a}{2+r^2}\right)^j \\ &= \mathrm{e}^{-\frac{a}{2+r^2}}\, k!\, \frac{(2r^2)^k}{(2+r^2)^{k+1}}\, L_k\!\left(\tfrac{a}{2+r^2}\right), \end{aligned} \tag{A.26}$$

where we employed the series representation of the Laguerre polynomials following from Eq. (3.21) upon setting $l = 0$,

$$L_p(x) = \sum_{j=0}^{p} \binom{p}{j} \frac{(-1)^j}{j!}\, x^j\,, \tag{A.27}$$

to perform the sum over j in the last step. Resorting to Eq. (A.27), from Eq. (A.26) we can then deduce that

$$L_p(-2\partial_\chi)\, \frac{1}{2+\chi r^2}\,\mathrm{e}^{-\frac{a}{2+\chi r^2}}\bigg|_{\chi=1} = \mathrm{e}^{-\frac{a}{2+r^2}} \sum_{k=0}^{p} \binom{p}{k} \frac{(-2r^2)^k}{(2+r^2)^{k+1}}\, L_k\!\left(\tfrac{a}{2+r^2}\right). \tag{A.28}$$

Finally, the sum in Eq. (A.28) can be performed explicitly with the help of the following identity [139]

$$\sum_{k=0}^{p} \binom{p}{k} \left(\frac{x}{1-x}\right)^k L_k(y) = \frac{1}{(1-x)^p}\, L_p(xy)\,, \tag{A.29}$$

which results in Eq. (A.21).

A.6 Expansion of large-order FG profiles in Laguerre basis

In this section, we show that the expansion coefficient of a flattened Gaussian (FG) profile of order $\mathcal{N}$ in a Laguerre basis given in Eq. (3.74),

$$c_{p,\mathcal{N}} = \sum_{j=p}^{\mathcal{N}} \frac{1}{2^j} \binom{j}{p}, \tag{A.30}$$

simplify significantly in the limit of large orders $\mathcal{N} \gg 1$. Note that Eq. (A.30) obviously implies that for generic $\mathcal{N}$ we have

$$c_{0,\mathcal{N}} = 2 \quad \text{and} \quad c_{\mathcal{N},\mathcal{N}} = 0\,. \tag{A.31}$$

Making use of the fact that the binomial coefficients fulfill

$$\binom{n}{k} + \binom{n}{k+1} = \binom{n+1}{k+1}, \tag{A.32}$$

and the obvious identity

$$c_{p,\mathcal{N}+1} = c_{p,\mathcal{N}} + \frac{1}{2^{\mathcal{N}+1}} \binom{\mathcal{N}+1}{p}, \tag{A.33}$$

which is a direct consequence of the definition of the coefficients in Eq. (A.30), one can readily show that the following recursion relation holds

$$c_{p+1,\mathcal{N}} = c_{p,\mathcal{N}} - \frac{1}{2^{\mathcal{N}}} \binom{\mathcal{N}+1}{p+1}. \tag{A.34}$$

From Eq. (A.34) we can infer that the (forward) finite difference

$$\Delta[c_{p,\mathcal{N}}](p) := c_{p+1,\mathcal{N}} - c_{p,\mathcal{N}}\,, \tag{A.35}$$

which measures the variation of the $c_{p,\mathcal{N}}$ with respect to a change in the integer value p, can be expressed compactly as

$$\Delta[c_{p,\mathcal{N}}](p) = -\frac{1}{2^{\mathcal{N}}} \binom{\mathcal{N}+1}{p+1}. \tag{A.36}$$

The second-order (forward) finite difference can then be analogously defined as

$$\Delta^2[c_{p,\mathcal{N}}](p) := \Delta[c_{p,\mathcal{N}}](p+1) - \Delta[c_{p,\mathcal{N}}](p)\,, \tag{A.37}$$

yielding

$$\Delta^2[c_{p,\mathcal{N}}](p) = -\frac{1}{2^{\mathcal{N}}} \frac{\mathcal{N}+1}{p+1} \binom{\mathcal{N}}{p} \left(\frac{\mathcal{N}-p}{p+2} - 1 \right). \tag{A.38}$$

For completeness, we remark that more advanced finite difference methods are not needed here because in the limit of $\mathcal{N} \gg 1$ on which we subsequently focus on, the refinements coming with such techniques are essentially rendered irrelevant. Together with Eq. (A.31), Eq. (A.36) implicates that the value of the $c_{p,\mathcal{N}}$ monotonically decreases with growing p from $c_{0,\mathcal{N}} = 2$ to $c_{\mathcal{N},\mathcal{N}} = 0$. On the other hand, Eq. (A.38)

implies the existence of a turning point. Clearly, for $\mathcal{N} \gg 1$ the latter is located at $p \simeq \mathcal{N}/2$. In a next step, we study the behavior of Eq. (A.36) in the vicinity of this value. To this end, we introduce a finite parameter $|\delta| < 1$, identify $p = (1+\delta)\mathcal{N}/2$, and study the behavior of

$$\Delta[c_{p,\mathcal{N}}](p)\big|_{p=\frac{\mathcal{N}}{2}(1+\delta)} = -\frac{1}{2^{\mathcal{N}}}\begin{pmatrix}\mathcal{N}+1\\ \frac{\mathcal{N}}{2}(1+\delta)+1\end{pmatrix} \tag{A.39}$$

for $\mathcal{N} \gtrsim (1+\delta)\mathcal{N}/2 \gg 1$, where Eq. (A.39) can be recast as

$$= -\frac{1}{2^{\mathcal{N}}}\frac{2}{1+\delta}\frac{\mathcal{N}!}{(\frac{\mathcal{N}}{2}(1+\delta))!(\frac{\mathcal{N}}{2}(1-\delta))!}\left(1+O(\tfrac{1}{\mathcal{N}})\right). \tag{A.40}$$

With Stirling's formula $(\mathcal{N}a)! = \sqrt{2\pi\mathcal{N}a}\,(\frac{\mathcal{N}a}{\mathrm{e}})^{\mathcal{N}a}(1+O(\frac{1}{\mathcal{N}}))$ for $\mathcal{N} \gg 1$ and finite a, we then obtain

$$\Delta[c_{p,\mathcal{N}}](p)\big|_{p=\frac{\mathcal{N}}{2}(1+\delta)} = -\frac{1}{\sqrt{2\pi\mathcal{N}(1-\delta^2)}}\frac{4}{1+\delta}\left[\left(\frac{1}{1+\delta}\right)^{1+\delta}\left(\frac{1}{1-\delta}\right)^{1-\delta}\right]^{\frac{\mathcal{N}}{2}}\left(1+O(\tfrac{1}{\mathcal{N}})\right), \tag{A.41}$$

which for $\delta = 0$ reduces to

$$\Delta[c_{p,\mathcal{N}}](p)\big|_{p=\frac{\mathcal{N}}{2}} = -\frac{4}{\sqrt{2\pi\mathcal{N}}}\left(1+O(\tfrac{1}{\mathcal{N}})\right). \tag{A.42}$$

As the expression in the square brackets in Eq. (A.41) vanishes for finite values of $|\delta| < 1$ and $\mathcal{N} \to \infty$, we have thus established that in the limit of $\mathcal{N} \gg 1$ we have

$$\sqrt{N}\,\Delta[c_{p,\mathcal{N}}](p) = -2\sqrt{\frac{2}{\pi}}\,\delta_{p,\mathcal{N}/2}\,. \tag{A.43}$$

Correspondingly, Eqs. (A.31), (A.36) and (A.43) allow us to infer that

$$c_{p,\mathcal{N}} \simeq 2\,\Theta(\mathcal{N}/2-p) \quad \text{for} \quad \mathcal{N} \gg 1\,. \tag{A.44}$$

For (3.79) this implies

$$c_{p,\mathcal{N},\mathcal{N}'} = 2[\Theta(\mathcal{N}/2-p) - \Theta(\mathcal{N}'/2-p)] \quad \text{for} \quad \mathcal{N} \gtrsim \mathcal{N}' \gg 1 \tag{A.45}$$

Finally, we note that with Eq. (A.44) we immediately obtain

$$\sum_{p=0}^{\mathcal{N}} c_{p,\mathcal{N}} = \mathcal{N}\,, \quad C_{\mathcal{N}}^2 = \sum_{p=0}^{\mathcal{N}} c_{p,\mathcal{N}}^2 = 2\mathcal{N}\,, \quad \sum_{p=0}^{\mathcal{N}} p\,c_{p,\mathcal{N}} = \frac{1}{4}\mathcal{N}^2\left(1+O(\tfrac{1}{\mathcal{N}})\right), \tag{A.46}$$

as well as for sums involving general powers of p,

$$\sum_{p=0}^{\mathcal{N}} p^n\,c_{p,\mathcal{N}} = \frac{1}{2^n}\frac{1}{n+1}\,\mathcal{N}^{n+1}\left(1+O(\tfrac{1}{\mathcal{N}})\right). \tag{A.47}$$

The results given in Eq. (A.46) are in line with the analogous expressions derived in Eq. (3.84) on

the basis of the finite-sum representation (A.30) and the result for $C_{\mathcal{N}}^2$ determined below Eq. (3.89). Moreover, with Eq. (A.45) it is straightforward to show that

$$\sum_{p=0}^{\mathcal{N}} p^n \, c_{p,\mathcal{N},\mathcal{N}'} = \frac{1}{2^n} \frac{1}{n+1} \left(\mathcal{N}^{n+1} - \mathcal{N}'^{n+1}\right) \left(1 + O(\tfrac{1}{\mathcal{N}})\right) \tag{A.48}$$

for $\mathcal{N} \gtrsim \mathcal{N}' \gg 1$ and thus $O(1/\mathcal{N}') = O(1/\mathcal{N})$. Also note that with Eqs. (A.44) and (A.45) one readily obtains

$$\sum_{p=0}^{\mathcal{N}} \mathrm{e}^{-\frac{p}{\mathcal{N}}x^2} c_{p,\mathcal{N}} = \frac{1}{x^2} \mathcal{N} \left(1 - \mathrm{e}^{-\frac{1}{2}x^2}\right) \left(1 + O(\tfrac{1}{\mathcal{N}})\right), \tag{A.49}$$

and

$$\sum_{p=0}^{\mathcal{N}} \mathrm{e}^{-\frac{p}{\mathcal{N}}x^2} c_{p,\mathcal{N},\mathcal{N}'} = \sum_{p=\mathcal{N}'/2}^{\mathcal{N}/2} \mathrm{e}^{-\frac{p}{\mathcal{N}}x^2} = \frac{1}{x^2} \mathcal{N} \left(\mathrm{e}^{-\frac{1}{2}\frac{\mathcal{N}'}{\mathcal{N}}x^2} - \mathrm{e}^{-\frac{1}{2}x^2}\right) \left(1 + O(\tfrac{1}{\mathcal{N}})\right). \tag{A.50}$$

A comparison with the previous identity confirms that Eq. (A.50) holds for the two cases of relevance in the present work, namely for either $\mathcal{N} \gtrsim \mathcal{N}' \gg 1$ or $\mathcal{N} \gg 1$ but at the same time $\mathcal{N}' = 0$.

Appendix B

Ehrenwörtliche Erklärung

Ich erkläre hiermit ehrenwörtlich, dass ich die vorliegende Arbeit selbständig, ohne unzulässige Hilfe Dritter und ohne Benutzung anderer als der angegebenen Hilfsmittel und Literatur angefertigt habe. Die aus anderen Quellen direkt oder indirekt übernommenen Daten und Konzepte sind unter Angabe der Quelle gekennzeichnet.
Weitere Personen waren an der inhaltlich-materiellen Erstellung der vorliegenden Arbeit nicht beteiligt. Insbesondere habe ich hierfür nicht die entgeltliche Hilfe von Vermittlungs- bzw. Beratungsdiensten in Anspruch genommen. Niemand hat von mir unmittelbar oder mittelbar geldwerte Leistungen für Arbeiten erhalten, die im Zusammenhang mit dem Inhalt der vorgelegten Habilitationsschrift stehen.
Die Arbeit wurde bisher weder im In- noch im Ausland in gleicher oder ähnlicher Form einer anderen Prüfungsbehörde vorgelegt.
Die geltende Habilitationsordnung der Friedrich-Schiller-Universität ist mir bekannt.
Ich versichere ehrenwörtlich, dass ich nach bestem Wissen die reine Wahrheit gesagt und nichts verschwiegen habe.

Jena, 26.06.2023 Felix Karbstein